國立臺灣大學醫學院醫學檢驗暨生物技術學系

博士論文

Department of Clinical Laboratory Sciences and Medical Biotechnology
College of Medicine
National Taiwan University

Doctoral Dissertation

探討兒童急性淋巴性白血病相關之微核醣核酸-181A 及微核醣核酸-151 的功能

Investigating the function of childhood acute lymphoblastic leukemia associated microRNAs: miR-181A and miR-151

顏靜慈

Ching-Tzu Yen

指導教授：林淑華 博士

Advisor: Shu-Wha Lin, Ph.D.

中華民國一百零四年十一月

November 2015

國立臺灣大學博士學位論文
口試委員會審定書

探討兒童急性淋巴性白血病相關之微核醣核酸-181A

及微核醣核酸-151 的功能

Investigating the functions of childhood acute lymphoblastic leukemia associated microRNAs: miR-181A and miR-151

本論文係顏靜慈君 D98424003 在國立臺灣大學醫學院醫學檢驗暨生物技術學系研究所完成之博士學位論文，於民國 104 年 11 月 5 日承下列考試委員審查通過及口試及格，特此證明

口試委員：

林俊華（指導教授）

俞松良　　黃度平

陳淑惠　　林淑容

楊佳芽　　林東燦

系主任、所長

前　言

微核醣核酸為演化上高度保留的內生性非編碼小片段 RNA，具影響各種生理功能的能力。除了調控個體發育及細胞功能，亦涉及癌症的病理機制。急性淋巴性白血病為最常見的兒童癌症，先前與臺大基因體中心基因微陣列及晶片核心實驗室合作分析兒童急性淋巴性白血病患者的微核醣核酸表現，找到了數個與急性淋巴性白血病次分群相關的微核醣核酸。本論文主要探討兩個急性淋巴性白血病相關之微核醣核酸基因：*MIR181A1* 及 *MIR151A*。第一部分著重於探討和 t(12;21)染色體轉位相關 RNA— *MIR181A1*。t(12;21) 為最常見的染色體異常且會形成 *ETV6/RUNX1* 融合致癌基因。本研究發現 *MIR181A1* 及 *MIR151A* 可相互調控，構成一個特殊的雙向負調控機制，並發現過量表現微核醣核酸 181a 可促進 *ETV6/RUNX1* 陽性白血病細胞的分化。第二部分則著重於探討 *MIR151A1* 基因的功能，此微核醣核酸在前 B 細胞急性淋巴性白血病中表現量遠高於 T 細胞急性淋巴性白血病。在本研究中，我們藉由基因重組工程產製 *Mir151* 基因剔除小鼠，並鑑定其表現型。

Preface

MicroRNAs (miRNAs) are endogenous noncoding small RNAs, which are highly conserved during biological evolution and implicated in virtually all aspects of biology. In addition to normal development and cellular function, they also involved in the pathogenesis of many cancers. Acute lymphoblastic leukemia (ALL) is a special type of cancer developed mostly in children. In collaboration with the NTU Microarray Core facility we have applied miRNA profiling to childhood ALL patients and identified several miRNAs correlated with various kinds of ALL subtypes. The thesis describes two ALL-associated miRNA genes, *MIR181A1* and *MIR151A*. The first part of the thesis focuses on t(12;21)-positive ALL associated miRNA—*MIR181A1*. t(12;21) is the most common chromosomal alteration which results in expression of *ETV6/RUNX1* fusion oncogene. We demonstrated novel regulatory network comprising *ETV6/RUNX1* and *MIR181A1* in which *ETV6/RUNX1* and *MIR181A1* can regulate each other. We further demonstrate that ectopic expression of miR-181a partially reversed the blockade of B cell differentiation in ETV6/RUNX1-expressing leukemic cells. The second part of the thesis focuses on *MIR151A*, which was identified to be differentially expressed in B-ALL. We generated the *Mir151* conventional knockout mice using recombineering technique and characterized their phenotypes.

誌謝

每篇被完成的論文，不光是作者的心血結晶，還隱含著許多人的貢獻，今日有此小小成果，心中由衷感激所有曾幫助我的人。

感謝給予我契機，讓我有幸踏入小兒血液腫瘤領域的林淑華老師及林東燦醫師，並且感謝林淑華老師及林淑容老師的細心教導，充分滋養了我的學術基礎及關於基因剔除小鼠的諸般知識與經驗，在撰寫期刊論文的同時，也習得了諸多寶貴的經驗與技巧，讓我得以茁壯成長。謝謝所有擔任口試委員的老師們，俞松良老師的精闢見解、楊性芳老師及曾慶平老師循循善導我的思路、以及陳淑惠醫師提供的臨床意見，使得我的論文更臻完整。還要感謝 ALL 團隊的所有成員，特別是建立了整個團隊研究基礎的楊永立醫師，耐心地教我 flow 分析方法及技巧的英卉學姐，還有不吝分享實驗經驗的勝凱，都給予我莫大的幫助。另外還要感謝中原大學基因功能研究室的諸位，在 mir-181a-1 研究上擔任開路先鋒的瑋柔、雖然照顧老鼠並不輕鬆，但有認真又窩心的曉穎和瑀絜分擔雜務，著實幫了不少忙；謝謝台大林淑華老師實驗室的同仁們，一直以來很慶幸有玉真學姐、軍宇學長及明憲在實驗及待人處事方面的經驗分享，另外要特別感謝夢倪體貼我趕論文時無暇顧及老鼠與實驗進度的龐大壓力，以及士鋒成功救援我那份差點毀損的論文電子檔。

我要將此份小小成就歸功於我的家人，我最親愛的爸爸媽媽和姊姊們，無條件支持任性的我念博士班的決定，即使我當了這麼多年的學生無法為家裡付出甚麼，在家時間也不多，卻從不給我壓力，總是微笑地鼓勵我，用充滿愛的家常料理撫慰我的身心。也謝謝我的婆家，對於這個總是忙於實驗的媳婦並未有太多要求，甚至把我當成自家女兒般地愛護與支持。

最後，最感謝的是我的先生 白振學，我們互相扶持走過念博士班最艱辛的歲月，也一起共享最美好的時光，就像彼此的左右手般，擁有不需言說的默契，是我的最佳實驗夥伴，也是我最重要的人生伴侶。今年年底，我們的第一個孩子即將出世，他在我腹中一起參與了 paper 及論文的撰寫和爸爸媽媽的畢業口試，感謝他在我最忙碌的時刻始終乖巧相伴，謝謝你，我的寶貝。

Abbreviation

7-AAD	7-aminoactinomycin
ABL1	ABL proto-oncogene 1
ALL	Acute lymphoblastic leukemia
AML	Acute myeloid leukemia
ANOVA	Analysis of variance
APC	Allophycocyanin
BAC	Bacterial artificial clone
B-ALL	B-cell precursor ALL
BCR	Breakpoint Cluster Region
bp	Base pair
BrdU	5'-bromo-2'-deoxyuridine
BSA	Bovine serum albumin
CBC	Complete blood counts
CD	Cluster of differentiation
CDS	Coding domain sequence
ChIP	Chromatin Immunoprecipitation
CLL	Chronic lymphocytic leukemia
CML	chronic myeloid leukemia
CRLF2	Cytokine receptor-like factor 2
DC	Differential count
DMEM	Dulbecco's Modified Eagle Medium
DPBS	Dulbecco's phosphate buffered saline
EDTA	Ethylenediaminetetraacetic acid
Epo	Erythropoietin
ERG	ETS-related gene
ETO	Eight-Twenty-One
ETV6	Ets variant 6
FBS	Fetal bovine serum
FITC	Fluorescein isothiocyanate
G0	Gap 0
G1	Gap 1
GAPDH	glyceraldehyde-3-phosphate dehydrogenase
HCC	Hepatocellular carcinoma
HCl	Hydrochloric acid
HDAC	Histone deacetylase

HEK	Human embryonic kidney
HEPES	4-(2-hydroxyethyl)-1-piperazineethanesulfonic acid
HLH	Helix-loop-helix
HRP	horseradish peroxidase
HSC	Hematopoietic stem cell
iAMP21	Intrachromosomal amplification of chromosome 21
IGH	Immunoglobulin Heavy chain locus
IKZF1	IKAROS family zinc finger
kb	kilobase
kg	kilogram
mg	miligram
MIR151	microRNA 151
MIR181A1	microRNA 181A1
miRNA	MicroRNA
MTT	3-(4,5- dimethylthiazol-2-yl)-2,5-diphenyltetrazolium bromide
NC	Negative control
N-CoR	Nuclear receptor co-repressor 1
PAX5	Paired box homeotic gene 5
PBS	Phosphate buffered saline
PCR	Polymerase chain reaction
PE	R-Phycoreythin
PerCP	Peridinin chlorophyll protein complex
PI	propidium iodide
PLAG1	Pleomorphic adenomas gene 1
pre-B cell	precursor B cell
pre-miRNA	precursor microRNA
pri-miRNA	primary microRNA
pro-B cell	progenitor B cell
PVDF	Polyvinylidene difluoride
PVDF	Immobilon polyvinylidene difluoride
qRT-PCR	Quantitative reverse transcription-polymerase chain reaction
RBC	Red blood cell
RIPA	Radioimmunoprecipitation assay
RISC	RNA-induced silencing complex
ROS	Reactive oxygen species
RPMI	Roswell Park Memorial Institute
RT-PCR	Reverse transcription-polymerase chain reaction

RUNX1	Runt-related transcription factor 1
SDS	Sodium dodecyl sulfate
SDS-PAGE	Sodium dodecyl sulfate polyacrylamide gel electrophoresis
SERCA2	Sarcoplasmic/endoplasmic reticulum Ca22+-ATPase 2
siRNA	short interfering RNA
SMRT	Silencing mediator of retinoic acid and thyroid hormone receptor
TSS	Transcriptional start site
UTR	untranslated region
VPA	Valproic acid

Table of Contents

The First Part

Childhood Acute Lymphoblastic Leukemia Associated MicroRNAs: I. A Double Negative Loop Comprising of *ETV6/RUNX1* and *MIR181A1*

摘要

急性淋巴性白血病為最常見的兒童癌症，而造成 *ETV6/RUNX1* 融合基因表現的 t(12;21) 染色體轉位則是在兒童急性前 B 細胞淋巴性白血病中最常見的染色體異常。微核醣核酸是一非編碼的小核醣核酸，長度僅 18–23 個核苷酸，是由 70-100 個核苷酸的微核醣核酸前驅物切割而來，其作用主要是在後基因轉錄階段抑制基因表達。幾乎所有的生理機制都受到微核醣核酸的影響，包括造血細胞分化，甚至已知有部分微核醣核酸參與在白血病癌化過程中。為探討與 *ETV6/RUNX1* 相關之微核醣核酸，本研究分析 50 個兒童前 B 細胞淋巴性白血病檢體中微核醣核酸的表達情形，其中包含 10 個 *ETV6/RUNX1* 陽性病例。透過與 *ETV6/RUNX1* 陰性病人細胞相比較，本研究找到 17 個在 *ETV6/RUNX1* 陽性病人細胞表達量顯著下降的微核醣核酸。在這些具顯著差異的微核醣核酸之中，由微核醣核酸 181a-1 前驅物 3′ 端衍生而來的成熟產物微核醣核酸 181a-1（miR-181a-1），其表現量的改變最具統計意義（下降近百分之七十五，P值 < 0.001）。此外，*MIR181A1* 基因中具有 RUNX1 蛋白的 DNA 結合位（TGTGGT），因此本研究選擇針對 *MIR181A1* 進行更深入的探討。

REH 細胞為 *ETV6/RUNX1* 陽性的前B細胞急性淋巴性白血病細胞株，本研究利用小片段干擾 RNA 抑制 REH 細胞的 ETV6/RUNX1 表達可使 miR-181a-1 表現量上升，此外在人類胚胎腎臟 293FT 細胞中過量表達 ETV6/RUNX1 融合蛋白則可抑制 miR-181a-1 表現量。本研究並以免疫染色質沉澱法（chromatin immunoprecipitation）在 REH 細胞株驗證被預測的 RUNX1 結合位，證明 *MIR181A1* 直接受到 ETV6/RUNX1 融合蛋白調控。相較於 miR-181a-1，被報導具有功能的是另一股微核醣核酸 181a（miR-181a），為尋找其下游標的，本研究將 REH 細胞轉染 miR-181a 並檢測 *PLAG1* 表達，已知在慢性淋巴性白血病（chronic lymphoblastic leukemia）中 *PLAG1* 為 miR-181a 標的。在過量表達 miR-181a 的 REH 細胞中，PLAG1 蛋白表達量下降；而在 *ETV6/RUNX1* 陽性臨

床檢體中 *PLAG1* mRNA 表達明顯增加。上述證據皆指出，如同慢性淋巴性白血病研究結果，*PLAG1* 基因在兒童急性淋巴性白血病亦為 miR-181a 標的。此外，在 miR-181a 轉染之 REH 細胞中 ETV6/RUNX1 蛋白表達量亦顯著下降，且與 *RUNX1* 3′端未轉譯區域（3′-untranslated region）上的 miR-181a 辨識序列（UGAAUGU）相關。本研究並利用 REH 細胞證明過量表達 miR-181a 會促進表現 ETV6/RUNX1 之前 B 細胞急性淋巴性白血病細胞由前 BI 階段（pre-BI stage）分化為未成熟 B 細胞（immature B cells）。且 miR-181a 亦可誘導 *ETV6/RUNX1* 陽性臨床病人檢體 CD10 抗原表達量減少，意即細胞有部分分化的現象。

統整上述研究成果，本研究顯示 *MIR181A1* 及 *ETV6/RUNX1* 可相互調控，並推論一涉及 *MIR181A1* 與 *ETV6/RUNX1* 的雙向負調控迴圈機制可能參與在由 ETV6/RUNX1 驅動之前B細胞急性淋巴性白血病分化停滯。

關鍵字：前 B 細胞急性淋巴性白血病，t(12;21)轉位，ETV6/RUNX1，微核醣核酸 181a-1，微核醣核酸 181a

Abstract

Acute lymphoblastic leukemia is the most common pediatric cancer, and the chromosomal translocation t(12;21), which resulting in expression of *ETV6/RUNX1* fusion gene, is the most frequent chromosomal lesion in childhood B-cell precursor (pre-B) ALL. MicroRNAs (miRNAs) are small noncoding RNAs with 18–23 nucleotides arisen from cleavage of 70-100 nucleotide precursors and mostly down regulate gene expression at post-transcriptional level. They have been implicated in virtually all aspects of biology including hematopoietic cell differentiation and some of them are also known to participate in leukemogenesis. To investigate the miRNAs that are associated with regulation of *ETV6/RUNX1* expression, we performed miRNA expression profiling on fifty leukemic samples from children with pre-BALL, including 10 cases positive for *ETV6/RUNX1*. We identified 17 miRNAs that were down-regulated in *ETV6/RUNX1*-positive, compared with *ETV6/RUNX1*-negative B-ALL. Of these miRNAs, miR-181a-1, one of the mature form derived from the 3′ arm of precursor hsa-mir-181a-1, gives the most significant fold-change (reduced by ~75%, $P<0.001$). In addition, *MIR181A1* contains a potential RUNX1 binding site (TGTGGT), thus we selected *MIR181A1* for further investigation.

In REH cells, an *ETV6/RUNX1*-positive B-ALL line, siRNA knockdown of ETV6/RUNX1 resulted in increased miR-181a-1 expression, while overexpression of

ETV6/RUNX1 fusion protein in HEK-293FT cells resulted in reduction of miR-181a-1 level. The predicted *RUNX1* binding site was also confirmed in REH cells by chromatin immunoprecipitation analysis, indicating *MIR181A1* is a direct target of the ETV6/RUNX1 fusion protein. To search for downstream targets of miR-181a, the functional counterpart of miR-181a-1, REH cells were transfected with miR-181a and the expression of *PLAG1*, shown to be a target of miR-181a-1 in chronic lymphoblastic leukemia (CLL) was examined. The PLAG1 protein level was decreased in miR-181a over-expressed REH cells. In addition, the *PLAG1* mRNA level was increased in *ETV6/RUNX1*-positive clinical samples. This indicated that *PLAG1* gene might be the down-stream target of miR-181a in childhood ALL as in CLL. Furthermore, we found ETV6/RUNX1 protein was also decreased in miR-181a-transfected REH cells, correlating with the existence of a miR-181a recognition sequence (UGAAUGU) at the 3'-untranslated region of *RUNX1*. Using REH cells, we showed ectopic expression of miR-181a could enhance ETV6/RUNX1-expressing B-ALL cells differentiate from pre-BI stage to immature B cells. In addition, miR-181a could induce partial differentiation of *ETV6/RUNX1*-positive clinical patient samples by diminishing CD10 expression.

Taken together, our results demonstrate that *MIR181A1* and *ETV6/RUNX1* regulate each other, and we propose that a double negative loop involving *MIR181A1* and

ETV6/RUNX1 may contribute to ETV6/RUNX1-driven differentiation arrest in B-ALL.

Key words：pre-B ALL，t(12;21) translocation，ETV6/RUNX1，miR-181a-1，miR-181a

List of Figures

List of Tables

List of Appendix

Chapter 1. Introduction

1.1. Childhood B-cell precursor acute lymphoblastic leukemia

Acute lymphoblastic leukemia (ALL), characterized by excessive proliferation and differentiation block of abnormal lymphoblast, is an a clinically and biologically heterogeneous hematologic malignancy originating from a multipotent hematopoietic stem cell (HSC). It is the most common childhood cancer, accounting for 31% of all tumors (1), and the leading cause of cancer-related death in children and young adult (2). According to the type of lymphocyte the leukemia cells come from, ALL has been classified into B-cell and T-cell lineage ALL. At approximately 80% (1), the majority of children with ALL have B-cell precursor ALL (B-ALL), which results from the accumulation of genetic alterations in pre-B cells and demonstrates a pre-B cell-like phenotype such as exhibiting cell surface markers of normal pre-B cells ($CD19^+$, $CD10^+$), and appears to be clonal expansion of normal pre-B cells stalled at a particular stage of the differentiation process (3, 4).

1.2. Genetic aberrations in B-ALL

Recurrent genetic aberrations that block pre-B cell differentiation and direct aberrant proliferation and cell survival is the hallmark of B-ALL and the driving force

of leukemogenesis. Using standard chromosomal and molecular genetic analysis, 75% of B-ALL cases can be detected harboring a recurring chromosomal abnormalities (2), which can be subdivide into numerical aberrations, such as hyperdiploidy (>50 chromosomes) and hypodiploidy (<44 chromosomes), and structural alteration like chromosomal rearrangement. Chromosomal rearrangements resulting from translocation, inversion, deletion, and duplication are common in B-ALL. These rearrangements often affect genes encoding regulators of hematopoiesis, tumor suppressors, oncogenes or tyrosine kinases. Four common translocations, t(12;21)(p13;q22), t(1;19)(q23;p13), t(9;22)(q34;q11.2), and t(4;11)(q21;q23), are most well-known and compart 30-35% of childhood ALL (Appendix I) (1, 5). These translocations disrupts the normal genes involved in regulating hematopoiesis and cause the formation of new fusion genes which are critical to leukemogenesis. Some of them, such as t(9;22) which results in a kinase fusion gene—*BCR/ABL1*, are powerful enough to induce leukemia individually (6), but some others may require additional genetic hits to induce overt leukemia (7).

Standard methods can detect genetic abnormalities in most of the patients but still have limitation. Recently, the aid of newly developed approaches including gene expression microarray profiling, DNA copy number analysis, and next-generation sequencing (NGS) technologies, have improved the number of lesions found in B-ALL and virtually all cases can be detected harboring a genetic alteration (8). Numerous

mutations that targeted genes in key cellular pathways in B-ALL are identified and are applied to characterize new subtypes or increase the new insights into known ALL subtypes, such as *BCR/ABL1*-like ALL (~15%) (9, 10), intrachromosomal amplification of chromosome 21 (iAMP21, ~2%) (11, 12), *IGH*- and *CRLF2*-rearrangement (5-7%) (13), *ERG*-deregulated ALL (~7%) (14), *PAX5*-deletion (3%) /mutation (5-7%) / rearrangement (2-3%) (5), and *IKZF1*-deregulated ALL (~15%) (9, 15).

1.3. *ETV6/RUNX1*-positive B-ALL

1.3.1. *ETV6/RUNX1* fusion gene

The t(12;21) (p13;q22) translocation, which results in *ETV6/RUNX1* fusion gene, was first reported by two different group in 1995 (16, 17). It is the most common chromosomal rearrangement in childhood B-ALL cases but less prevalent in adult patients (1, 18). The incidence of t(12;21) in B-ALL is approximately 15-25%, and patients with this translocation usually have excellent outcome (19). This rearrangement is not able to be detected by conventional cytogenetic analysis but is readily detected by fluorescent in situ hybridization and molecular techniques, such as RT-PCR and quantitative RT-PCR (20-22).

The *ETV6* gene, which is very large (240 kb) and consists of eight exons coding for an ETS-like putative transcription factor containing a helix-loop-helix (HLH) and a

DNA-binding domain is on human chromosome 12p13 (23). The *RUNX1* gene, which belongs to the runt domain gene family of transcription factors, is on human chromosome 21q22 and spans 260 kb consisting of 12 exons (24). Both *ETV6* and *RUNX1* genes demonstrated critical roles in hematopoiesis in knockout mice studies (25-27), and they are also frequently targeted by rearrangements and mutations in leukemia (28, 29).

The breakpoints on *ETV6* gene are clustered in a 15 kb region between exon 5 and 6 (23), and the breakpoints on *RUNX1* gene may occur either in the ~100 kb intron 1 or intron 2 (Appendix IIA) (18, 30). Most of all, the *ETV6/RUNX1* fusion transcript shows a joining of exon 5 of *ETV6* to the second exon of *RUNX1*, while the junction occurred at the third exon of *RUNX1* is less frequently seen (Appendix IIB) (30). Wherever the breakpoints occurred, these all result in fusion of the 5′ portion of *ETV6* and almost the entire coding region of *RUNX1* gene.

1.3.2. Structure and function of ETV6/RUNX1 fusion protein

The ETV6/RUNX1 fusion protein is composed of the N-terminal non-DNA-binding region of ETV6 and nearly complete RUNX1 protein, including the DNA-binding and activation region, which is responsible for the essential function of the fusion protein (Appendix III) (16, 18, 31). The ETV6 protein acts as a DNA-binding

transcriptional repressor, while RUNX1 can be a DNA-binding transcriptional activator or repressor depending on the promoter specificity or cell context (18). In contrast to RUNX1, transiently expressed ETV6/RUNX1 fusion protein generally represses the activities of reporter constructs driven by regulatory regions derived from hematopoietic-specific genes (18). The ETV6/RUNX1 fusion protein acts as an aberrant transcription factor that can interfere with the normal functions of wild-type ETV6 and RUNX1 through multiple mechanisms. ETV6/RUNX1 can dimerize with wild-type ETV6 through the HLH domain and disrupt the activity of ETV6 (31, 32). ETV6/RUNX1 may also bind to RUNX1 target DNA sequences and recruit transcriptional corepressors including mSinA, N-coR, and histone deacetylase-3 (HDAC3) via the fusion part of ETV6, resulting in dysregulated RUNX1-dependent transcription (Appendix IV) (31, 33, 34).

1.3.3. Role of ETV6/RUNX1 in leukemogenesis of B-ALL

Analysis of monozygotic twins with concordant leukemia and retrospective screening of neonatal blood spots of patients with leukemia indicate that chromosomal translocations characteristic of pediatric leukemia often arise prenatally (35). However, in normal cord blood ETV6/RUNX1 is detected at a frequency that is 100-fold greater than the risk of the corresponding leukemia (36). Mouse models demonstrate that

expression of ETV6/RUNX1 in murine bone morrow stem cells impedes B cell differentiation from the earliest stages of B cell development with a particular marked impact at the transition from pro-B to pre-B cell stages. Although the accumulation of both multipotent and B-cell progenitors in vivo, ETV6/RUNX1 is insufficient to induce leukemia by itself (37, 38). Collectively, these data suggests that ETV6/RUNX1 is a frequent prenatal first hit in childhood leukemia which can initiate a preleukemic phenotype remaining covert for up to 15 years but is insufficient for clinical leukemia.

1.4. MicroRNAs

1.4.1. Overview

MicroRNAs (miRNAs) are a group of single-stranded, endogenously initiated non-coding RNAs which are first discovered in the early 1990s (39). They are transcribed by RNA polymerase II as part of capped and polyadenylated primary transcripts (pri-miRNAs) that can be either protein-coding or non-coding. The primary transcript is cleaved by the Drosha ribonuclease III enzyme to produce an approximately 70 to 100- nucleotide stem-loop precursor miRNA (pre-miRNA), which is exported to cytoplasm and is further cleaved by the Dicer ribonuclease to generate the 20-23 nucleotides mature miRNA products from 3′ and/or 5′ arms (40). When two mature miRNAs originate from opposite arms of the same pre-miRNA and express

similar amounts, they are represented as -3p and -5p (41). In human cells, the mature miRNAs incorporate into a RNA-induced silencing complex (RISC) and then target mRNAs for degradation or translational repression via partial or perfect complementarity to the mRNA 3' untranslated region (3' UTR) through specific seed sequences (Appendix V) (40, 42). By this way, miRNAs can downregulate gene expression at the post-transcriptional level. In the recent years, there has been increasing evidence that miRNAs also bind in the coding region to inhibit translation (43), implying that miRNAs may flexibly tune the time-scale and magnitude of post-transcriptional regulation through combination of multiple ways (44). Thus, miRNAs have the ability to control fundamental cellular functions such as survival, differentiation, apoptosis, and cell cycle.

1.4.2. MicroRNAs in hematopoiesis and leukemogenesis

A variety of miRNAs have been identified as important regulators of hematopoiesis (45). For instance, miR-221/222 inhibits the erythropoiesis (46), miR-223 is essential to modulate myeloid differentiation (47), miR-181a and miR-150 are dynamically regulated during T-cell and B-cell development, respectively, and premature expression of certain miRNAs in hematopoietic progenitors may impair T- and B-cell development at the stage transition during maturation (48-50).

MiRNA expression in hematological malignancies has also been extensively studied. Some information about factors that modulate miRNA expression is now available. Dysregulation of miRNA expression is frequently associated with cytogenetic abnormalities, and indeed certain abnormalities have direct impacts on aberrant miRNAs expressions (45). RUNX1/ETO, the most common acute myeloid leukemia–associated fusion protein resulting from t(8;21), was first reported to directly repress miR-223 expression by triggering chromatin remodeling and epigenetic silencing, which in turn blocks the differentiation of myeloid precursor cells (51).

1.4.3. *MIR181A1* gene

MIR181A1 gene is located on human chromosome 1q32.1 and is only 62 bp distant from *MIR181B1* gene, they are considered sharing the same primary transcript. There is only one exon in *MIR181A1* gene and expressed a pre-miRNA with 110 bp in length referred to hsa-mir-181a-1. Hsa-mir-181a-1 will further generate two mature miRNAs including miR-181a-3p and -5p, which are referred to miR-181a-1 and miR-181a, respectively (Figure 1A). *MIR181A1* belongs to the miR-181 family which consists of mir-181a/b1, mir-181a/b2 and mir-181c/d, producing four highly similar mature 5p miRNAs (miR-181a, miR-181b, miR-181c and miR-181d, respectively) with identical seed sequence and a slight difference in 1~4 bp from three polycistronic transcripts

(Figure 1B).

Although both 3p and 5p of hsa-mir-181a can be detected in tissues, previous reports only demonstrated that miR-181a targets various mRNAs and has physiological roles and pathological meanings (52-54), while the function of miR-181a-1 remains unclear. In healthy cells, miR-181a regulates B-cell development, influences T-cell sensitivity to antigens by modulating T-cell receptor signaling, and is involved in early steps of hematopoiesis (55). A tumor suppressor activity of miR-181a is reported in chronic lymphocytic leukemia (CLL) (56, 57), glioma (53), and astrocytoma (54). In addition, ectopic expression of miR-181a has been shown to sensitizes acute myeloid leukemia (AML) cell lines to chemotherapy (58), and enhance the effect of radiation treatment on malignant glioma cells via down-regulation of the Bcl-2 protein (59).

1.4.4. MicroRNAs associated with ETV6/RUNX1

Recent studies have shown that aberrant miRNA expression also plays an important role in malignant transformation of ETV6/RUNX1 ALL. A highly expressed miR-125b-2 cluster was found in ETV6/RUNX1 ALL and may provide leukemic cells with a survival advantage against growth inhibitory signals in a p53-independent mechanism (60). In addition, ETV6/RUNX1 was shown to regulate the cellular level of the Survivin protein and apoptosis via suppression of miR-494 and miR-320a

expression by direct binding to the promoter regions of their encoding genes (61).

1.5. Research motive and the aim

It is believed that ETV6/RUNX1 expression may allow quiescent, preleukemic cells to exist in the bone marrow via transcriptional deregulation of downstream genes. There is ample evidence that leukemogenesis driven by ETV6/RUNX1 is mediated in part by conferring survival signals through direct modulation of multiple targets such as *EPOR*, *MDM2*, and miRNA genes (61-63). However, miRNAs involved in the ETV6/RUNX1-mediated B-cell differentiation arrest is not well understood. For this purpose, we designed and performed the experiments to identify the miRNAs which are regulated by ETV6/RUNX1 and elucidated the underlying regulatory mechanism.

Chapter 2. Materials and Methods

2.1. Materials

2.1.1. Reagents

Product name	Company
1 kb DNA Ladder	Bertec
100 bp DNA Ladder	Bertec
20x Human GAPDH VIC/MGB	Applied Biosystems
2-Mercaptoethanol	Sigma
2x TaqMan Universal PCR Master Mix	Applied Biosystems
Acrylamide	Sigma
Agar, Bacteriological	ALPHA biosciences
Agarose	Invitrogen
Ammonium persulfate	Sigma
Ampicillin	Sigma
bis-Acrylamide	Sigma
Boric acid	J.T.Baker
Bovine serum albumin (BSA)	Sigma
BPB	Sigma
Calf Intestine Alkaline Phosphatase (CIP)	Fermentus
Chlorofrom	J.T.Baker
Dithiothreitol (DTT)	Invitrogen
DMEM	Hyclone
dNTPs	GeneDirex
Dulbecco's phosphate buffered saline (DPBS)	Gibco
EDTA	J.T.Baker
EDTA•Na_2	J.T.Baker
Ethanol	Sigma
Ethidium Bromide (EtBr)	Amersco
Fetal bovine serum (FBS)	Biological Industries
Formaldehyde	Sigma
Glucose	Sigma
Glycerol	Mallinckrodt

Glycine	J.T.Baker
HEPES	Gibco
Isopropanol	Fluka
L-glutamine	Gibco
Methnol	Sigma
OPTI-MEM I	Invitrogen
PageRugular Pre-Stained Protein Ladder	Fermentus
Penicillin/Streptomycin (P/S)	Gibco
Phosphate buffered saline (PBS)	Biowest
Polybrene	Sigma
Protease inhibitor cocktails	Roche
Puromycin	Sigma
RIPA buffer	Thermo
RPMI-1640	Gibco
Skimmed milk	安佳
Sodium bicarbonate	Gibco
sodium dodecyl sulfate (SDS)	Pierce
Sodium pyruvate	Gibco
StemSpam™ CC100	StemCell Technologies
StemSpam™ SFEMII	StemCell Technologies
TEMED	Sigma
Tris base	J.T.Baker
Trypan blue	Biowest
Trypsin	Gibco
Tryptone	ALPHA biosciences
Tween 20	Sigma
Valproic acid sodium salt (VPA)	Sigma
Xylene	Sigma
Yeast extract	ALPHA biosciences

2.1.2. Kits

Product name	Company
Bradford protein assay	Bio-Rad
BrdU-FITC flow kit	BD
Cell Proliferation Kit I (MTT)	Roche
Chromatin Immunoprecipitation (ChIP) Assay Kit	Upstate

Dual-Luciferase Reporter Assay	Promega
FastStart universal SYBR green master (ROX)	Roche
FavorPrep plasmid extraction midi kit	FAVORGEN
FavorPrep plasmid extraction mini kit	FAVORGEN
FITC Annexin V apoptosis detection kit	BD
Immobiion Western Chemilum HRP substrate	Millipore
Lipofectatime 2000	Invitrogen
Neon™ transfection system 10 μL kit	Invitrogen
PEG-it kit	SBI
Pre-miR™ miRNA Precursor Molecule (hsa-mir-181a)	Ambion
Pre-miR™ Negative Control #1	Ambion
Qiagen Plasmid Maxi kit	Qiagen
QuikChange Lightning Site-Directed Mutagenesis kit	Agilent
RnaseOut	Invitrogen
siPORT™ *NeoFX*™ Transfection Agent	Ambion
siRNA	Invitrogen
SuperScript III Reverse Transcriptase	Invitrogen
T4 DNA Ligase	NEB
Taq DNA polymerase	Geneaid
TaqMan miRNA expression assay	Applied Biosystems
TaqMan® MicroRNA Cells-to-CT™ Kit	Ambion
TaqMan® miRNA RT kit	Ambion
TransIT-LT1	Mirus Bio.
Trizol reagent	Invitrogen

2.1.3. Antibodies

Product name	Company
mouse monoclonal anti-PLAG1 (H00005324-M02)	Abnova
mouse polyclonal anti-β-actin (NB600-501)	Novus
rabbit polyclonal anti-RUNX1 (ab50541)	Abcam
HRP-conjugated Goat anti-mouse IgG (AP124P)	Millipore
HRP-conjugated Goat anti-rabbit IgG (AP132P)	Millipore

2.1.4. Vectors

Product name	Source
pGL3-SV40 Promoter Vector	Promega
pRL-SV40 Vector	Promega
pLKO.1.Null-T vector	RNAi core facility, Acadamia Sinia
pMD.G vector	RNAi core facility, Acadamia Sinia
pCMVΔR8.91 vector	RNAi core facility, Acadamia Sinia
pCMV-XL4-ETV6 (NM_001987.3)	Origene
pCMV-XL4-RUNX1 (NM_001754.3)	Origene

2.1.5. Instruments

Instrument name	Company
7300 Real-Time PCR machine	Appied Biosystems
GeneAmp PCR machine	Appied Biosystems
AllegraTM 21R centriguge	Beckman Coulter
Avanti® J-E high speed centrifuge	Beckman Coulter
KUBOTA 2420 centriguge	KUBOTA
Eppendorf microcentriguge (F45-24-11)	Eppendorf
Orbital shacking incubator (OSI500R)	TKS
Analytical balance (TE124s)	Sartorius
Ultrasound sonicator (UP200H)	Hielscher
LAB ROTATOR	Digisystem
Microporator MP-100	Digital Bio Tech.
Cell cuture incubator (MCO-15AC)	SANYO
Synergy^{HT} ELISA reader	BioTek
SpectraMaxR M5 multi-detection reader	Molecular Devices
FUSION-SOLO Chemiluminescence imaging system	Vilber Lourmat
FACSCalibur	BD
Nanodrop	Thermo

2.2. Methods

2.2.1. Patients

All of the B-cell precursor ALL patient samples were obtained at the time of diagnosis and prior to treatment. Viable diagnostic bone marrow (BM) or peripheral blood (PB) was obtained from 50 children who were diagnosed with B-ALL between July 1996 and July 2014 at National Taiwan University Hospital (NTUH) and National Cheng Kung University Hospital (NCKUH). The diagnosis of ALL was made based on the morphologic findings of BM aspirates, as well as on immunophenotype analyses of leukemic cells by flow cytometry. Conventional cytogenetics analyses were performed as part of the routine workup. Patients were prospectively assigned to one of three risk groups (standard, high, and very high) based on their presenting clinical features and the biological features of their leukemic cells. Patients were considered to have standard-risk (SR) ALL if they were between 1 and 9 years old with a presenting leukocyte count less than 10×10^9 cells/L or were between 2 and 7 years old with a presenting leukocyte count between 10×10^9 and 50×10^9 cells/L. Patients were considered to have high-risk (HR) ALL if they were between 1 and 9 years old with a presenting leukocyte count between 50×10^9 and 100×10^9 cells/L, or between 1 and 2 or 7 and 10 years old with a presenting leukocyte count between 10×10^9 and 50×10^9

cells/L. Patients with at least one of the following were assigned to the very-high-risk (VHR) group: age younger than 1 year, initial leukocyte count greater than 100×10^9 cells/L, or presence of *BCR-ABL*, *MLL-AF4* or other *MLL* rearrangements in B-ALL. The Institutional Review Board of National Taiwan University Hospital approved the study. In accordance with the Declaration of Helsinki, we obtained written informed consent from the parents of each patient before collection.

2.2.2. RNA preparation

Mononuclear cells from bone marrow or peripheral blood were Ficoll purified and immediately stored in liquid nitrogen. Cryopreserved samples were thawed and washed in 2% FBS-supplemented 1X PBS prior to RNA extraction. Total RNA was extracted using Trizol reagent according to the manufacturer's instructions.

2.2.3. Quantitative real-time PCR

Transcripts of human *ETV6*/*RUNX1* were quantified by TaqMan real-time PCR using published primer probe combinations (22), and the TaqMan endogenous control assay for *GAPDH* was combined in the same reaction. Expression of *PLAG1* and the reference gene *GAPDH* was determined by SYBR Green real-time PCR and measured in two independent assays. The primer and probe sequences used in this study were

shown in Table 1. All of the assays were run in duplicate.

2.2.4. MicroRNA expression profile

MiRNA expression profiling was performed using the ABI PRISM 7900 Real Time PCR System and stem-loop reverse transcription-quantitative PCR miRNA arrays containing 397 mature human miRNAs. 365 miRNAs were assayed using TaqMan miRNA arrays with 100 ng of RNA as the input for each reverse transcriptase reaction according to the manufacturer's protocol. Each individual miRNA in primary ALL blasts and cell line experiments was measured using TaqMan miRNA assays. All miRNA assays were run concurrently with a calibration control, U6 snRNA and were run in triplicate.

2.2.5. Cell culture

The REH cell line (human B-cell precursor leukemia, *ETV6/RUNX1*-positive) from American Type Culture Collection was grown in 6-well plates at 10^5 to 10^6 cells/mL, depending on experimental conditions. REH cells were cultured in RPMI medium supplemented with 10 mM HEPES, 1 mM sodium pyruvate, 4.5 g/L glucose, 1.5 g/L sodium bicarbonate, and 10% FBS. HEK-293FT cells were cultured in 24-well plates and 60-mm dishes for the luciferase reporter assay and lentivirus packaging,

respectively. HEK-293FT cells were grown in DMEM supplemented with 6 mM L-glutamine, 1 mM sodium pyruvate, and 10% FBS. Primary leukemic cells were obtained from patients with active precursor B-ALL. Primary ALL blasts were isolated from freshly harvested bone marrow aspirates by density centrifugation using Ficoll-Paque followed by two washes with RPMI medium. After freezing-thawing, primary ALL blasts were cultured in SFEMII supplemented with a cytokine cocktail containing recombinant human Flt3 ligand, stem cell factor, and thrombopoietin to support the proliferation of hematopoietic progenitors.

2.2.6. Cell viability

The viability of cultured cells was determined by assaying the reduction of MTT to formazan using the Cell Proliferation Kit I. Briefly, 100 μL REH cells or primary ALL blasts were plated in 96-well plates, and 50 μg MTT per 100 μL 1X DPBS was added to each well at different times. Cells were then incubated at 37℃ for 4 hours, and 100 μL 10% SDS in 0.01 M HCl was added to dissolve the formazan crystals. Absorbance was measured at 550 nm and 690 nm with a Synergy HT multi-detection microplate reader.

2.2.7. Proliferation and cell cycle

A BrdU flow kit was used to determine cell cycle kinetics and to measure BrdU

incorporation into DNA of proliferating cells. Briefly, cells (1.5×10^5 cells/mL) were seeded in 6-well tissue culture plates and cultured for 48 hours followed by the addition of 10 μM BrdU, and the incubation was continued for an additional 30 minutes. Cells were fixed in a solution containing paraformaldehyde and the detergent saponin, and then they were incubated for 1 hour at 37℃ with DNase (30 μg per sample). FITC-conjugated anti-BrdU (1:50 dilution in wash buffer) was added, and incubation was continued for 20 minutes at room temperature. Cells were washed, and DNA was stained using 7-AAD (20 μL per sample), followed by flow cytometric analysis**.** The BrdU content (FITC) and total DNA content (7-AAD) were determined using FCS Express software. All experiments were carried out three times.

2.2.8. Apoptosis assay

Apoptosis was evaluated by staining with annexin V/PI and flow cytometric analysis. Briefly, REH cells were harvested, washed, and resuspended in annexin V binding buffer. Then, the cells were stained with annexin V-FITC in the dark at room temperature for 10 minutes, centrifuged, and gently resuspended in annexin V binding buffer. Finally, 10 μL PI staining solution was added and gently mixed, and cells were kept on ice in the dark and immediately subjected to flow cytometry. All experiments were carried out three times.

2.2.9. Flow cytometric analysis of lineage markers

To assess cell-surface markers, cells were suspended in 1% BSA/PBS and stained with the appropriate dilution of the antibodies for 15 minutes at room temperature. Before detection, cells were washed with 1% BSA/PBS and resuspended in 1% paraformaldehyde/PBS. Monoclonal antibodies recognizing the following cell-surface markers were used for flow cytometry: CD19, CD10, CD20, CD45, IgM, κ-chain, and λ-chain. Marker analyses were performed by using flow cytometry.

2.2.10. Chromatin immunoprecipitation

We used the chromatin immunoprecipitation (ChIP) kit to perform the assays. Briefly, cells were harvested, and chromatin was cross-linked with formaldehyde at a final concentration of 1%. After lysis of the cells, samples were sonicated to an average DNA length of 300 to 500 bp. The chromatin was immunoprecipitated overnight with antibodies against RUNX1 and HDAC3. The HDAC inhibitor valproic acid (VPA) was used to release the binding of HDAC3; REH cells were treated with 2 mM VPA for 24 hours before harvesting. Chromatin was also purified from cross-linked DNA that had not been immunoprecipitated to serve as an input DNA control. A genomic region close to the putative RUNX1-binding site (P1), which is 3 kb upstream of the *MIR181A1* transcription start site predicted by CoreBoost_HM

(http://rulai.cshl.edu/tools/CoreBoost_HM/) (64), and another *MIR181A1* upstream region (P2) was amplified by PCR. As a positive control, the primer set PC was used to amplify the promoter region of *MIR223* as previously described (51). All of the primers used for PCR were listed in Table 1. The entire experiment was carried out three times with similar results.

2.2.11. Western blotting

Cells were pelleted, washed with cold PBS, and lysed for 30 minutes on ice in RIPA buffe with protease inhibitor cocktail. Lysates were cleared by centrifugation at 14,000 × *g* at 4°C for 15 minutes, and 35 μg total protein was separated by SDS-PAGE and transferred to an PVDF membrane. The membrane was blocked and incubated overnight with primary antibodies. After a final incubation with secondary antibodies conjugated with HRP (1:5000 dilution), immune complexes were detected with HRP chemiluminescent substrate. Antibodies and dilutions used were: anti-RUNX1 (1:1000), anti-PLAG1 (1:500), and anti-β-actin (1:5000).

2.2.12. siRNA transfection

For *ETV6*/*RUNX1* silencing with a siRNA, REH cells were transfected with a mixture of siRNAs targeting the fusion region of *ETV6*/*RUNX1* or a nonfunctional

control, siRNA-S (65, 66). The siRNA sequences were shown in Table 2. The siRNAs were transfected into REH cells via electroporation with a MP-100 microporator in a 100-μL gold tip under the following conditions: 1×10^6 cells/mL antibiotic-free culture medium, 230 nM siRNA, one pulse of 1,150 V for 30 milliseconds. After 48 hours of transfection, cells were harvested to assess target gene expression.

2.2.13. miRNA precursor transfection

The miRNA precursors hsa-mir-181a and negative control 1 are partially double-stranded RNAs that mimic endogenous precursor miRNAs. Each miRNA precursor was transfected into cells at a final concentration of 50 nM using siPORT NeoFx transfection agent. Two rounds of transfection were performed with a 48-hour interval between the first and second round. The effects manifested by the introduction of the precursor miRNAs into the cells were assayed after the second round of transfection.

2.2.14. ETV6/RUNX1 and RUNX1 protein overexpression

The pCMV6-XL4 vector expressing either ETV6/RUNX1 (pCMV-XL4-E/R) or RUNX1 (pCMV-XL4-RUNX1) protein was transfected into HEK-293FT cells using the transfection reagent TransIT-LT1 according to the manufacturer's instructions. An

empty pCMV6-XL4 vector without insert was used as a transfection control. Cells were harvested after 72 hours of transfection and further analyzed the protein and miR-181a-1 expression by Western blot and qRT-PCR, respectively. The entire experiment was carried out three times with similar results.

2.2.15. Lentiviral construct and infection

The sequence of *MIR181A1* was PCR amplified from human bone marrow mononuclear cells and then cloned into vector pLKO_TRC001, which contains a PGK-puromycin acetyltransferase insert, and labeled as pLKO.1.181A1. An empty TRC1 vector, pLKO.1.Null-T, was used as a negative control. Production and infection of lentivirus followed the protocol from the National RNAi Core facility. Briefly, lentivirus was generated by transfection of HEK-293FT cells using the transfection reagent TransIT-LT1. The vectors used were pLKO.1.null-T or pLKO.1.181A1, and the packaging vectors were pMD.G and pCMVΔR8.91. Single infection of REH cells and two sequential infections of primary ALL cells with concentrated lentiviral particles were carried out in 24-well plates. Lentivirus-infected cells were selected by adding puromycin (2 μg/mL) to the culture medium and collected after screening for a week.

2.2.16. Luciferase reporter assay

The luciferase activity assay was performed using the Dual-Luciferase Reporter Assay System (Promega). A 678-bp fragment of the *RUNX1* 3′ UTR containing a binding site for miR-181a (UGAAUGU) was cloned into the XbaI site at the distal end of the luciferase reporter gene of pGL3-promoter vector. This construct was used to transiently transfect HEK-293FT cells with Lipofectamine 2000 together with pRL-TK Renilla, a transfection control used to calibrate the luciferase activity, and pLKO.1.181A1 (miR-181a-expressing vector) or pLKO.1.Null-T (negative control for miR-181a-expressing vector). A mutated version of the binding sequence (AGAUCUG) containing a BglⅡ site was obtained by site directed mutagenesis and was used as the target site control. Cells were lysed, and the luciferase activity was measured 48 hours after transfection.

2.2.17. Statistical analyses

In miRNA profiling analysis, to avoid low abundant expression issue, miRNA with coefficient of variation (CV) < 0.2 was removed in the first step. In the second step, the student's t test was used to evaluate different miRNA expression between *ETV6/RUNX1*-positive (n=10) and *ETV6/RUNX1*-positive (n=40) groups. Finally, in order to control multiple testing issue, false discovery rate method was performed to

adjust p value obtained from student's t test (67). Data are represent the means ± SE or ± SD as indicated in the figure legends. The two-tailed unpaired Student's t test or ANOVA were used to test the difference between groups for continuous variables. For categorical data, Fisher's exact was performed to test the difference between groups. Calculation methods of P values were denoted in the figure legends or bottom of tables. All tests were two-tailed and P values <0.05 were considered significant.

Chapter 3. Results

3.1 ETV6/RUNX1 directly downregulates *MIR181A1*

3.1.1 *ETV6/RUNX1*-associated miRNA expressions in clinical samples

Extensive miRNA profiling was carried out on the diagnostic samples of a cohort of 50 childhood B-ALL patients in the cooperation with National Taiwan University microarray core facility (Figure 2). Ten *ETV6/RUNX1*-positive and forty *ETV6/RUNX1*-negative cases were included in this cohort. The clinical features including gender, onset age, WBC count at first diagnosis, and distribution of risk groups showed no statistical difference between the *ETV6/RUNX1*-positive and *ETV6/RUNX1*-negative samples (Table 3). Because ETV6/RUNX1 retains the DNA-binding ability of RUNX1, the fusion protein acts as a dominant-negative repressor to downregulate RUNX1 target genes. Therefore, a reduction of specific miRNAs in *ETV6/RUNX1*-positive samples compared with *ETV6/RUNX1*-negative samples was evaluated. Seventeen miRNAs (let-7a, let-7b, miR-19a, miR-130b, miR-155, miR-181a-1, miR-181c, miR-181d, miR-195, miR-221, miR-222, miR-30e-3p, miR-342, miR-423, miR-425, miR-660, miR-92) were significantly downregulated in *ETV6/RUNX1*-positive ALL samples (Table 4). According to miRBase database (a searchable database of published miRNA sequences and

annotation, http://mirbase.org/) these miRNAs can be classified into 13 miRNA clusters. In the use of CoreBoost_HM we predicted the transcriptional start site (TSS) of these miRNA clusters, moreover, we identified that 92% of the *ETV6/RUNX1*-associated miRNA clusters (12/13) possess the potential RUNX1 binding sites (TGT/cGGT) in the region between upstream 4 kb and downstream 1 kb of their TSS (Table 5).

Of these miR-181a-1, which is derived from the 3′ arm of its precursor miRNA, hsa-mir-181a-1 (Figure 1), had the most significant *P*-value and showed a remarkable 4-fold reduction (Table 4). The decreased expression of miR-181a-1 in *ETV6/RUNX1*-positive leukemias was validated in another cohort of B-ALL primary blasts analyzed by real-time quantitative RT-PCR. The relative miR-181a-1 levels in *ETV6/RUNX1*-positive and *ETV6/RUNX1*-negative samples of validation set were 0.14 ± 0.08 and 0.06 ± 0.03, respectively (Figure 3A). We also measure miR-181a level, which is derived from the 5′ arm of hsa-mir-181a-1 and was not included in the miRNA expression profile. Expression level of miR-181a was not associated with *ETV6/RUNX1* status (Figure 3B), however, was positive correlated with miR-181a-1 expression level in patient samples (Figure 3C).

3.1.2 siRNA knockdown of ETV6/RUNX1 up-regulates miR-181a-1 expression

Whether ETV6/RUNX1 regulates miR-181a-1 expression was further assessed by

knockdown of *ETV6/RUNX1* and overexpression of ETV6/RUNX1 in cell lines. We conducted siRNA-mediated knockdown of *ETV6/RUNX1* in t(12;21)-positive REH cells, which express the ETV6/RUNX1 fusion protein (Figure 4). A mixture of two *ETV6/RUNX1*-specific siRNAs (siE/R), which target the fusion region of *ETV6/RUNX1*, was used to suppress *ETV6/RUNX1* expression (65). As a transfection control, we used a nonfunctional siRNA (siRNA-S) that had no effect on *ETV6/RUNX1* expression (66). Compared with siRNA-S, both mRNA and protein of *ETV6/RUNX1* were significantly decreased by ~40% and ~35% after knockdown with siE/R without interfering the RUNX1 protein expression (Figure 5). Further examination showed that miR-181a-1 levels increased significantly in REH cells that were treated with siE/R (221 ± 50.8%) but not in those treated with siRNA-S (117 ± 13%) (Figure 6).

3.1.3 Overexpression of ETV6/RUNX1 down-regulates miR-181a-1 expression

Overexpression of ETV6/RUNX1 or RUNX1 protein was carried out by transfection of pCMV6-vectors expressing ETV6/RUNX1 or RUNX1 into HEK-293FT cells in the use of an empty vector as a transfection control (Figure 7). Compared with the empty vector, while expression of RUNX1 protein increased the miR-181a-1 level (114 ± 8.1%), expression of ETV6/RUNX1 protein significantly resulted in mR-181a-1 reduction (75 ± 14.6%) (Figure 8). This overexpression experiment confirmed that

ETV6/RUNX1 may inhibit miR-181a-1 generation.

These studies with cell lines and clinical leukemic specimens indicated that ETV6/RUNX1 negatively regulates miR-181a-1.

3.1.4 ETV6/RUNX1 binds the regulatory region of *MIR181A1*

To reveal the interaction between ETV6/RUNX1 and the regulatory region of *MIR181A1*, we performed ChIP using the ETV6/RUNX1-positive REH cells and a RUNX1-specific antibody. Bioinformatic analyses identified the predicted TSS of *MIR181A1* and a putative RUNX1-binding site with the sequence of TGTGGT located 3.8 kb upstream of the transcription start site (P1 site, Figure 9). Binding of RUNX1 at P1 was demonstrated by specific precipitation of this DNA region, but not at an irrelevant site (P2), with anti-RUNX1 in the ChIP analysis (Figure 10).

3.1.5 Transcriptional co-repressor HDAC3 is recruited to the regulatory region of *MIR181A1*

Previous reports have shown that the transcriptional repressor activity of ETV6/RUNX1 is associated with its aberrant recruitment of the N-CoR/SMRT-HDAC3 complex (33, 34, 68), thus we performed ChIP on REH cells using anti-HDAC3. Our data revealed that HDAC3 also binds at P1 but not the *GAPDH* coding region (Figure

11). Valproic acid (VPA) is an aliphatic compound specifically targeting class I (HDAC1, 2, 3, 8), II (HDAC4, 5, 6, 7, 9, 10) and class IV (HDAC11) HDACs by binding to their zinc-containing catalytic domain.(69) Previous reports have shown that VPA treatment might induce selective proteasomal degradation of HDAC2 (70) as well as disrupt the assembly of the RUNX1/ETO-HDAC1 repressor complex on RUNX1 target gene promoters (71). In our study, we found that VPA treatment also could remove HDAC3 from the P1 RUNX1 binding site and was used as a negative control for HDAC3-ChIP (Figure 11, left).

Taken together, these results supported the idea that ETV6/RUNX1 may directly suppress *MIR181A1* expression.

3.2 *MIR181A1* targets *PLAG1* oncogene in B-ALL

3.2.1. Upregulation of *PLAG1* mRNA in clinical samples

The consequence and mechanism(s) of hsa-mir-181a-1 downregulation in *ETV6/RUNX1*-positive leukemia were further investigated. It has been shown that miR-181a, a mature form of hsa-mir-181a-1 derived from the 5′ arm (Figure 1), functions by targeting several mRNAs (54, 57, 72). To identify new miR-181a target genes, we conducted a database search utilizing TargetScan (http://www.targetscan.org), an online miRNA target prediction interface, and reviewed the literature associated with

oncogene targeting by miR-181a. With miRNA target prediction programs, we identified 1,194 potential miR-181a target genes, including *PLAG1*, which is a transcription factor and proto-oncogene. Ectopic overexpression of PLAG1 is associated with tumorigenesis in humans and is negatively regulated by miR-181a in CLL cells (57, 73). We found that the relative *PLAG1* mRNA levels were higher in our *ETV6/RUNX1*-positive clinical samples (8.47 ± 5.29) than in the *ETV6/RUNX1*-negative samples (1.85 ± 2.71) (Figure 12).

3.2.2. Overexpression of miR-181a inhibits PLAG1 expression in REH cells

This increase in *PLAG1* mRNA may have been caused by downregulation of miR-181a owing to ETV6/RUNX1. To investigate this hypothesis, we overexpressed miR-181a in REH cells, which exhibited a low miR-181a background, and resulted in a ~300 fold increased in miR-181a level (Figure 13). We observed that *PLAG1* mRNA was not affected, while there was a near 50% reduction in PLAG1 protein in cells transfected with miR-181a mimics compared with those transfected with nonspecific miRNA mimics or in untransfected cells (Figure 3B). Our results indicated that miR-181a represses the oncogene— *PLAG1* in B-ALL as in CLL.

Together, these data showed that miR-181a-1 expression was reduced in *ETV6/RUNX1*-positive leukemia; in contrast, the level of its target gene *PLAG1* was

increased, suggesting that ETV6/RUNX1 may upregulate oncogenic *PLAG1* via transcriptional repression of *MIR181A1*.

3.3 *MIR181A1* negatively regulates *ETV6/RUNX1*

3.3.1. Overexpression of miR-181a downregulates ETV6/RUNX1 in REH cells

The presence of *RUNX1* and *ETV6/RUNX1* among the database-predicted target genes implies an unknown mechanism of *RUNX1* and *ETV6/RUNX1* regulation by miR-181a. To investigate this possibility, we overexpressed miR-181a in REH cells by transfection of miRNA mimics (Figure 13), which resulted in a decrease of ETV6/RUNX1 protein by ~23% but not the *ETV6/RUNX1* mRNA level (Figure 15), indicating that miR-181a might negatively regulate *ETV6/RUNX1*.

3.3.2. miR-181a targets the miR-181a recognition sequence located in *RUNX1*-3' UTR

The negative effect of miR181a on *ETV6/RUNX1* expression was further assessed with the luciferase reporter assay, which examined the interaction between miR181a and *ETV6/RUNX1* in the *RUNX1* 3' UTR. We constructed wild-type and mutated fragments containing the last 678 bp of the *RUNX1* 3′ UTR (Figure 16A), which contains an miR-181a recognition sequence, and inserted them immediately

downstream of the luciferase reporter gene (Figure 16B). The miR-181a expression vector or empty vector was co-transfected with the different luciferase 3' UTR constructs into HEK-293FT cells. The results showed that miR-181a downregulated the luciferase reporter gene activity when the luciferase gene was fused with wild-type (NC: 100 ± 9.86%; 181a: 81.74 ± 7.11%) but not mutated *RUNX1* 3' UTR (NC: 100 ± 9.86%; 181a: 94.97 ± 4.26%) (Figure 16C). These experiments demonstrated that miR-181a targets *ETV6/RUNX1*, and they suggested that the fusion gene and miR-181a can regulate each other.

3.4 The cellular effects of *MIR181A1* on B-ALL cells

3.4.1. Ectopic expression of *MIR181A1* impedes REH cell growth

To elucidate the cellular function of *MIR181A1* in B-ALL and how *MIR181A1* participates in the preleukemic events induced by ETV6/RUNX1, REH cells were transduced by a lentiviral vector carrying *MIR181A1* (181A1-LV) to express miR-181a and miR-181a-1 stably and constitutively (Figure 17). We found that ectopic overexpression of *MIR181A1* resulted in growth retardation of the cells, and 181A1-LV-transduced REH cells showed a nearly 40% decrease in both MTT activity (Figure 18A) and cell density after 72 hours of seeding (Figure18B-C).

3.4.2. Apoptotic cells increases in *MIR181A1*-lentivirus transduced REH cells

The growth retardation of 181A1-LV transduced cells might be caused by increased cell death or decreased proliferation. To investigate the possible mechanism, lentivirus-transduced cells were stained with annexin V and PI to detect the apoptotic cells (Figure 19A). Compared with REH cells, the infection control (NC) did not show difference in annexin V–positive (apoptotic) cell population, while 181A1-LV transduction induced an nearly 8% increase in apoptosis (Figure 19B).

3.4.3. The percentage of G0/G1 phase population increases in *MIR181A1*-lentivirus transduced REH cells

We further assessed the proliferation activity by biparametric BrdU/DNA flow cytometry. The total DNA was stained by 7-AAD dye and proliferative cells were labeled by BrdU incorporation and detected by anti-BrdU-FITC. G0/1, S, or G2/M phase was defined by 7-AAD staining intensities, and proliferative cells that were actively synthesizing DNA were characterized by BrdU-positive (Figure 20A). We found that *MIR181A1* expression resulted in slightly decrease in the percentage of S and G2/M phase cells without statistical significance, while the most obvious change was the increase of the proportion of cells in G0/G1 phase (Figure 20B).

3.4.4. Ectopic expression of *MIR181A1* enhances REH cell differentiation

The oncogenic effect of ETV6/RUNX1 has been postulated to operate through impairment of B-cell differentiation in a bone marrow transplantation model, and consequently it results in the accumulation of pro-B-cells (38). We investigated whether the greatly reduced *MIR181A1* expression seen in *ETV6/RUNX1*-positive pro-B ALL blasts plays a role in the ETV6/RUNX1-mediated blockade of B-cell differentiation. The stages of B lymphocyte maturation are characterized by specific expression patterns of immunoglobulins and other membrane proteins. To gain insight into the effect of miR-181a overexpression on REH cell maturation, we stained cells for differentiation markers and found an increase in CD10-negative (Figure 21), CD20-positive (Figure 22), surface IgM-positive (Figure 23), κ-chain-positive (Figure 24), and λ-chain-positive (Figure 25) cell populations in 181A1-LV-transduced cells compared with NC. In normal progression of B cell differentiation, decreased CD10 expression and increased CD20, IgM, κ-chain, and λ-chain expression represent a gradual maturation of B lymphoid cells from pre-B I cells to immature B cells (74), indicating *MIR181A1* expression may induce REH cells toward partial differentiation.

3.4.5. *MIR181A1* expression enhances apoptosis of differentiated cells

Because the decrease in CD10 expression was the most notable change of

181A1-LV-transduced cells, we further stained cells for CD10 and annexin V (Figure 26A). As expected that there was no difference between REH cells and cells transduced with NC. *MIR181A1* transduction induced apoptosis in both CD10-positive and CD10-negative population. Moreover, we found that most apoptotic 181A1-transduced cells were CD10-negative (Figure 26B), implying a loss of survival ability in these differentiated cell.

3.4.6. Ectopic expression of *MIR181A1* induces partial differentiation of *ETV6/RUNX1*-positive primary ALL blasts

Loss of the marker CD10 and a gain of CD20 have been associated with differentiation of normal B-cell precursors from HSCs to naive mature B lymphocytes in the bone marrow (75). The infection of primary blasts isolated from the bone marrow of B-ALL patients with a lentiviral vector expressing miR-181a increased the level of miR-181a/miR-181a-1 by an average of 2.5-fold (1.5 to 3-fold)/ 3-fold (1.3 to 5.2-fold) in three *ETV6/RUNX1*-positive samples compared with the controls (Figure 27). We have also confirmed that the *ETV6/RUNX1*-positive primary ALL blasts survived after lentivirus infection and puromycin selection were *ETV6/RUNX1*-positive (Figure 28). We observed that lentiviral infection may alter certain properties of primary ALL blasts, thus we mainly compared the NC and 181A1-LV transduced cells. This induction

altered the lymphocytic differentiation as shown by the decrease in the high expression of CD10 in cells in two of three *ETV6/RUNX1*-positive samples, though the intensity of CD20 were not changed in all three samples (Figure 29-31). We also explore the effect of *MIR181A1* transduction in one *ETV6/RUNX1*-negative sample, but no significant change in surface CD10 and CD20 expression was found (Figure 32). We were also determine the growth rate of lentivirus-infected primary ALL blasts, however, the patient cells seemed just survived in our culture medium rather than proliferation and the growth activity was gradually lost after thawing out (Figure 33), which may cause the low induction of miR-181a expression and reduce the influence of miR-181a.

Taken together, our data suggests that the level of miR-181a expression may be important for the perturbation of the lymphocytic differentiation program in ETV6/RUNX1-expressing ALL.

Chapter 4. Discussion

Despite having an extremely short sequence, miRNAs have diverse functions via targeting of multiple genes simultaneously. They have been implicated in virtually all aspects of biology, including cell proliferation, cell differentiation, cell cycle, apoptosis, developmental timing, metabolism, and hematopoiesis. They participate in endogenous transcriptional networks that control early development, lineage decision, and differentiation in many cell types, including hematopoietic cells (76).

4.1 Selection of *Mir181A1* to be investigated

Because miRNAs are critical to hematopoiesis and their dysregulation is a ubiquitous feature of leukemia, we attempted to understand the driving force of this abnormal phenomenon and the consequence of aberrant miRNA expression. By applying miRNA profiling to 50 B-ALL patients, we determined the gene expression signatures of specific ALL subtypes. Owing to *ETV6/RUNX1* is the most frequent gene fusion present in ALL and it acts as an aberrant transcription factor via its DNA-binding domain to directly dysregulate RUNX1 targets, we presumed that ETV6/RUNX1 may occupy the RUNX1-binding motif located in the regulatory regions of certain miRNAs and disrupt their normal functions. The miRNA expression profile showed that most miRNAs are downregulated in *ETV6/RUNX1*-positive samples, indicating that

ETV6/RUNX1 perturbs the activities of miRNAs primarily through gene repression. We identified miR-181a-1 as the most differentially underexpressed miRNA in patients carrying t(12;21). This is consistent with the expression profile of another cohort; Schotte et al. measured 397 miRNAs in 81 pediatric ALL cases and also demonstrated that miR-181a-1 expression is 5-fold lower in patients with t(12;21) than in patients with other ALL subtypes (77). It was performed on the same technology platform, meaning this result is replicable using the same platform even with different populations of patients. A previous study has reported that miR-494 and miR-320a levels are regulated by ETV6/RUNX1, as demonstrated by their expression profiles in shRNA-knockdown REH cells (61). However, we did not find a decrease of these two miRNAs in *ETV6/RUNX1*-positive samples in our data; this may be due to differences in the experimental strategies.

4.2 The relationship between *ETV6/RUNX1* and *MIR181A1*

To address how ETV6/RUNX1 regulates miR-181a-1, we over-expressed ETV6/RUNX1 in HEK-293FT cells, performed siRNA-mediated knockdown of the *ETV6/RUNX1* fusion gene and the ChIP assay in an ETV6/RUNX1-expressing leukemic cell line. Our data revealed a downregulation of miR-181a-1 in ETV6/RUNX1-overexpressed HEK-293FT cells and an upregulation of miR-181a-1 in

ETV6/RUNX1-knockdown cells, and we further demonstrated a direct ETV6/RUNX1 binding to the regulatory region of *MIR181A1*. Evidence shows that aberrant recruitment of chromatin repressors such as HDAC3 and N-CoR/SMRT—via interaction with the ETV6 moiety of ETV6/RUNX1—correlates with the oncogenic activities of ETV6/RUNX1 (33, 34). We also found that HDAC3 was recruited to the regulatory region of *MIR181A1*, whereas this binding disappeared after treatment with HDAC inhibitor. Our results suggest that ETV6/RUNX1 acts as a negative regulator to inhibit *MIR181A1* expression directly.

The miR-181 family is highly conserved and comprises six miRNAs transcribed from three separate gene loci and organized into three clusters including miR-181a/b-1, miR-181a/b-2, and miR-181c/d. The finding that both miR-181a-1 and miR-181c/d are significantly downregulated in ETV6/RUNX1 ALL (Table 4) and that all members of the miR-181 family share the same seed sequence at their 5′ arms and in targets led us to investigate the downstream genes regulated by miR-181a. We confirmed that *PLAG1* is under the control of miR-181a in REH cells and primary blasts, just as *PLAG1* is reported to be oncogenic and controlled by deregulated miR-181a in CLL (78). In addition, not only was miR-181a suppressed by ETV6/RUNX1, but feedback inhibition of miR-181a on ETV6/RUNX1 was observed in the cell line experiments, though the suppression of ETV6/RUNX1 by miR-181a was rather mild. Our miRNA expression

profile has demonstrated that not only miR-181a-1, but also other members of miR-181 family were down-regulated. These family members have the identical seed region therefore it is possible that they target the ETV6/RUNX1 together which may exert more powerful effect. Together, our results suggest that miR-181a-1 and ETV6/RUNX1 can regulate each other.

4.3 A double negative loop comprising *ETV6/RUNX1* and *MIR181A1*

In fact, such a regulatory network between transcription factors and miRNAs has been described before; for example, regulatory circuitry comprising miR-223 and transcription factors NFI-A and C/EBPα has been shown to sustain the level of miR-223, which may be important in granulopoiesis (79). Moreover, recently a 'mutual negative feedback loop' involving MYC and miR-548m was described in non-Hodgkin B-cell lymphomas, in that this regulatory loop is important for sustaining a high level of MYC and low level of miR-548m during lymphomagenesis and drug resistance (80). According to previous similar findings and our current data, we propose a we propose a new mechanism of ETV6/RUNX1 action: a double negative loop in which ETV6/RUNX1 can bind to the regulatory region of *MIR181A1* to keep hsa-mir-181a-1 expression low, which consequently reduces the miR-181a-mediated translational repression of ETV6/RUNX1. By doing so, ETV6/RUNX1 can enhance its own

oncogenic potential (Figure 34).

4.4 The effects of *MIR181A1* on B-ALL cells

Differentiation arrest is a hallmark of acute leukemia. Indeed, ETV6/RUNX1 can generate transformed HSCs and sustain the preleukemic clone (37, 38). *ETV6/RUNX1*-positive B-ALL represents the clonal expansion of hematopoietic precursors blocked at the pre-B cell stage of lymphoid differentiation. The transduction of miR-181a into ETV6/RUNX1-expressing REH cells resulted in many phenotypic alterations, including a retarded growth rate, an increase in apoptosis and G0/G1 population, and a reduction in CD10 marker expression at the cell surface. Decreased CD10 expression implies the differentiation of REH cells from pre B I to pre B II stage, and a small proportion of cells even expressed CD20, IgM, κ-chain, and λ-chain, which represent an immunophenotype of immature B cells (74, 75). Furthermore, ectopic expression of miR-181a in primary leukemia cells carrying t(12;21) also exhibited a trend in decreased CD10 expression, though the effect of miR-181a was not consistent in all clinical samples. We speculate that this inconsistence may be caused by the sample variations in non-homogenous leukemic cell population, survival rate after thawing out, and efficiency of lentiviral transduction. Taken together, our data implies a previously undiscovered role for miR-181a in B-lymphoid maturation.

The phenotypes of VPA-treated REH cells including moderate increase of apoptosis and G0/G1 population, and differentiation antigen shift (81) are nearly identical to those we observed that were induced by increased miR-181a level, and those changes that resulted from HDAC inhibition may be partially explained by a relief from *MIR181A1* repression mediated by ETV6/RUNX1 through recruitment of HDAC3.

Previous studies have demonstrated the impact of miR-181 on the differentiation of both the myeloid and lymphoid lineages (82-84). The expression of miR-181 family members gradually decreases during granulocytic and macrophage-like differentiation, and evidence shows that miR-181 is a negative regulator of this process (82, 83). In murine bone marrow, the miR-181 family is preferentially expressed in B-lymphoid cells, and ectopic expression of miR-181 in murine hematopoietic stem-progenitor cells leads to an increase of B-lymphopoiesis both *in vivo* and *in vitro* (84). Among the miR-181 family members, miR-181a is the most enriched throughout the murine B-cell developmental stages and gradually increases from the pro-B cell stage and reaches highest level at the immature B-cell stage in bone marrow (85). In the development program of human blood cells, miR-181a expression level is high in hematopoietic stem-progenitor cells but lower in mature B cells (83, 86). However, detail analysis of miR-181a expression in each differentiation stage of human B cells is limited.

In this study, we demonstrate a new regulatory network comprising *ETV6/RUNX1* and *MIR181A1* in which *ETV6/RUNX1* and *MIR181A1* can regulate each other. We further demonstrate that ectopic expression of miR-181a partially reversed the blockade of B cell differentiation in ETV6/RUNX1-expressing leukemic cells. Our results suggest a novel mechanism by which ETV6/RUNX1 might exert its preleukemic effect by inhibiting its negative regulator, *MIR181A1*, to perturb the progression of early-stage development of the B-cell lineage.

Chapter 5. Conclusion and Prospective

Since *MIR181A1* expression was suppressed in *ETV6/RUNX1*-positive ALL cells, which were stalled at the pre-B stage and could be overcome by recovery of miR-181a expression, we propose that miR-181a may have a role in promoting pre-B cell differentiation. However, it needs more efforts to elucidate the function of miR-181a in normal B cell development. *In vivo* strategies such as using B lineage-specific knockout mice, or a xenograft mouse model using human HSCs with induction of miR-181a expression at specific time point will be required.

In addition, the mature products miR-181a, miR-181b, miR-181c or miR-181d are thought to have regulatory roles at post-transcriptional level through complementarity to target mRNAs. While these mature miRNAs have similar predicted target mRNA and most of them are downregulated in ETV6/RUNX1 ALL, whether the members of miR-181 family other than miR-181a also involved in such a double negative loop would need further investigation.

In conclusion, our study enhances our understanding in the interaction of ETV6/RUNX1 and miRNAs, increases the knowledge of *MIR181A1* function in human B-cell development, helps to unravel one of the molecular mechanism underlying ETV6/RUNX1-mediated attenuation of B-cell differentiation, and offers the opportunity

to identify new targets for development of therapeutic approaches to *ETV6/RUNX1*-positive leukemia.

Bibliography

1. Pui CH, Carroll WL, Meshinchi S, Arceci RJ. Biology, risk stratification, and therapy of pediatric acute leukemias: an update. *Journal of clinical oncology : official journal of the American Society of Clinical Oncology* 2011 Feb 10; **29**(5)**:** 551-565.

2. Mullighan CG. Molecular genetics of B-precursor acute lymphoblastic leukemia. *The Journal of clinical investigation* 2012 Oct; **122**(10)**:** 3407-3415.

3. Lo Nigro L. Biology of childhood acute lymphoblastic leukemia. *Journal of pediatric hematology/oncology* 2013 May; **35**(4)**:** 245-252.

4. Pui CH, Robison LL, Look AT. Acute lymphoblastic leukaemia. *Lancet* 2008 Mar 22; **371**(9617)**:** 1030-1043.

5. Ghazavi F, Lammens T, Van Roy N, Poppe B, Speleman F, Benoit Y, *et al.* Molecular basis and clinical significance of genetic aberrations in B-cell precursor acute lymphoblastic leukemia. *Experimental hematology* 2015 Aug; **43**(8)**:** 640-653.

6. Huettner CS, Zhang P, Van Etten RA, Tenen DG. Reversibility of acute B-cell leukaemia induced by BCR-ABL1. *Nature genetics* 2000 Jan; **24**(1)**:** 57-60.

7. van der Weyden L, Giotopoulos G, Rust AG, Matheson LS, van Delft FW, Kong J, *et al.* Modeling the evolution of ETV6-RUNX1-induced B-cell precursor acute lymphoblastic leukemia in mice. *Blood* 2011 Jul 28; **118**(4)**:** 1041-1051.

8. Roberts KG, Mullighan CG. Genomics in acute lymphoblastic leukaemia: insights and treatment implications. *Nature reviews Clinical oncology* 2015 Jun; **12**(6)**:** 344-357.

9. Mullighan CG, Su X, Zhang J, Radtke I, Phillips LA, Miller CB, *et al.* Deletion of IKZF1 and prognosis in acute lymphoblastic leukemia. *The New England journal of medicine* 2009 Jan 29; **360**(5)**:** 470-480.

10. Den Boer ML, van Slegtenhorst M, De Menezes RX, Cheok MH, Buijs-Gladdines JG, Peters ST, *et al.* A subtype of childhood acute lymphoblastic leukaemia with poor treatment outcome: a genome-wide classification study. *The Lancet Oncology* 2009 Feb; **10**(2)**:** 125-134.

11. Moorman AV, Richards SM, Robinson HM, Strefford JC, Gibson BE, Kinsey SE, *et al.* Prognosis of children with acute lymphoblastic leukemia (ALL) and intrachromosomal amplification of chromosome 21 (iAMP21). *Blood* 2007 Mar 15; **109**(6)**:** 2327-2330.

12. Harrison CJ, Moorman AV, Schwab C, Carroll AJ, Raetz EA, Devidas M, *et al.* An international study of intrachromosomal amplification of chromosome 21 (iAMP21): cytogenetic characterization and outcome. *Leukemia : official journal of the Leukemia Society of America, Leukemia Research Fund, UK* 2014 May; **28**(5)**:** 1015-1021.

13. Mullighan CG, Collins-Underwood JR, Phillips LA, Loudin MG, Liu W, Zhang J, *et al.* Rearrangement of CRLF2 in B-progenitor- and Down syndrome-associated acute lymphoblastic leukemia. *Nature genetics* 2009 Nov; **41**(11)**:** 1243-1246.

14. Clappier E, Auclerc MF, Rapion J, Bakkus M, Caye A, Khemiri A, *et al.* An intragenic ERG deletion is a marker of an oncogenic subtype of B-cell precursor acute lymphoblastic leukemia with a favorable outcome despite frequent IKZF1 deletions. *Leukemia : official journal of the Leukemia Society of America, Leukemia Research Fund, UK* 2014 Jan; **28**(1)**:** 70-77.

15. Mullighan CG, Miller CB, Radtke I, Phillips LA, Dalton J, Ma J, *et al.* BCR-ABL1 lymphoblastic leukaemia is characterized by the deletion of Ikaros. *Nature* 2008 May 1; **453**(7191)**:** 110-114.

16. Golub TR, Barker GF, Bohlander SK, Hiebert SW, Ward DC, Bray-Ward P, *et al.* Fusion of the TEL gene on 12p13 to the AML1 gene on 21q22 in acute lymphoblastic leukemia. *Proceedings of the National Academy of Sciences of the United States of America* 1995 May 23; **92**(11)**:** 4917-4921.

17. Romana SP, Mauchauffe M, Le Coniat M, Chumakov I, Le Paslier D, Berger R, *et al.* The t(12;21) of acute lymphoblastic leukemia results in a tel-AML1 gene

fusion. *Blood* 1995 Jun 15; **85**(12)**:** 3662-3670.

18. Zelent A, Greaves M, Enver T. Role of the TEL-AML1 fusion gene in the molecular pathogenesis of childhood acute lymphoblastic leukaemia. *Oncogene* 2004 May 24; **23**(24)**:** 4275-4283.

19. Shurtleff SA, Buijs A, Behm FG, Rubnitz JE, Raimondi SC, Hancock ML, *et al.* TEL/AML1 fusion resulting from a cryptic t(12;21) is the most common genetic lesion in pediatric ALL and defines a subgroup of patients with an excellent prognosis. *Leukemia : official journal of the Leukemia Society of America, Leukemia Research Fund, UK* 1995 Dec; **9**(12)**:** 1985-1989.

20. Romana SP, Poirel H, Leconiat M, Flexor MA, Mauchauffe M, Jonveaux P, *et al.* High frequency of t(12;21) in childhood B-lineage acute lymphoblastic leukemia. *Blood* 1995 Dec 1; **86**(11)**:** 4263-4269.

21. Yang YL, Lin SR, Chen JS, Hsiao CC, Lin KH, Sheen JM, *et al.* Multiplex reverse transcription-polymerase chain reaction as diagnostic molecular screening of 4 common fusion chimeric genes in Taiwanese children with acute lymphoblastic leukemia. *Journal of pediatric hematology/oncology* 2010 Nov; **32**(8)**:** e323-330.

22. Gabert J, Beillard E, van der Velden VHJ, Bi W, Grimwade D, Pallisgaard N, *et al.* Standardization and quality control studies of 'real-time' quantitative reverse transcriptase polymerase chain reaction of fusion gene transcripts for residual disease detection in leukemia - A Europe Against Cancer Program. *Leukemia : official journal of the Leukemia Society of America, Leukemia Research Fund, UK* 2003 Dec; **17**(12)**:** 2318-2357.

23. Baens M, Peeters P, Guo C, Aerssens J, Marynen P. Genomic organization of TEL: the human ETS-variant gene 6. *Genome research* 1996 May; **6**(5)**:** 404-413.

24. Levanon D, Glusman G, Bangsow T, Ben-Asher E, Male DA, Avidan N, *et al.* Architecture and anatomy of the genomic locus encoding the human leukemia-associated transcription factor RUNX1/AML1. *Gene* 2001 Jan 10; **262**(1-2)**:** 23-33.

25. Mukouyama Y, Chiba N, Hara T, Okada H, Ito Y, Kanamaru R, *et al.* The AML1 transcription factor functions to develop and maintain hematogenic precursor cells in the embryonic aorta-gonad-mesonephros region. *Developmental biology* 2000 Apr 1; **220**(1)**:** 27-36.

26. Yokomizo T, Ogawa M, Osato M, Kanno T, Yoshida H, Fujimoto T, *et al.* Requirement of Runx1/AML1/PEBP2alphaB for the generation of haematopoietic cells from endothelial cells. *Genes to cells : devoted to molecular & cellular mechanisms* 2001 Jan; **6**(1)**:** 13-23.

27. Wang LC, Swat W, Fujiwara Y, Davidson L, Visvader J, Kuo F, *et al.* The TEL/ETV6 gene is required specifically for hematopoiesis in the bone marrow. *Genes & development* 1998 Aug 1; **12**(15)**:** 2392-2402.

28. Look AT. Oncogenic transcription factors in the human acute leukemias. *Science* 1997 Nov 7; **278**(5340)**:** 1059-1064.

29. Bohlander SK. ETV6: a versatile player in leukemogenesis. *Seminars in cancer biology* 2005 Jun; **15**(3)**:** 162-174.

30. van Dongen JJ, Macintyre EA, Gabert JA, Delabesse E, Rossi V, Saglio G, *et al.* Standardized RT-PCR analysis of fusion gene transcripts from chromosome aberrations in acute leukemia for detection of minimal residual disease. Report of the BIOMED-1 Concerted Action: investigation of minimal residual disease in acute leukemia. *Leukemia : official journal of the Leukemia Society of America, Leukemia Research Fund, UK* 1999 Dec; **13**(12)**:** 1901-1928.

31. Morrow M, Samanta A, Kioussis D, Brady HJ, Williams O. TEL-AML1 preleukemic activity requires the DNA binding domain of AML1 and the dimerization and corepressor binding domains of TEL. *Oncogene* 2007 Jun 28; **26**(30)**:** 4404-4414.

32. Gunji H, Waga K, Nakamura F, Maki K, Sasaki K, Nakamura Y, *et al.* TEL/AML1 shows dominant-negative effects over TEL as well as AML1. *Biochemical and biophysical research communications* 2004 Sep 17; **322**(2)**:** 623-630.

33. Guidez F, Petrie K, Ford AM, Lu H, Bennett CA, MacGregor A, *et al.*

Recruitment of the nuclear receptor corepressor N-CoR by the TEL moiety of the childhood leukemia-associated TEL-AML1 oncoprotein. *Blood* 2000 Oct 1; **96**(7)**:** 2557-2561.

34. Wang L, Hiebert SW. TEL contacts multiple co-repressors and specifically associates with histone deacetylase-3. *Oncogene* 2001 Jun 21; **20**(28)**:** 3716-3725.

35. Greaves MF, Maia AT, Wiemels JL, Ford AM. Leukemia in twins: lessons in natural history. *Blood* 2003 Oct 1; **102**(7)**:** 2321-2333.

36. Mori H, Colman SM, Xiao Z, Ford AM, Healy LE, Donaldson C, *et al.* Chromosome translocations and covert leukemic clones are generated during normal fetal development. *Proceedings of the National Academy of Sciences of the United States of America* 2002 Jun 11; **99**(12)**:** 8242-8247.

37. Tsuzuki S, Seto M, Greaves M, Enver T. Modeling first-hit functions of the t(12;21) TEL-AML1 translocation in mice. *Proceedings of the National Academy of Sciences of the United States of America* 2004 Jun 1; **101**(22)**:** 8443-8448.

38. Fischer M, Schwieger M, Horn S, Niebuhr B, Ford A, Roscher S, *et al.* Defining the oncogenic function of the TEL/AML1 (ETV6/RUNX1) fusion protein in a mouse model. *Oncogene* 2005 Nov 17; **24**(51)**:** 7579-7591.

39. Lee RC, Feinbaum RL, Ambros V. The C. elegans heterochronic gene lin-4 encodes small RNAs with antisense complementarity to lin-14. *Cell* 1993 Dec 3; **75**(5)**:** 843-854.

40. Winter J, Jung S, Keller S, Gregory RI, Diederichs S. Many roads to maturity: microRNA biogenesis pathways and their regulation. *Nature cell biology* 2009 Mar; **11**(3)**:** 228-234.

41. Bartel DP. MicroRNAs: genomics, biogenesis, mechanism, and function. *Cell* 2004 Jan 23; **116**(2)**:** 281-297.

42. Shivdasani RA. MicroRNAs: regulators of gene expression and cell differentiation. *Blood* 2006 Dec 1; **108**(12)**:** 3646-3653.

43. Hausser J, Syed AP, Bilen B, Zavolan M. Analysis of CDS-located miRNA target sites suggests that they can effectively inhibit translation. *Genome research* 2013 Apr; **23**(4)**:** 604-615.

44. Brummer A, Hausser J. MicroRNA binding sites in the coding region of mRNAs: extending the repertoire of post-transcriptional gene regulation. *BioEssays : news and reviews in molecular, cellular and developmental biology* 2014 Jun; **36**(6)**:** 617-626.

45. Vasilatou D, Papageorgiou S, Pappa V, Papageorgiou E, Dervenoulas J. The role of microRNAs in normal and malignant hematopoiesis. *European journal of haematology* 2010 Jan 1; **84**(1)**:** 1-16.

46. Felli N, Fontana L, Pelosi E, Botta R, Bonci D, Facchiano F, *et al.* MicroRNAs 221 and 222 inhibit normal erythropoiesis and erythroleukemic cell growth via kit receptor down-modulation. *Proceedings of the National Academy of Sciences of the United States of America* 2005 Dec 13; **102**(50)**:** 18081-18086.

47. Gilicze AB, Wiener Z, Toth S, Buzas E, Pallinger E, Falcone FH, *et al.* Myeloid-derived microRNAs, miR-223, miR27a, and miR-652, are dominant players in myeloid regulation. *BioMed research international* 2014; **2014:** 870267.

48. Neilson JR, Zheng GX, Burge CB, Sharp PA. Dynamic regulation of miRNA expression in ordered stages of cellular development. *Genes & development* 2007 Mar 1; **21**(5)**:** 578-589.

49. Xiao C, Calado DP, Galler G, Thai TH, Patterson HC, Wang J, *et al.* MiR-150 controls B cell differentiation by targeting the transcription factor c-Myb. *Cell* 2007 Oct 5; **131**(1)**:** 146-159.

50. Zhou B, Wang S, Mayr C, Bartel DP, Lodish HF. miR-150, a microRNA expressed in mature B and T cells, blocks early B cell development when expressed prematurely. *Proceedings of the National Academy of Sciences of the United States of America* 2007 Apr 24; **104**(17)**:** 7080-7085.

51. Fazi F, Racanicchi S, Zardo G, Starnes LM, Mancini M, Travaglini L, *et al.*

Epigenetic silencing of the myelopoiesis regulator microRNA-223 by the AML1/ETO oncoprotein. *Cancer cell* 2007 Nov; **12**(5)**:** 457-466.

52. O'Connell RM, Rao DS, Chaudhuri AA, Baltimore D. Physiological and pathological roles for microRNAs in the immune system. *Nature reviews Immunology* 2010 Feb; **10**(2)**:** 111-122.

53. Shi L, Cheng Z, Zhang J, Li R, Zhao P, Fu Z, *et al.* hsa-mir-181a and hsa-mir-181b function as tumor suppressors in human glioma cells. *Brain research* 2008 Oct 21; **1236:** 185-193.

54. Ouyang YB, Lu Y, Yue S, Giffard RG. miR-181 targets multiple Bcl-2 family members and influences apoptosis and mitochondrial function in astrocytes. *Mitochondrion* 2012 Mar; **12**(2)**:** 213-219.

55. Gao W, Yu Y, Cao H, Shen H, Li X, Pan S, *et al.* Deregulated expression of miR-21, miR-143 and miR-181a in non small cell lung cancer is related to clinicopathologic characteristics or patient prognosis. *Biomedicine & pharmacotherapy = Biomedecine & pharmacotherapie* 2010 Jul; **64**(6)**:** 399-408.

56. Visone R, Rassenti LZ, Veronese A, Taccioli C, Costinean S, Aguda BD, *et al.* Karyotype-specific microRNA signature in chronic lymphocytic leukemia. *Blood* 2009 Oct 29; **114**(18)**:** 3872-3879.

57. Pallasch CP, Patz M, Park YJ, Hagist S, Eggle D, Claus R, *et al.* miRNA deregulation by epigenetic silencing disrupts suppression of the oncogene PLAG1 in chronic lymphocytic leukemia. *Blood* 2009 Oct 8; **114**(15)**:** 3255-3264.

58. Bai H, Cao Z, Deng C, Zhou L, Wang C. miR-181a sensitizes resistant leukaemia HL-60/Ara-C cells to Ara-C by inducing apoptosis. *Journal of cancer research and clinical oncology* 2012 Apr; **138**(4)**:** 595-602.

59. Chen G, Zhu W, Shi D, Lv L, Zhang C, Liu P, *et al.* MicroRNA-181a sensitizes human malignant glioma U87MG cells to radiation by targeting Bcl-2. *Oncology reports* 2010 Apr; **23**(4)**:** 997-1003.

60. Gefen N, Binder V, Zaliova M, Linka Y, Morrow M, Novosel A, *et al.* Hsa-mir-125b-2 is highly expressed in childhood ETV6/RUNX1 (TEL/AML1) leukemias and confers survival advantage to growth inhibitory signals independent of p53. *Leukemia : official journal of the Leukemia Society of America, Leukemia Research Fund, UK* 2010 Jan; **24**(1)**:** 89-96.

61. Diakos C, Zhong S, Xiao Y, Zhou M, Vasconcelos GM, Krapf G, *et al.* TEL-AML1 regulation of survivin and apoptosis via miRNA-494 and miRNA-320a. *Blood* 2010 Dec 2; **116**(23)**:** 4885-4893.

62. Torrano V, Procter J, Cardus P, Greaves M, Ford AM. ETV6-RUNX1 promotes survival of early B lineage progenitor cells via a dysregulated erythropoietin receptor. *Blood* 2011 Nov 3; **118**(18)**:** 4910-4918.

63. Kaindl U, Morak M, Portsmouth C, Mecklenbrauker A, Kauer M, Zeginigg M, *et al.* Blocking ETV6/RUNX1-induced MDM2 overexpression by Nutlin-3 reactivates p53 signaling in childhood leukemia. *Leukemia : official journal of the Leukemia Society of America, Leukemia Research Fund, UK* 2014 Mar; **28**(3)**:** 600-608.

64. Wang X, Xuan Z, Zhao X, Li Y, Zhang MQ. High-resolution human core-promoter prediction with CoreBoost_HM. *Genome research* 2009 Feb; **19**(2)**:** 266-275.

65. Zaliova M, Madzo J, Cario G, Trka J. Revealing the role of TEL/AML1 for leukemic cell survival by RNAi-mediated silencing. *Leukemia : official journal of the Leukemia Society of America, Leukemia Research Fund, UK* 2011 Feb; **25**(2)**:** 313-320.

66. Diakos C, Krapf G, Gerner C, Inthal A, Lemberger C, Ban J, *et al.* RNAi-mediated silencing of TEL/AML1 reveals a heat-shock protein- and survivin-dependent mechanism for survival. *Blood* 2007 Mar 15; **109**(6)**:** 2607-2610.

67. Benjamini YaH, Yosef. Controlling the false discovery rate: a practical and powerful approach to multiple testing. *Journal of the Royal Statistical Society, Series B* 1995; **57**(1)**:** 289-300.

68. Karagianni P, Wong J. HDAC3: taking the SMRT-N-CoRrect road to repression. *Oncogene* 2007 Aug 13; **26**(37)**:** 5439-5449.

69. Moreno DA, Scrideli CA, Cortez MA, de Paula Queiroz R, Valera ET, da Silva Silveira V, *et al.* Differential expression of HDAC3, HDAC7 and HDAC9 is associated with prognosis and survival in childhood acute lymphoblastic leukaemia. *British journal of haematology* 2010 Sep; **150**(6)**:** 665-673.

70. Kramer OH, Zhu P, Ostendorff HP, Golebiewski M, Tiefenbach J, Peters MA, *et al.* The histone deacetylase inhibitor valproic acid selectively induces proteasomal degradation of HDAC2. *The EMBO journal* 2003 Jul 1; **22**(13)**:** 3411-3420.

71. Liu S, Klisovic RB, Vukosavljevic T, Yu J, Paschka P, Huynh L, *et al.* Targeting AML1/ETO-histone deacetylase repressor complex: a novel mechanism for valproic acid-mediated gene expression and cellular differentiation in AML1/ETO-positive acute myeloid leukemia cells. *The Journal of pharmacology and experimental therapeutics* 2007 Jun; **321**(3)**:** 953-960.

72. Li X, Zhang J, Gao L, McClellan S, Finan MA, Butler TW, *et al.* MiR-181 mediates cell differentiation by interrupting the Lin28 and let-7 feedback circuit. *Cell death and differentiation* 2012 Mar; **19**(3)**:** 378-386.

73. Van Dyck F, Declercq J, Braem CV, Van de Ven WJ. PLAG1, the prototype of the PLAG gene family: versatility in tumour development (review). *International journal of oncology* 2007 Apr; **30**(4)**:** 765-774.

74. Mesquita Junior D, Araujo JA, Catelan TT, Souza AW, Cruvinel Wde M, Andrade LE, *et al.* Immune system - part II: basis of the immunological response mediated by T and B lymphocytes. *Revista brasileira de reumatologia* 2010 Sep-Oct; **50**(5)**:** 552-580.

75. Perez-Andres M, Paiva B, Nieto WG, Caraux A, Schmitz A, Almeida J, *et al.* Human peripheral blood B-cell compartments: a crossroad in B-cell traffic. *Cytometry Part B, Clinical cytometry* 2010; **78 Suppl 1:** S47-60.

76. Fazi F, Nervi C. MicroRNA: basic mechanisms and transcriptional regulatory

networks for cell fate determination. *Cardiovascular research* 2008 Sep 1; **79**(4)**:** 553-561.

77. Schotte D, De Menezes RX, Akbari Moqadam F, Khankahdani LM, Lange-Turenhout E, Chen C, *et al.* MicroRNA characterize genetic diversity and drug resistance in pediatric acute lymphoblastic leukemia. *Haematologica* 2011 May; **96**(5)**:** 703-711.

78. Patz M, Pallasch CP, Wendtner CM. Critical role of microRNAs in chronic lymphocytic leukemia: overexpression of the oncogene PLAG1 by deregulated miRNAs. *Leukemia & lymphoma* 2010 Aug; **51**(8)**:** 1379-1381.

79. Fazi F, Rosa A, Fatica A, Gelmetti V, De Marchis ML, Nervi C, *et al.* A minicircuitry comprised of microRNA-223 and transcription factors NFI-A and C/EBPalpha regulates human granulopoiesis. *Cell* 2005 Dec 2; **123**(5)**:** 819-831.

80. Lwin T, Zhao X, Cheng F, Zhang X, Huang A, Shah B, *et al.* A microenvironment-mediated c-Myc/miR-548m/HDAC6 amplification loop in non-Hodgkin B cell lymphomas. *The Journal of clinical investigation* 2013 Nov; **123**(11)**:** 4612-4626.

81. Starkova J, Madzo J, Cario G, Kalina T, Ford A, Zaliova M, *et al.* The identification of (ETV6)/RUNX1-regulated genes in lymphopoiesis using histone deacetylase inhibitors in ETV6/RUNX1-positive lymphoid leukemic cells. *Clinical cancer research : an official journal of the American Association for Cancer Research* 2007 Mar 15; **13**(6)**:** 1726-1735.

82. Wang X, Gocek E, Liu CG, Studzinski GP. MicroRNAs181 regulate the expression of p27Kip1 in human myeloid leukemia cells induced to differentiate by 1,25-dihydroxyvitamin D3. *Cell Cycle* 2009 Mar 1; **8**(5)**:** 736-741.

83. Georgantas RW, 3rd, Hildreth R, Morisot S, Alder J, Liu CG, Heimfeld S, *et al.* CD34+ hematopoietic stem-progenitor cell microRNA expression and function: a circuit diagram of differentiation control. *Proceedings of the National Academy of Sciences of the United States of America* 2007 Feb 20; **104**(8)**:** 2750-2755.

84. Chen CZ, Li L, Lodish HF, Bartel DP. MicroRNAs modulate hematopoietic

lineage differentiation. *Science* 2004 Jan 2; **303**(5654)**:** 83-86.

85. Spierings DC, McGoldrick D, Hamilton-Easton AM, Neale G, Murchison EP, Hannon GJ, *et al.* Ordered progression of stage-specific miRNA profiles in the mouse B2 B-cell lineage. *Blood* 2011 May 19; **117**(20)**:** 5340-5349.

86. Landgraf P, Rusu M, Sheridan R, Sewer A, Iovino N, Aravin A, *et al.* A mammalian microRNA expression atlas based on small RNA library sequencing. *Cell* 2007 Jun 29; **129**(7)**:** 1401-1414.

Figures

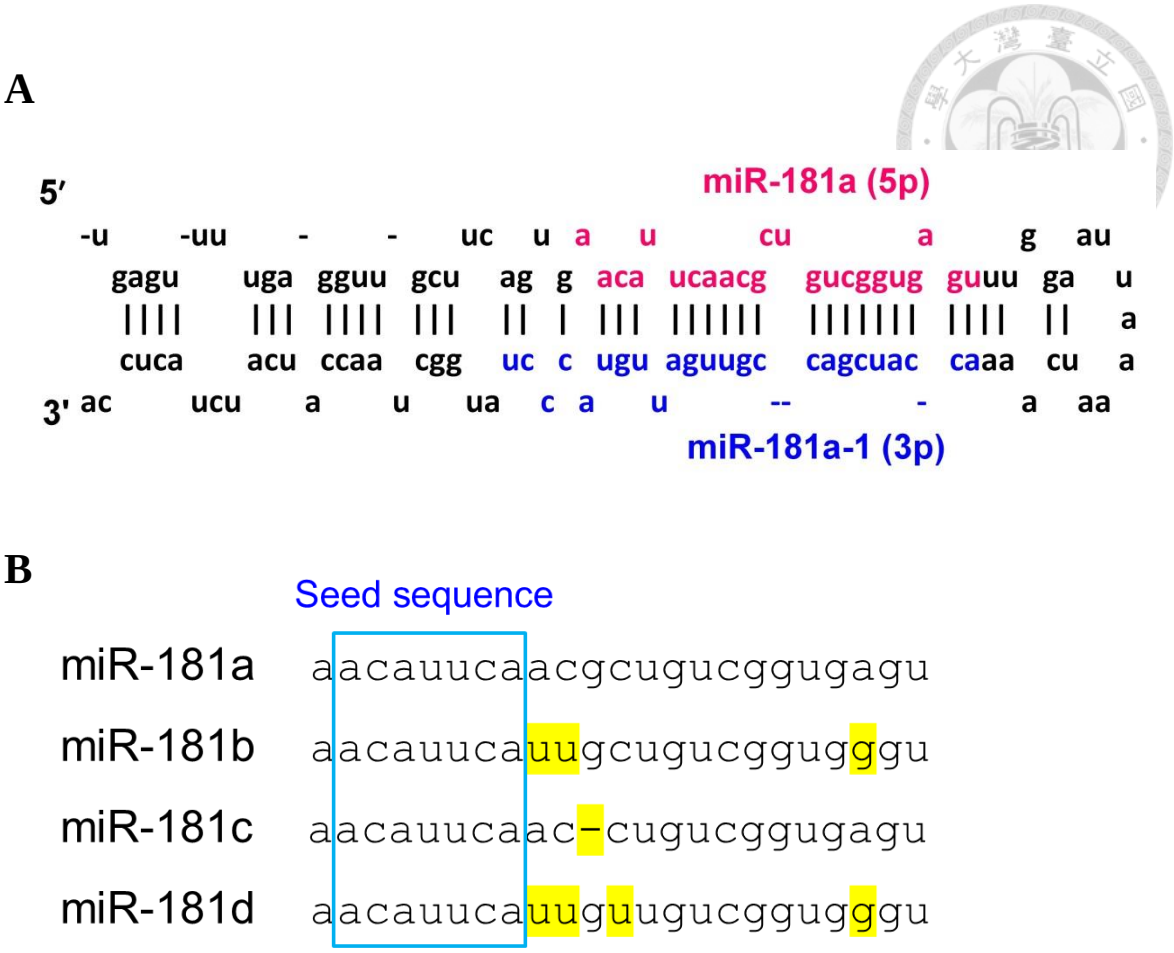

Figure 1. hsa-mir-181a-1 and 5p sequence of miR-181 family.

(A) Stem-loop sequence of hsa-mir-181a-1. Human precursor mir-181a-1 is in length with 110 bp arisen from *MIR181A1* primary transcript. Two mature forms miR-181a (red) and miR181a-1 (blue) derived from 5′ and 3′ arm of precursor, respectively, are indicated. (B) The whole sequence of 5p and the seed sequence of each member in human miR-181 family is represented as 5′ to 3′ end.

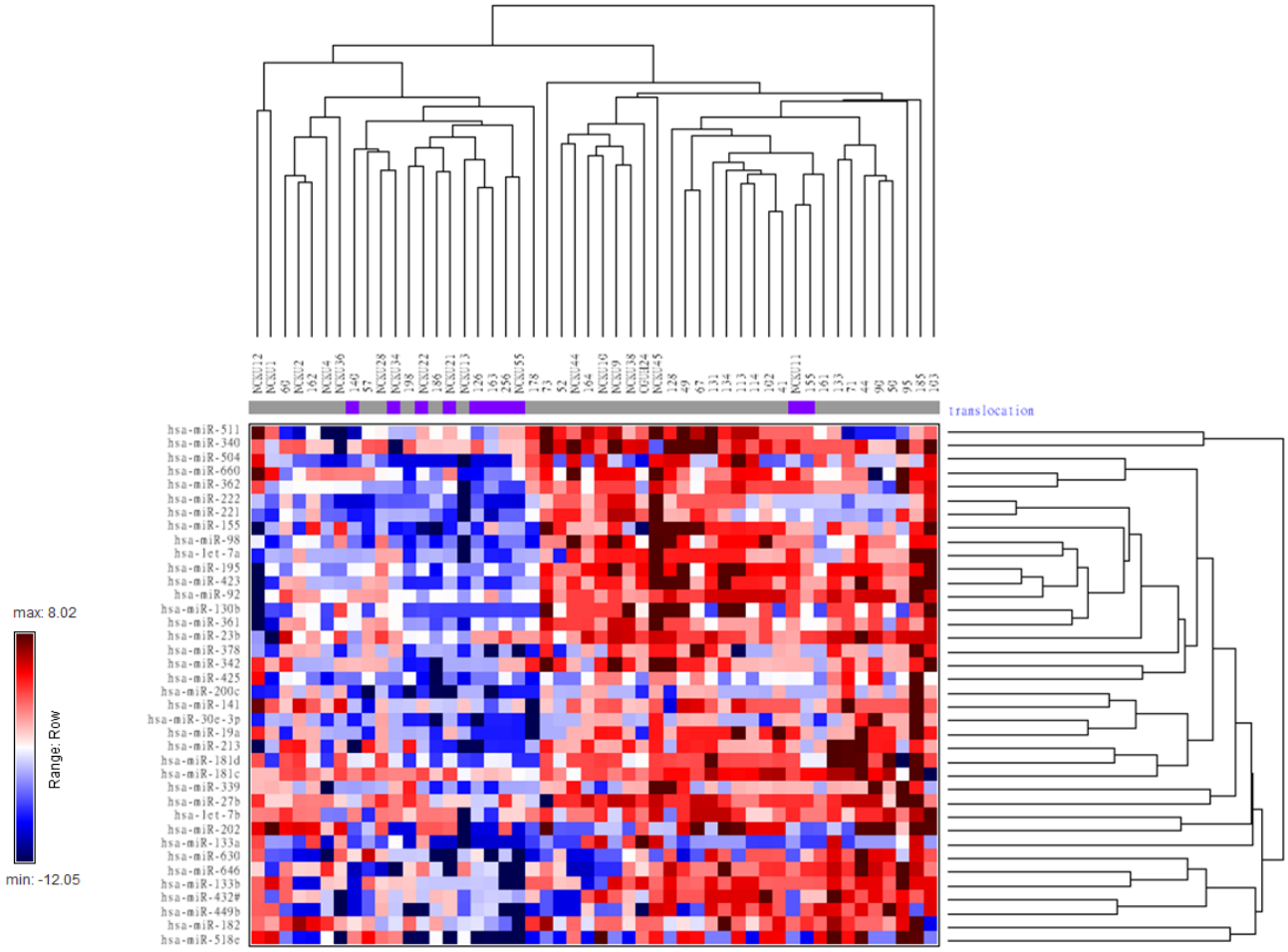

Figure 2. MicroRNA expression profile in childhood B-ALL patients.

50 childhood B-ALL patients were recruited including *E/R*-positive, n=10 (purple); *E/R*-negative, n=40 (gray). 365 miRNA were analyzed by ABI Taqman qRT-PCR based miRNA arrays which were carried out by Microarray core facility, Yu's Lab, NTU.

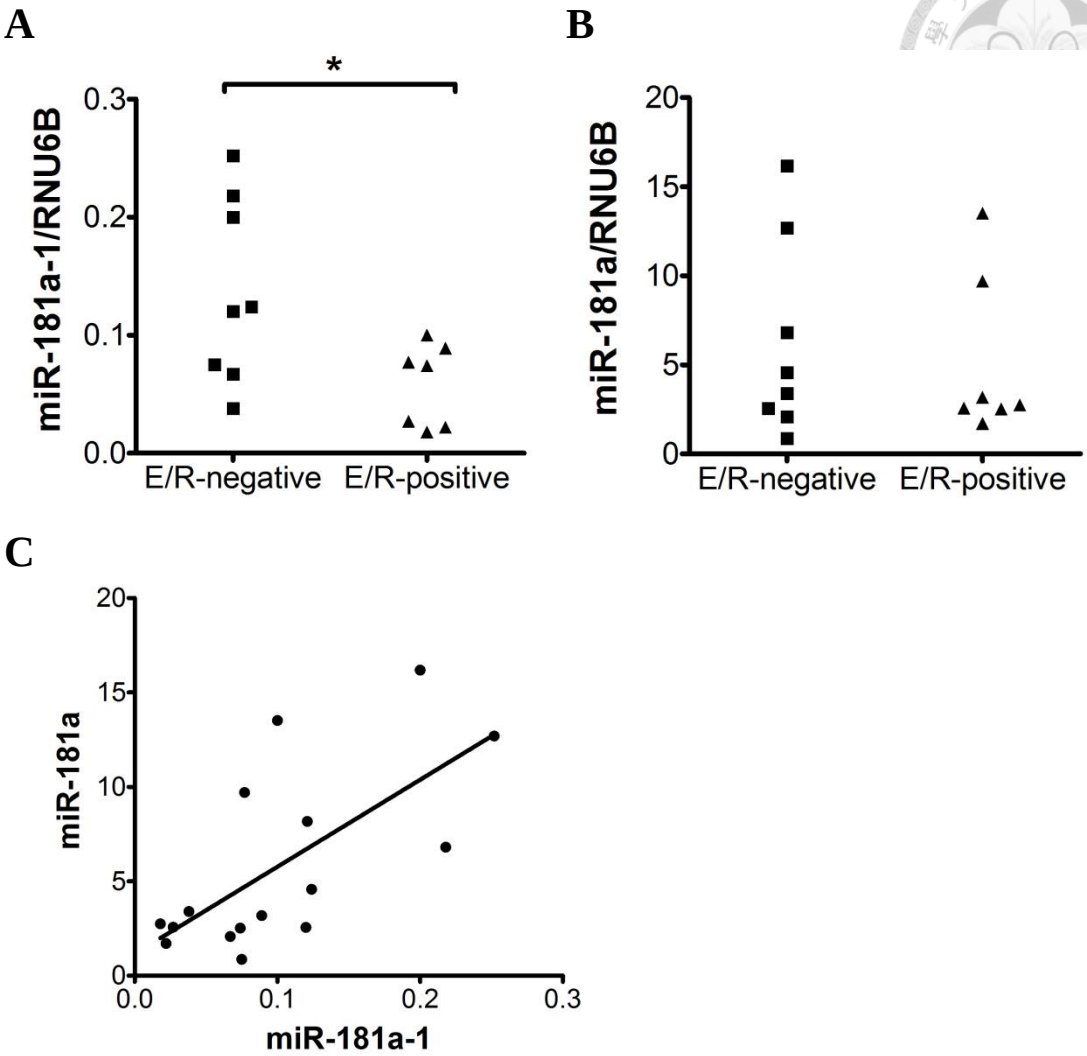

Figure 3. Validation of individual miRNA expression.

15 childhood B-ALL patients were included (*E/R*-positive, n = 7; *E/R*-negative, n = 8). (A) miR-181a-1 (*E/R*-positive samples: 0.14 ± 0.08; *E/R* -positive samples: 0.06 ± 0.03) and (B) miR-181a (*E/R* -positive samples: 6.15 ± 5.49; *E/R* -positive samples: 5.13 ± 4.58) levels were measured by TaqMan microRNA assays. * $P \leq 0.05$ (ANOVA) (C) Association between miR-181a-1 and miR-181a expression level in primary B-ALL cells. Pearson correlation coefficient = 0.67, P = 0.0045.

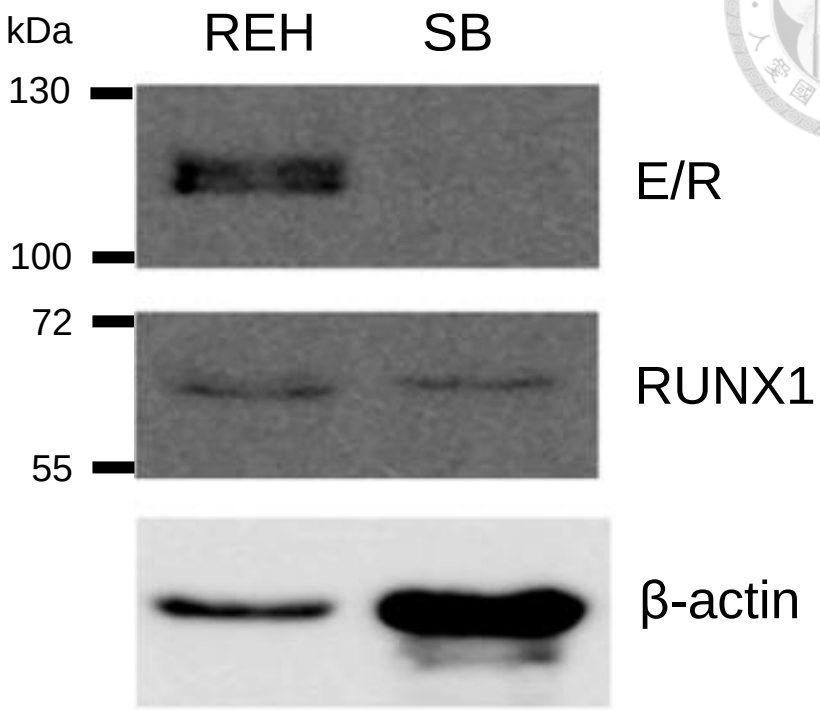

Figure 4. Expression of ETV6/RUNX1 fusion protein and wild type RUNX1 protein in B-ALL cell lines.

REH cells (left lane) are t(12;21)-positive which express both ETV6/RUNX1 fusion protein (predicted size: 100 kDa) and RUNX1 protein (predicted size: 55kDa), and CCRF-SB cells (right lane) do not carry any common translocation which only express RUNX1 protein. Protein expression was detected by Western blot using anti-RUNX1 antibody and β-actin was used as an internal control. E/R: ETV6/RUNX1.

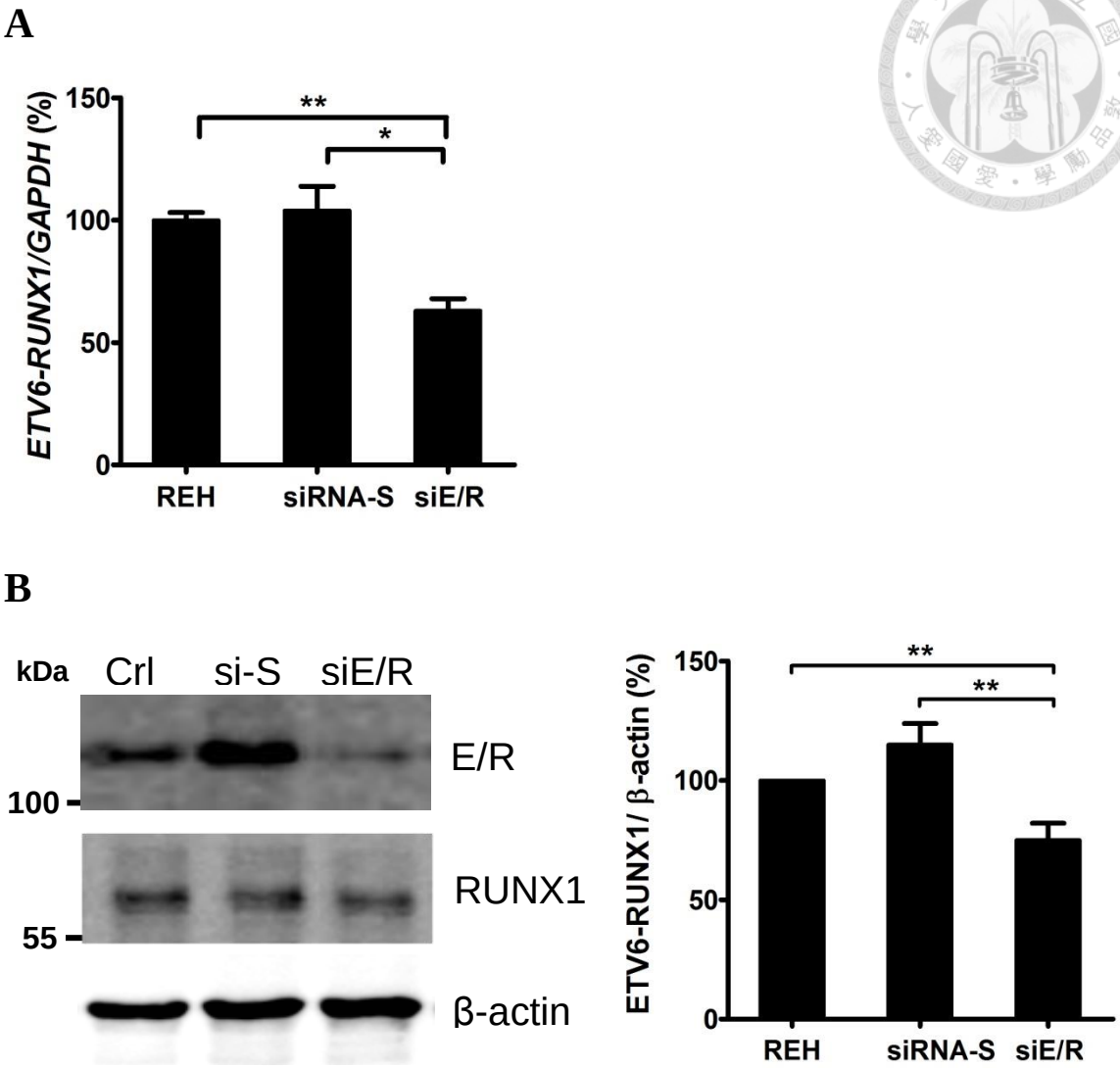

Figure 5. siRNA-mediated knockdown of *ETV6/RUNX1* fusion gene. ETV6/RUNX1-positive REH cells (transfection control) were transfected with siRNAs. After 48 hours of transfection with functional siETV6/RUNX1 (siE/R) or nonfunctional siRNA (siRNA-S, siRNA transfection control), (A) *ETV6/RUNX1* mRNA was detected by Taqman qRT-PCR, and *GAPDH* was used as a calibration control for mRNA expression. (B) ETV6/RUNX1 protein was analyzed by Western blotting with anti-RUNX1; anti-β-actin was used as a loading control. Quantification was conducted by densitometric analysis. Bars represent the mean ± SEM of at least three independent experiments. $^{*}P \leq 0.05$, $^{**}P \leq 0.01$ (ANOVA).

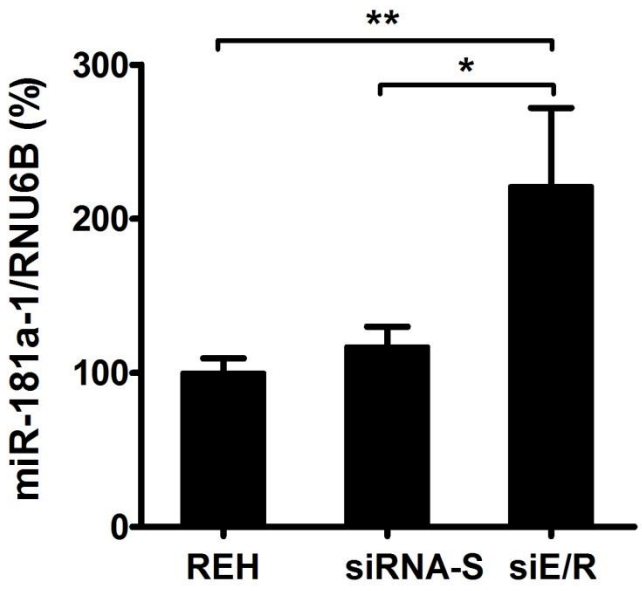

Figure 6. Effect of siRNA knockdown of *ETV6/RUNX1* on miR-181a-1 expression.

Expression of miR-181a-1 was determined by TaqMan microRNA assay and RNU6B was used as a calibration control for miRNA expression. Bars represent the mean ± SEM of at least three independent experiments. $^{*}P \leq 0.05$, $^{**}P \leq 0.01$ (ANOVA).

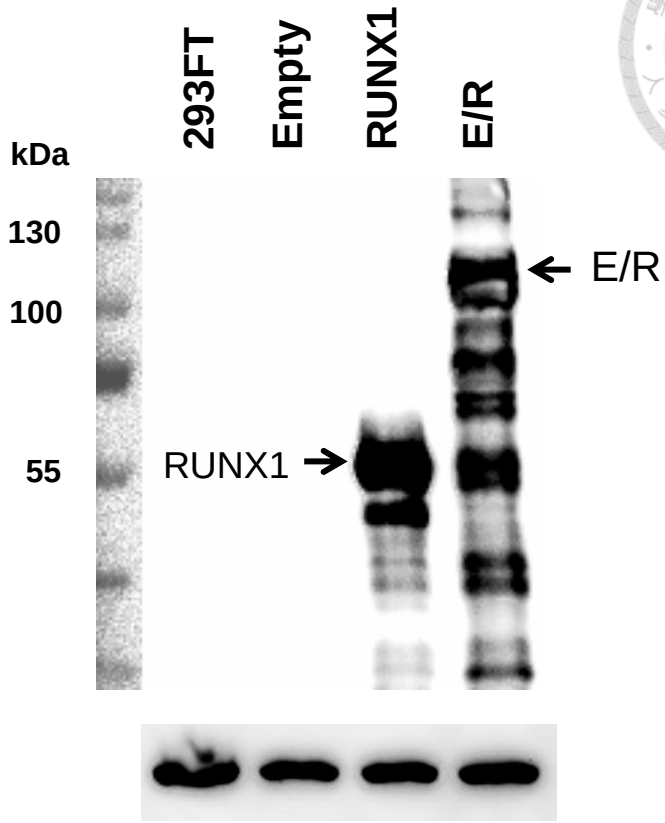

Figure 7. Overexpression of RUNX1 or ETV6/RUNX1 in HEK-293FT cells. HEK-293FT cells were transfected with CMV-XL4 vector expressing either RUNX1 (RUNX1) or ETV6/RUNX1 (E/R) protein. An empty vector (Empty) was used as a transfection control. Protein expression was detected by Western blot using anti-RUNX1 antibody and β-actin was used as an internal control. 30 μg protein per well was loaded.

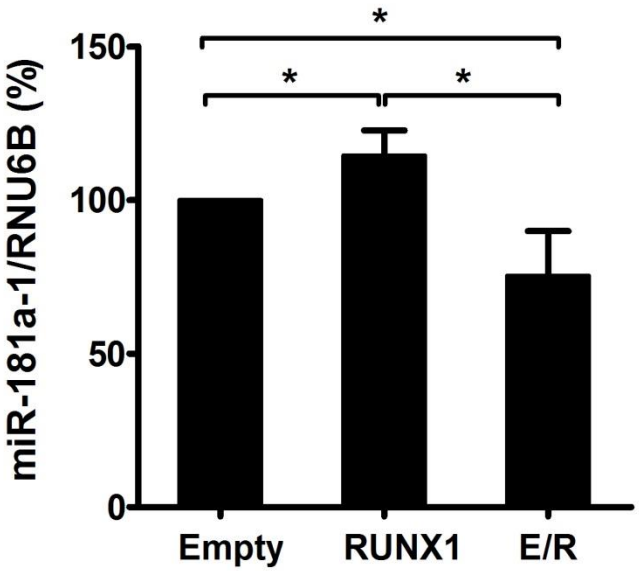

Figure 8. Effects of RUNX1 and ETV6/RUNX1 overexpression on miR-181a-1 expression.

Expression of miR-181a-1 was determined by TaqMan microRNA assay and RNU6B was used as a calibration control for miRNA expression. Bars represent the mean ± SD of three independent experiments. $^{*}P \leq 0.05$, (ANOVA).

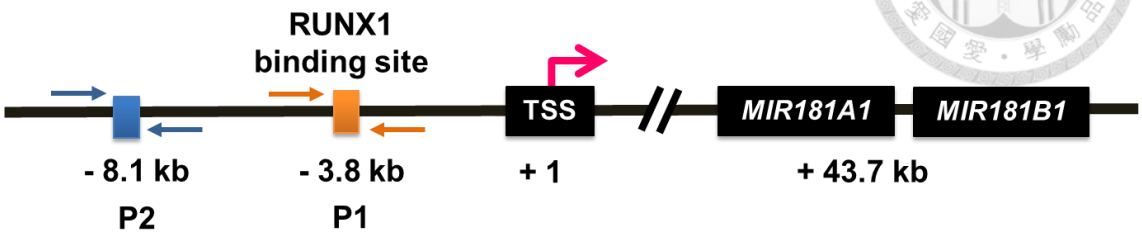

Figure 9. Schematic representation of the genomic structure of human *MIR181A1* gene.

MIR181A1 gene is located on human chromosome 1 in cluster with *MIR181B1* gene, the distance between *MIR181A1* and *MIR181B1* is 62 bp. The location of *MIR181A1* gene and the RUNX1-binding site are numbered relative to the Transcriptional start site (TSS, +1). Arrows indicate the locations of the primers used in the ChIP assay. P1 primers (orange) were used to amplify the region close to ETV6/RUNX1 binding site, and P2 primers (blue) were used to amplify the region away from ETV6/RUNX1 binding site as a negative control for ChIP assay with anti-RUNX1.

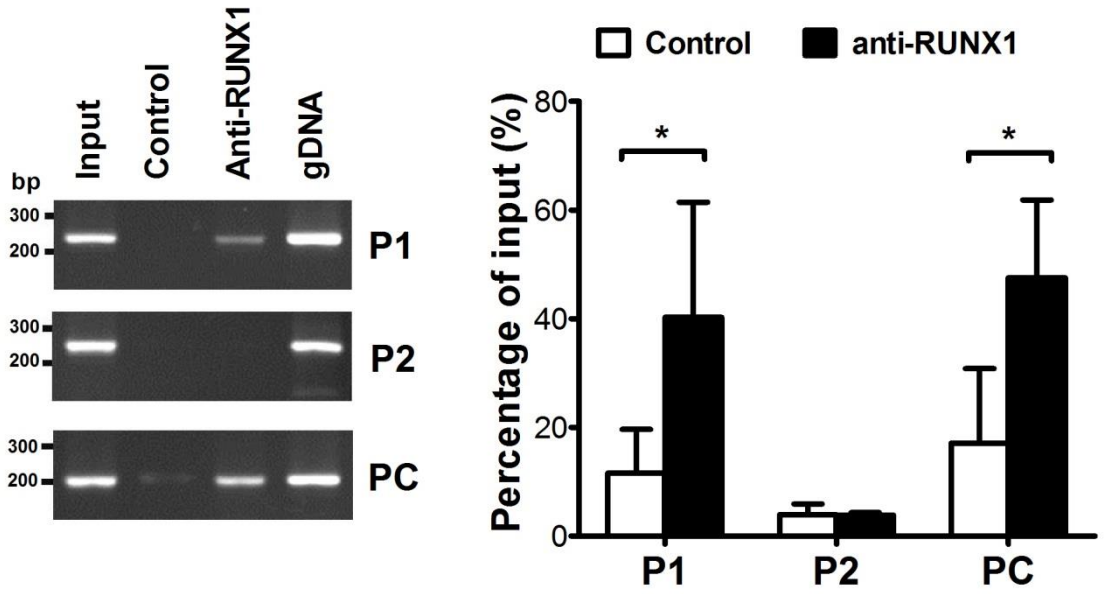

Figure 10. ETV6/RUNX1 binds to regulatory region of *MIR181A1*.

ChIP was carried out using anti-RUNX1 or in the absence of specific antibody (Control) (left). DNA sequences surrounding the putative RUNX1-binding site were amplified by PCR using P1 primers. To evaluate the specificity of RUNX1 binding, a positive control and a negative control were performed using PC and P2, respectively, for the ChIP assay. Amplification of the upstream region near the RUNX1-binding site on *MIR223*, which is a known direct target of RUNX1, was performed using PC primers. P2 primers were designed to amplify a distal region lacking the RUNX1-binding site. Input shows the amplification from sonicated chromatin, and genomic DNA (gDNA) was used as a positive PCR control. The PCR products were quantified by densitometry (right). Bars show the mean ± SD from three independent experiments. $^{*}P \leq 0.05$ (ANOVA).

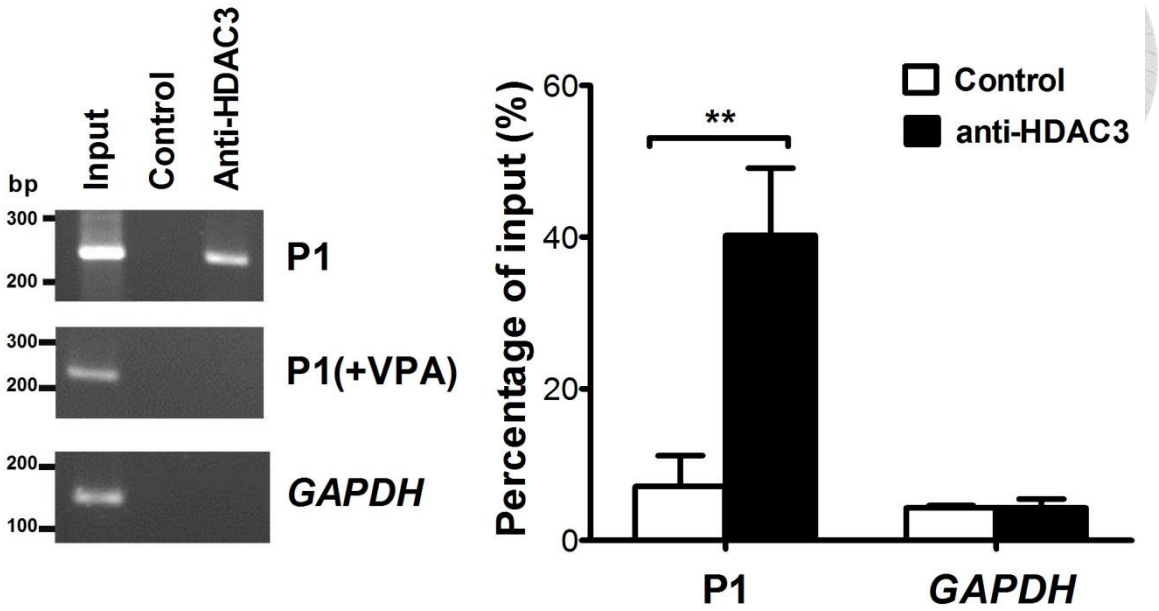

Figure 11. HDC3 binds to regulatory region of *MIR181A1*.

ChIP was carried out using anti-HDAC3 or in the absence of specific antibody (Control) (left). DNA sequences surrounding the putative RUNX1-binding site were amplified by PCR using P1 primers. To evaluate the specificity of HDAC3 binding, treatment with valproic acid (VPA, a HDAC inhibitor) and amplification of the promoter region of *GAPDH* were used as controls for the ChIP assay. Input shows the amplification from sonicated chromatin and was used as a positive PCR control. The PCR products were quantified by densitometry (right). Bars show the mean ± SD from three independent experiments. ** $P \leq 0.01$ (ANOVA).

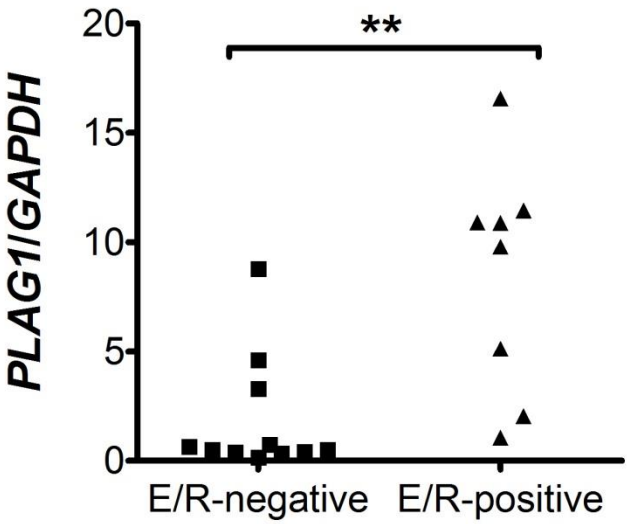

Figure 12. Expression of *PLAG1* mRNA in B-ALL clinical samples.
19 childhood B-ALL patients were included (*E/R*-positive, n = 8; *E/R*-negative, n = 11). *PLAG1* mRNA level was assessed by SYBR green qRT-PCR. Each dot represents an individual sample. ** $P \leq 0.01$ (t-test).

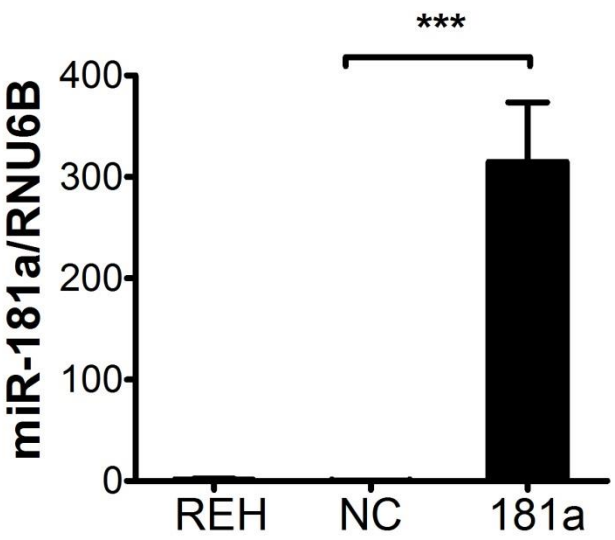

Figure 13. Overexpression of miR-181a in REH cells by transfection with precursor miRNA.

A final 50 nM concentration of nontargeting-miR (NC) or pre-mir-181a (181a) were transfected twice with a 48hr-interval and transfected cells were harvested after 48hr of the second transfection for further examination. Expression level of miR-181a was detected by TaqMan microRNA assay. Bars represent the mean ± SD of three independent experiments. *** $P \leq 0.001$ (ANOVA).

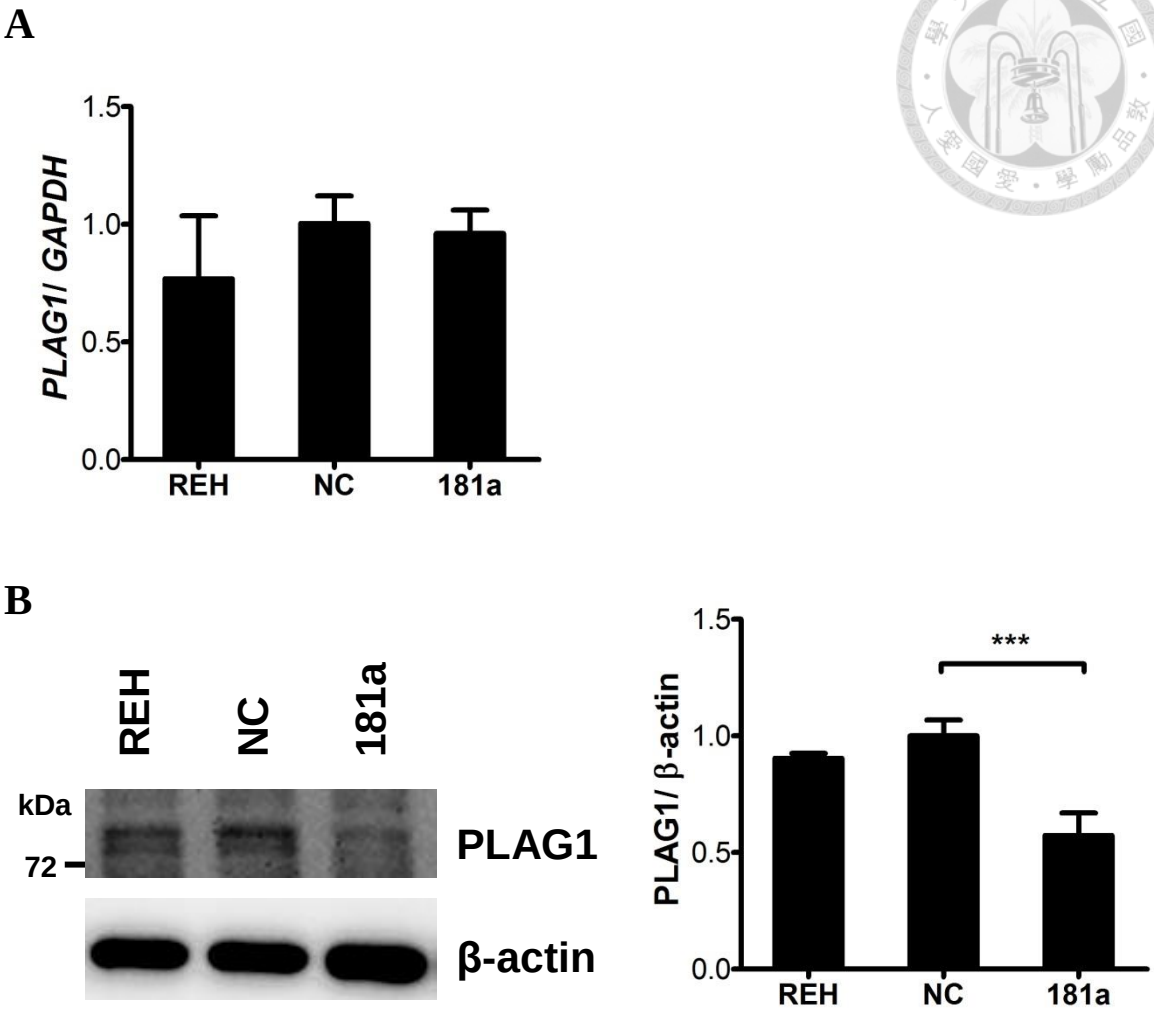

Figure 14. PLAG1 expression in miRNA precursor transfected REH cells. Expression of (A) *PLAG1* mRNA in REH cell (no transfection control), NC-transfected REH cells (miRNA transfection control), and 181a-transfected REH cells was determined by SYBR green qRT-PCR, and (B) PLAG1 protein was analyzed by Western blot with anti-PLAG1 (left). Quantification was conducted by densitometric analysis (right). *GAPDH* and anti-β-actin were used as internal controls for mRNA and protein expression, respectively. Bars represent the mean ± SD of three independent experiments. *** $P \leq 0.001$ (ANOVA).

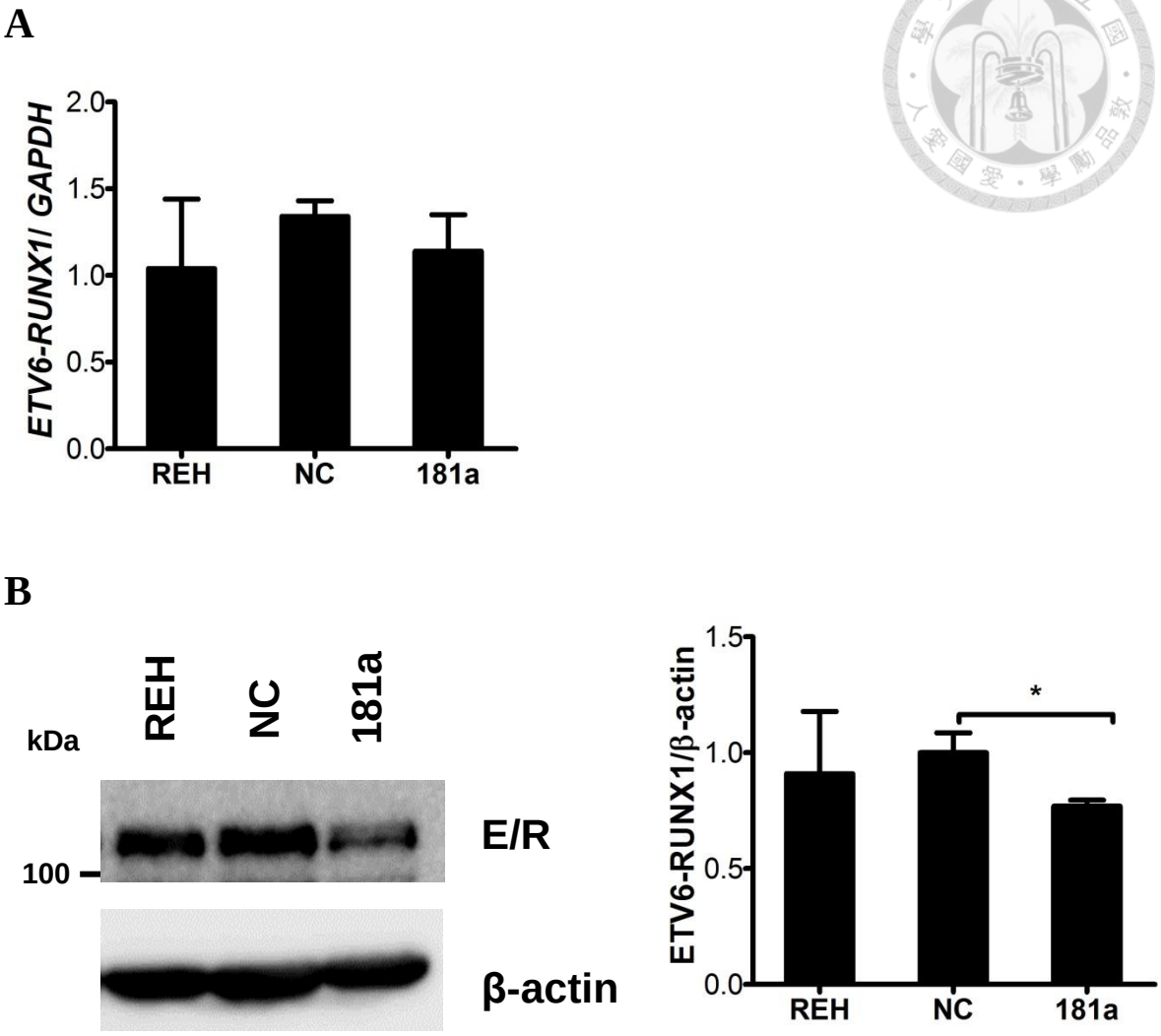

Figure 15. ETV6/RUNX1 expression in miRNA mimics transfected REH cells.

Expression of (A) *ETV6/RUNX1* mRNA in REH cell (no transfection control), NC-transfected REH cells (miRNA transfection control), and 181a-transfected REH cells was determined by Taqman qRT-PCR, and (B) ETV6/RUNX1 fusion protein was analyzed by Western blot with anti-RUNX1 (left). Quantification was conducted by densitometric analysis (right). *GAPDH* and anti-β-actin were used as internal controls for mRNA and protein expression, respectively. Bars represent the mean ± SD of three independent experiments. $^{*}P \leq 0.05$ (ANOVA).

A

WT *RUNX1*-3' UTR 5' GGGGAAA**UGAAUGU**G 3'
miR-181a 3' UGUCGCA**ACUUACA**A 5'

mutated *RUNX1*-3' UTR 5' GGGGAAA**ACAUCUG**G 3'
miR-181a 3' UGUCGCA**ACUUACA**A 5'

3758 nt

RUNX1 | *RUNX1-3′* UTR

B

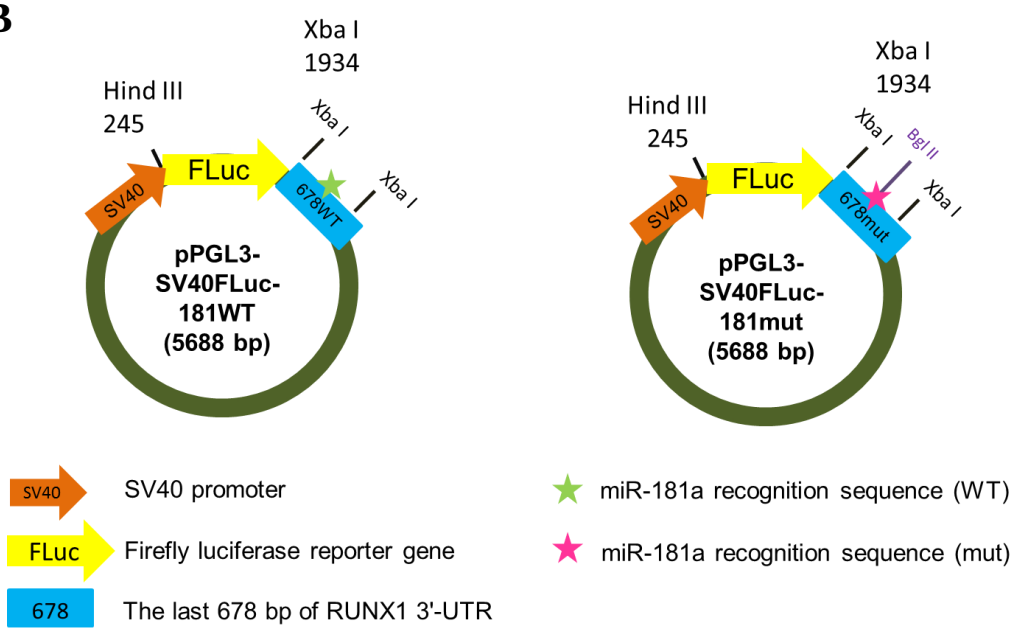

C

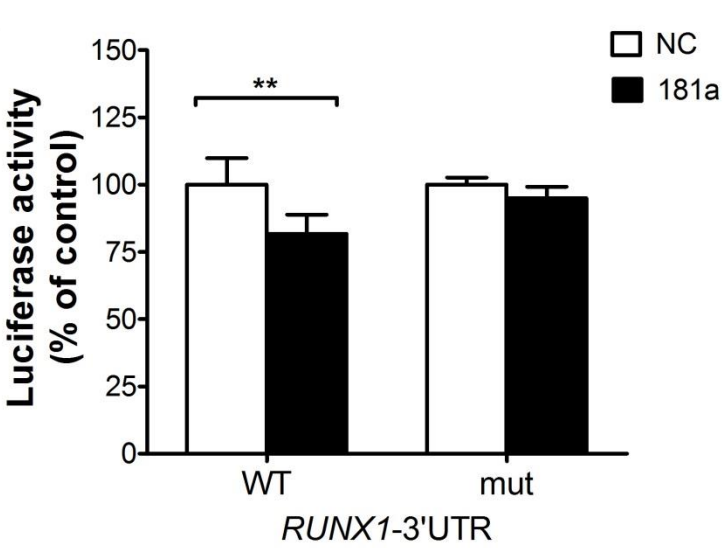

Figure 16. miR-181a targets the 3′-UTR of *RUNX* and *ETV6/RUNX1*.
(A) The putative miR-181a binding site in the *RUNX1* 3′ UTR, both wild type and mutated version. (B) The last 678 bp of the human RUNX1 3' UTR containing normal (WT) or mutated (mut) miR-181a targeting sequences were cloned and inserted to the downstream of a pGL3-SV40Fluc vector in which a Firefly reporter gene (FLuc) was driven by a SV40 promotor (SV40). A Bgl II restriction enzyme site was added into the mutated version of miR-181a targeting sequence for easy recognition by restriction enzyme mapping. (C) pGL3-SV40FLuc-181WT/mut and pRLuc-TK (a Renilla luciferase control reporter vector used as a calibration control for transfection efficiency) were transfected into 293FT cells with expression vectors for miR-181a (181a) or negative control shRNA (NC). Luciferase activity was adjusted by FLuc/RLuc. Bars represent the mean ± SD of three independent experiments. ** $P \leq 0.01$ (ANOVA).

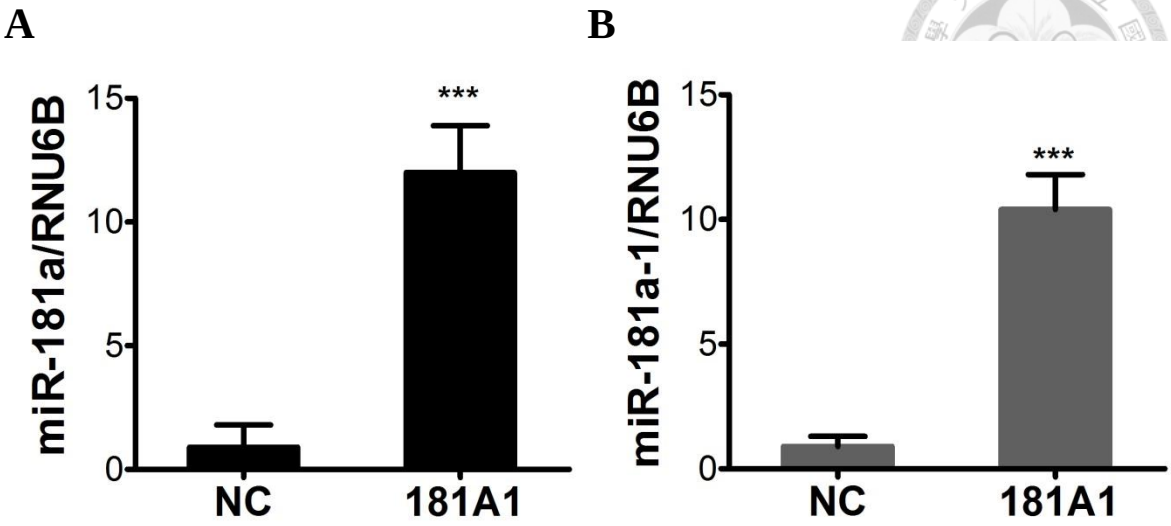

Figure 17. Stable expression of *MIR181A1* in REH cells via lentiviral transduction.

REH cells were infected with lentiviral vector expressing the negative control shRNA (NC) or miR-181a (181A1). Infected cells were undergone a week of puromycin selection. Relative (A) miR-181a and (B) miR-181a-1 level were determined by Taqman microRNA assays. Bars show the mean ± SD from three independent experiments. *** $P \leq 0.001$ (ANOVA).

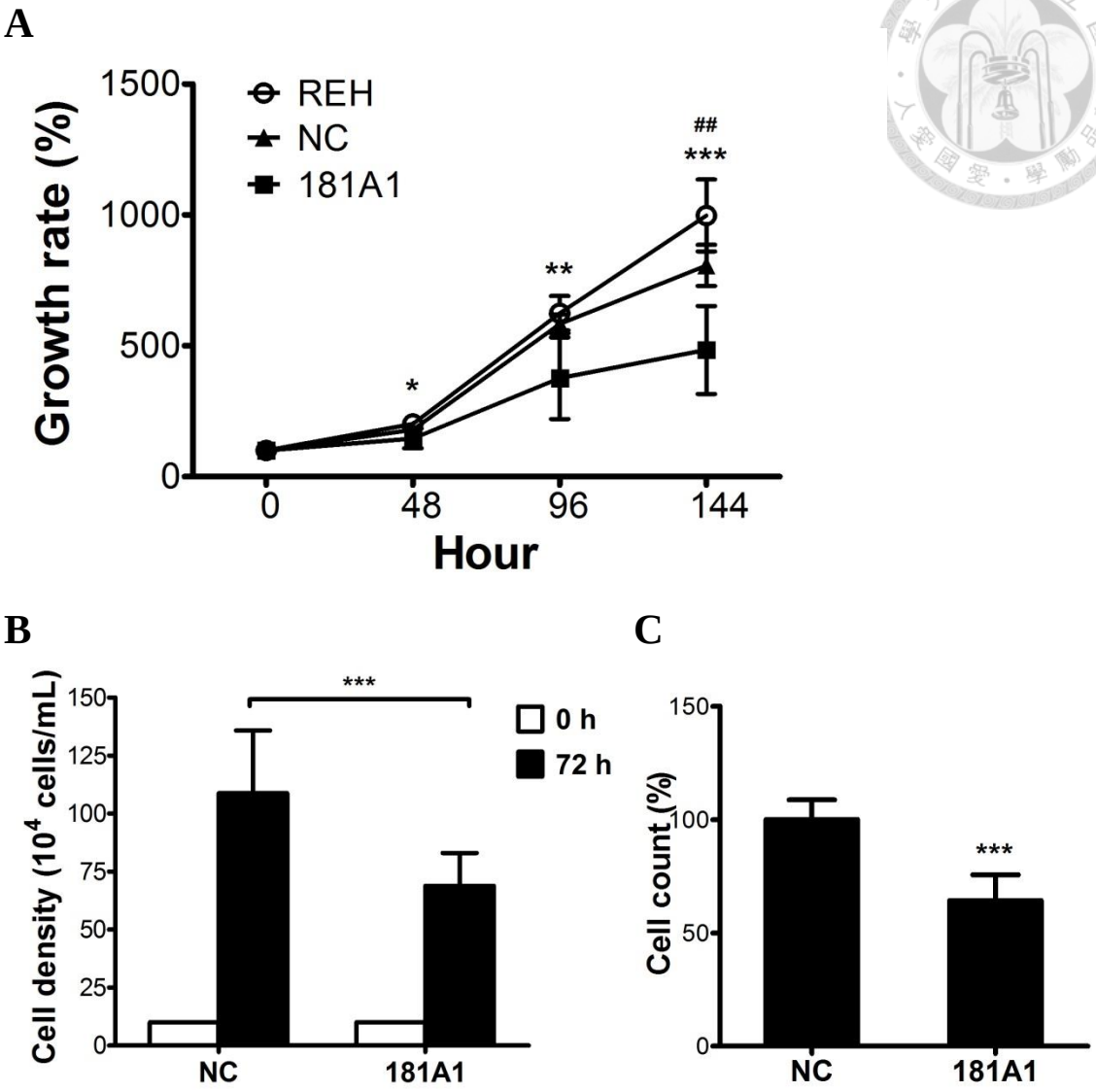

Figure 18. Assessment of cell growth of lentivirus transduced REH cell.

(A) Growth curve was determined as following: 10,000 cells per well were seeding in a 96-well plate and cultured for 48, 96, and 144 hours, and then assessed with the MTT assay. (B) Cells were seeded at a density of $1*10^5$ cells/ml and cultured. 72hr later, cells were stained with trypan blue and counted. (C) Cell count at 72hr was demonstrated as percentage of infection control (NC). Bars show the mean ± SD from three independent experiments. 181A1 vs. NC $^{*}P \leq 0.05$, $^{**}P \leq 0.01$, $^{***}P \leq 0.001$; NC vs. REH $^{\#\#}P \leq 0.01$ (ANOVA).

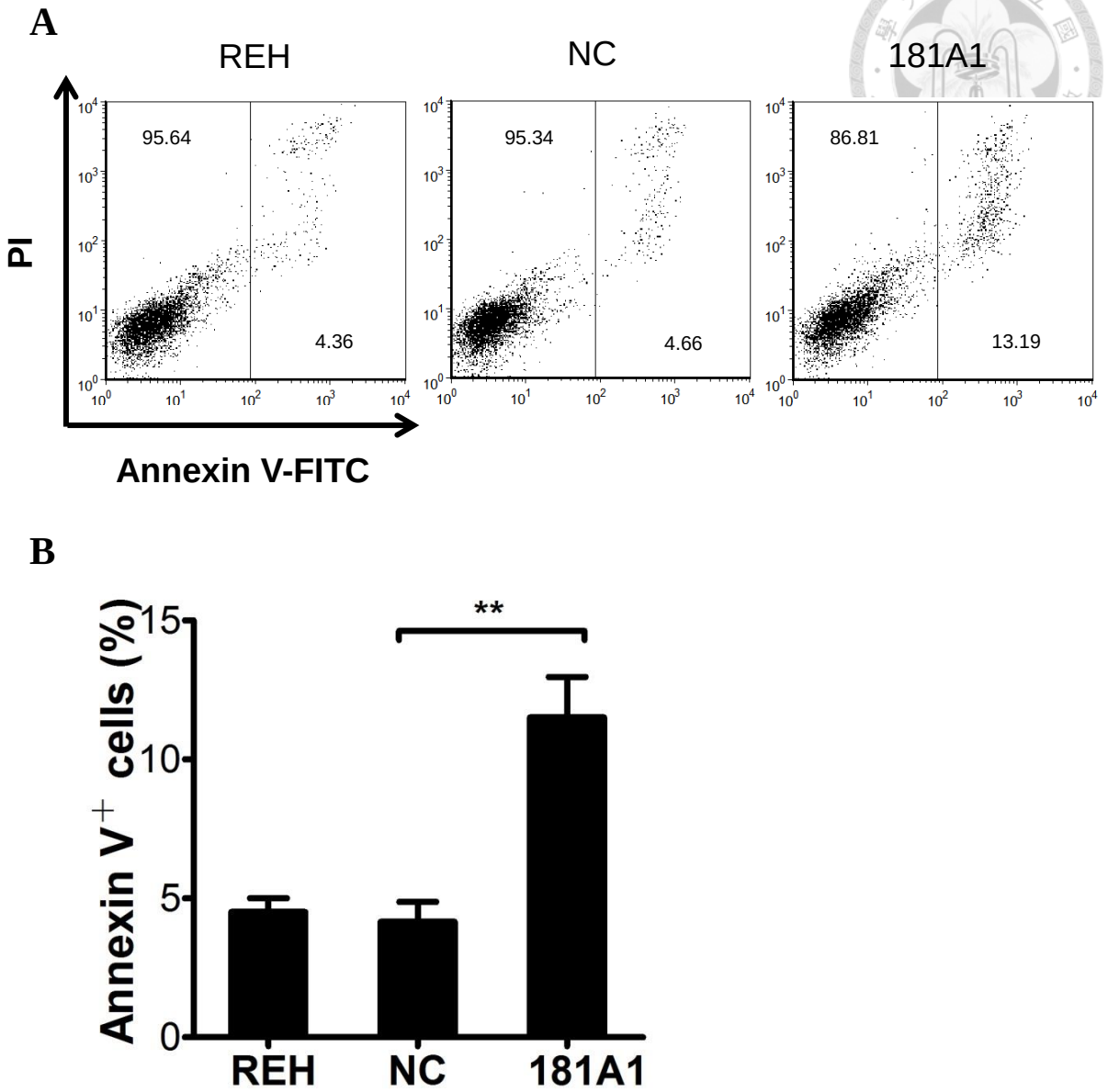

Figure 19. Apoptosis analysis of lentivirus transduced REH cell.

(A) Lentiviral transduced REH cells were seeded at a density of $1*10^5$ cells/ml and cultured. 72hr later, cells were collected and assessed the apoptotic cells by flow cytometric analysis of annexin V/PI staining of lentivirus-transduced cells. (B) Representative histograms demonstrate the proportion of annexin V-positive cells. Bars show the mean ± SD from three independent experiments. ** $P \leq 0.01$ (ANOVA).

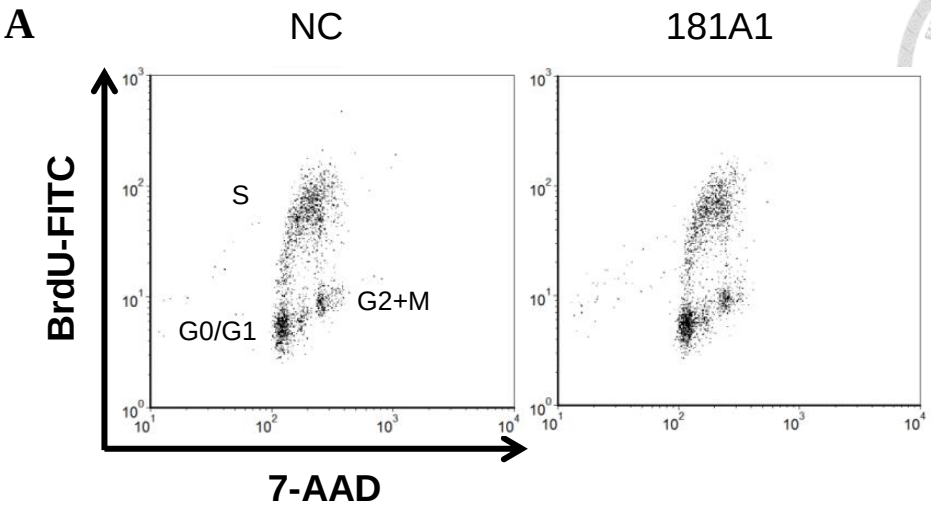

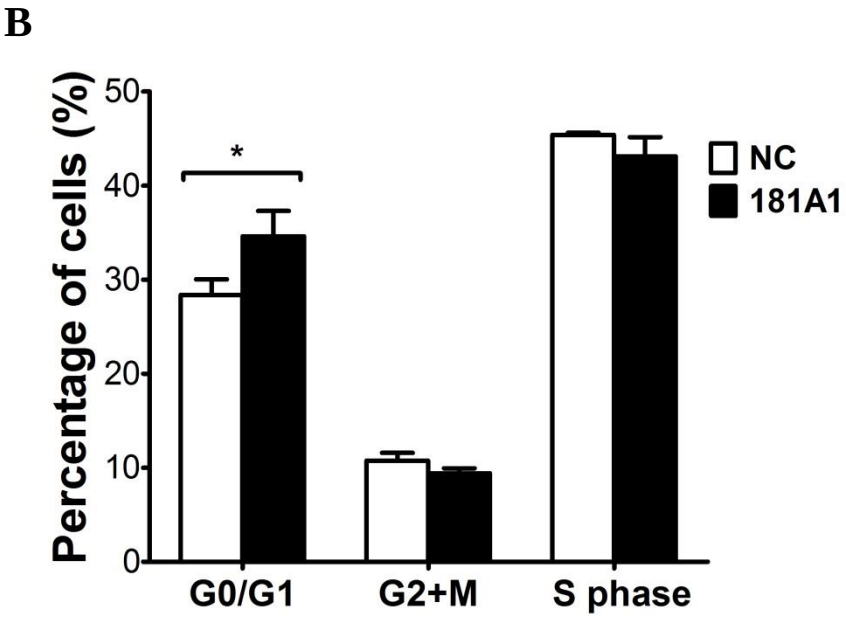

Figure 20. Analysis of cell cycle and proliferation of lentivirus transduced REH cells.

Cells were seeded at a density of $1*10^5$ cells/ml and cultured for 72hr, and then cell cycle and cell proliferation were assessed by Biparametric BrdU/DNA analysis. (A) During the last 30 minutes of culture, 1 mM BrdU was added to the cells, and then the cells were stained with anti-BrdU and 7-aminoactinomycin D (7-AAD) and detected by flow cytometry. (B) The percentage of cells in each of the cell-cycle phases (G0/G1, S, and G2+M) was quantified. Bars show the mean ± SD from three independent experiments. * $P \leq 0.05$ (ANOVA).

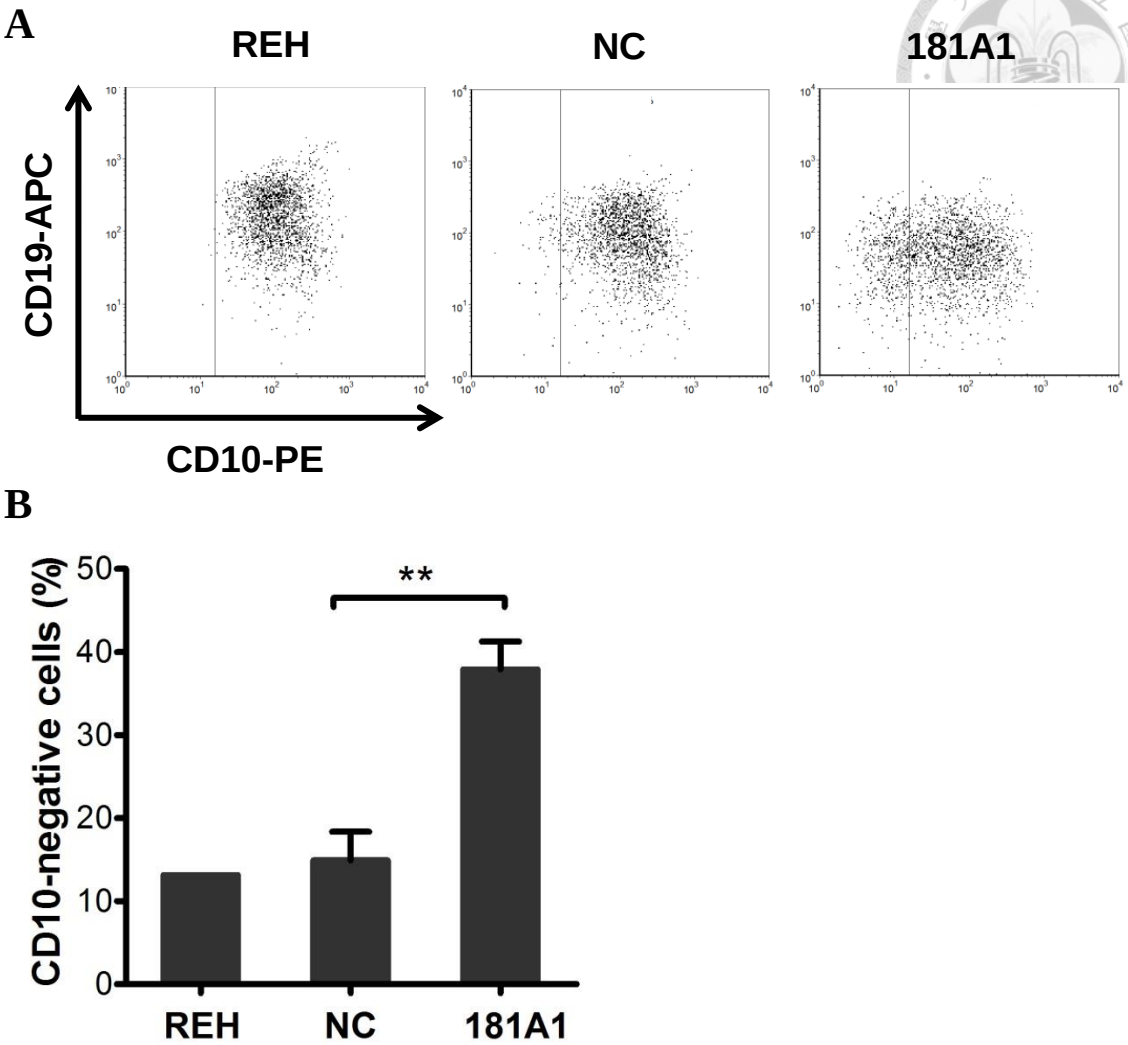

Figure 21. Analysis of CD10 expression on lentivirus-infected REH cells. (A) Percentage of lentivirus-infected REH cells stained for cell-surface marker CD10-PE/CD34-PerCP/CD19-APC as analyzed by flow cytometry. (B) The results were quantified and are presented as the average ± SD of three independent evaluations. (REH: 13.1%; NC: 14.9 ± 3.43%; 181A1: 37.9 ± 3.35), ** $P \leq 0.01$ (ANOVA).

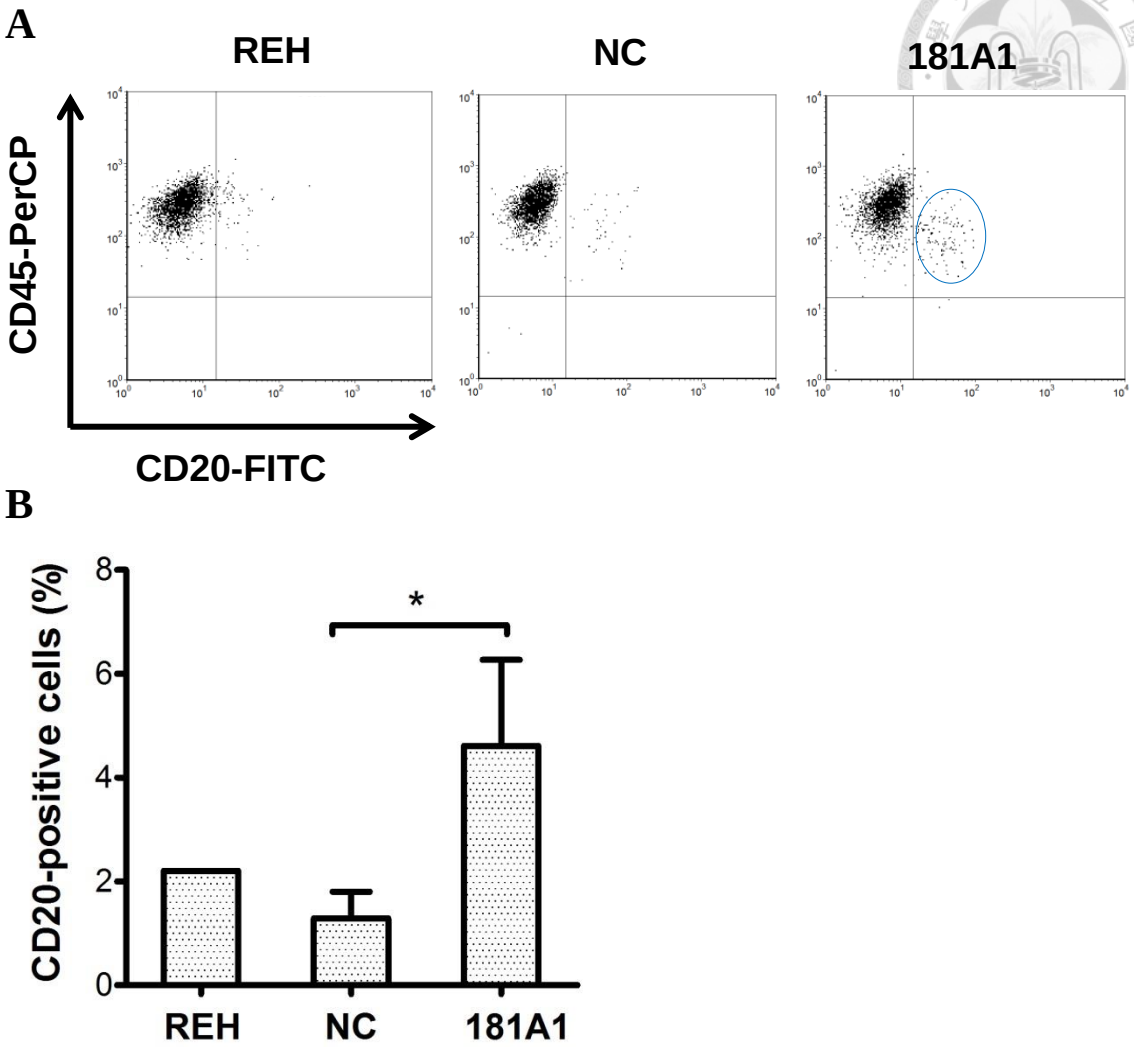

Figure 22. Analysis of CD20 expression on lentivirus-infected REH cells. (A) Percentage of lentivirus-infected REH cells stained for cell-surface marker CD20-FITC/CD45-PerCP as analyzed by flow cytometry. (B) The results were quantified and are presented as the average ± SD of three independent evaluations. (REH: 2.2%; NC: 1.29 ± 0.51%; 181A1: 4.61 ± 1.66), * $P \leq 0.05$ (ANOVA).

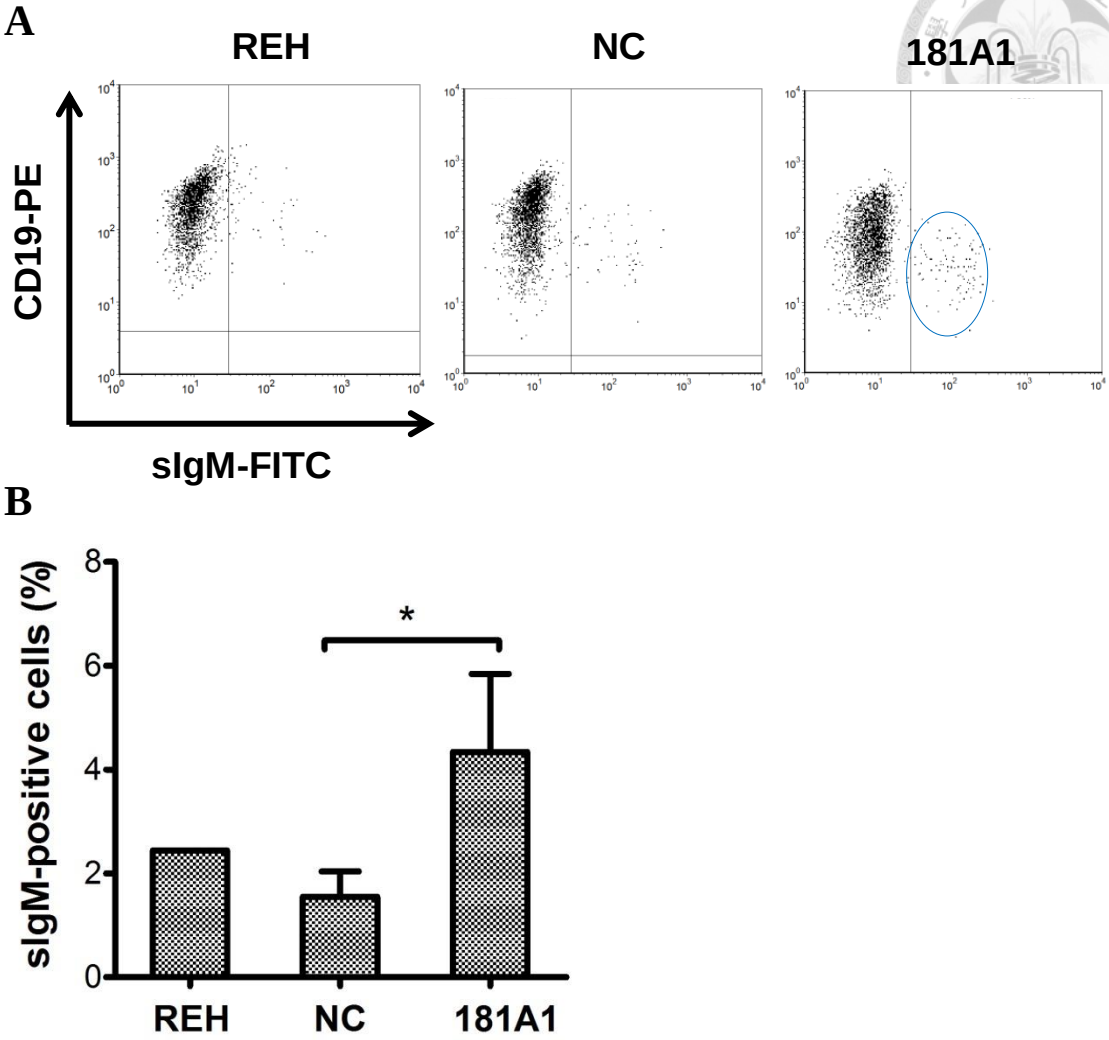

Figure 23. Analysis of surface IgM expression on lentivirus-infected REH cells.

(A) Percentage of lentivirus-infected REH cells stained for cell-surface marker IgM-FITC/CD19-PE/CD45-PerCP as analyzed by flow cytometry. (B) The results were quantified and are presented as the average ± SD of three independent evaluations. (REH: 2.44%; NC: 1.55 ± 0.49%; 181A1: 4.34 ± 1.5), * $P \leq 0.05$ (ANOVA).

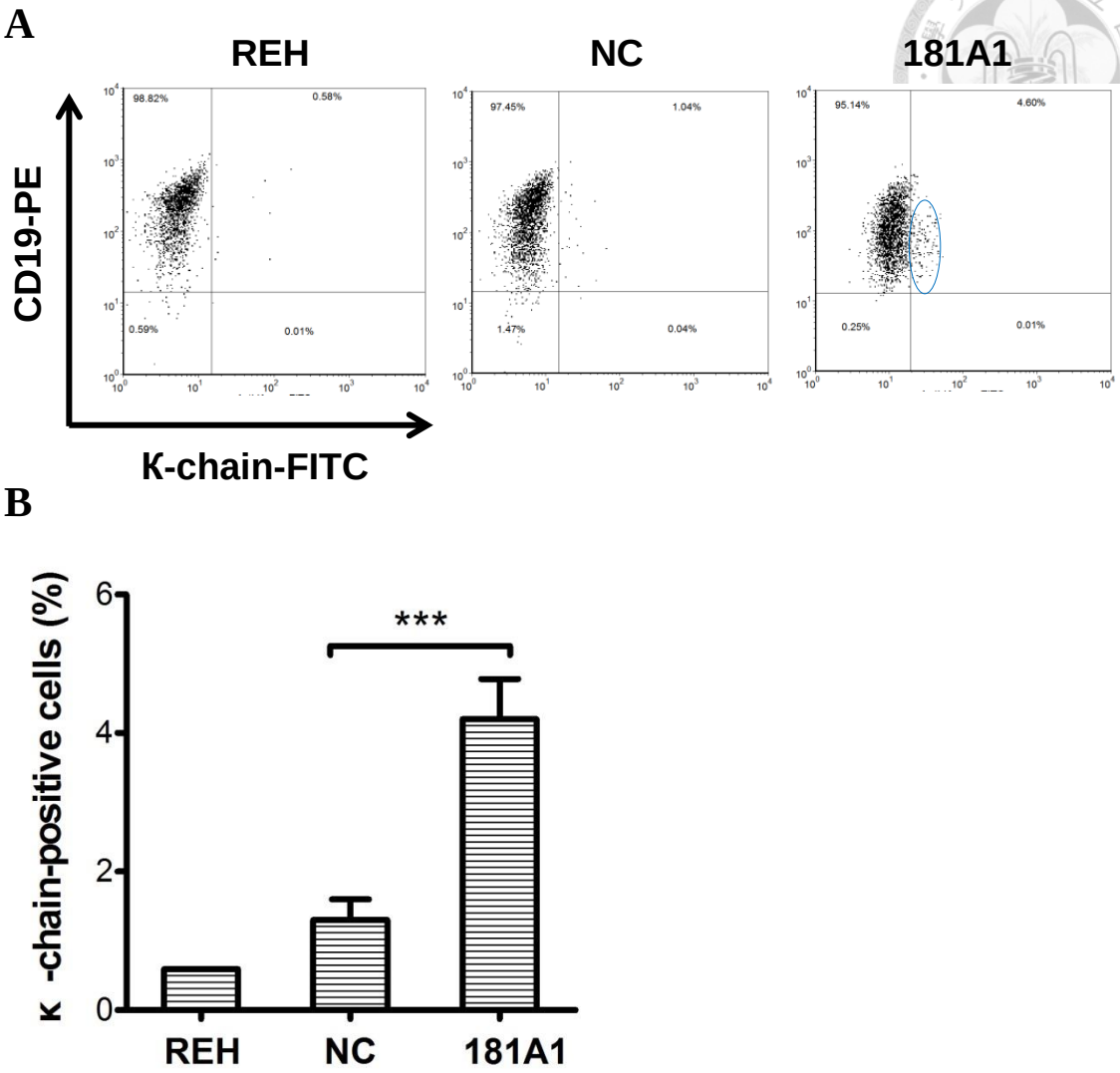

Figure 24. Analysis of κ-chain expression on lentivirus-infected REH cells. (A) Percentage of lentivirus-infected REH cells stained for cell-surface marker κ-chain-FITC/CD19-PE/CD45-PerCP as analyzed by flow cytometry. (B) The results were quantified and are presented as the average ± SD of three independent evaluations. (REH: 0.59%; NC: 1.3 ± 0.3%; 181A1: 4.2 ± 0.58), *** $P \leq 0.001$ (ANOVA).

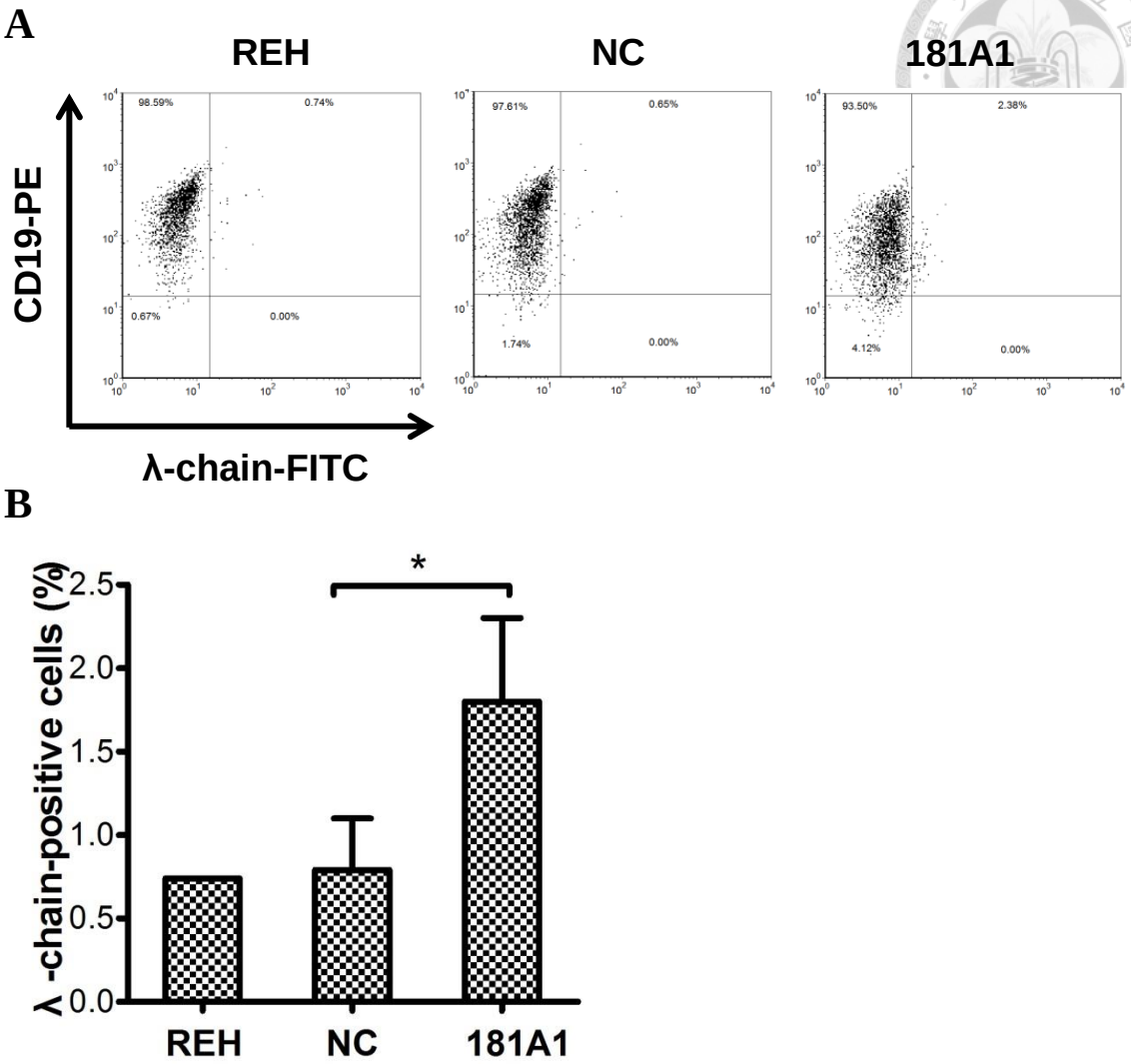

Figure 25. Analysis of λ-chain expression on lentivirus-infected REH cells. (A) Percentage of lentivirus-infected REH cells stained for cell-surface marker λ-chain-FITC/CD19-PE/CD45-PerCP as analyzed by flow cytometry. (B) The results were quantified and are presented as the average ± SD of three independent evaluations. (REH: 0.74%; NC: 0.79 ± 0.31%; 181A1: 1.8 ± 0.5), * $P \leq 0.05$ (ANOVA).

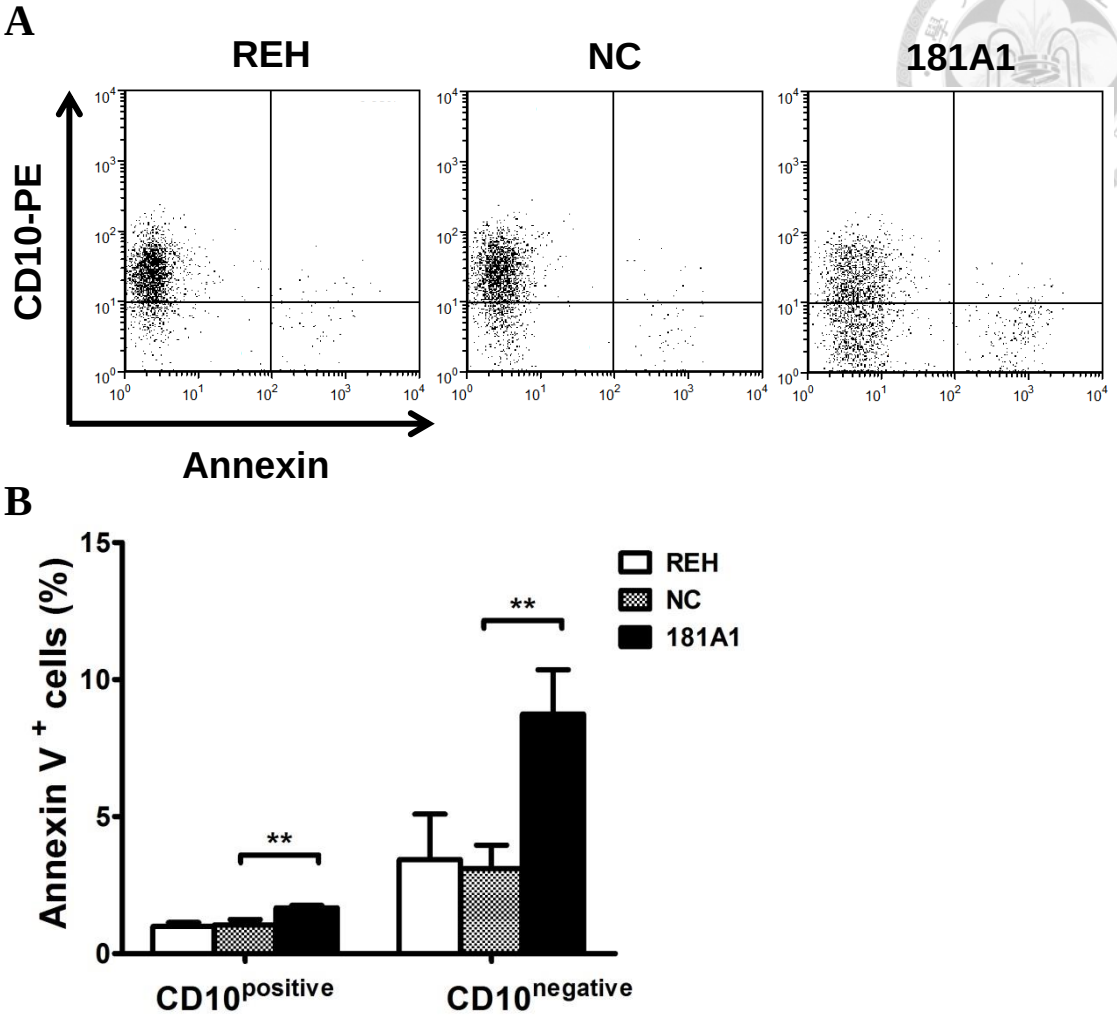

Figure 26. Analysis of CD10 expression on apoptotic REH cells.

(A) Percentage of lentivirus-infected REH cells stained for cell-surface marker Annexin V-FITC/CD10-PE was analyzed by flow cytometry. (B) The results were quantified and are presented as the average ± SD of three independent evaluations. Annexin $V^{+}CD10^{+}$: REH 0.99 ± 0.15%; NC 1.05 ± 0.19%; 181A1: 1.67 ± 0.09; Annexin $V^{+}CD10^{-}$: REH 3.43 ± 1.66%; NC 3.1 ± 0.86%; 181A1: 8.74 ± 1.62. ** $P \leq 0.01$ (ANOVA).

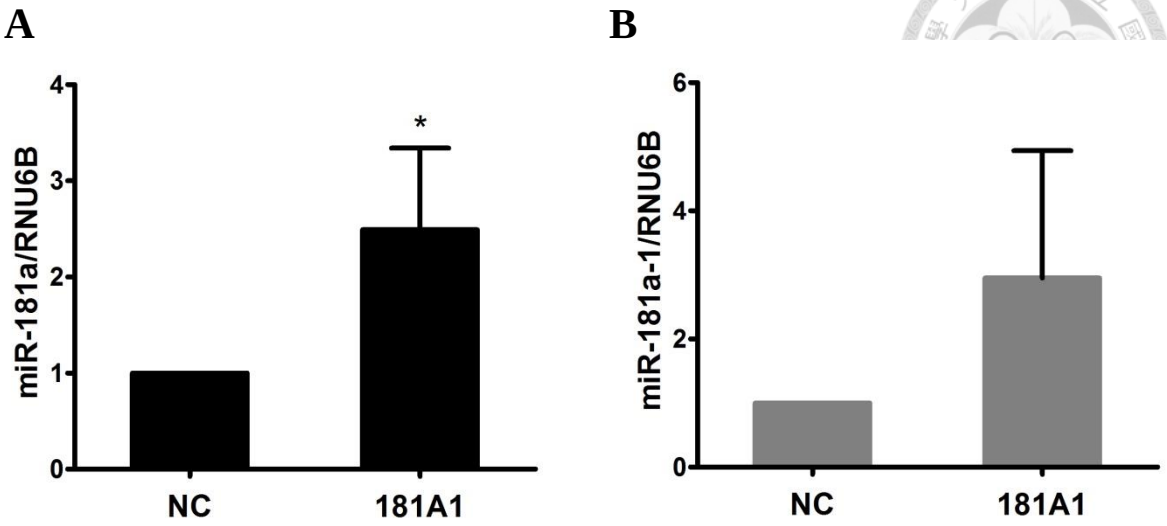

Figure 27. Ectopic expression of *MIR181A1* in primary ALL cells via lentiviral transduction.

Patient cells were infected with lentiviral vector expressing the negative control shRNA (NC) or miR-181a (181A1). Infected cells were undergone a week of puromycin selection. Relative (A) miR-181a and (B) miR-181a-1 level were determined by Taqman microRNA assays. Bars show the mean ± SD from three independent experiments. *** $P \leq 0.001$ (ANOVA).

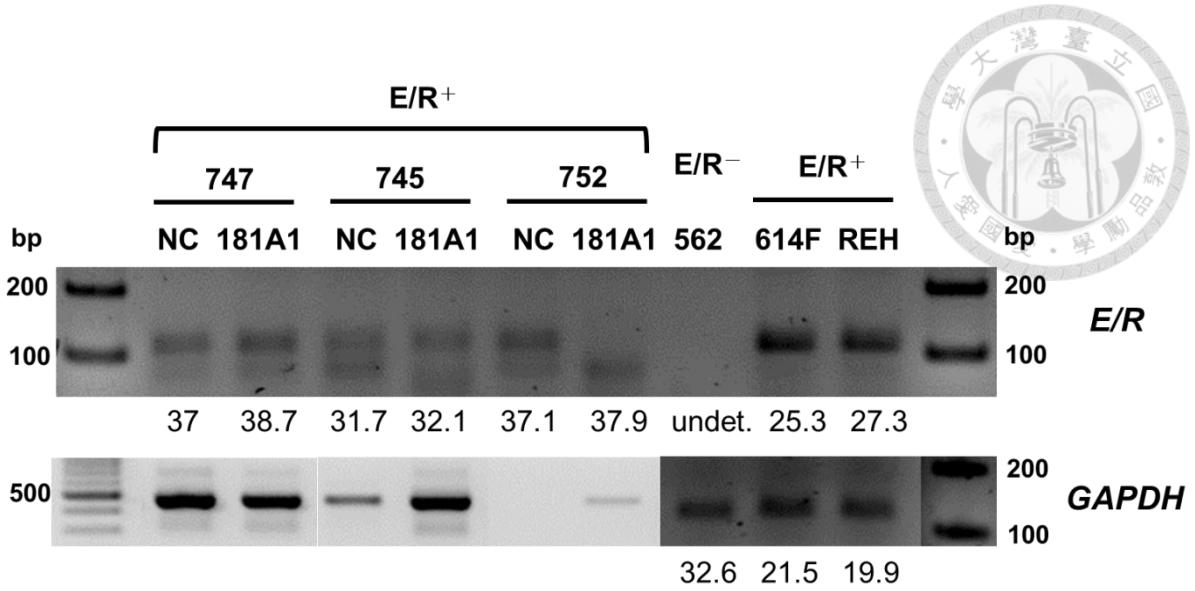

Figure 28. Detection of *ETV6/RUNX1* mRNA in cultured primary ALL cells. Patient cells infected with lentiviral vector and undergone a week of puromycin selection were detected the *ETV6/RUNX1* (upper) and endogenous *GAPDH* (lower) expression by qRT-PCR or RT-PCR. The Ct value was indicated below each sample.

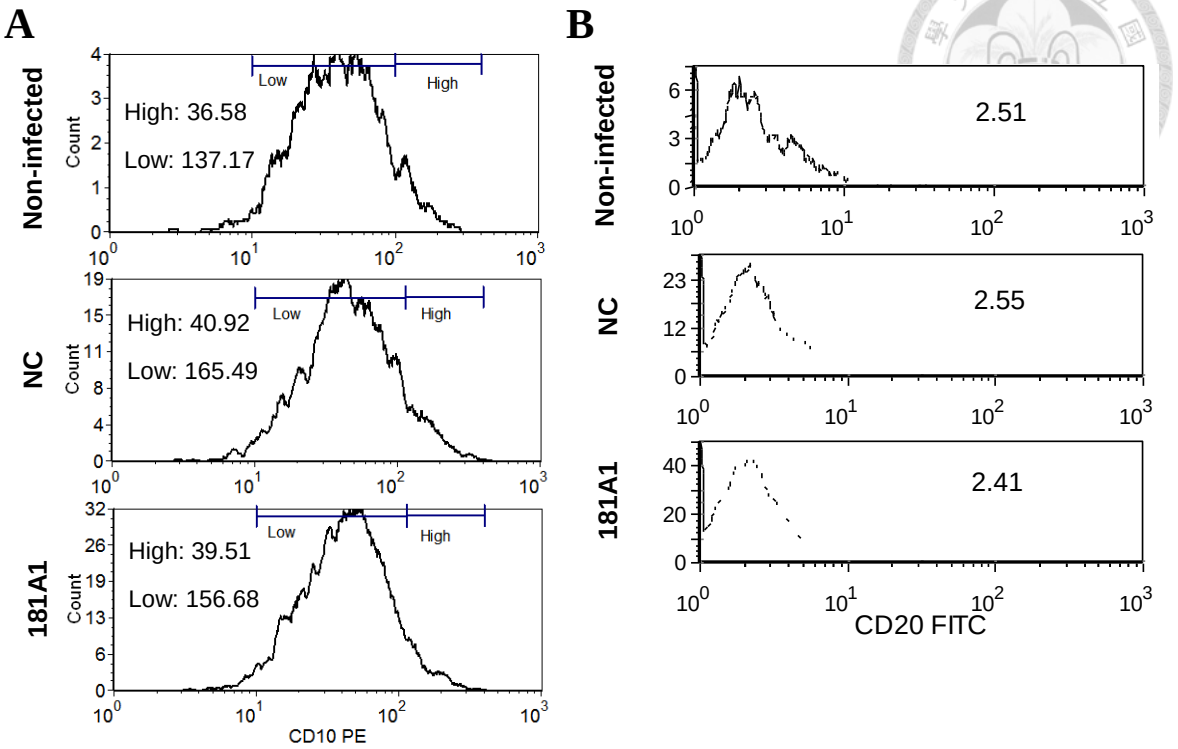

C

	Non-infected	NC	181A1
CD10^{High} (%)	9.95	10.1	6.95
CD10^{Low} (%)	88.16	87.98	91.05

Figure 29. Surface marker analysis of lentivirus-infected *ETV6/RUNX1*-positive primary ALL cells derived from patient #747.

After puromycin selection, lentivirus-infected patient cells were stained for cell-surface markers CD20-FITC/CD10-PE/CD34-PerCP/CD19-APC and analyzed by flow cytometry. Mean fluorescence intensity (MFI) of (A) CD10 and (B) CD20 expression in CD45^{+}CD19^{+} cells were as indicated in the graphics. (C) Detail analysis of the percentage of CD10^{High} and CD10^{Low} in CD45^{+}CD19^{+} lentiviral-transduced cells.

A

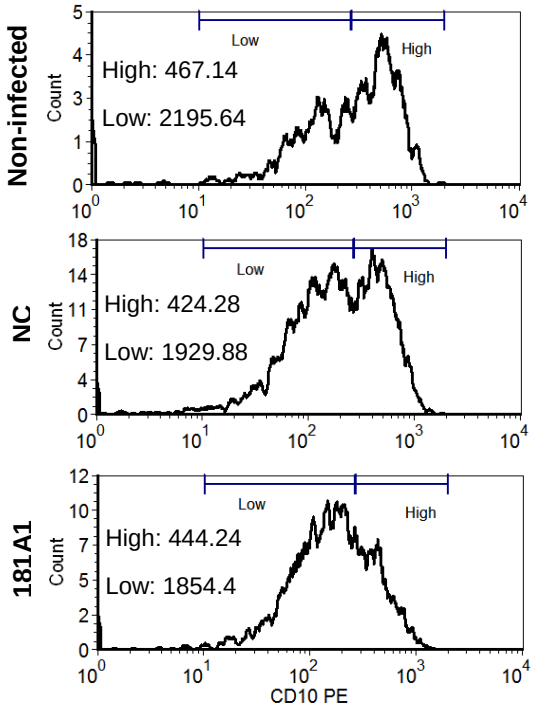

B

	Non-infected	NC	181A1
CD10^{High} (%)	42.77	40.09	29.48
CD10^{Low} (%)	54.17	58.1	69.02

Figure 30. Surface marker analysis of lentivirus-infected *ETV6/RUNX1*-positive primary ALL cells derived from patient #752.

After puromycin selection, lentivirus-infected patient cells were stained for cell-surface markers CD10-PE/CD34-PerCP/CD19-APC and analyzed by flow cytometry. Mean fluorescence intensity (MFI) of (A) CD10 expression in CD10^{High} and CD10^{Low} population of CD45^{+}CD19^{+} cells were as indicated in the graphics. (B) Detail analysis of the percentage of CD10^{High} and CD10^{Low} in CD45^{+}CD19^{+} lentiviral-transduced cells.

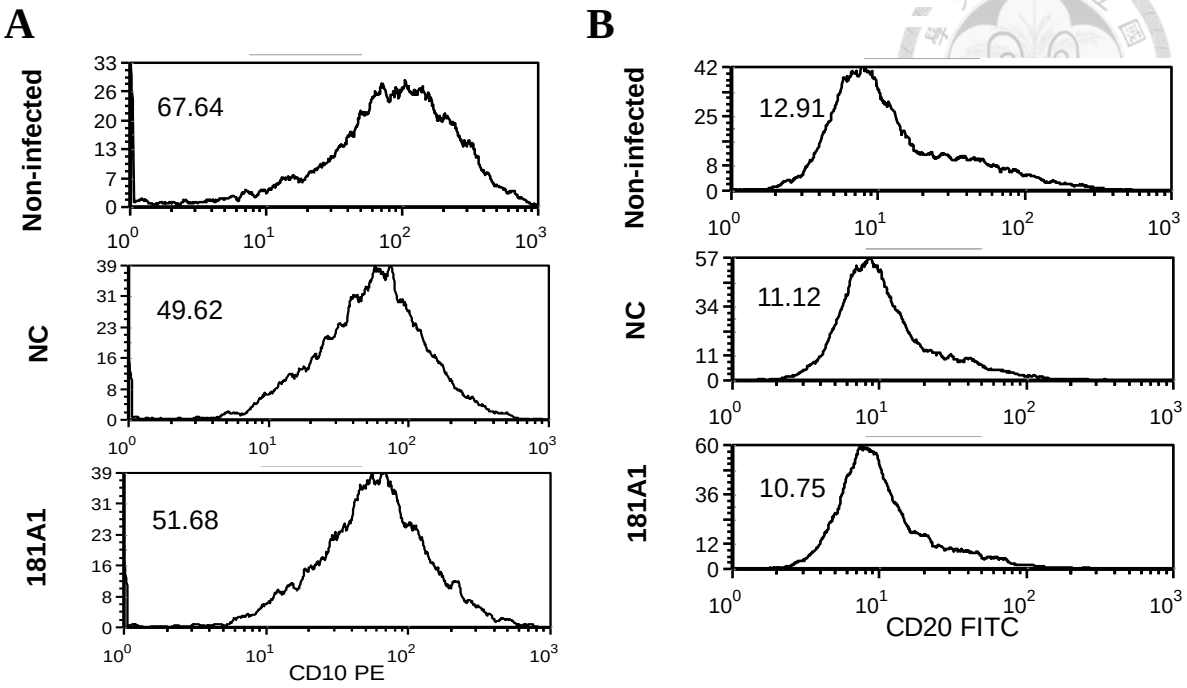

Figure 31. Surface marker analysis of lentivirus-infected *ETV6/RUNX1*-positive primary ALL cells derived from patient #745.

After puromycin selection, lentivirus-infected patient cells were stained for cell-surface markers CD20-FITC/CD10-PE/CD34-PerCP/CD19-APC and analyzed by flow cytometry. Mean fluorescence intensity (MFI) of (B) CD10 and (C) CD20 expression of $CD45^{+}CD19^{+}$ cells were as indicated in the graphics.

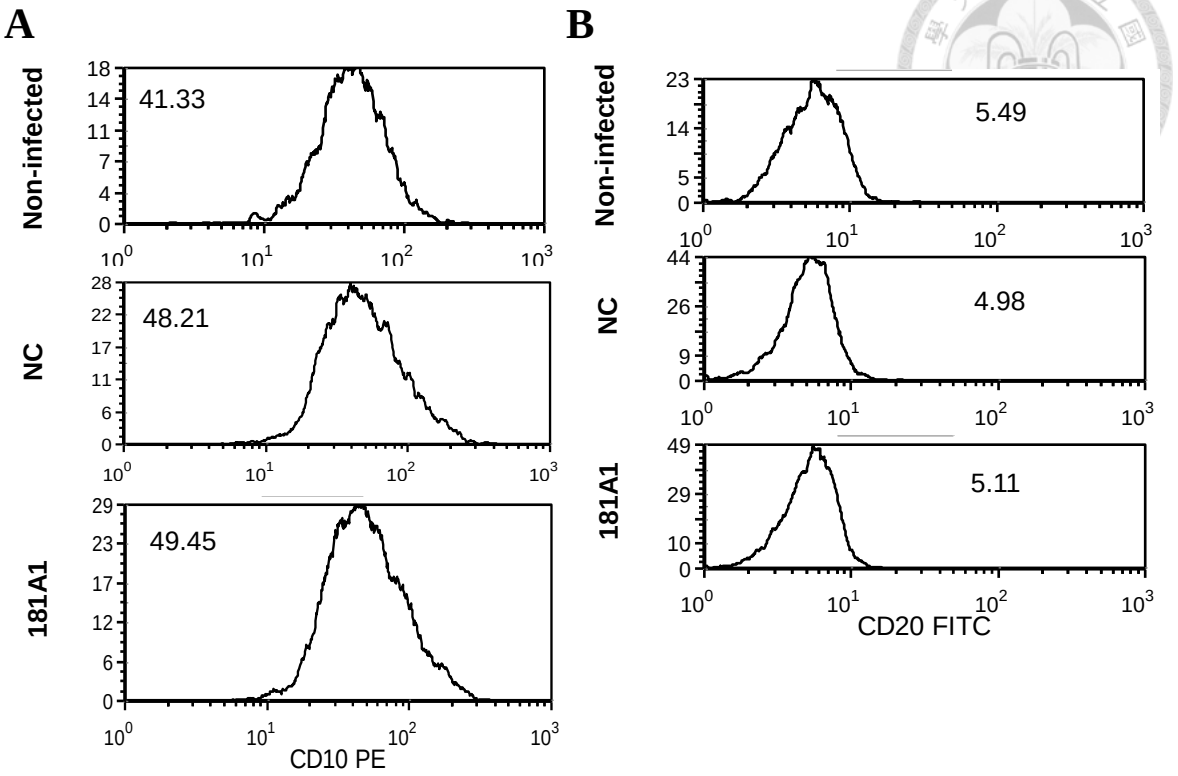

Figure 32. Surface marker analysis of lentivirus-infected *ETV6/RUNX1*-negative primary ALL cells derived from patient #754.

After puromycin selection, lentivirus-infected patient cells were stained for cell-surface markers CD20-FITC/CD10-PE/CD34-PerCP/CD19-APC and analyzed by flow cytometry. Mean fluorescence intensity (MFI) of (A) CD10 and (B) CD20 expression in $CD45^{+}CD19^{+}$ cells were as indicated in the graphics.

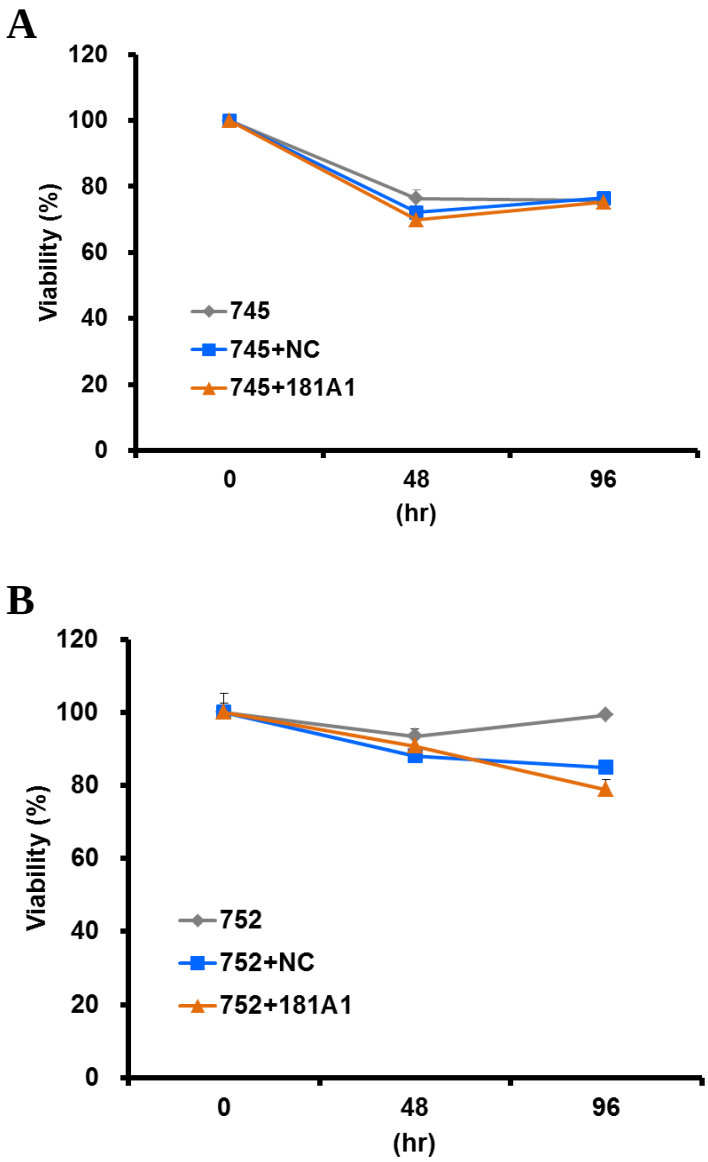

Figure 33. Viability of lentivirus-infected primary ALL cells derived from patient #745 (*E/R*-positive) and #752 (*E/R*-positive).

After puromycin selection, growth curve of lentivirus-infected primary ALL cells derived from (A) patient #745 and (B) patient #752 were determined as following: 10,000 cells per well were seeding in a 96-well plate and cultured for 48 and 96 hours, and then assessed with the MTT assay.

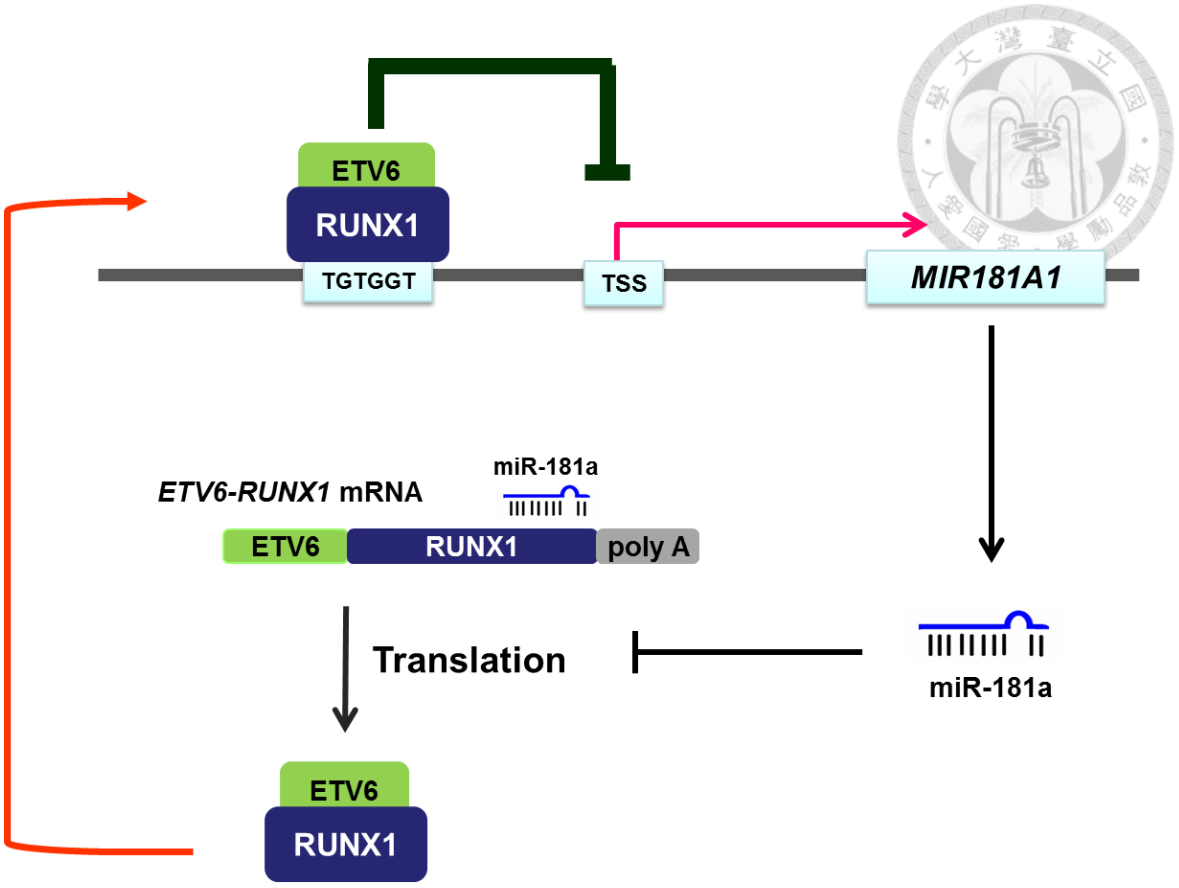

Figure 34. Schematic representation of the double negative loop comprising *ETV6/RUNX1* and *MIR181A1*.

In leukemia cells with frequent chromosome rearrangement t(12;21)(p13;q22), ETV6/RUNX1 oncoprotein occupies the putative RUNX1-binding site upstream of *MIR181A1* and restricts transcription by recruiting co-repressors such as HDAC3. This repression of *MIR181A1* expression consequently upregulates the target of miR-181a, ETV6/RUNX1—the oncoprotein itself, and enhances ETV6/RUNX1's oncogenic potential

Tables

Table 1. Primer sequences

for ChIP assay	
P1	
Forward	5'-CACCATACACAAACCACTTG -3'
Reverse	5'-GAGCTCTGTGTATGATTGTC-3'
P2	
Forward	5'-AG CTCAGTAGAGAGATGTTG-3'
Reverse	5'-GGCACACAAGCTAAA ACTTG-3'
GAPDH coding region	
Forward	5'-GAAGGTGAAGGTCGGAGT-3'
Reverse	5'-ACCTTGAG CTCTCCTTGC-3'
for SYBR-green qRT-PCR	
GAPDH	
Forward	5'-GAAGGTGAAGGTCGGAGT-3'
Reverse	5'-GAAGATGGTGATGGGATTTC-3'
PLAG1	
Forward	5'-ACATGGCTACTCATTCTCCTGA-3'
Reverse	5'-GTCGTGTGTATGGAGGTGATTC-3'
For *ETV6/RUNX1* Taqman qRT-PCR	
ENF301	5'-CTCTGTCTCCCCGCCTGAA-3'
ENR361	5'-CGGCTCGTGCTGGCAT-3'
ENPr341 (ABI probe)	5'-6FAM-TCCCAATGGGCATGGCGTGC-MGBNFQ-3'

Table 2. siRNA sequences

siE/R-siRNA 1	
Sense	5'-CCAUUGGGAGAAUAGCAGAAUGCAU-3'
Antisense	5'-AUGCAUUCUGCUAUUCUCCCAAUGG-3'
siE/R-siRNA 5	
Sense	5'-UGGGAGAAUAGCAGAAUGCAUACUU-3'
Antisense	5'-AAGUAUGCAUUCUGCUAUUCUCCCA-3'
Scramble-siRNA S	
Sense	5'-GAAGACGGUAAAUACGUUCGAUAAU-3'
Antisense	5'-AUUAUCGAACGUAUUUACCGUCUUC-3'

Table 3. Clinical features of the ALL patients included in miRNA expression profiling study

	Non t(12;21)		t(12;21)		
	n	%	n	%	*P*
Gender					
Female	20	50	4	40	0.728*
Male	20	50	6	60	
Onset age					
Mean ± SD	6.15 ± 3.23		5.77 ± 2.97		0.738†
Less than 10	36	90	9	90	1.000*
More than 10	4	10	1	10	
WBC count × k/μL					
Less than 100	32	80	9	90	0.665*
More than 100	8	20	1	10	
t(9;22)					
Non	37	92.5	10	100	1.000*
With	3	7.5	0	0	
Risk groups					
SR	20	50	6	60	0.899*
HR	9	22.5	2	20	
VHR	11	27.5	2	20	

SR: standard risk; HR: high risk; VHR: very high risk

*Calculated by Fisher's Exact test

†Calculated by Student's *t*-test

Table 4. The statistic signature of 17 miRNAs

miRNA*	Expression level, t(12;21)/non t(12;21)	*P*
hsa-miR-181a-1	0.254	<.00005
hsa-miR-92	0.327	0.002
hsa-miR-222	0.194	0.004
hsa-miR-342	0.461	0.004
hsa-miR-181d	0.524	0.004
hsa-miR-155	0.353	0.005
hsa-miR-423	0.371	0.005
hsa-miR-195	0.391	0.012
hsa-miR-130b	0.472	0.019
hsa-miR-221	0.098	0.024
hsa-let-7b	0.505	0.037
hsa-let-7a	0.527	0.037
hsa-miR-30e-3p	0.443	0.039
hsa-miR-19a	0.456	0.039
hsa-miR-660	0.525	0.045
hsa-miR-181c	0.385	0.046
hsa-miR-425	0.465	0.050

* Selected by differential expression in patients with or without t(12;21)

Table 5. The signature of 13 miRNAs/miRNA clusters and the locations of RUNX1 binding sites

miRNA/miRNA cluster	Location	Input (NCBI36)	TSS* (+1)	RUNX1 binding site†
hsa-miR-181a-1	1q32.1	chr1 197094905 197144905 −	197138675	-3845
hsa-miR-30e-3p	1p34.2	chr1 40942614 40992614 +	40947610	-3749, -3185, -2321
hsa-miR-425	3p21.31	chr3 49033146 49083146 −	49041875	-3879, -3488, -2863, -1349
hsa-miR-19a/92a-1	13q31.3	chr13 90750860 90800860 +	90798075‡	-242
hsa-miR-342	14q32.2	chr14 99595745 99645745 +	99601480	-1909, -1322, -548, +31
hsa-miR-195	17p13.1	chr17 6862065 6912065 −	6919137‡	-2916, -889
hsa-miR-423	17q11.2	chr17 25418223 25468223 +	25468010	-3293, -2389
hsa-miR-181c/d	19p13.13	chr19 13796513 13846513 +	13837455	158
hsa-miR-155	21q21.3	chr21 25818163 25868163 +	26934221‡	no binding site is found
hsa-miR-130b	22q11.21	chr22 20287270 20337270 +	20326560	-1999, -545
hsa-let-7a-3/7b	22q13.31	chr22 44837293 44887293 +	44846680	-3453, -1882
hsa-miR-221/222	Xp11.3	chrX 45490638 45540638 −	45518410	-3561, -675
hsa-miR-660	Xp11.23	chrX 49604494 49654494 +	49613885	-3396, -3320, +708

TSS, transcriptional start site. *TSS is predicted by CoreBoost_HM.

†RUNX1 binding site in the upstream 4kb and downstream 1kb of TSS.

‡TSS of host gene

Appendixes

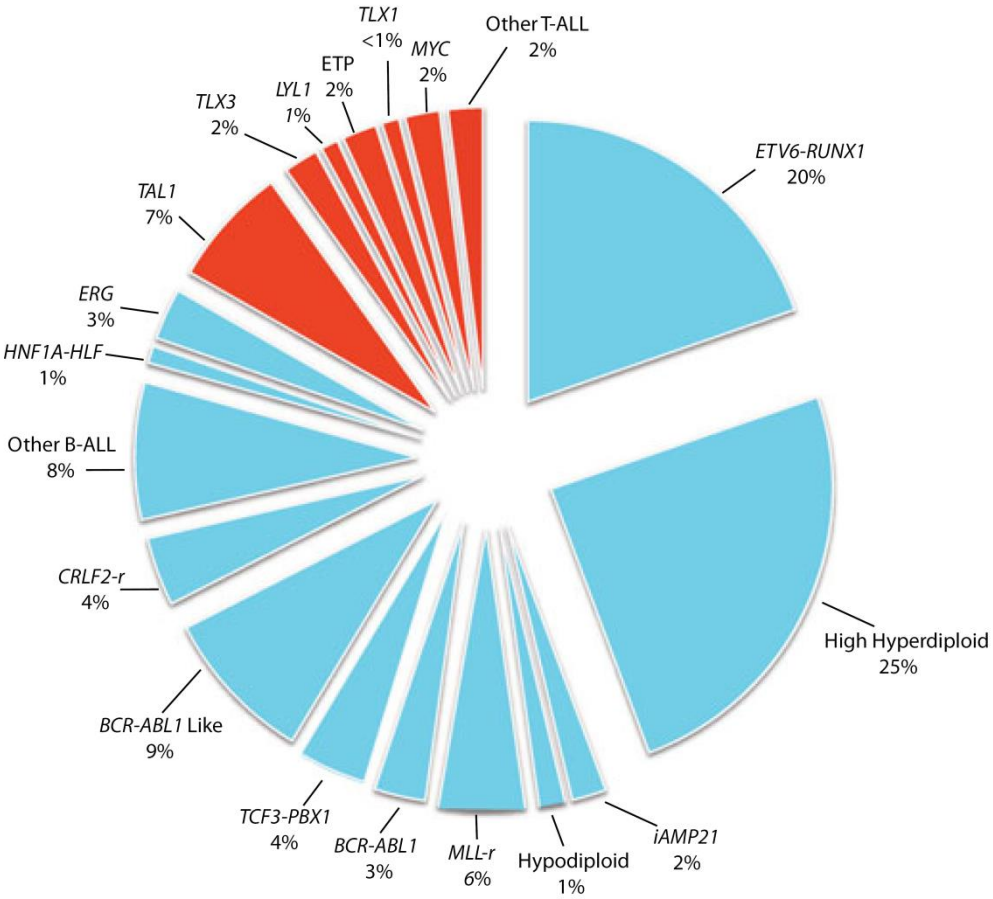

Appendix I. Frequency of cytogenetic subtypes of childhood ALL. Blue part: B-ALL; red part: T-ALL

Adapted from Teachey DT, Hunger SP. Predicting relapse risk in childhood acute lymphoblastic leukaemia. *British journal of haematology* 2013 Sep; **162**(5)**:** 606-620.

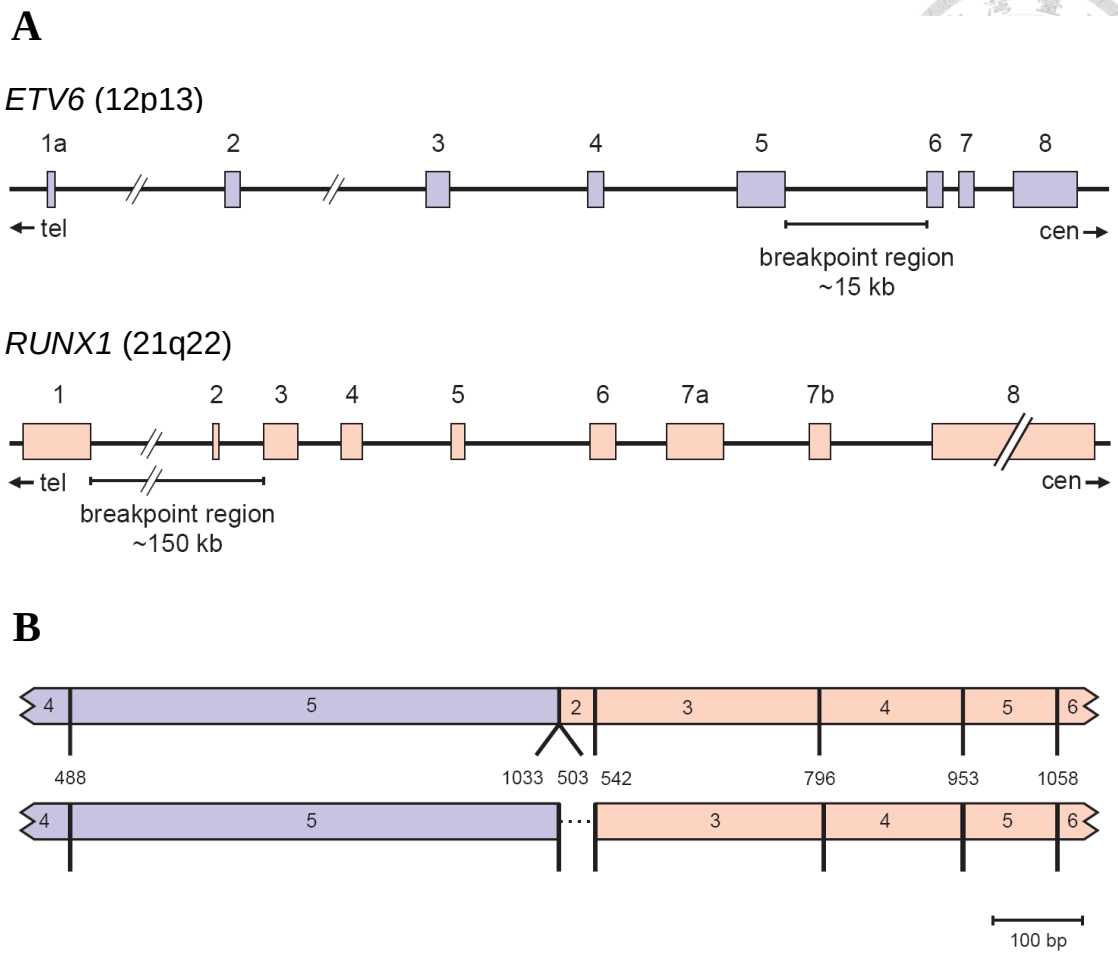

Appendix II. Schematic diagram of the exon/intron structure of the *ETV6* and *RUNX1* genes involved in t(12;21)(p13;q22).

Modified and adapted from van Dongen JJ, Macintyre EA, Gabert JA, Delabesse E, Rossi V, Saglio G, et al. Standardized RT-PCR analysis of fusion gene transcripts from chromosome aberrations in acute leukemia for detection of minimal residual disease. Report of the BIOMED-1 Concerted Action: investigation of minimal residual disease in acute leukemia. *Leukemia : official journal of the Leukemia Society of America, Leukemia Research Fund*, UK 1999 Dec; **13**(12): 1901-1928.

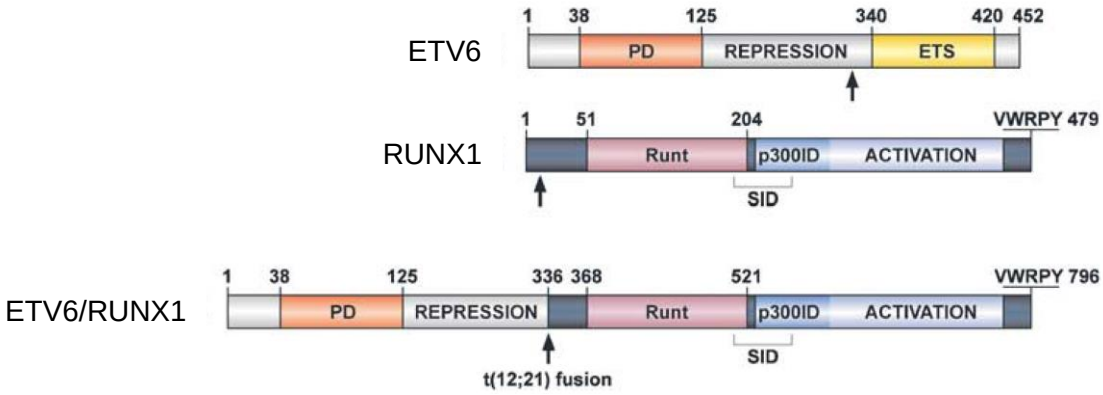

Appendix III. A schematic representation of the full-length ETV6, RUNX1 and ETV6/RUNX1 proteins. (PD: oligomerisation pointed domain, Repression: central repression domain, ETS: ETS DNA binding domain, RUNT: RUNT DNA binding domain, SID: mSin3A interaction domain, p300ID: a region reported to interact with the p300 HAT, Activation: transcriptional activation domain)

Modified and adapted from Zelent A, Greaves M, Enver T. Role of the TEL-AML1 fusion gene in the molecular pathogenesis of childhood acute lymphoblastic leukaemia. Oncogene 2004 May 24; 23(24): 4275-4283.

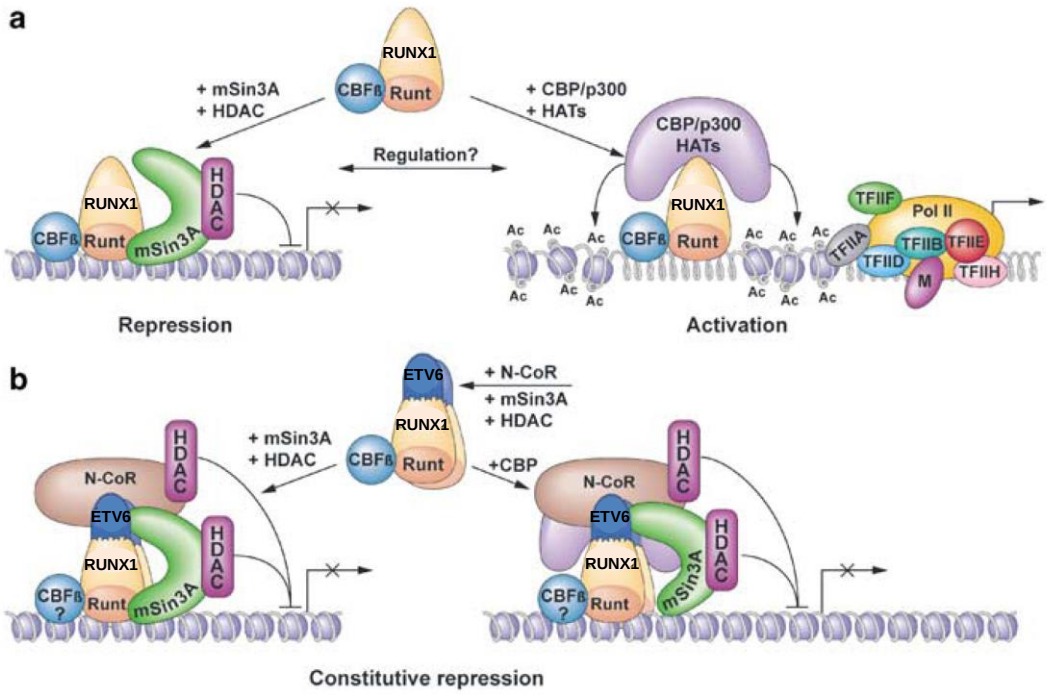

Appendix IV. A hypothetical model for the molecular mechanism of ETV6/RUNX1 action.

Modified and adapted from Zelent A, Greaves M, Enver T. Role of the TEL-AML1 fusion gene in the molecular pathogenesis of childhood acute lymphoblastic leukaemia. Oncogene 2004 May 24; 23(24): 4275-4283.

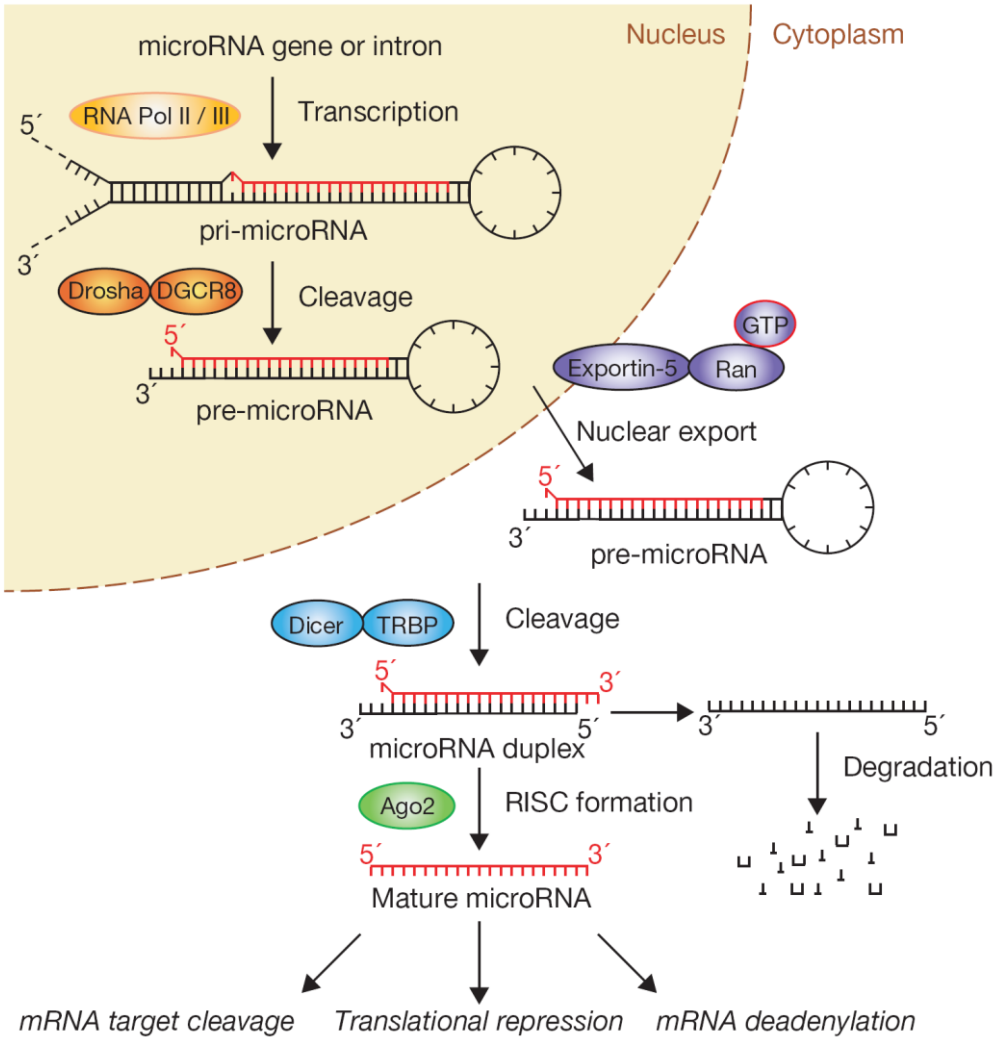

Appendix V. The canonical pathway of microRNA biosynthesis.

Adapted from Winter J, Jung S, Keller S, Gregory RI, Diederichs S. Many roads to maturity: microRNA biogenesis pathways and their regulation. Nature cell biology 2009 Mar; 11(3): 228-234.

The Second Part

Childhood Acute Lymphoblastic Leukemia Associated MicroRNAs: II. Establishment of *Mir151* conventional knockout mice

摘要

微核醣核酸在後轉錄階段可藉由負向調控編碼基因的表現，影響細胞的各種生理層面。目前已知微核醣核酸 151 會與宿主基因 *PTK2* 一起表達，在先前研究中則顯示微核醣核酸 151 與癌症及心臟肥大症相關，但整體來說，關於微核醣核酸 151 的報導相當少。儘管已有數個目標基因被發表，包括 *RhoGDIA*、*CCNE1*、和 *ATP2A2* 基因，微核醣核酸 151 的生理功能及病理角色仍不清楚。先前針對 60 個兒童急性淋巴性白血病檢體分析微核醣核酸表達，發現微核醣核酸 151 在前 B 細胞急性淋巴性白血病中表現量遠高於 T 細胞急性淋巴性白血病，為了解微核醣核酸 151 在此現象中扮演的角色，本研究利用基因重組工程技術產製微核醣核酸 151（*Mir151*）基因剔除小鼠並已確認在 DNA 及 RNA 表現上皆為 *Mir151* 缺失。本研究並進一步探討 *Mir151* 基因剔除鼠的表現型，發現年輕小鼠（小於 1 歲）的紅血球生成增加並伴隨腎臟紅血球生成素轉錄的上升，此現象在缺氧環境下更為顯著且可能與 Hif-α 的調控機制相關。在長期觀測結果中，我們發現 *Mir151* 缺失並未影響長期存活，但年紀較長的小鼠（大於 1.5 歲）中，有 33% $Mir151^{+/-}$ 及 23% $Mir151^{-/-}$小鼠產生自發性肺癌。本研究並更進一步利用 urethane 在年輕小鼠誘導肺癌產生，結果卻與預期不同，*Mir151* 缺乏在年輕小鼠身上具有保護作用。

統整上述結果，本研究揭露了微核醣核酸 151 先前未被發現的生理及病理角色，並為之後的研究提供新的研究方向。

關鍵字：微核醣核酸 151，基因剔除小鼠，紅血球生成素，慢性缺氧，自發性肺癌

Abstract

MicroRNAs (miRNAs) are the major key players to negatively regulate the expression of coding genes in post-transcriptional level and control almost all aspects of biology of the cells. *MIR151A* expresses a miRNA that co-expresses with *PTK2* gene and has been reported to be involved in cancers and cardiac hypertrophy. The description about *MIR151A* in previous reports is rare. Although several target mRNAs including *RhoGDIA*, *CCNE1*, and *ATP2A2* have been identified, the physiological function and pathological role of *MIR151A1* remains a puzzle. We have performed a miRNA expression profiling on 60 childhood ALL patients and identified miR-151 to be differentially expressed in B-ALL. To elucidate the role of miR-151 involved in this phenomenon, we generated and the *Mir151* conventional knockout mice using recombineering technology and confirmed the deficiency of *Mir151* gene on both DNA and RNA level. We further characterized phenotypes of *Mir151* knockout mice and found in young mice (< 1year) an increased erythropoiesis concordant with the elevated renal *Epo* transcription, which was more prominent under hypoxic and may associate with a Hif-α-regulated mechanism. In elder mice (>1.5 year), we found that *Mir151* deficiency did not affect the long-term survival, whereas spontaneous lung tumors were developed in 33% *Mir151*$^{+/-}$ and 23% *Mir151*$^{-/-}$ mice. We further performed a

urethane-induced lung cancer model on young N10F2 mice, however, an unexpected protective effect of was exerted in young mice deficient in *Mir151*.

Taken together, our results reveal the undiscovered physiological and pathological role of *MIR151A*, which may provide new aspects for future research.

Key words：miR-151，genetic knockout mice，erythropoietin，chronic hypoxia, spontaneous developed lung cancer

List of Figures

List of Tables

List of Appendix

Chapter 6. Introduction

6.1. MicroRNAs

MiRNAs are the major key players to negatively regulate the expression of coding genes in post-transcriptional level (1). These small non-coding RNA with 18–23 nucleotides in length arisen from cleavage of 70-100 nucleotide precursors are phylogenetically conserved and essential. Up to date more than 1,000 miRNA genes in the human genome have been validated (2). Besides, tissue-specific expression of miRNA was also observed (3). MiRNAs are estimated to regulate more than one third of all mRNA transcripts. RNA-induced silencing complex (RISC) directs miRNAs to hybridize with the 3′-UTR or coding domain sequence (CDS) of specific mRNA targets to enhance mRNA destabilization, degradation and/or inhibit translation for protein synthesis (4, 5). Most miRNA–mRNA targeting occurs through base pairing between a short sequence located at the 5′ end of the miRNA, called the seed sequence, and its mRNA target. This seed sequence, ranging from nucleotide positions 2–8 in the miRNA, largely defines the its downstream targets and hence is the basis of most target prediction programs (6).

In contrast to the promoter-based regulation of mRNA synthesis, miRNAs are regarded as moderate modulators of the transcriptional response, fine-tuning gene

expression largely by negative regulation in a process that requires stoichiometric binding to mRNA targets (2). Since one individual mRNAs can be targeted by multiple miRNAs, and a single miRNA can target hundreds of mRNAs, it also making these small RNAs powerful regulators of cell fate decisions. In addition, aberrant expression of miRNAs has emerged to be a common feature of cancers, as their roles in cancers can be either tumor suppressors or oncomirs dependent on cancer types (7-10).

6.2. microRNA 151a

microRNA 151a is a miRNA that co-expresses with focal adhesion kinase (FAK, official gene name: *PTK2*) and has been reported to be involved in cancer (10-13) and cardiac hypertrophy (14). Research reports focusing on this miRNA are rare in relative to other well-studied miRNAs, such as miR-221 and miR-222, miR-125b, and miR-181.

6.2.1. Human *MIR151A* gene

Human *MIR151A* gene is located on chromosome 8q24.3, residing within intron-22 of the host gene encoding protein tyrosine kinase 2 (*PTK2*), also known as focal adhesion kinase (FAK), a key signaling molecule involved in the regulation of cell motility (Figure 1; Appendix VI). Only one exon existed in *MIR151A* gene and expressed a pre-miRNA with 90 bp in length referred to hsa-mir-151. According to

Sanger miRBase database, hsa-mir-181a-1 is further processed into two mature products including miR-151a-3p and -5p (Figure 1A).

6.2.2. Clinical association and target mRNAs of *MIR151A*

A previous report and our unpublished data, which used the different microarray platform, have shown that in patients with T-cell ALL compared to B-cell ALL, miR-151 was identified as discriminative (15). In cancer associated studies, down regulation of miR-151 was seen in the abnormal miRNA expression profile in mononuclear and $CD34^+$ cells from patients with chronic myeloid leukemia (CML) compared with healthy controls (16). It has been reported that chromosome 8q24.3 is a common recurrent amplification region in hepatocellular carcinoma (HCC). Previous study showed that increasing *MIR151A* expression was correlated with intrahepatic metastasis and *MIR151A* exerted this function through directly targeting *RhoGDIA* by miR-151-5p, a putative metastasis suppressor in HCC (10). Also in prostate cancer, copy number gain of the *MIR151A* gene in the primary tumor may indicate the presence of metastatic disease (17). Another target mRNA Cyclin E1 (*CCNE1*) gene, was demonstrated to be regulated by miR-151-5p in nasopharyngeal carcinoma, and a miR-151-5p binding site polymorphism in the 3′-UTR of *CCNE1* gene was involved in susceptibility and stage of nasopharyngeal carcinoma (18). Although both of

miR-151-5p and 3p can be detected in tissues, the function of miR-151-3p remained unclear for a long time. Until recently the first target mRNA of miR-151-3p was published. miR-151–3p was shown to directly target *ATP2A2*, a gene encoding for a slow skeletal and cardiac muscle specific Ca^{2+} ATPase (SERCA2) thus downregulating slow muscle gene expression in skeletal muscle cells (19).

6.2.3. Mouse *Mir151* gene

Mouse *Mir151* gene, which is located on chromosome 15 and resides within intron-22 of the host gene (*PTK2*), is highly homologous to human *MIR151* gene. It also generates two mature miRNA products, miR-151-5p and 3p (Figure 1B). The seed sequences are highly conserved in human and mouse, although there is a little difference in 3p sequence outside the seed region (Figure 1C).

6.3. Research motive and the strategy

The discovery of miRNAs as modifiers of disease processes can help identify cellular effectors and define molecular mechanisms of disease processes. Unlike the widely studied miRNAs, miR-151-associated reports is limited thus the physiological and pathological role of *MIR151* remains extremely unclear, and a genetic knockout mice may provide an opportunity to investigate the function of *MIR151*. In this study,

we established the conventional knockout mice lack of *Mir151* in the attempt to investigate the physiological function of *Mir151*, and whether *Mir151* participates in cancer biology.

Chapter 7. Materials and Methods

7.1. Materials

7.1.1. Reagents

Product name	Company
1 kb DNA Ladder	Bertec
100 bp DNA Ladder	Bertec
2x TaqMan Universal PCR Master Mix	Applied Biosystems
Agar, Bacteriological	ALPHA biosciences
Agarose	Invitrogen
Ampicillin	Sigma
Boric acid	J.T.Baker
BPB	Sigma
Calf Intestine Alkaline Phosphatase (CIP)	Fermentus
Chlorofrom	J.T.Baker
$CoCl_2$	Sigma
Dithiothreitol (DTT)	Invitrogen
dNTPs	GeneDirex
EDTA	J.T.Baker
EDTA•K_2	J.T.Baker
Ethanol	Sigma
Ethidium Bromide (EtBr)	Amersco
Formalin	Sigma
Glycerol	Mallinckrodt
Isopropanol	Fluka
Phosphate buffered saline (PBS)	Biowest
T-PER buffer	Thermo
Tris base	J.T.Baker
Tryptone	ALPHA biosciences
Urethane	Sigma
Yeast extract	ALPHA biosciences

7.1.2. Kits

Kit	Company
FastStart universal SYBR green master (ROX)	Roche
FavorPrep plasmid extraction midi kit	FAVORGEN
FavorPrep plasmid extraction mini kit	FAVORGEN
Qiagen Plasmid Maxi kit	Qiagen
RnaseOut	Invitrogen
SuperScript III Reverse Transcriptase	Invitrogen
T4 DNA Ligase	NEB
Taq DNA polymerase	Geneaid
TaqMan miRNA expression assay	Applied Biosystems
TaqMan® miRNA RT kit	Ambion
Trizol reagent	Invitrogen

7.1.3. Vectors

Vector	Source
pL253	TMMC, NTU
pL451	TMMC, NTU
pL452	TMMC, NTU

7.1.4. Equipment

Instrument name	Company
7300 Real-Time PCR machine	Appied Biosystems
Abbott Cell-Dyn 3700	GMI
AllegraTM 21R centriguge	Beckman Coulter
Analytical balance (TE124s)	Sartorius
Avanti® J-E high speed centrifuge	Beckman Coulter
Eppendorf microcentriguge (F45-24-11)	Eppendorf
GeneAmp PCR machine	Appied Biosystems
Hitachi 7170A Automatic Analyzer	HITACHI
hypoxia chamber	homemade
LAB ROTATOR	Digisystem
Nanodrop	Thermo

7.2. Methods

7.2.1. Targeting vector construction

The recombineering technology (20) was used in the construction of targeting vector for *Mir151* deletion (Appendix VII). BAC (Bacterial artificial clone) carrying isogenic genomic DNA of *Mir151* (bMQ-355P20) under the 129sv/J genetic background was purchased from Source BioScience LifeSciences. The sequences used for homologous recombination were amplified from the BAC using PCR (AB and YZ fragment, see Appendix VIII) and then clone into pL253 vector, called “Vector A”. Vector A was linearized by restriction enzyme digestion and co-transformed with bMQ-355P20 BAC into EL350 E.coli by electroporation. Vector A which retrieved the chromosomal fragment from BAC through homologous recombination was called “Retrieve A”. To insert the loxP sequences into the flanked regions of *Mir151* gene, homologous DNA fragment CD/EF and GH/IJ were cloned into pL452 and pL451 vector, called “Vector B” and “Vector C”, respectively (Appendix VIII). “A+B” was produced by transforming the “Retrieve A” and “Vector B” together into EL350 E.coli and the loxP-Neo^{r}-loxP sequence originated form Vector B would integrate into the 3′ end of *Mir151* through homologous recombination. Next, the addiction of Arabinose induced Cre recombinase

expression in EL350 E.coli and deleted one of the loxP site and Neo^r, called “A+B-B”. With similar principle, the introduction of Frt-PGK-Neor-Frt-loxP sequence from “Vector C” into 5′ end which called “A+B-B+C” was performed in the next. Finally, after linearized the “retrieve A+B-B+C” with Not I restriction enzyme, the targeting vector containing neomycin resistance gene and thymidine kinase for positive and negative selection in ES cell culture was ready for ES cell targeting. The primer sequences used for targeting vector construction were shown in Table 1.

7.2.2. Gene targeting of ES cells and generation of *Mir151* conventional knockout (KO) mice

The E14TG2a (HPRT-) ES cell line was cultured, propagated, and transfected with the targeting construct by electroporation. HAT (0.1mM hypoxanthine, 4μM aminopterin, and 0.16 mM thymidine) and ganciclovir (10 μM) was used to select for ES cell colonies grown from electroporation. Surviving cell colonies were isolated, established as clones, and genotyped by Southern blotting to ensure homologous recombination. Southern blotting and genomic DNA isolation were performed following standard procedures to identify the desired ES cell clones. The correct clones were subsequently introduced into blastocysts of C57BL/6J mice by microinjection. Chimeric mice were bred with wild-type (WT) C57BL/6J mice to obtain heterozygous first generation

(B6129-N1F1) mice, which were intercrossed to generate homozygous N1F2 mice. *Mir151* heterozygous N1F1 male mice were also backcrossed with C57BL/6JNarl female mice for ten generations and performed speed congenic at N4 to obtained *Mir151* conventional knockout mice on a C57BL/6JNarl background. Genotyping of N1F2 mice was performed by Southern blotting and by PCR. The PCR reaction mixture contained 0.3- to 1-μg tail DNA, 200 μM dNTPs, 200 nM each of the primers, and 1 U Taq DNA polymerase in 25 μL reaction buffers supplied by the manufacturer. The primer sequences used for genotyping were shown in Table 1. ES cell gene targeting, excision of neomycin resistance gene, blastocyst injection, and chimera production were supported by the Transgenic Mouse Model Core Facility of the National Research Program for Genomic Medicine, the National Science Council of Taiwan.

7.2.3. Animals

N1F2 male and female mice were used in all of the experiments in this study. N10F2 male mice (6~8 weeks) were only used in urethane induced model. All mice were housed and bred in the Laboratory Animal Center of the Department of Bioscience Technology of Chung Yuan Christian University (CYCU). The mice (n = 5/cage) were maintained in a room with a constant temperature of 22 ± 1℃, relative humidity of 55 ± 10% and 12-h light/dark cycle, and fed standard rodent chow and purified distilled

water ad libitum. Mice for long-term observation were kept and weighed every month until the end of their life. The dead bodies of mice were collected, dissected, taken pictures, and major organs including liver, heart, spleen, lung, kidney were preserved in 10% formalin. All animal experiments were approved by the Institutional Animal Care and Use Committee of CYCU.

7.2.4. RNA preparation and reverse transcription

Tissues including lung, heart, brain, kidney, spleen, liver, thymus, and lymph node were collected, washed with cold 1X PBS, and homogenized in T-PER buffer. Total RNA was extracted using Trizol reagent according to the manufacturer's instructions. For mRNA qRT-PCR, 5μg total RNA was first reverse transcribed into cDNA by reverse transcriptase using oligo dT and random hexamer as primers. For miRNA detection, the TaqMan® miRNA RT kit and RT primers from Taqman miRNA assay were used following the manufacturer's instructions.

7.2.5. Quantitative real-time PCR

Expression of miR-151-3p and 5p were determined by TaqMan real-time PCR using Taqman microRNA assays. All miRNA assays were run concurrently with a calibration control, snoRNA-202, and were run in triplicate. Transcript of *Ptk2, Epo, Phd3, Pgk,*

Vegf A and the reference gene *Gapdh* was determined by SYBR Green real-time PCR and measured in two independent assays. The primer sequences used for qRT-PCR were shown in Table 1.

7.2.6. Complete blood counts and differential counts

Whole blood was collected by puncture of the retro-orbital plexus of mice using capillary tubes with anticoagulant. Complete blood counts (CBCs) and Differential counts (DCs) was performed on EDTA・K_2-anticoagulated blood using an automated counting device with the aid of Taiwan Mouse Clinc's service.

7.2.7. Clinical chemistry

Whole blood was collected by puncture of the retro-orbital plexus of mice using capillary tubes without an anticoagulant. Serum was diluted five times with distilled water and serum blood chemistry was analyzed by an automated device. Parameters analyzed included levels of total protein , albumin (ALB), globulin, total bilirubin (BUN), aspartate aminotransferase (GOT), alanine aminotransferase (GPT), alkaline phosphatase (ALP), amylase, lactate dehydrogenase (LDH), and γ -glutamyltransferase, triglyceride (TG), total cholesterol (T-CHO), high density lipoprotein-cholesterol (HDL-C), Na, K, Cl, Mg, P, Ca, Uric acid (UA), Fe, UIBC, and

TIBC

7.2.8. Chronic hypoxia

N1F2 male mice of each genotype (18-20 weeks, weighing 33-54 g) were separated into two groups. One group (hypoxic mice) was exposed to 10% O_2 in a well-ventilated, temperature-controlled hypoxia chamber for 6 hours. The other control group (normoxic mice, control) which exposed to 10% O_2 for 0 hour was maintained under ambient normoxic conditions. At the end of exposure, mice were sacrificed, the kidneys were quickly removed and then performed RNA extraction immediately or rapidly frozen in liquid nitrogen. The frozen organs were stored at –80℃.

7.2.9. $CoCl_2$ treatment

N1F2 male mice of each genotype (34-36 weeks, weighing 34-57 g) were separated into two groups and injected i.p. with 60 mg/kg cobaltous chloride ($CoCl_2$) solution in 1X PBS or 1X PBS as control group. Animals were sacrificed 6 hours after $CoCl_2$ injection. The kidneys were quickly removed and performed RNA extraction immediately or rapidly frozen in liquid nitrogen. The frozen organs were stored at –80℃.

7.2.10. Tumor analysis

Lung tissues were fixed in 10% formalin followed by 70% EtOH. Tumors were counted and measured. The individual tumor size was measured. Tumors were graded on a 4-stage grading system: macroscopic normal and on hematoxylin and eosin (H&E) slides with typical adenomatous hyperplasia as grade I; nodule $\leqq$ 2 (smaller than 1/4 lobe), normal part is still remained in the same lobe as grade II; nodule > 2 or larger than 1/4 lobe, normal part is still remained in the same lobe as grade III; Completely loss of normal tissue in the same lobe as grade IV.

7.2.11. Urethane-induced lung cancer model

The *Mir151*$^{+/+}$, *Mir151*$^{+/-}$, and *Mir151*$^{-/-}$ mice (N1F2 n=7 for each group, N10F2 n = 12 for each genotype), matched by age (N1F2 23 weeks, N10F2 6–8 weeks old) and weight (N1F2 31-47 g, N10F2 16–19 g) were used. These mice were injected i.p. with 1 mg/g body weight urethane in normal saline once weekly for 6 (N1F2) or 4 (N10F2) consecutive weeks. At the end of the experiments, mice were sacrificed and dissected their lungs. Lung tumor numbers and sizes were evaluated under a dissecting microscope. Tumors were isolated from the normal part and quickly frozen in liquid nitrogen for further analysis.

7.2.12. Histological analysis

All tissues were fixed in 10% buffered formalin for 24 h, embedded in paraffin, cut into 5–7-μm sections, and stored at 4°C in the dark. For histological analysis, the sections were dewaxed before staining with hematoxylin and eosin (21). All kidney sections were examined by Dr. SL Lin (Nephrology, Department of Medicine, National Taiwan University Hospital), and lung sections were examined by Dr. WC Lin (Department of Pathology, National Taiwan University Hospital)

7.2.13. Statistical analyses

Statistical analysis was performed by using ANOVA or Mann-Whitney test of Prism software (GraphPad, California, USA). Data are expressed as mean with SDs. A value of $p<0.05$ was considered significant.

Chapter 8. Results

8.1. Generation and identification of *Mir151* conventional knockout mice

8.1.1. Generation of *Mir151* conventional knockout mice

Targeting vector replaced a ~15.2 kb genomic DNA sequence covering part intron 22 of *Ptk2* gene and *Mir151* by homologous recombination. To generate *Mir151* conventional knockout (KO) allele, the targeted ES cells were transfected with plasmid encoding Cre recombinase (Figure 2). The ES cells carrying KO allele were injected to E3.5 blastocysts from 129sv/J strain. Chimera mice bearing over 90% coat color chimerism were obtained. The male chimera mice were bred with C57BL/6JNarl female mice to yield N1F1 pups with germline transmission. Heterozygous N1F1 mice were then intercrossing to generate N1F2 mice with each genotype ($Mir151^{+/+}$, $Mir151^{+/-}$, and $Mir151^{-/-}$) for characterization. To obtain *Mir151* conventional knockout mice on a C57/BL6JNarl background, we also backcrossed the N1F1 male mice with C57/BL6JNarl female mice for ten generation.

8.1.2. Identification of gene status in DNA and RNA level

We have designed a multiplex PCR method to identify three genotype

simultaneously in one reaction (Figure 3A). Three primers including a forward primer specific to wild type (WT) allele (m151F2), a forward primer specific to KO allele (m151F3), and a common reverse primer (m151R) were used. The amplicon size of WT and KO allele was 393 bp and 494 bp, respectively. The genotype was confirmed by Southern blotting (Figure 3B) and PCR method was used in routine (Figure 3C).

To determine the expression of *Mir151* in major organs, the tissues derived from N1F2 mice and a Taqman qRT-PCR was applied. We found that both miR-151-5p and 3p were enriched in heart and lung, while the hematopoiesis-associated organs including liver, spleen, thymus, and lymph node expressed relative low level of *Mir151* (Figure 4A). We also confirmed the ablation of mature miR-151 expression, including 3p and 5p (Figure 4B). Undisrupted *Ptk2* transcription after deletion of *Mir151* was demonstrated by SYBR green qRT-PCR using the primer set specific to the exon flanked to *Mir151* (Figure 4C).

8.2. Characterization of *Mir151* conventional knockout mice

8.2.1. *Mir151* is not essential to survival

We have collected 361 N1F2 pups and recorded their survival at day 10 after birth. The distribution of three genotype was $Mir151^{+/+}$: $Mir151^{+/-}$: $Mir151^{-/-}$ = 1 : 1.91 : 0.92 (Table 2), that was nearly identical to Mendel's first law (1 : 2 : 1). Our result indicates

that *Mir151* loss has no significant deleterious effects on survival. We also found that *Mir151*$^{-/-}$ knockout mice were viable, developed well, and fertile.

8.2.2. A kinetic change of erythropoiesis

We have generated a cohort including 10 *MiR151*$^{+/+}$ and 9 *MiR151*$^{-/-}$ male N1F2 mice, the body weight was measured twice a week, and examined the complete blood count (CBC) every months. We found that *MiR151*$^{-/-}$ mice showed a significantly higher RBC count, hemoglobin concentration, and hematocrit during the age between 4 to 8 months, compared with their *MiR151*$^{+/+}$ littermates (Figure 5). This alteration was not continuously persisted in *MiR*151$^{-/-}$ mice and disappeared after 9 months. We also examined the clinical chemistry (age: 6~8 months), however, we did not found any significant alteration in *MiR*151$^{-/-}$ mice (Table 3). Overall, we observed that the RBC count, hemoglobin, and hematocrit kept homeostasis in *MiR151*$^{+/+}$ mice, but were induced and kept in higher value between the age of 4-8 months and accompanied by gradually decline in *MiR151*$^{-/-}$ mice until the last time point of the experiment (1-year-old).

8.2.3. Elevated renal *Epo* mRNA level in young *MiR151*$^{-/-}$ mice

Erythropoiesis is regulated by erythropoietin (Epo), a 30.4 kDa glycoprotein

hormone known as the master regulator of red blood cell production through promoting erythroid progenitor cell viability, proliferation, and differentiation (22). Production of Epo is tightly regulated by development, tissue-specific, and physiological signals. It is produced by hepatocytes in the embryonic stage, and during the late gestation the site responsible to Epo production switches form the fetal liver to the kidney (23). Because the erythropoietin synthesis is dependent on the transcriptional activity of *Epo* gene (24), we analyzed the transcript level of renal and hepatic *Epo* in mice with age corresponding to 3, 6, and 9 months (Figure 6). In agreement with the CBC result, an expected up-regulation of renal *Epo* transcription was detected in *MiR151*$^{-/-}$ mice at 6 months old but not in *MiR151*$^{+/+}$ littermates, whereas the hepatic *Epo* mRNA remained at low level.

8.2.4. Induction of renal *Epo* by chronic hypoxia

Epo is highly sensitive to the balance between oxygen supply and demand. A previous study using isolated rat kidneys with hypoxic perfusate has demonstrated the increased renal Epo secretion (25). To enhance *Epo* expression, we performed chronic hypoxia using the hypoxia chamber (Fig. 7) and evaluated the induction of *Epo* transcription (Fig. 8). Mice were exposed to 10% O_2 for 0 and 6 hours. At this age, *Epo* transcripts at basal level were already elevated in *MiR151*$^{+/-}$ and *MiR151*$^{-/-}$ mice

(*MiR151*$^{+/+}$, *MiR151*$^{+/-}$, and *MiR151*$^{-/-}$ were 1, 2, and 3.5 fold, respectively). Low oxygen level significantly enhanced *Epo* transcription in all genotypes after 6 hours exposure to hypoxia (by ~20-fold). It is interesting that hypoxia-induced increase of *Epo* mRNA in all genotypes demonstrated a relative high and regular manner which was identical to normoxic condition (0 hour) (*MiR151*$^{+/+}$, *MiR151*$^{+/-}$, and *MiR151*$^{-/-}$ were 1, 2, and 3.5 fold, respectively).

8.2.5. No increase in renal Epo-producing cells in *MiR151*$^{-/-}$ mice

The understanding of which cells produce Epo in kidneys was not clarified until the use of genetically modified mice which help to identify that interstitial fibroblasts in the cortex and outer medulla are renal Epo-producing cells (26). In the progression of renal fibrosis, a common feature of chronic kidney disease (CKD), interstitial fibroblasts will differentiate into myofibroblasts which are the major collagen producing cells. During the initial stage of renal fibrosis, interstitial fibroblasts will proliferate concordant with increased *Epo* expression, and then lost the Epo producing ability when become myofibroblasts, resulting in renal anemia at the end stage of the disease. To elucidate whether the kinetic change of *Epo* level in *MiR151*$^{-/-}$ mice was duo to undergo renal fibrosis, the histological analysis of kidney section was performed (Figure 9). However, the proliferation of interstitial fibroblasts at 6 months was not observed and

mice were free from renal fibrosis when 9 months

Taken together, our data suggests that *MiR151* may have a role in regulating renal *Epo* transcription through an unknown mechanism.

8.2.6. Increase of Hif-α target gene expressions in young *MiR151*$^{-/-}$ mice

The mechanisms controlling the expression of the *Epo* gene is oxygen-dependent. Increase of Epo synthesis in response to hypoxic stimuli is also based on enhanced transcriptional activity of the *Epo* gene, and hypoxia-inducible factors (HIFs) are responsible for the linkage between changes in tissue oxygenation and altered *Epo* transcription (23). Data from animal studies (27, 28) and clinical investigations (29, 30) showed that hypoxia-inducible factor-2α (HIF-2α) is the critical regulator of *Epo* under physiologic and stress conditions in adults. We speculated that *MiR151*$^{-/-}$ mice may undergo mild hypoxia because of the up-regulated *Epo* in kidney but not in liver. To address whether this alteration in *MiR151*$^{-/-}$ mice was mediated by Hif-α, we determined the expression of Hif-α target genes including *Epo*, *Phd3*, *Pgk*, and *Vegf A*, in kidney of 6-month-old mice (Figure 8). In comparison with *MiR151*$^{+/+}$ littermates, *Epo* and *Phd3* expression were significantly increased in *MiR151*$^{-/-}$ mice, while no difference was shown in *Pgk* and *Vegf A* gene. We also observed that the upregulated *Epo* mRNA level was most obvious and reversely correlated with the *MiR151* gene dosage. However, it is

unexpected that *MiR151*$^{+/-}$ has physiological higher *Pgk* and *Vegf A* mRNA levels.

8.2.7. Induction of *Epo* expression by $CoCl_2$ treatment

Under normoxic conditions, HIF-α subunits are degraded rapidly by the ubiquitin-proteasome pathway (31). To evaluate whether the high *Epo* transcription in *MiR151*$^{-/-}$ mice was associated with Hif-α expression in the kidney, we injected i.p. with $CoCl_2$, which is a chemical reagent that can stabilize Hif-α. Renal *Epo* expression was significantly increased in *MiR151*$^{-/-}$ mice after $CoCl_2$ treatment, while the induction in *MiR151*$^{+/+}$ was moderate (Figure 11).

Our data indicates that Hif-α may participate in the phenotype of increasing erythropoiesis observed in *MiR151*$^{-/-}$ mice.

8.3. Long-term observation of *Mir151* conventional knockout mice

8.3.1. No difference in survival

We generated a cohort of 124 N1F2 mice for long-term observation, including 58 males (*MiR151*$^{+/+}$, *MiR151*$^{+/-}$, and *MiR151*$^{-/-}$ were 18, 17, 23) and 66 females (*MiR151*$^{+/+}$, *MiR151*$^{+/-}$, and *MiR151*$^{-/-}$ were 21, 19, 26). These mice were kept without any invasive experiment and weighed every month until death. In the comparison with wild type littermate, the life span and survival in *MiR151*$^{+/-}$, and *MiR151*$^{-/-}$ mice were no

significant difference (Figure 12).

8.3.2. Spontaneous developed lung cancer in old *Mir151* knockout mice

The deaths of all of the N1F2 mice recruited in the long-term observation were naturally occurred. To elucidate the cause of death, we collected the dead bodies for dissection and further histological analysis as more as we could. The data from total 58 mice whose bodies remained intact were obtained. While some of the mice dead in infection, some were looked normal, we found that lung cancer was developed in 33% *MiR151*$^{+/-}$ (6/18) and 23% *MiR151*$^{-/-}$ mice (6/26) but not in wild type littermates (0/14) (Figure 13). The histological analysis showed that the subtype of lung cancer developed in *Mir151* knockout mice was adenocarcinoma. Tumors were further subdivided according to the severity (Table 4).

8.3.3. Increase number of urethane-induced lung tumors in elder *Mir151* knockout mice

The death of mice developed spontaneous lung cancer often occurred after 1.5 years. To speed up the development of cancer, we conducted a carcinogen-inducible lung tumorigenesis model with the i.p. injection of urethane, a known carcinogen (Figure 14). Urethane administration is shown to be reliably reproducible and

subsequent tumorigenesis develops in a time-dependent manner (32). N1F2 mice were used to performed this experiment. After 20 weeks of first injection, mice were sacrificed. All of the tumors were observed, measured, and dissected under dissecting microscopy (Figure 15). As expected, number of urethane-induced tumors in *Mir151* knockout mice were more than wild type littermates (Figure 16).

8.4. Depletion of *Mir151* protected young mice from urethane-induced lung cancer

To enhance the understanding of the role of *Mir151* in the initial stage of tumorigenesis, and to prevent from the disturbance duo to B6129 mixed genetic background, we performed the he urethane-induced lung cancer model on N10F2 mice (6~8 weeks) (Figure 17). After 36 weeks of first injection, mice were sacrificed and removed the lung quickly after heart perfusion. Tumors were subdivided according to the size, dissected, and separated from the normal part of the lung. Unexpectedly, we found the result was opposite to elder mice that the urethane-induced tumors in *Mir151* knockout mice were ameliorated compared to wild type littermates, and were demonstrated a decreasing manner associated with gene dosage (Figure 18).

Chapter 9. Discussion

9.1. Increased erythropoiesis in young mice

This study was initiated by the data of miRNA array profiling that we found miR-151 was differentially expressed in B-ALL rather than in T-ALL, thus we proposed that *Mir151* may have roles in hematopoiesis and performed continuous CBC/DC analysis on N1F2 mice. *Mir151* knockout mice were observed the increased erythropoiesis concordant with elevated renal *Epo* mRNA level without hepatic *Epo* expression. Besides, the clinical chemistry of *Mir151* knockout mice were normal in the comparison with littermate controls, indicating the transient increase of erythropoiesis was not caused by anemia. These finding let us hypothesized that *Mir151* knockout mice may undergo mild hypoxia and the phenomenon described above was the results of compensation. To address whether this alteration was mediated by Hif-α, known to regulate gene expression under hypoxic condition, we detected expression of Hif-α protein and Hif-α target genes in kidney under normoxia, hypoxia, and $CoCl_2$ treatment. Although *Epo* and *Phd3* were elevated in normoxia and the induction of *Epo* was robust in all conditions, we could not identify the increased of Hif-α protein duo to the unresolved trouble in methodology. Besides, the unexpected up-regulated *Pgk* and *Vegf*

A mRNA were seen in heterozygous but not homozygous knockout mice may duo to the sample size was too small.

Together, we speculate Hif-α and other underlying mechanism may participate in the phenotype of increasing erythropoiesis observed in young *MiR151* knockout mice.

9.2. Spontaneous developed and urethane-induced lung cancer in elder mice v.s. the protective effect of *Mir151* loss in young mice.

The different results of spontaneous and induced lung cancer developed in elder and young mice may be caused by many reasons. First, the age. As we speculate that *MiR151* knockout mice may undergo mild hypoxia inside their body, there may be more physiological damages such as hypoxia-induced reactive oxygen species (ROS) accumulated with time in elder mice. Second, *Mir151* may express in a space- and time-scale dependent manner. Although we have identified that *Mir151* is enriched in lung, we did not measure the dynamic expression of *Mir151* in lung tissue across their life. Third, multiple genes with opposite function can be regulated by *Mir151*. For instance, miR-151-5p regulates *RhoGDIA*, a putative metastasis suppressor in HCC (10). Another miR-151-5p target *CCNE1*, which encodes a G1 phase cyclin (Cyclin E) essential for S-phase entry, has been shown to trigger hyperplasia and lung adenocarcinoma in transgenic mice (18, 33). Besides, there must be more *Mir151* target

genes waiting for identifying. Forth, the difference in genetic background. Spontaneous developed and more serious carcinogen-induced lung cancer were observed in elder N1F2 mice which had mixed genetic background (50% C57BL/6J and 50% 129sv/J) and modifier genes may interfere the real impact of *Mir151* deficiency on phenotypes of these mice.

9.3. The potential application of *Mir151* knockout mice

The recent discovery of a miR-151-3p target gene *ATP2A2* (19), which encodes for a slow skeletal and cardiac muscle specific Ca^{2+} ATPase (SERCA2) has provide a new insight into the understanding of *MIR151A*. SERCA2 is essential for Ca^{2+} uptake during excitation–contraction coupling in cardiomyocytes. Impaired Ca^{2+} uptake resulting from decreased expression and reduced activity of SERCA2a is a hallmark of heart failure (34), and the efficacy of SERCA2a restoration has been proven in improving the disease (35-37). Due to the important role of SERCA2 in both healthy and disease hearts, and *Mir151* depletion in whole body has no significant deleterious effects on organogenesis and survival, it could be a future therapeutics.

Chapter 10. Conclusion and Prospective

In conclusion, our preliminary data obtained from N1F2 mice has revealed that *Mir151* is not essential to survival, the physiological effect of *Mir151* deficiency is mild, and has showed the inconsistent results of urethane-induced lung tumorigenesis compared with N10F2 mice. Using the *Mir151* conventional knockout mice with pure C57BL/6J genetic background, increasing the sample size, and giving appropriate stimulus to mice such as chronic hypoxia, carcinogen-, or oncogene-induced cancer model may contribute to understand the physiological function and pathological role of *Mir151* gene in the future.

In addition to conventional knockout mice, we have also generated the *Mir151* conditional knockout mice which can be used to specific deplete *Mir151* in the use of Cre recombinase driven by myocardial-specific promoter. It may provide an opportunity to confirm whether the *Mir151* regulates heart expressed SERCA2 *in vivo* and evaluate the therapeutic potential of miR-151 in heart failure.

Bibliography

1. Lagos-Quintana M, Rauhut R, Lendeckel W, Tuschl T. Identification of novel genes coding for small expressed RNAs. *Science* 2001 Oct 26; **294**(5543)**:** 853-858.

2. Friedlander MR, Lizano E, Houben AJ, Bezdan D, Banez-Coronel M, Kudla G, *et al.* Evidence for the biogenesis of more than 1,000 novel human microRNAs. *Genome biology* 2014; **15**(4)**:** R57.

3. Choudhury NR, de Lima Alves F, de Andres-Aguayo L, Graf T, Caceres JF, Rappsilber J, *et al.* Tissue-specific control of brain-enriched miR-7 biogenesis. *Genes & development* 2013 Jan 1; **27**(1)**:** 24-38.

4. Kim VN. MicroRNA biogenesis: coordinated cropping and dicing. *Nature reviews Molecular cell biology* 2005 May; **6**(5)**:** 376-385.

5. Fabian MR, Sonenberg N, Filipowicz W. Regulation of mRNA translation and stability by microRNAs. *Annual review of biochemistry* 2010; **79:** 351-379.

6. Subramanyam D, Blelloch R. From microRNAs to targets: pathway discovery in cell fate transitions. *Current opinion in genetics & development* 2011 Aug; **21**(4)**:** 498-503.

7. He L, Thomson JM, Hemann MT, Hernando-Monge E, Mu D, Goodson S, *et al.* A microRNA polycistron as a potential human oncogene. *Nature* 2005 Jun 9; **435**(7043)**:** 828-833.

8. Shi L, Cheng Z, Zhang J, Li R, Zhao P, Fu Z, *et al.* hsa-mir-181a and hsa-mir-181b function as tumor suppressors in human glioma cells. *Brain research* 2008 Oct 21; **1236:** 185-193.

9. Gatt ME, Zhao JJ, Ebert MS, Zhang Y, Chu Z, Mani M, *et al.* MicroRNAs 15a/16-1 function as tumor suppressor genes in multiple myeloma. *Blood* 2010 Oct 20.

10. Ding J, Huang S, Wu S, Zhao Y, Liang L, Yan M, *et al.* Gain of miR-151 on

chromosome 8q24.3 facilitates tumour cell migration and spreading through downregulating RhoGDIA. *Nature cell biology* 2010 Apr; **12**(4)**:** 390-399.

11. Lips EH, van Eijk R, de Graaf EJ, Oosting J, de Miranda NF, Karsten T, *et al.* Integrating chromosomal aberrations and gene expression profiles to dissect rectal tumorigenesis. *BMC cancer* 2008; **8:** 314.

12. Luedde T. MicroRNA-151 and its hosting gene FAK (focal adhesion kinase) regulate tumor cell migration and spreading of hepatocellular carcinoma. *Hepatology* 2010 Sep; **52**(3)**:** 1164-1166.

13. Uchida M, Tsukamoto Y, Uchida T, Ishikawa Y, Nagai T, Hijiya N, *et al.* Genomic profiling of gastric carcinoma in situ and adenomas by array-based comparative genomic hybridization. *The Journal of pathology* 2010 May; **221**(1)**:** 96-105.

14. Sayed D, Hong C, Chen IY, Lypowy J, Abdellatif M. MicroRNAs play an essential role in the development of cardiac hypertrophy. *Circulation research* 2007 Feb 16; **100**(3)**:** 416-424.

15. Fulci V, Colombo T, Chiaretti S, Messina M, Citarella F, Tavolaro S, *et al.* Characterization of B- and T-lineage acute lymphoblastic leukemia by integrated analysis of MicroRNA and mRNA expression profiles. *Genes, chromosomes & cancer* 2009 Dec; **48**(12)**:** 1069-1082.

16. Agirre X, Jimenez-Velasco A, San Jose-Eneriz E, Garate L, Bandres E, Cordeu L, *et al.* Down-regulation of hsa-miR-10a in chronic myeloid leukemia CD34+ cells increases USF2-mediated cell growth. *Molecular cancer research : MCR* 2008 Dec; **6**(12)**:** 1830-1840.

17. Barnabas N, Xu L, Savera A, Hou Z, Barrack ER. Chromosome 8 markers of metastatic prostate cancer in African American men: gain of the MIR151 gene and loss of the NKX3-1 gene. *The Prostate* 2011 Jun 1; **71**(8)**:** 857-871.

18. Liu Y, Cai H, Liu J, Fan H, Wang Z, Wang Q, *et al.* AmiR-151binding site polymorphism in the 3'-untranslated region of the cyclin E1 gene associated with nasopharyngeal carcinoma. *Biochemical and biophysical research communications* 2013 Feb 14.

19. Wei H, Li Z, Wang X, Wang J, Pang W, Yang G, *et al.* microRNA-151-3p regulates slow muscle gene expression by targeting ATP2a2 in skeletal muscle cells. *Journal of cellular physiology* 2015 May; **230**(5)**:** 1003-1012.

20. Liu P, Jenkins NA, Copeland NG. A highly efficient recombineering-based method for generating conditional knockout mutations. *Genome research* 2003 Mar; **13**(3)**:** 476-484.

21. Yu IS, Lin SR, Huang CC, Tseng HY, Huang PH, Shi GY, *et al.* TXAS-deleted mice exhibit normal thrombopoiesis, defective hemostasis, and resistance to arachidonate-induced death. *Blood* 2004 Jul 1; **104**(1)**:** 135-142.

22. Jelkmann W. Regulation of erythropoietin production. *The Journal of physiology* 2011 Mar 15; **589**(Pt 6)**:** 1251-1258.

23. Stockmann C, Fandrey J. Hypoxia-induced erythropoietin production: a paradigm for oxygen-regulated gene expression. *Clinical and experimental pharmacology & physiology* 2006 Oct; **33**(10)**:** 968-979.

24. Eckardt KU, Kurtz A. Regulation of erythropoietin production. *European journal of clinical investigation* 2005 Dec; **35 Suppl 3:** 13-19.

25. Pagel H, Jelkmann W, Weiss C. Erythropoietin production in the isolated perfused kidney. *Biomedica biochimica acta* 1990; **49**(2-3)**:** S271-274.

26. Pan X, Suzuki N, Hirano I, Yamazaki S, Minegishi N, Yamamoto M. Isolation and characterization of renal erythropoietin-producing cells from genetically produced anemia mice. *PloS one* 2011; **6**(10)**:** e25839.

27. Gruber M, Hu CJ, Johnson RS, Brown EJ, Keith B, Simon MC. Acute postnatal ablation of Hif-2alpha results in anemia. *Proceedings of the National Academy of Sciences of the United States of America* 2007 Feb 13; **104**(7)**:** 2301-2306.

28. Kapitsinou PP, Liu Q, Unger TL, Rha J, Davidoff O, Keith B, *et al.* Hepatic HIF-2 regulates erythropoietic responses to hypoxia in renal anemia. *Blood* 2010 Oct 21; **116**(16)**:** 3039-3048.

29. Percy MJ, Furlow PW, Lucas GS, Li X, Lappin TR, McMullin MF, *et al.* A gain-of-function mutation in the HIF2A gene in familial erythrocytosis. *The New England journal of medicine* 2008 Jan 10; **358**(2)**:** 162-168.

30. Bernhardt WM, Wiesener MS, Weidemann A, Schmitt R, Weichert W, Lechler P, *et al.* Involvement of hypoxia-inducible transcription factors in polycystic kidney disease. *The American journal of pathology* 2007 Mar; **170**(3)**:** 830-842.

31. Epstein AC, Gleadle JM, McNeill LA, Hewitson KS, O'Rourke J, Mole DR, *et al.* C. elegans EGL-9 and mammalian homologs define a family of dioxygenases that regulate HIF by prolyl hydroxylation. *Cell* 2001 Oct 5; **107**(1)**:** 43-54.

32. Kellar A, Egan C, Morris D. Preclinical Murine Models for Lung Cancer: Clinical Trial Applications. *BioMed research international* 2015; **2015:** 621324.

33. Ma Y, Fiering S, Black C, Liu X, Yuan Z, Memoli VA, *et al.* Transgenic cyclin E triggers dysplasia and multiple pulmonary adenocarcinomas. *Proceedings of the National Academy of Sciences of the United States of America* 2007 Mar 6; **104**(10)**:** 4089-4094.

34. Meyer M, Schillinger W, Pieske B, Holubarsch C, Heilmann C, Posival H, *et al.* Alterations of sarcoplasmic reticulum proteins in failing human dilated cardiomyopathy. *Circulation* 1995 Aug 15; **92**(4)**:** 778-784.

35. Kawase Y, Ly HQ, Prunier F, Lebeche D, Shi Y, Jin H, *et al.* Reversal of cardiac dysfunction after long-term expression of SERCA2a by gene transfer in a pre-clinical model of heart failure. *Journal of the American College of Cardiology* 2008 Mar 18; **51**(11)**:** 1112-1119.

36. Jessup M, Greenberg B, Mancini D, Cappola T, Pauly DF, Jaski B, *et al.* Calcium Upregulation by Percutaneous Administration of Gene Therapy in Cardiac Disease (CUPID): a phase 2 trial of intracoronary gene therapy of sarcoplasmic reticulum Ca2+-ATPase in patients with advanced heart failure. *Circulation* 2011 Jul 19; **124**(3)**:** 304-313.

37. Wahlquist C, Jeong D, Rojas-Munoz A, Kho C, Lee A, Mitsuyama S, *et al.* Inhibition of miR-25 improves cardiac contractility in the failing heart. *Nature* 2014 Apr 24; **508**(7497)**:** 531-535.

Figures

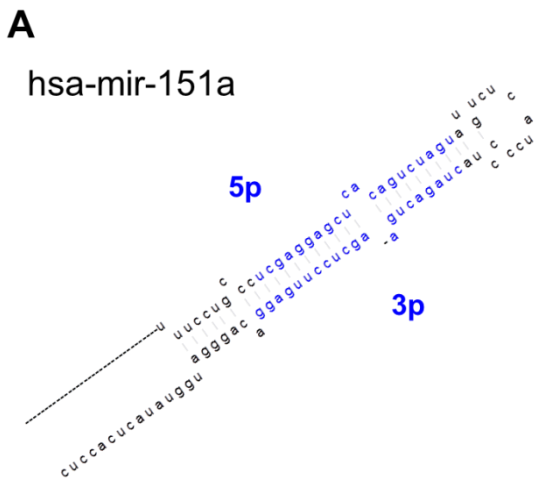

C

	miR-151-5p	miR-151-3p
Homo sapiens	5' - ucgaggagcucacagucuagu - 3'	5' - cuagacugaagcuccuugagg - 3'
Mus musculus	5' - ucgaggagcucacagucuagu - 3'	5' - cuagacugaggcuccuugagg - 5'

Figure 1. miR-151

Precursor structure and sequence of (A) human mir-151a and (B) mouse mir-151. (C) Sequence of mature miR-151. blue: seed region, red: the difference between human and mouse miR-151-3p.

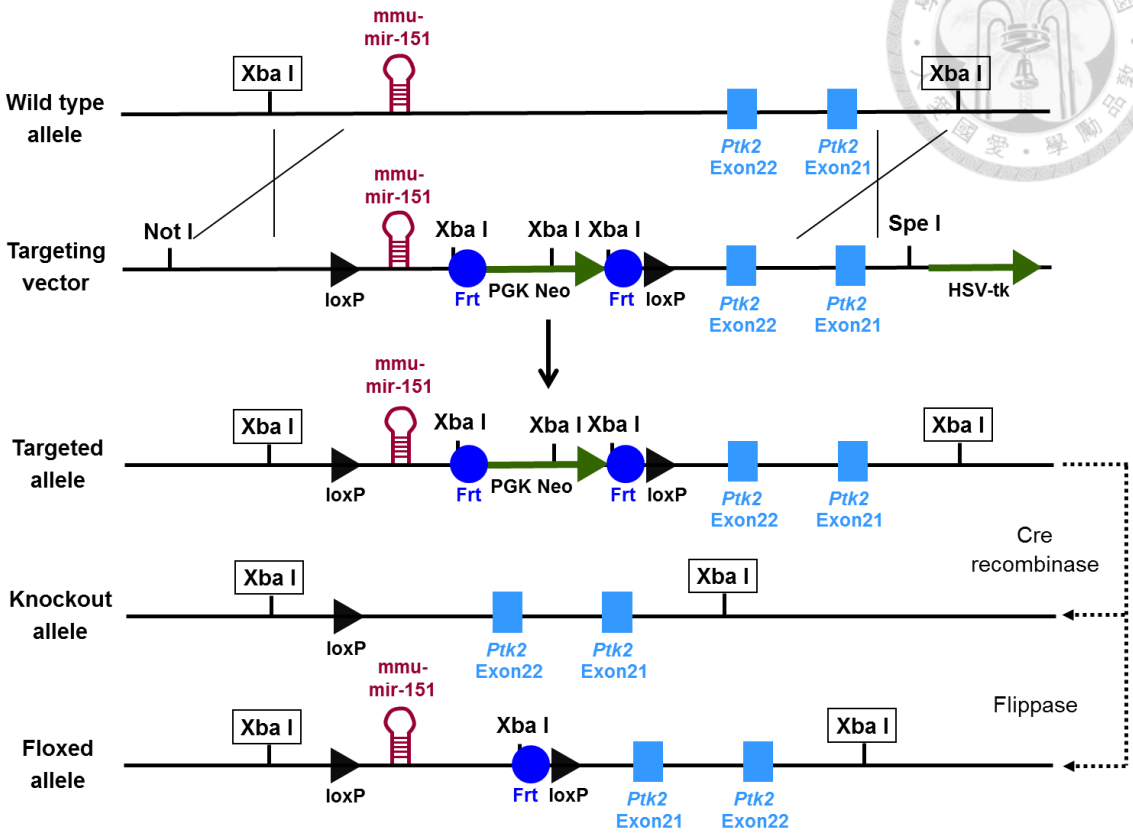

Figure 2. Knockout strategy of *Mir151* gene.

Schematic strategy for introduction of the loxP sites flanked the region containing the mmu-mir-151 sequence. Mouse *Mir151* gene is located in a large intron between exon 20 and exon 21 of *Ptk2* gene. Two loxP sequences (indicated by black triangle), two Frt sequences, and a neomycin-resistant gene (indicated by green arrow) were inserted to the flanked region of *Mir151* using a targeting vector. The wild type allele was replaced by the targeting allele through homologous recombination. The ES cells undergone neomycin selection could be transfected with either the Cre recombinase or the Flippase to delete the region between the two loxP or Frt sequences, respectively. The former became a *Mir151* conventional knockout allele, while the latter became a conditional knockout allele.

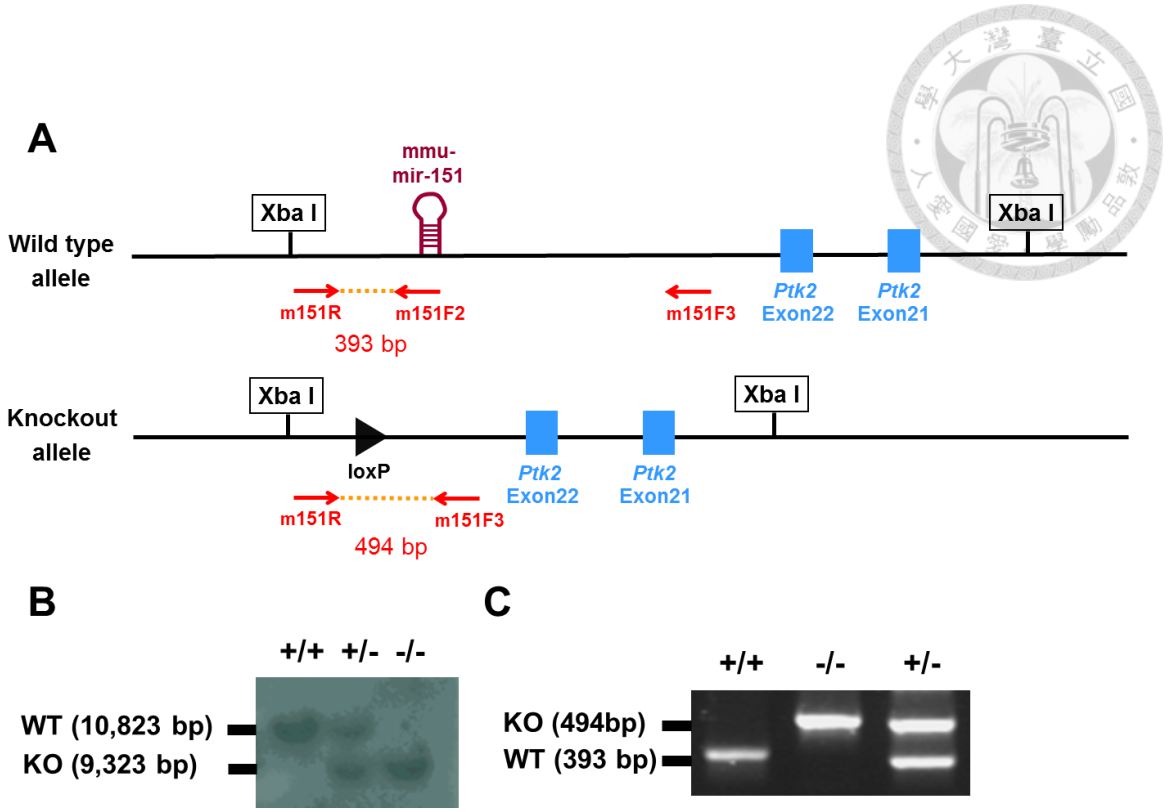

Figure 3. Genotyping results.

(A) The primer design for genotyping. A multiplex PCR strategy using two forward primers (m151F2 and m151F3) and one reverse primer (m151R) was applied to detect wild type (WT) allele (393 bp) and knockout (KO) allele (494 bp) simultaneously. (B) Validation of the successful recombination was conducted by Southern blotting, the DNA fragment size of WT and KO allele was 10.8 kb and 9.3 kb, respectively. (C) Genotyping PCR was used as a routine method. The amplicon size of each genotype is as followed: Mir151$^{+/+}$ 393 bp, Mir151$^{-/-}$ 494 bp, and Mir151$^{+/-}$ 393 and 494 bp.

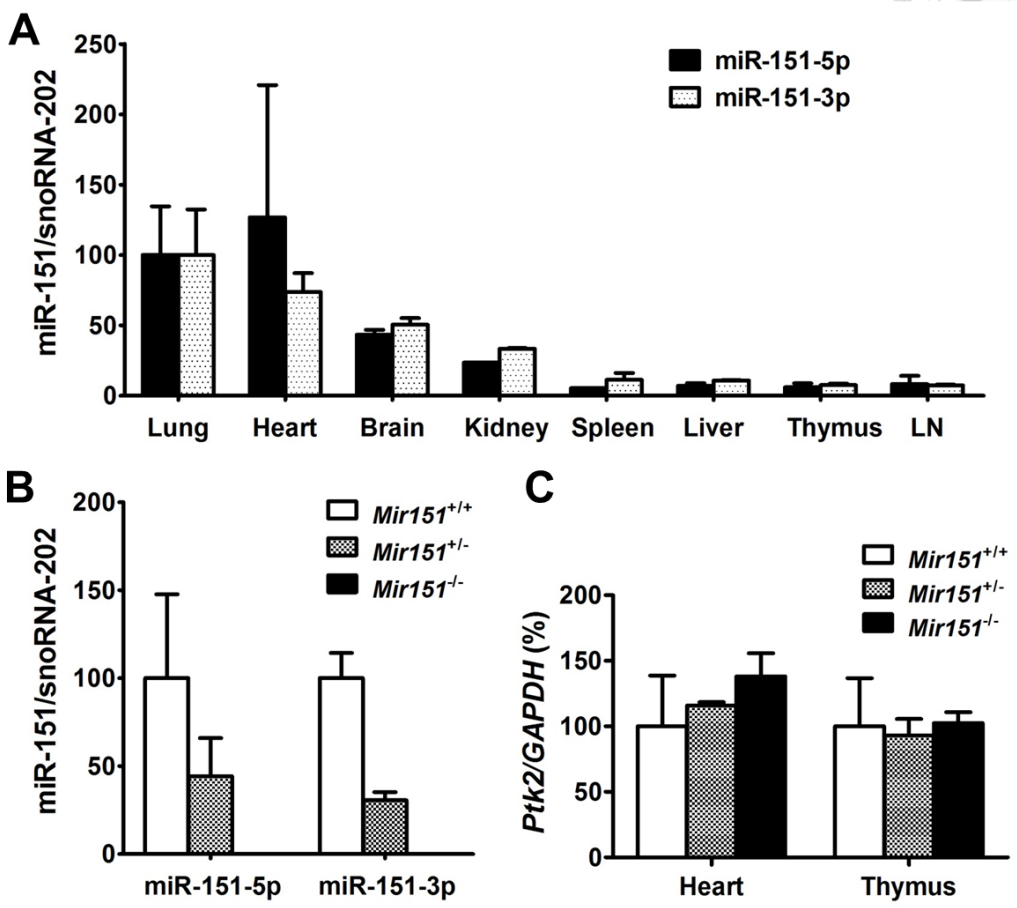

Figure 4. Expression of *Mir151* and *Ptk2* (host gene).

Relative expression of 5p and 3p of mmu-mir-151 (A) in major organs of wild type mice (n=2) and (B) in heart tissue of each genotype (n=2) were detected by Taqman microRNA assays. (C) *Ptk2* (*Mir151* host gene) mRNA level was assessed in heart and thymus tissue, which expressed highest and lowest *Mir151* level, by SYBR green qRT-PCR (n=2 for each genotype). snoRNA-202 and *Gapdh* gene were used as internal controls for miRNA and mRNA, respectively. Bars represent the mean ± SD.

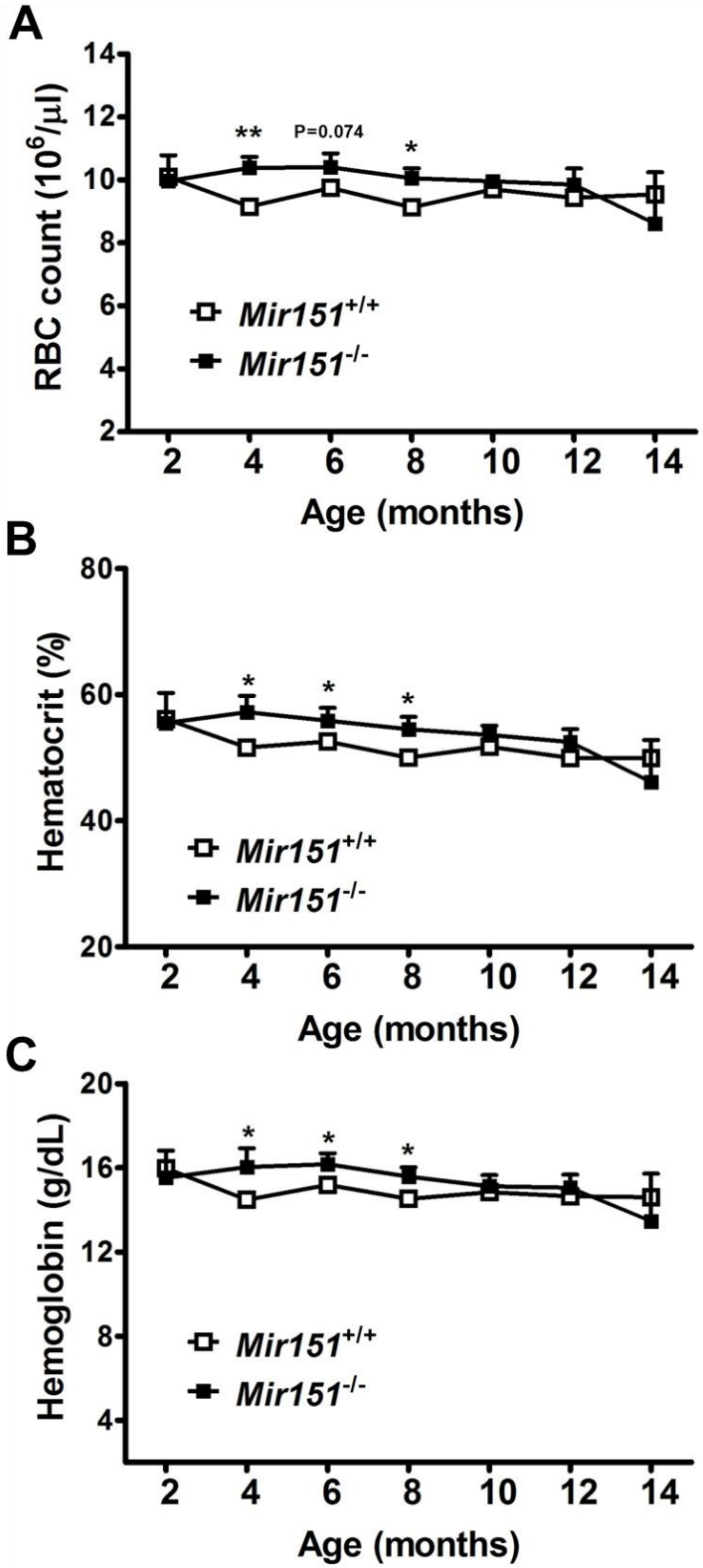
A
RBC count (10^6/μl)
14
12
10
8
6
4
2
**
P=0.074
*
Mir151+/+
Mir151-/-
2
4
6
8
10
12
14
Age (months)
B
Hematocrit (%)
80
60
40
20
*
*
*
Mir151+/+
Mir151-/-
2
4
6
8
10
12
14
Age (months)
C
Hemoglobin (g/dL)
20
16
12
8
4
*
*
*
Mir151+/+
Mir151-/-
2
4
6
8
10
12
14
Age (months)

Figure 5. CBCs and DCs analysis

The CBCs and DCs of *Mir151* wild type and knockout mice were monitored every month for more than one year. CBCs and DCs analysis were carried out with whole blood collected by puncture of the retro-orbital plexus of mice using capillary tubes with EDTA•K_2 as anticoagulant. The (A) RBC count, (B) hemoglobin, and (C) hematocrit of knockout mice were increased from 4 to 6 months and then gradually decreased, while these in wild type mice remained stable though out the long-term observation. (*Mir151*$^{+/+}$ n=8, *Mir151*$^{-/-}$ n=9) KO v.s WT * $P \leq 0.05$, ** $P \leq 0.01$ (ANOVA)

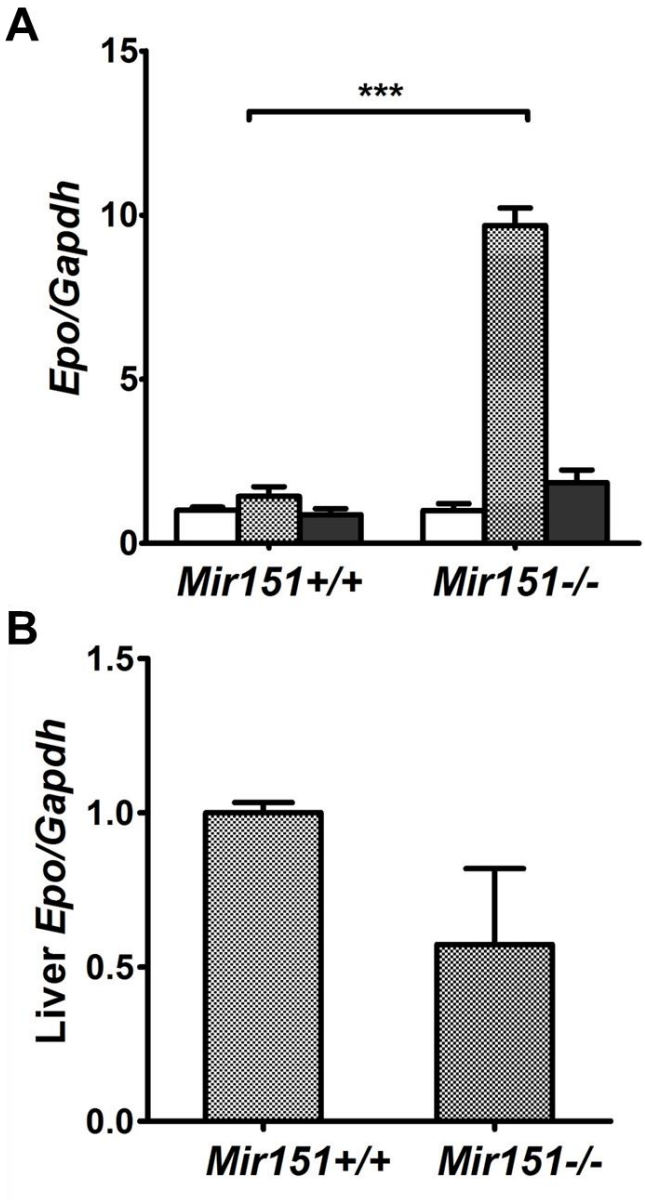

Figure 6. *Epo* mRNA level in mouse kidney and liver.

Mir151 N1F2 wild type and knockout mice were sacrificed at the age of 3, 6, and 9 months and then extracted the total RNA from kidney and liver. (A) Renal *Epo* mRNA level in 3-, 6-, and 9-months-aged mice (n=4 per group at each time-point) and (B) liver *Epo* mRNA level in 6-months-aged mice (n=2) were determined by SYBR green qRT-PCR. *Epo* transcript was detected by SYBR green qRT-PCR, and *Gapdh* gene was used as an internal control. Gene expression was shown in relative to 3 months-aged wild type mice. Bars represent the mean ± SD. *** $P \leq 0.001$ (ANOVA)

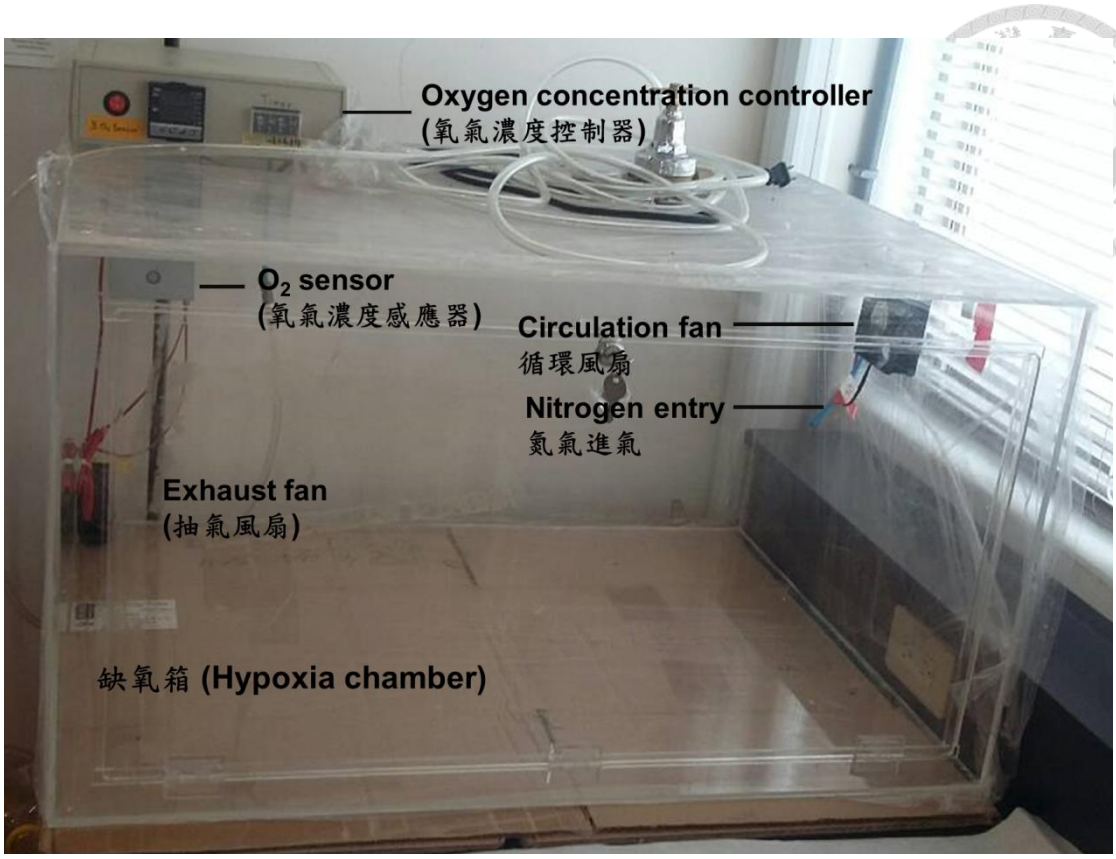

Figure 7. The hypoxia chamber for *in vivo* study.

With an oxygen sensor and continuous nitrogen supply, this system can reduce oxygen concentration in hypoxia chamber and maintained the oxygen level at 10±0.5%. The exhaust fan excludes the atmospheric air in the chamber, and the circulation fan makes uniform distribution of nitrogen and residual air in the chamber. In the control of timer, the exhaust fan turns around 30 seconds in every five minutes. Three capped cages can be put into the chamber simultaneously.

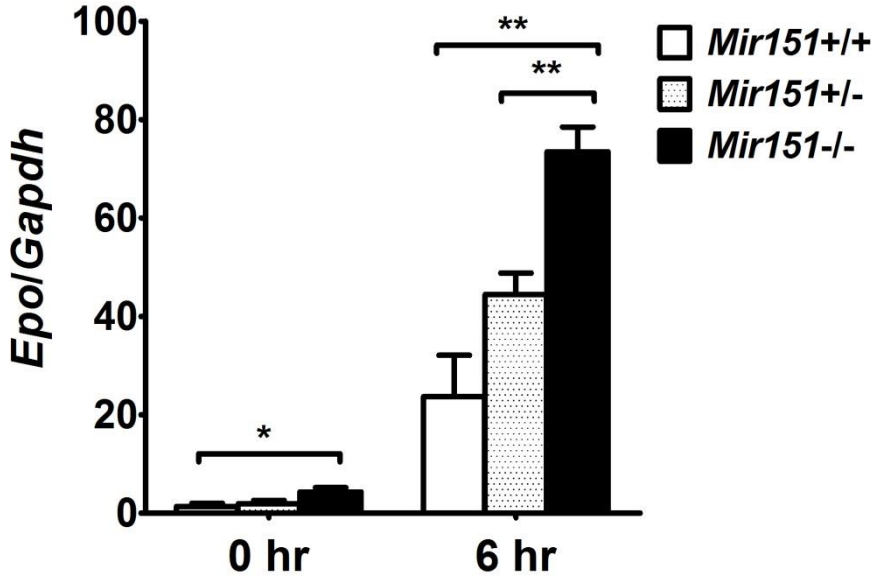

Figure 8. Chronic hypoxia induced the renal *Epo* mRNA level

N1F2 male mice (5 months old) were exposed to 10±0.5% O_2 in the hypoxia chamber under the well control of oxygen sensor. After 0 and 6 hour exposure to chronic hypoxia, the mice were sacrificed and collected the kidney. Renal *Epo* mRNA was measured by SYBR green qRT-PCR and normalized by *Gapdh*. Bars represent the mean ± SD. (n=3 for each group) * $P \leq 0.05$, ** $P \leq 0.01$ (ANOVA)

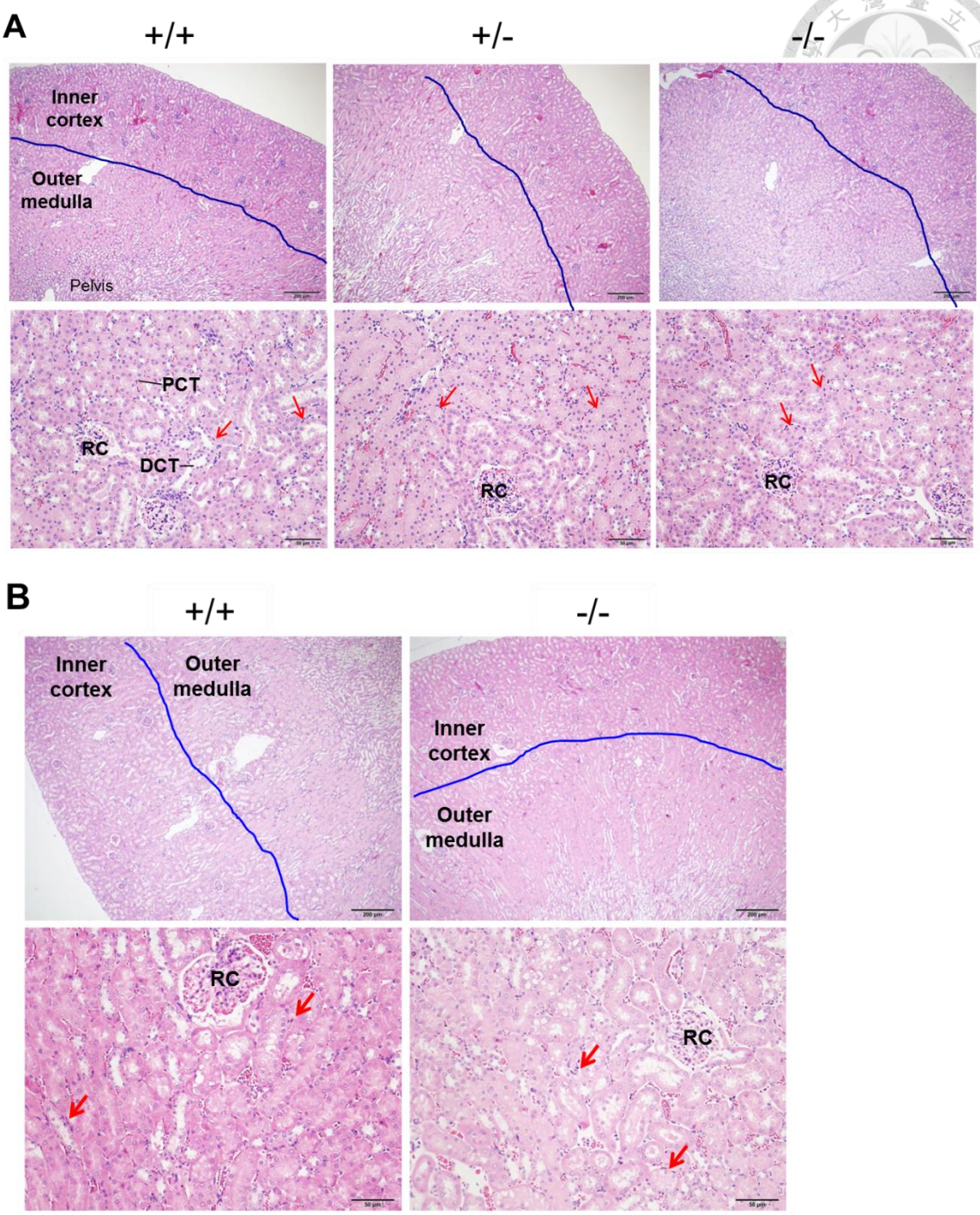

Figure 9. Kidney section stained with hematoxylin and eosin.
(A) 5-month-old mice and (B) 9-month-old N1F2 mice did not revealed the increase of interstitial fibroblasts and renal fibrosis. (A) and (B) top ×50 ; bottom ×200. RC: renal corpuscle; PCT: proximal convoluted tubule; DCT: distal tubule; Red arrow: interstitial fibroblast

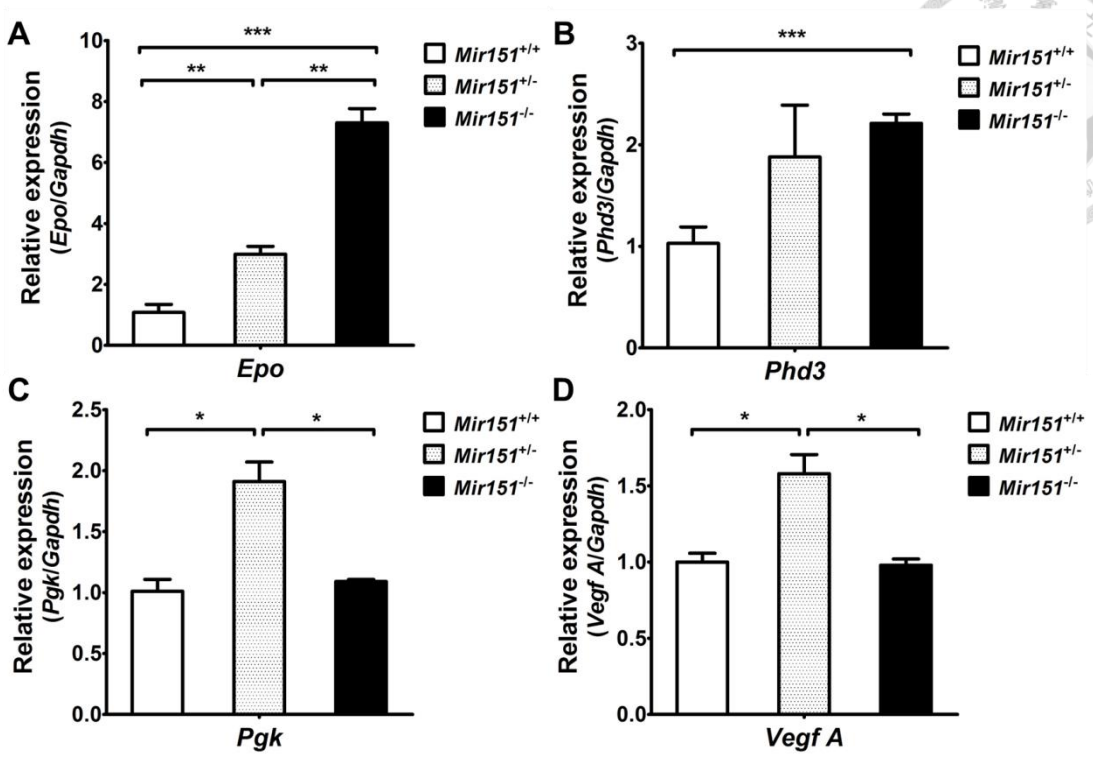

Figure 10. Expression of Hif-α target genes in the kidney

Total RNA was extracted from whole kidney lysate from N1F2 male mice (6 months). Expression of Hif-α target gene including (A) *Epo*, (B) *Phd3*, (C) *Pgk*, and (D) *Vegf A* was determined by SYBR green qRT-PCR. *Gapdh* gene was used as an internal control, and the gene expression in wild type mice was used as a calibrator. Bars represent the mean ± SD. (n=3 for each genotype) * $P \leq 0.05$, ** $P \leq 0.01$, *** $P \leq 0.001$ (ANOVA)

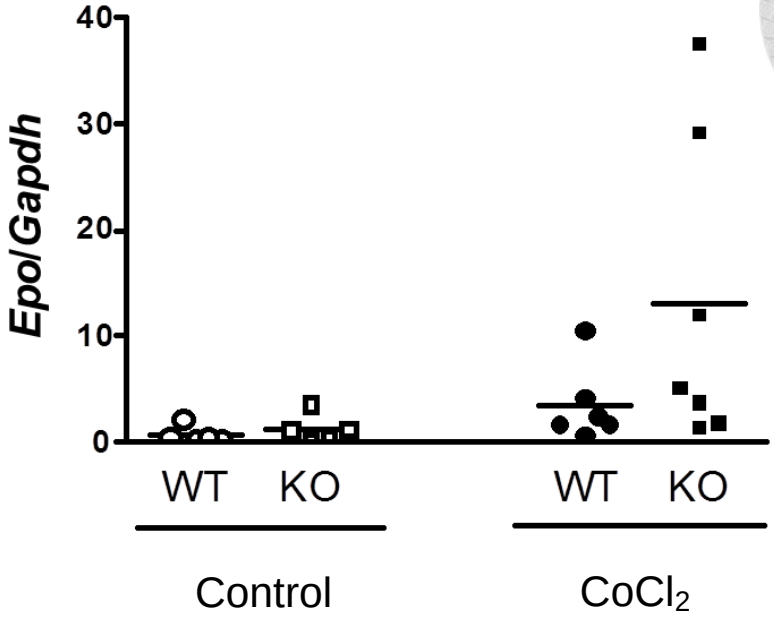

Figure 11. $CoCl_2$ treatment increased the expression of renal *Epo* mRNA.
9-month-aged N1F2 male mice were injected i.p with 60mg/kg of $CoCl_2$ (n=7). Control mice were injected with PBS (n=5). After 6 hour of injection, the mice were sacrificed and collected the kidney. Renal *Epo* mRNA was measured by SYBR green qRT-PCR and normalized by *Gapdh*.

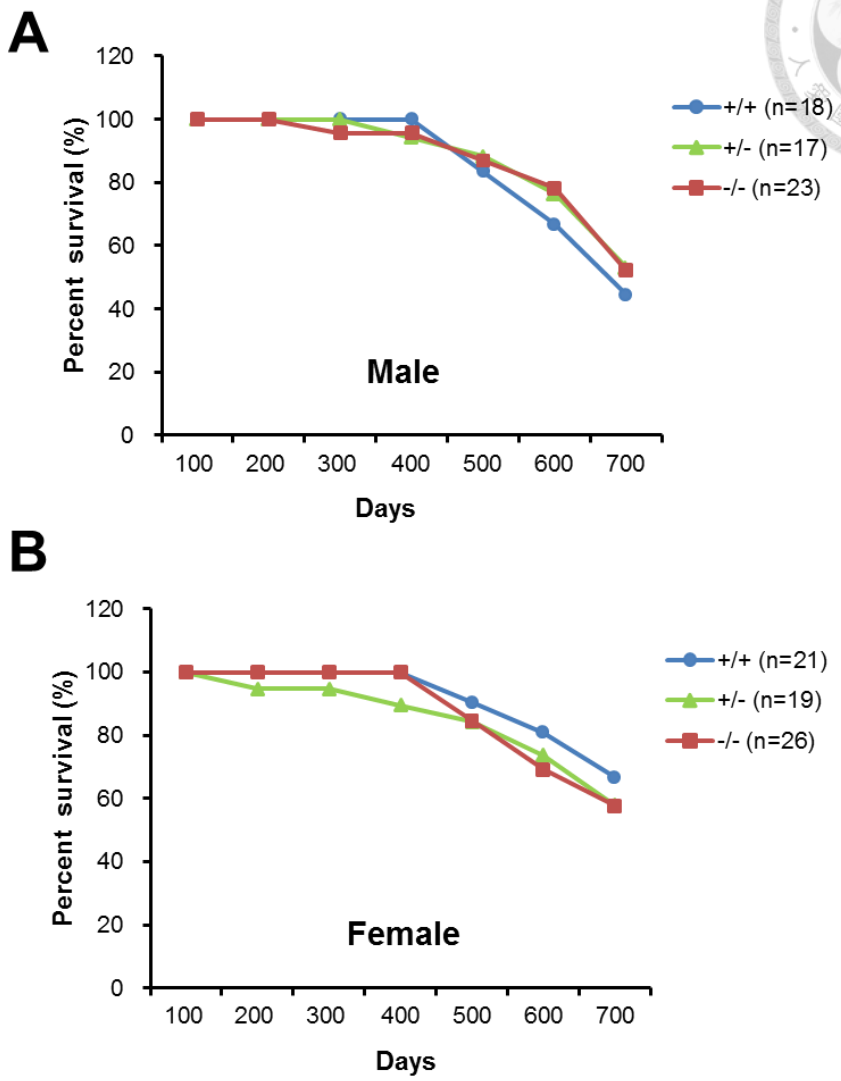

Figure 12. Survival curve.

A cohort including 124 N1F2 mice (58 male and 66 female) were kept and monitored for more than two years. No difference in survival of these three genotype was found.

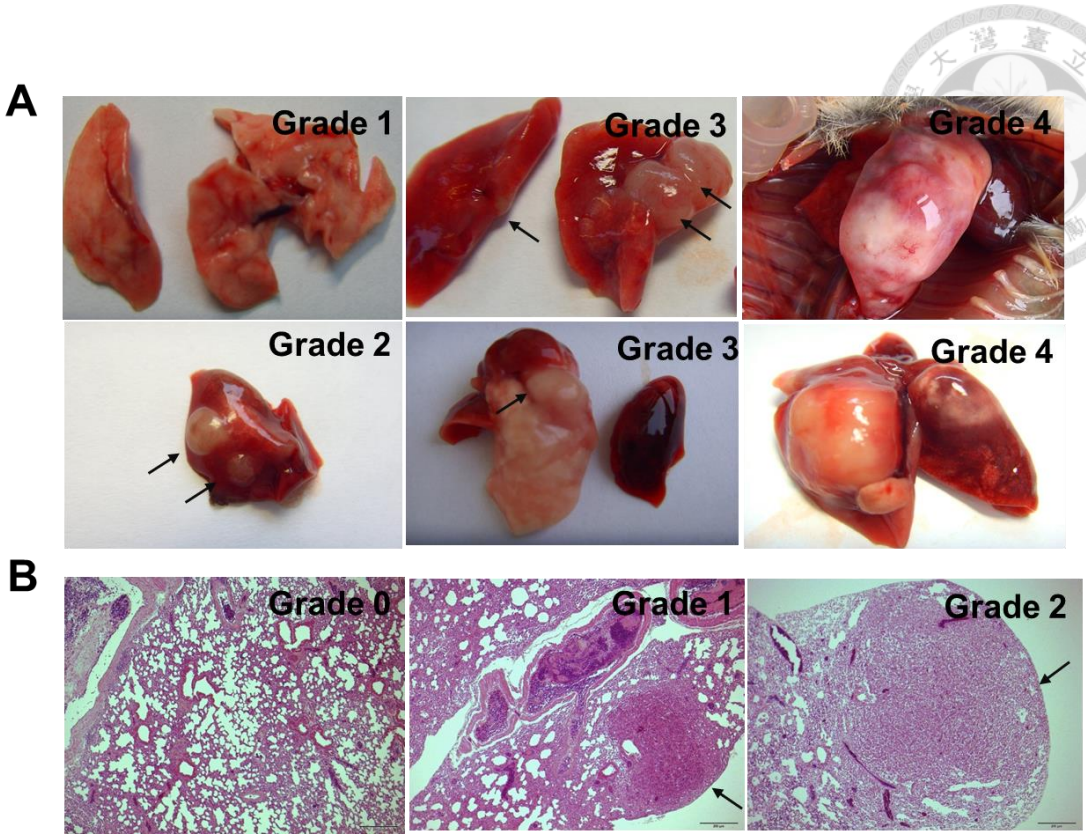

Figure 13. Examination of the lung in dead mice.

Lung cancer was spontaneously occurred in 23% homozygous and 33% heterozygous N1F2 *Mir151* knockout mice at their end stage. (A) The disease progression was subdivided according to the tumor size. [0: macro- and microscopic normal; 1: macroscopic normal, but tumor lesion can be observed in lung section under microscope; 2: nodule ≦ 2 (smaller than 1/4 lobe), normal part is still remained in the same lobe; 3: nodule > 2 or larger than 1/4 lobe, normal part is still remained in the same lobe; 4: Completely loss of normal tissue in the same lobe.] (B) Lung section stained with hematoxylin and eosin.

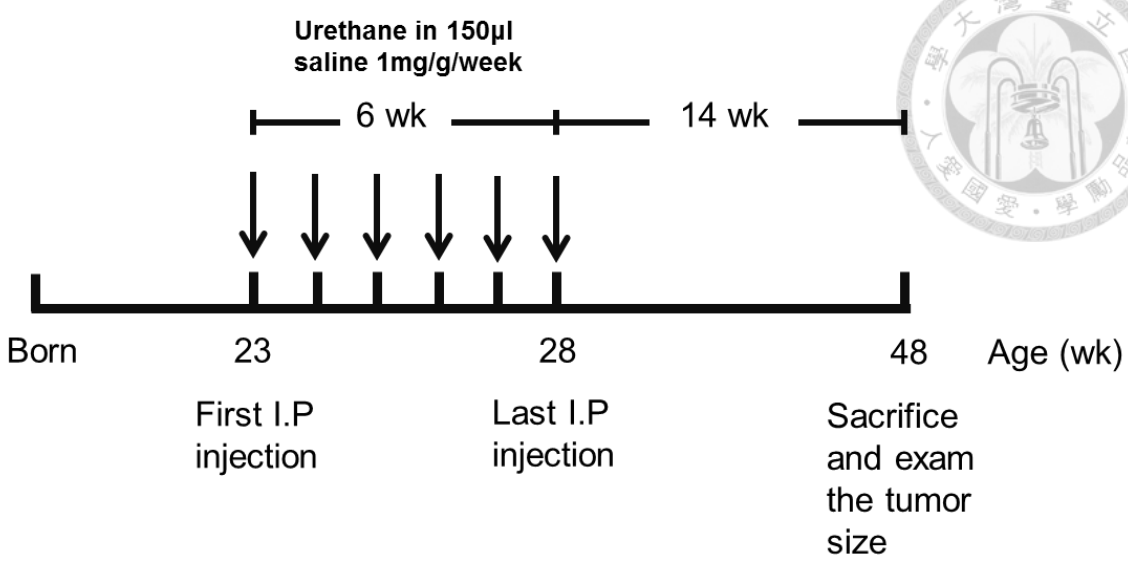

Figure 14. Urethane induction protocol for elder mice.

Mir151 N1F2 knockout mice (23 weeks old) as well as their littermate controls started to inject I.P. with 1 mg/g body weight urethane once weekly for 6 consecutive weeks. 20 weeks after the first urethane injection, mice were sacrificed, dissected their lungs, and examined the tumor size.

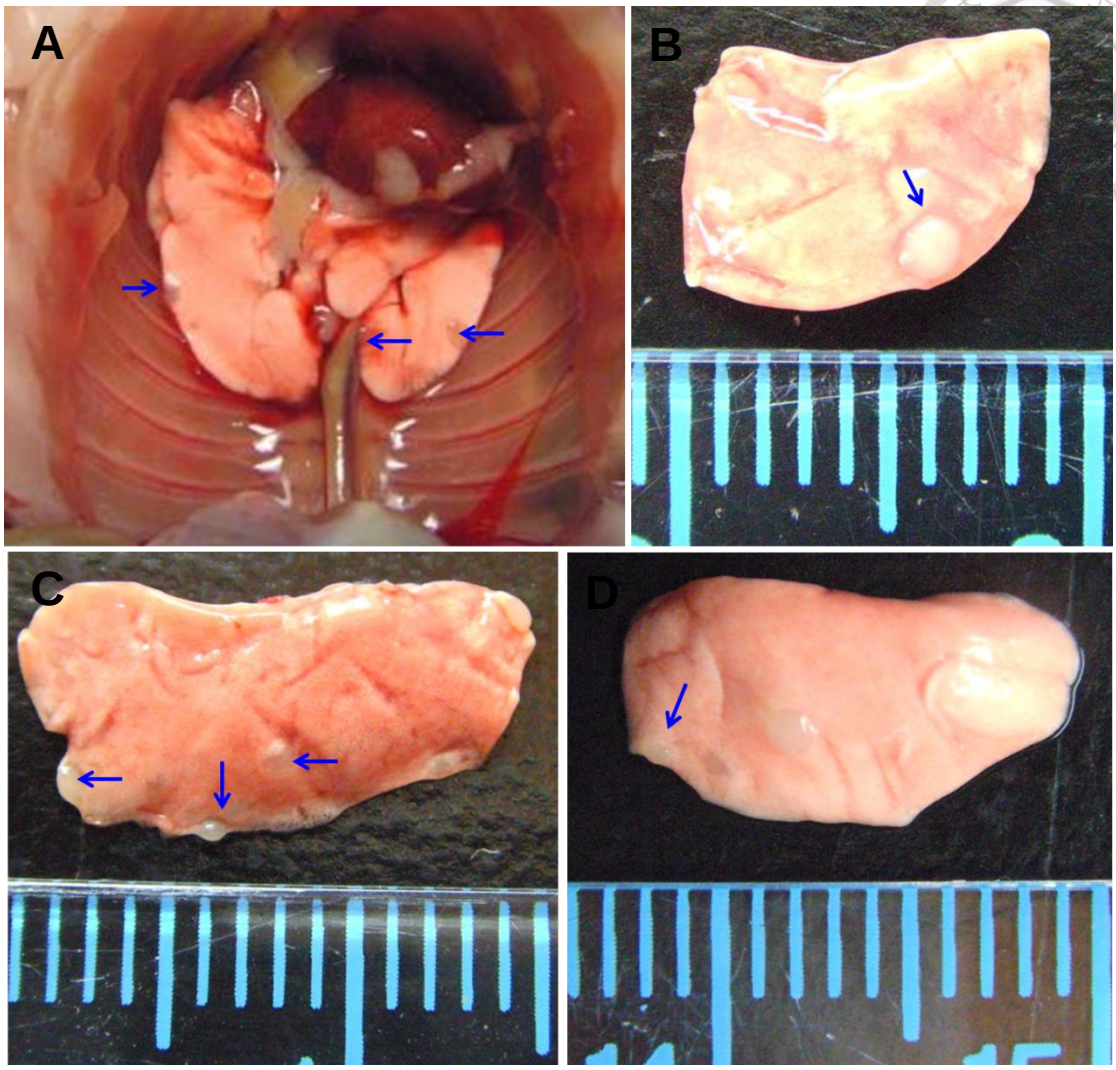

Figure 15. Lung cancer induced by urethane injection.

(A) After open the chest of urethane-treated mice, the developing nodules can be observed on the lung surface. (B) Tumor size larger than 1 mm. (C) More than one nodule developed in one lobe. (C) Tumor size smaller than 1mm.

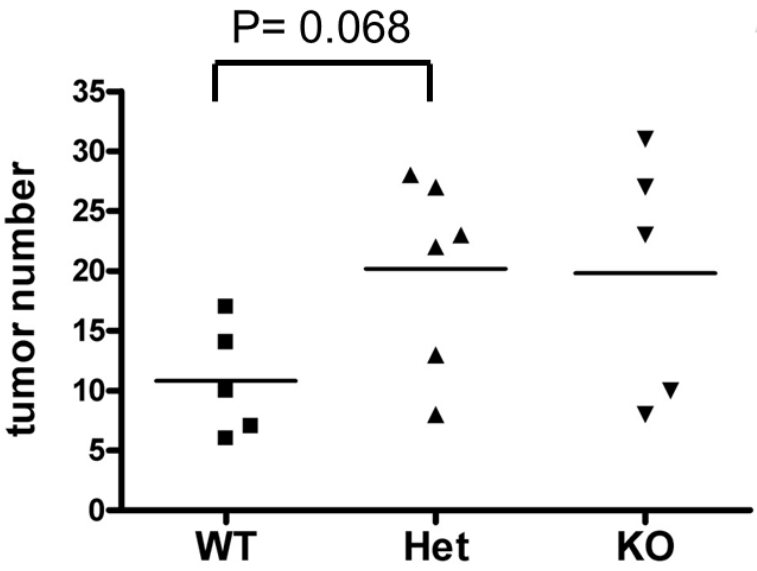

Figure 16. Quantification of tumor numbers induced by urethane in elder mice.

Tumor numbers were observed and counted under dissecting microscope. (WT n=5, Het n=6, and KO n=5) Het v.s WT, P=0.068 (Mann-Whitney test).

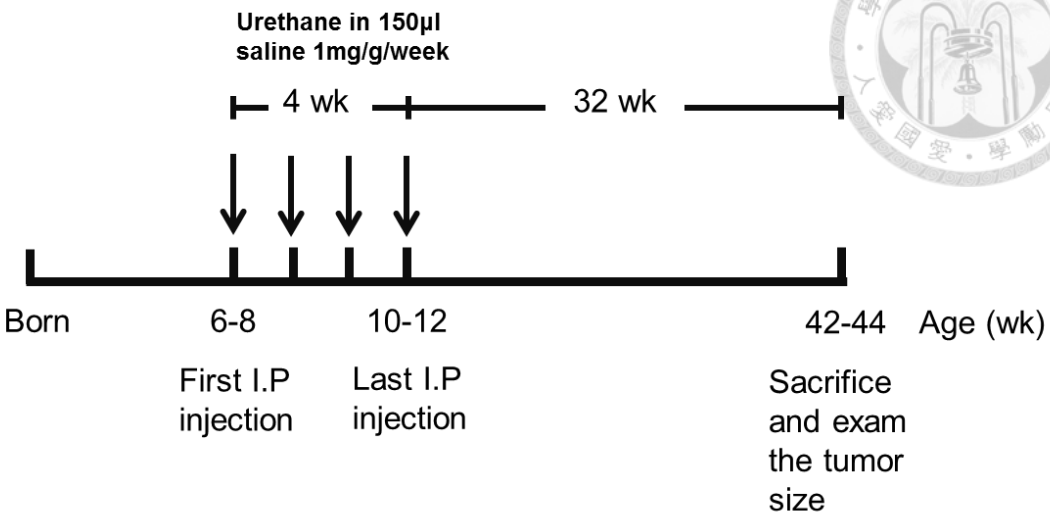

Figure 17. Urethane induction protocol for young mice.

Mir151 N10F2 knockout mice as well as their littermate controls started to inject I.P. at 6–8 weeks of age with 1 mg/g body weight urethane once weekly for 4 consecutive weeks. 36 weeks after the first urethane injection, mice were sacrificed, dissected their lungs, and examined the tumor size.

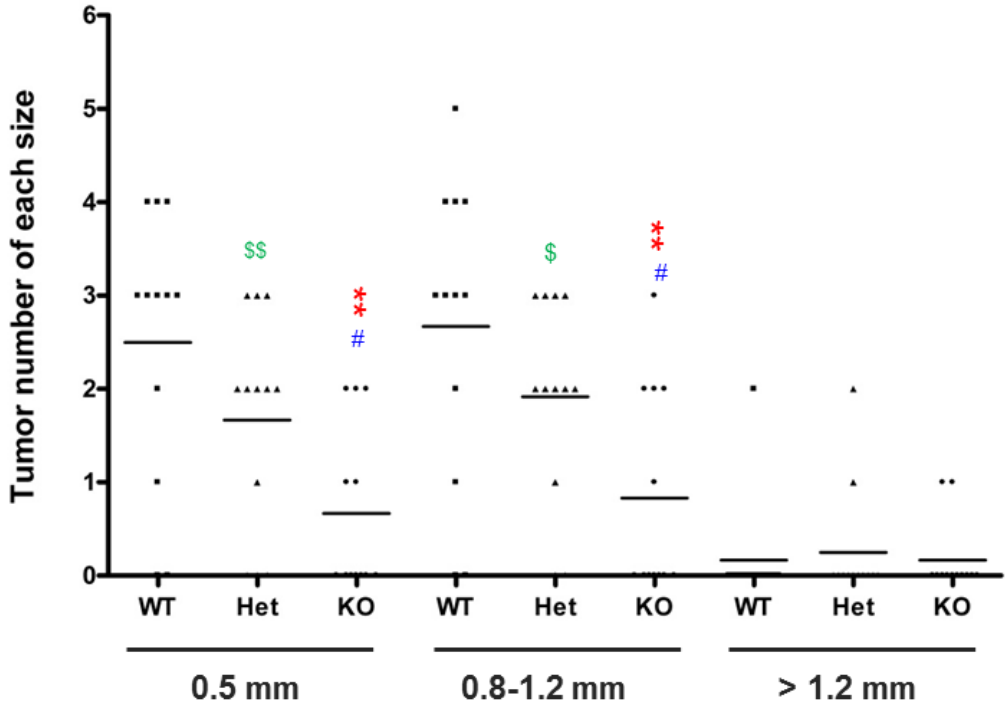

Figure 18. Quantification of tumor numbers induced by urethane in young mice.

Tumor numbers were subdivided according to the size: 0.5 mm (small), 0.8-1.2 mm (medium), and > 1.2 mm (large). *Mir151* N10F2 knockout mice showed a significant decreased in small and medium size. (n=12 for each genotype) ** KO v.s WT, $P \leq 0.01$; # KO v.s Het, $P \leq 0.05$; $ Het v.s WT, $P \leq 0.05$; $$ Het v.s WT, $P \leq 0.01$ (Mann-Whitney test)

Tables

Table 1. Primer sequences

For SYBR green qRT-PCR		For targeting vector construct	
Gene	**Primer sequence**	**Primer name**	**Sequence**
Gapdh		151-AU	5'-GAAAGAGTATCCCTGTGACCC-3'
Forward	5'-CTGGAGAAACCTGCCAAGTA-3'	151-BD	5'-AACTCTCCTGCTGTGAGTGG-3'
Reverse	5'-AAGAGTGGGAGTTGCTGTTG-3'	151-CU	5'-GACGCTTCATTCCAAGACGTC-3'
Ptk2		151-DD	5'-TTCTGTGCTCACGAGGGTGAAC-3'
Forward	5'-AGGCGGCCCAGGTTTACT3'	151-EU	5'-AAGGACACAGAGACAACTTCC-3'
Reverse	5'-CACCTTCTCCTCCTCCAGGAT-3'	151-FD	5'-GTAGTATGGCCAACAGAAGAC-3'
Epo		151-GU	5'-CGTGTCTATACGGAAAGGAG-3'
Forward	5'-CATCTGCGACAGTCGAGTTCTG-3'	151-HD	5'-AAGAGACAGTGGCAGTTGTG-3'
Reverse	5'-CACAACCCATCGTGACATTTTC-3'	151-IU	5'-CAGTGGAACTATTGAGCTCTC-3'
Phd3		151-JD	5'-ATATGCAGCCTGAAACAGCTCC-3'
Forward	5'-TCGCTTCCTCCCGAACTCT-3'	151-YU	5'-TATGTGCAGAGCAGGAAGAAGC-3'
Reverse	5'-CAGAAACGAGGGTGGCTAACTT-3'	151-ZD	5'-AGTGCATGGTGGGACAATTGACC-3'
Pgk			
Forward	5'-GGAAGCGGGTCGTGATGA-3'	**For genotyping**	
Reverse	5'-GCCTTGATCCTTTGGTTGTTTG-3'	**Primer name**	**Sequence**
Vegf A		m151F2	5'-TGGGACTGAGAGCTGAGAAAG-3'
Forward	5'-CCACGTCAGAGAGCAACATCA-3'	m151F3	5'-TTCTTGTGGGAGTGTGTCAAGG-3'
Reverse	5'-TCATTCTCTCTATGTGCTGGCTTT-3'	m151R	5'-AGACGCTTCATTCCAAGACGTC-3'

Table 2. N1F2 Pup number of each genotype at day 10 post birth				
	***Mir151*$^{+/+}$**	***Mir151*$^{+/-}$**	***Mir151*$^{-/-}$**	**Total number**
Expected	90	181	90	361
Observed	94	180	87	361

Table 3. Clinical biochemistry of *Mir151* Conventional KO female mice *

Item	Unit	+/+ (n=4)	-/- (n = 5)	*p*-value
Body weight befrore fasting	g	29.18 ± 3.9	30.80 ± 5.61	0.6395
Body weight after fasting	g	28.45 ± 4.05	29.72 ± 5.71	0.7195
GOT	U/L	77.5 ± 22.55	56.25 ± 8.54	0.0732
GPT	U/L	47.5 ± 28.72	27.5 ± 8.66	0.1827
Total protiein	g/dL	5.88 ± 0.48	5.60 ± 0.22	0.2874
Globulin	g/dL	3.13 ± 0.25	3.13 ± 0.25	0.8786
Albumin/Globulin	-	e	4.00 ± 0.41	0.7156
Amylase	U/L	4605.0 ± 654.5	3937.5 ± 619.07	0.1362
TG	mg/dL	121.25 ± 19.74	142.5 ± 35.0	0.2256
T-CHO	mg/dL	135.0 ± 7.07	117.5 ± 35.0	0.2497
HDL-C	mg/dL	46.25 ± 8.54	40.00 ± 15.81	0.3934
Na	mmol/L	133.72 ± 2.5	133.72 ± 2.5	0.6845
K	mmol/L	5.5 ± 0.91	5.38 ± 0.63	1.0000
Cl	mmol/L	133.75 ± 2.5	133.75 ± 2.5	0.8786
UA	mg/dL	3.0 ± 0	3.25 ± 0.29	0.6517
Mg	mmol/L	1.05 ± 0.11	0.88 ± 0.09	0.0952
P	mg/dL	7.63 ± 0.63	6.75 ± 0.65	0.0780
Ca	mmole/L	2.24 ± 0.06	2.15 ± 0.11	0.2093
ALP	UL	215.00 ± 43.01	198.75 ± 51.05	0.6983
CRP	mg/dL	0.1	0.1	ND
LDH	UL	591.25 ± 262.47	536.25 ± 256.66	0.5605
BUN	mg/dL	29.75 ± 4.13	26.38 ± 4.57	0.2433
UIBC	µg/dL	210.00 ± 40.21	246.25 ± 25.94	0.0994
Fe	µg/dL	216.25 ± 47.68	187.5 ± 40.1	0.2711
TIBC	µg/dL	426.25 ± 11.09	433.75 ± 23.23	0.3316

* Age: 26-30 weeks

Table 4. The 4-stage grading system

	Grade				
	0	1	2	3	4
+/+	14	0	0	0	0
+/- *	12	0	4	0	2
-/- *	20	1	1	3	1

* Compared to WT mice, $p<0.05$ (non-parametric analysis)

0: macro- and microscopic normal
1: macroscopic normal, but tumor lesion can be observed using microscopy
2: nodule $\leqq$ 2 (smaller than 1/4 lobe), normal part is still remained in the same lobe
3: nodule > 2 or larger than 1/4 lobe, normal part is still remained in the same lobe
4: Completely loss of normal tissue in the same lobe

Appendixes

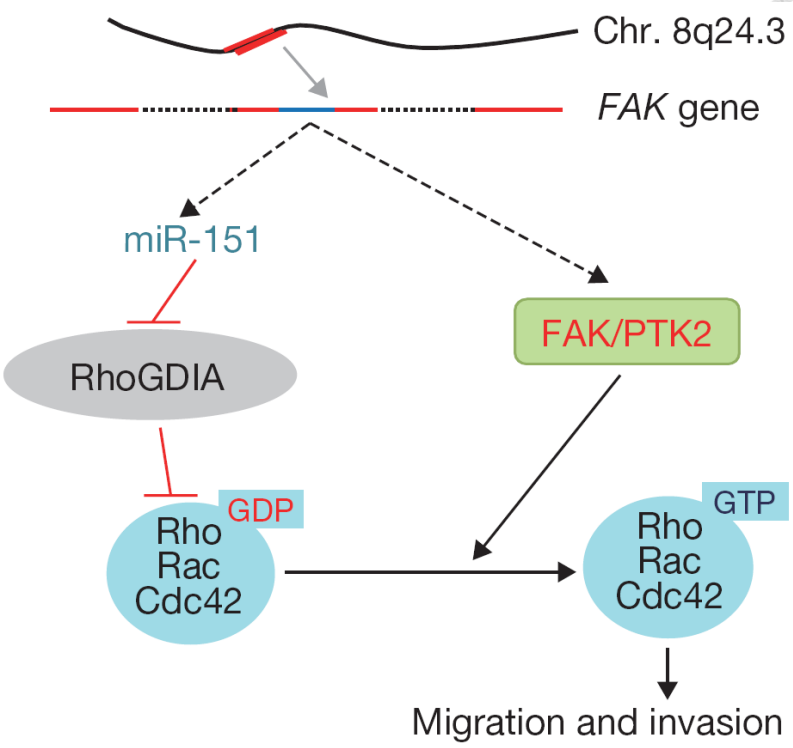

Appendix VI. Proposed model illustrating the expression, function and mechanism of miR-151 in HCC invasion and metastasis.

Adapted from Ding J, Huang S, Wu S, Zhao Y, Liang L, Yan M, et al. Gain of miR-151 on chromosome 8q24.3 facilitates tumour cell migration and spreading through downregulating RhoGDIA. Nature cell biology 2010 Apr; 12(4): 390-399.

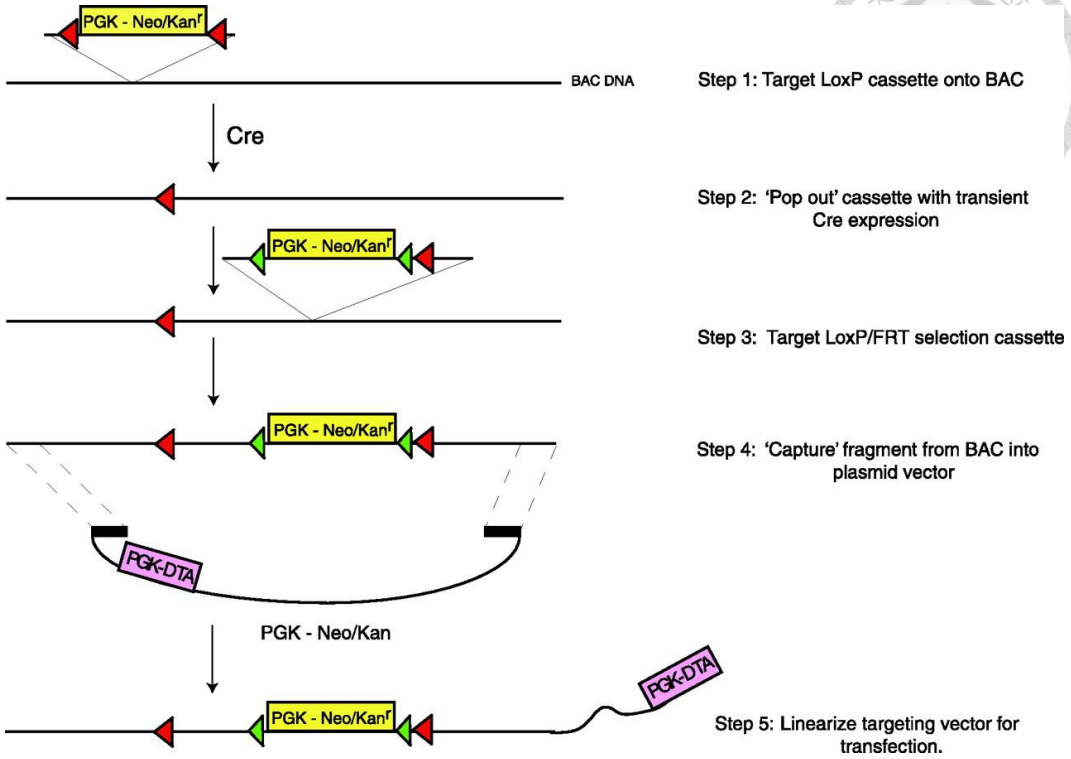

Appendix VII. Recombineering technology.

Contemporary approaches for modifying the mouse genome. Physiol Genomics. 2008 Aug 15;34(3):225-38.

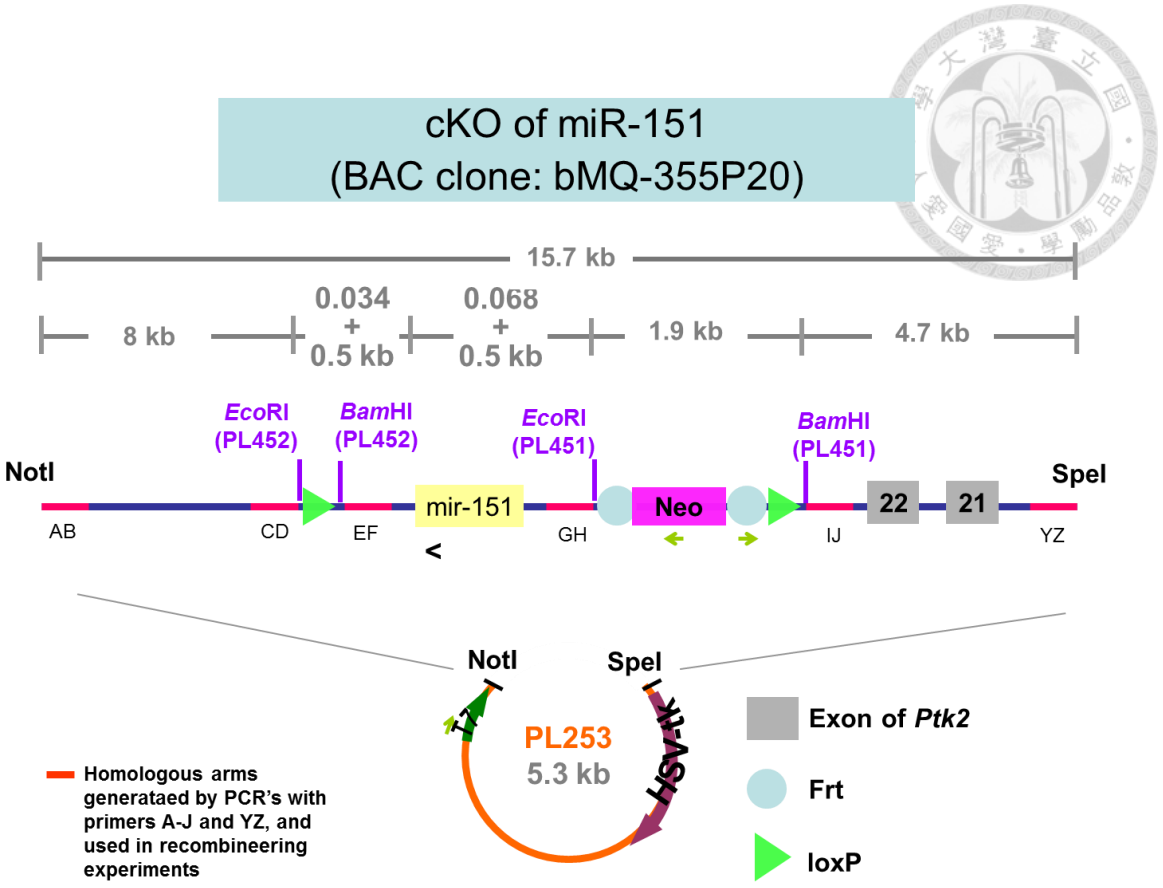

Appendix VIII. Design of targeting vector for *Mir151*.

Data source: Transgenic Mouse Model Core Facility, NTU.

Appendix VIII. Publications

1. Yang YL, Yen CT, Pai CH, Chen HY, Yu SL, Lin CY, Hu CY, Jou ST, Lin DT, Lin SR, and Lin SW. (accepted 2015, Oct). A double negative loop comprising *ETV6/RUNX1* and *MIR181A1* contributes to differentiation block in t(12;21)-positive acute lymphoblastic leukemia. *Plos one*. (co-first author)
2. Huang YJ, Lin YL, Chiang CI, Yen CT, Lin SW, Kao JT. (2012, Jan). Functional importance of apolipoprotein A5 185G in the activation of lipoprotein lipase. *Clinica Chemica Acta; international journal of clinical chemistry*, 18;413(1-2):246-50.
3. Yang YL, Lin SR, Chen JS, Hsiao CC, Lin KH, Sheen JM, Cheng CN, Wu KH, Lin SW, Yu SL, Chen HY, Lu MY, Chang HH, Yen CT, Lin JF, Su YH, Li YP, Lin CY, Jou ST, Lin DT. (2010, Oct). Multiplex reverse transcription-polymerase chain reaction as diagnostic molecular screening of 4 common fusion chimeric genes in Taiwanese children with acute lymphoblastic leukemia. *Journal of Pediatric Hematology/Oncology*, 32(8):e323-30.
4. Yang YL, Lin SR, Chen JS, Lin SW, Yu SL, Chen HY, Yen CT, Lin CY, Lin JF, Lin KH, Jou ST, Hu CY, Chang SK, Lu MY, Chang HH, Chang WH, Lin KS, Lin DT. (2010, Jan). Expression and prognostic significance of the apoptotic genes BCL2L13, Livin, and CASP8AP2 in childhood acute lymphoblastic leukemia.. *Leukemia Research*, 34(1):18-23.

A double negative loop comprising *ETV6/RUNX1* and *MIR181A1* contributes to differentiation block in t(12;21)-positive acute lymphoblastic leukemia

Yung-Li Yang[1,2¶], Ching-Tzu Yen[3¶], Chen-Hsueh Pai[3], Hsuan-Yu Chen[4], Sung-Liang Yu[3], Chien-Yu Lin[4], Chung-Yi Hu[3], Shiann-Tarng Jou[2], Dong-Tsamn Lin[1,2], Shu-Rung Lin[5,6&*], and Shu-Wha Lin[3&*]

[1]Departments of Laboratory Medicine, National Taiwan University Hospital, College of Medicine, National Taiwan University, Taipei, Taiwan;
[2]Departments of Pediatrics, National Taiwan University Hospital, College of Medicine, National Taiwan University, Taipei, Taiwan;
[3]Departments of Clinical Laboratory Sciences and Medical Biotechnology, College of Medicine, National Taiwan University, Taipei, Taiwan;
[4]Institute of Statistical Science, Academia Sinica, Taipei, Taiwan;
[5]Department of Bioscience Technology, College of Science, Chung-Yuan Christian University, Taoyuan, Taiwan
[6]Center for Nanotechnology and Center for Biomedical Technology, College of Science, Chung-Yuan Christian University, Taoyuan, Taiwan

Running Head: *ETV6/RUNX1* and *MIR181A1* in ALL

[*]Corresponding Authors
E-mail: mtshuwha@ntu.edu.tw (SWL)
E-mail: shurung@cycu.edu.tw (SRL)

[¶]These authors contributed equally to this work.
[&]These authors also contributed equally to this work.

Accepted [Oct/2015]

Abstract

Childhood acute lymphoblastic leukemia (ALL) with t(12;21), which results in expression of the *ETV6/RUNX1* fusion gene, is the most common chromosomal lesion in precursor-B (pre-B) ALL. We identified 17 microRNAs that were downregulated in *ETV6/RUNX1*$^{+}$ compared with *ETV6/RUNX1*$^{-}$ clinical samples. Among these microRNAs, miR-181a-1 was the most significantly reduced (by ~75%; $P < 0.001$). Using chromatin immunoprecipitation, we demonstrated that ETV6/RUNX1 directly binds the regulatory region of *MIR181A1*, and knockdown of *ETV6/RUNX1* increased miR-181a-1 level. We further showed that miR-181a (functional counterpart of miR-181a-1) could target *ETV6/RUNX1* and cause a reduction in the level of the oncoprotein ETV6/RUNX1, cell growth arrest, an increase in apoptosis, and induction of cell differentiation in *ETV6/RUNX1*$^{+}$ cell line. Moreover, ectopic expression of miR-181a also resulted in decreased CD10 hyperexpression in *ETV6/RUNX1*$^{+}$ primary patient samples. Taken together, our results demonstrate that *MIR181A1* and *ETV6/RUNX1* regulate each other, and we propose that a double negative loop involving *MIR181A1* and *ETV6/RUNX1* may contribute to ETV6/RUNX1-driven arrest of differentiation in pre-B ALL.

Introduction

The t(12;21) translocation, which fuses *ETV6* and *RUNX1*, is the most common chromosomal alteration in childhood precursor B-cell (pre-B) acute lymphoblastic leukemia (ALL) [1]. The initial fusion of *ETV6/RUNX1* is believed to allow quiescent, preleukemic cells to exist in the bone marrow, and the disease-promoting changes in the *ETV6/RUNX1*-positive preleukemic stage usually take place through second hits that arise in the late pro-B cell stage [2]. The oncogenic property of ETV6/RUNX1 is related to its aberrant function as a rogue transcription factor that can interfere with the normal functions of wild-type ETV6 and RUNX1 through multiple mechanisms. For example, ETV6/RUNX1 can dimerize with wild-type ETV6 via the helix-loop-helix domain of ETV6, thereby disrupting ETV6 function [3, 4]. ETV6/RUNX1 also can bind to RUNX1 target DNA sequences and recruit transcriptional corepressors including mSinA, N-coR, and histone deacetylase-3 (HDAC3) via the ETV6 portion of the fusion protein, resulting in dysregulated RUNX1-dependent transcription [3, 5, 6]. Evidence has revealed that aberrant recruitment of transcriptional repressors correlates with the oncogenic activities of ETV6/RUNX1 so as to constitutively repress a number of genes required for hematopoiesis, including *JunD*, *ACK1*, *PDGFRB*, and *TCF4*, which are involved in cell cycle regulation [7, 8]. The leukemogenic consequences of ETV6/RUNX1 through the aforementioned mechanisms are induction of survival signals and inhibition of cell differentiation by ETV6/RUNX1's direct modulation of multiple targets such as *EPOR*, *MDM2*, and certain miRNA genes [9-11].

MicroRNAs (miRNAs) execute diverse functions by targeting the mRNAs of multiple genes simultaneously. Recent advances have indicated that miRNAs are important regulators of hematopoiesis; moreover, miRNA-mediated control of gene dosage is critical for lineage fate determination of hematopoietic cells, and disruption of this regulation may lead to malignant transformation [12, 13]. Moreover, dysregulation of miRNA expression is frequently associated with cytogenetic abnormalities, and in turn certain of these abnormalities have a direct impact on aberrant expression of miRNAs [13]. For instance, miR-155 is essential to B-cell development and is aberrantly upregulated in B-cell malignancies including diffuse large B cell lymphoma (DLBCL), follicular lymphoma (FL), and chronic lymphocytic leukemia (CLL) [14-16]. In patients expressing the aberrant fusion protein AML1/ETO, the most common acute myeloid leukemia–associated fusion resulting from t(8;21), the fusion oncoprotein was the first ever reported to directly repress miR-223 expression by triggering chromatin remodeling and epigenetic silencing,

which in turn block myeloid precursor cell differentiation [17]. Emerging evidence from research on miRNAs and hematological malignancy has provided deeper insight into the relation between miRNAs and their target genes. In addition to the simple negative regulation of target mRNAs by miRNAs, miRNA–target relationships may also involve complex feedback and feed-forward loops. These loops help to maintain a desired protein inhibition/activation state and often participate in lineage determination in hematopoiesis and lymphomagenesis [12].

It is presumed that ETV6/RUNX1 may occupy the RUNX1-binding motif located in the regulatory regions of certain miRNA genes and thereby disrupt their transcription. Recent studies have shown that aberrant miRNA expression plays an important role in malignant transformation of ETV6/RUNX1 ALL. A highly expressed miR-125b-2 cluster was found in ETV6/RUNX1 ALL, which may provide leukemic cells with a survival advantage against growth inhibitory signals [18]. In addition, downregulation of two miRNAs i.e., miR-494 and miR-320a, by ETV6/RUNX1 via direct binding to the regulatory regions of miRNA genes has been shown to support *ETV6/RUNX1*-positive leukemic cell survival through the loss of inhibition of survivin, an anti-apoptotic protein and the target of miR-494 and miR-320a [11]. Although much is known about these miRNAs and their dysregulation in ETV6/RUNX1 ALL, it remains unclear how and which other miRNAs are involved in ETV6/RUNX1-mediated leukemogenesis.

In an attempt to understand the driving force and the consequence of aberrant miRNA expression in ETV6/RUNX1 ALL, we performed miRNA profiling and lentiviral delivery of miRNAs into pre-B ALL blasts from patients. We identified *MIR-181A1* as the most prominent target of ETV6/RUNX1, and we demonstrate that *ETV6/RUNX1* and *MIR-181A1* form a novel regulatory double negative loop. Our results suggest a mechanism by which ETV6/RUNX1 might exert its preleukemic effect by perturbing the early-stage progression of the B-cell lineage.

Materials and Methods

Patients

All of the patient samples were obtained at the time of diagnosis and prior to treatment. The study was approved by the Institutional Review Board of National Taiwan University Hospital. In accordance with the Declaration of Helsinki, we obtained written informed consent from the parents of each patient before collection.

Cell culture

The REH cells (*ETV6/RUNX1*-positive human pre-B ALL, from ATCC) and human embryonic kidney 293FT cells were cultured in RPMI (Invitrogen) and DMEM (HyClone) medium, respectively, and supplemented with 10% fetal bovine serum (Biological Industries). Human primary pre-B ALL blasts were grown in SFEMII (StemCell Technologies) supplemented with a cytokine cocktail supporting cell growth (StemSpan CC100, StemCell Technologies).

RNA preparation and gene expression analysis

Total RNA was extracted by Trizol (Invitrogen) and used for reverse transcription (RT) as described [19]. Quantitative real-time PCR (qPCR) was performed on an ABI PRISM 7300. *ETV6/RUNX1* transcripts were detected by TaqMan qPCR using published primer probe combinations [20], and the TaqMan endogenous control assay for *GAPDH* (Applied Biosystems) was used.

MicroRNA expression profiling was performed using the ABI PRISM 7900 and stem-loop RT-qPCR miRNA arrays containing 397 mature human miRNAs (Applied Biosystems) as described [21]. For quantifying individual miRNA each was measured using TaqMan miRNA assays (Applied Biosystems). All miRNA assays were run concurrently with a calibration control, U6 snRNA.

ChIP

We used the chromatin immunoprecipitation (ChIP) kit (Upstate) to perform the assays. The chromatin was immunoprecipitated with antibodies against RUNX1 and HDAC3 (Abcam). The HDAC inhibitor valproic acid (VPA) was used to release the binding of HDAC3; REH cells were treated with 2 mM VPA for 24 hours before harvesting. Chromatin was also purified from cross-linked DNA that had not been immunoprecipitated to serve as an input control. A genomic region containing the putative RUNX1-binding site located at 3.8 kb upstream of the *MIR181A1* transcription start site (TSS) predicted by CoreBoost_HM (http://rulai.cshl.edu/tools/CoreBoost_HM/) [22], and another *MIR181A1* upstream region which does not contain the RUNX1-binding site were amplified by PCR. As a positive control for RUNX1 ChIP, the primer set PC amplifying the *MIR223* promoter was used as previously described [17]. PCR for the *GAPDH* coding region was carried out as a negative control for HDAC3 ChIP. Primers were listed in Table A in S1 file, available on the *PLOS ONE* Web site.

Western blotting

Cells were pelleted, washed with cold PBS, and lysed in RIPA buffer (Thermo) with protease inhibitor cocktail (Roche). 35 μg total protein was separated by SDS-PAGE and transferred to an Immobilon PVDF membrane (Pall). The membrane was blocked and incubated overnight with primary antibodies. After a final incubation with secondary antibodies conjugated with horseradish peroxidase (1:5000 dilution; Millipore), immune complexes were detected with HRP chemiluminescent substrate (Millipore). Antibodies and dilutions used were: anti-RUNX1 (1:1000, Abcam) and anti-β-actin (1:5000, Novus).

Lentiviral construct and infection

The sequence of *MIR181A1* was PCR amplified from human bone marrow mononuclear cells and then cloned into vector pLKO_TRC001 (National RNAi core, Taiwan), which contains a PGK-puromycin acetyltransferase insert, and labeled as pLKO.1.181A1. An empty TRC1 vector, pLKO.1.Null-T (National RNAi Core, Taiwan), which expresses a negative control shRNA (sequence: TCAGTTAACCACTTTTT) was used as an infection control. Production, concentration, and infection of lentivirus followed the protocol from the National RNAi Core, Taiwan. Single infection of REH cells and two sequential infections of primary pre-B ALL blasts with lentiviral particles were carried out. Infected cells were selected by adding puromycin (2 μg/mL) to the culture medium and collected after screening for a week.

miRNA precursors and siRNA transfection

The two miRNA precursors hsa-mir-181a and negative control 1 (Ambion) are partially double-stranded RNAs that mimic endogenous precursor miRNAs. Each was transfected into cells at a final concentration of 50 nM using siPORT NeoFx transfection agent (Ambion). Two rounds of transfection were performed with a 48-hour interval between the first and second round.

For ETV6/RUNX1 silencing with a short interfering RNA (siRNA), REH cells were transfected with a mixture of siRNAs targeting the fusion region of *ETV6/RUNX1* (Stealth siRNAs, Invitrogen) or a nonfunctional control, siRNA-S (Stealth siRNAs, Invitrogen) [23, 24]. The siRNAs were transfected into REH cells via electroporation with a MP-100 microporator (Labtech) in a 100-μL gold tip under the following conditions: 1×10^6 cells/mL antibiotic-free culture medium, 230 nM siRNA, one pulse of 1,150 V for 30 milliseconds.

Luciferase reporter assay

The luciferase activity assay was performed using the Dual-Luciferase Reporter Assay System (Promega). A 678-bp fragment of the RUNX1 3′ UTR containing a binding site for miR-181a (UGAAUGU) was cloned into the XbaI site at the distal end of the luciferase reporter gene of pGL3-promoter vector (Promega). This construct was used to transiently transfect 293FT cells with Lipofectamine 2000 (Invitrogen) together with pRL-TK Renilla (Promega), a transfection control used to calibrate the luciferase activity, and pLKO.1.181A1 (miR-181a-expressing vector) or pLKO.1.Null-T (negative control for miR-181a-expressing vector). A mutated version of the binding sequence (AGAUCUG) containing a BglⅡsite was used as the target site control. Cells were lysed, and the luciferase activity was measured 48 hours after transfection.

Cell viability, cell cycle, proliferation, and apoptosis assays

The cell viability was determined by Cell Proliferation Kit I (MTT) (Roche). A BrdU flow kit (BD) was used to determine cell cycle and proliferating cells. Apoptosis was evaluated by annexin V: FITC apoptosis detection kit (BD).

Flow cytometry analysis of lineage markers

Monoclonal antibodies recognizing the following cell-surface markers were used for flow cytometry: CD10, CD19, CD20, CD45, IgM, κ-chain, and λ-chain (BD). Flow cytometry was performed using FACScalibur (BD). Data were analyzed using FCS Express software (De Novo Software).

Statistical analyses

In miRNA profiling analysis, to avoid low abundant expression issue, miRNA with coefficient of variation (CV) < 0.2 was removed in the first step. In the second step, the student's t test was used to evaluate different miRNA expression between *ETV6/RUNX1*-positive (n=10) and *ETV6/RUNX1*-negative (n=40) groups. Finally, in order to control multiple testing issues, false discovery rate method was performed to adjust p value obtained from student's t test [25]. Data are represented the means ± SE or ± SD as indicated in the figure legends. The Student's t test or ANOVA were used to test the difference between groups for continuous variables. For categorical data, Fisher's exact was performed to test the difference between groups. Calculation methods of P values were denoted in the figure legends or bottom of tables. All tests were two-tailed and P values <0.05 were considered significant.

Results

miR-181a-1 is downregulated in *ETV6/RUNX1*-positive leukemias, and the regulatory region of *MIR181A1* is bound by ETV6/RUNX1 and HDAC3

Extensive miRNA profiling was carried out on the diagnostic samples of a cohort of 50 pre-B ALL patients, including 10 *ETV6/RUNX1*-positive and 40 *ETV6/RUNX1*-negative cases (clinical feature of patients see Table B in S1 file). Because ETV6/RUNX1 retains the DNA-binding ability of RUNX1, the fusion protein acts as a dominant-negative repressor to downregulate RUNX1 target genes. Therefore, a reduction of specific miRNAs in *ETV6/RUNX1*-positive samples compared with *ETV6/RUNX1*-negative samples was evaluated. Seventeen miRNAs were significantly downregulated in *ETV6/RUNX1*-positive ALL samples (Table 1), and of these, miR-181a-1, which is derived from the 3′ arm of precursor hsa-mir-181a-1 (Fig 1A), had the most significant *P*-value and showed a remarkable 4-fold decrease (Table 1). The decreased expression of miR-181a-1 in *ETV6/RUNX1*-positive leukemias was validated in another cohort of pre-B ALL cases analyzed by real-time qRT-PCR (Fig 1B).

Table 1. The statistic signature of 17 miRNAs

miRNA*	Expression level, ETV6/RUNX1^{+}/ ETV6/RUNX1^{-}	*P*
hsa-miR-181a-1	0.254	<.00005
hsa-miR-92	0.327	.002
hsa-miR-222	0.194	.004
hsa-miR-342	0.461	.004
hsa-miR-181d	0.524	.004
hsa-miR-155	0.353	.005
hsa-miR-423	0.371	.005
hsa-miR-195	0.391	.012
hsa-miR-130b	0.472	.019
hsa-miR-221	0.098	.024
hsa-let-7b	0.505	.037
hsa-let-7a	0.527	.037
hsa-miR-30e-3p	0.443	.039
hsa-miR-19a	0.456	.039
hsa-miR-660	0.525	.045
hsa-miR-181c	0.385	.046

hsa-miR-425	0.465	.050

* Selected by differential expression in patients with or without ETV6/RUNX1 fusion gene.

Whether ETV6/RUNX1 regulates miR-181a-1 expression was further assessed by siRNA-mediated knockdown of *ETV6/RUNX1* in REH cells, which express the ETV6/RUNX1 fusion protein (Figs 1C and 1D). A mixture of two *ETV6/RUNX1*-specific siRNAs (siE/R), which target the fusion region of *ETV6/RUNX1*, was used to suppress *ETV6/RUNX1* expression [23]. As a transfection control, we used a nonfunctional siRNA (siRNA-S) that had no effect on *ETV6/RUNX1* expression [24]. Compared with siRNA-S, both mRNA and protein of ETV6/RUNX1 were significantly reduced by ~40% and ~35% after knockdown with siE/R (Figs 1C and 1D). Further examination showed that miR-181a-1 levels increased significantly in REH cells that were treated with siE/R but not in those treated with siRNA-S (Fig 1E). These studies with REH cells and clinical leukemic specimens indicated that ETV6/RUNX1 negatively regulates miR-181a-1 level.

To reveal the interaction between ETV6/RUNX1 and the regulatory region of *MIR181A1*, we performed ChIP using the REH cells and a RUNX1-specific antibody. Bioinformatic analyses identified the predicted transcription start site (TSS) of *MIR181A1* and a putative RUNX1-binding site with the sequence of TGT/cGGT located 3.8 kb upstream of the TSS (P1 site, Fig 2A; Table C in S1 file). Binding of RUNX1 and ETV6/RUNX1 at P1 was demonstrated by specific precipitation of this DNA region, but not at an irrelevant site (P2), with anti-RUNX1 in the ChIP analysis (Fig 2B). Moreover, ChIP with anti-HDAC3 also revealed the binding of HDAC3 at P1 (Fig 2C). These results are in agreement with previous reports that the transcriptional repressor activity of ETV6/RUNX1 is associated with its aberrant recruitment of the N-CoR/SMRT-HDAC3 complex [5-7]. Taken together, these results supported the idea that ETV6/RUNX1 directly regulates *MIR181A1* expression.

miR-181a targets *ETV6/RUNX1*

The consequence and mechanism(s) of *MIR181A1* downregulation in ETV6/RUNX1 ALL were further investigated. It has been shown that miR-181a, a mature form derived from the 5′ arm of precursor hsa-mir-181a-1 (Fig 1A), functions by targeting several mRNAs [26-28]. To identify new miR-181a target genes, we conducted a database search utilizing TargetScan (http://www.targetscan.org), an online miRNA target prediction interface, and searched for oncogenes targeting by miR-181a. With miRNA target prediction programs, we identified 1,194 potential miR-181a target genes. The presence of *RUNX1* among the database-predicted target

genes implies an unknown mechanism of *ETV6/RUNX1* regulation by miR-181a. To investigate this hypothesis, we first overexpressed miR-181a in REH cells by transfection of miRNA mimics (Fig 3A), which resulted in a decrease of ETV6/RUNX1 (Fig 3B). The negative effect of miR-181a on *ETV6/RUNX1* expression was further assessed with the luciferase reporter assay, which examined the interaction between miR-181a and the 3' UTR of *RUNX1* and *ETV6/RUNX1* (Fig 3C). We constructed fragments containing the last 678 bp of the *RUNX1* 3′ UTR, which contains wild-type or mutated miR-181a recognition sequence, and inserted them immediately downstream of the luciferase reporter gene. The miR-181a expression vector or empty vector was co-transfected with the different luciferase 3' UTR constructs into 293FT cells. The results showed that miR-181a downregulated the luciferase reporter gene activity when the luciferase gene was fused with wild-type but not mutated *RUNX1* 3' UTR (Fig 3D). These experiments demonstrated that miR-181a targets *ETV6/RUNX1*, and they suggested that the fusion gene and *MIR181A1* can regulate each other.

Ectopic expression of miR-181a in REH cells impedes cell growth and enhances cell differentiation

The oncogenic effect of ETV6/RUNX1 has been postulated to operate through impairment of B-cell differentiation in a bone marrow transplantation model, and consequently it results in the accumulation of pro-B cells [29]. We investigated whether the greatly reduced *MIR181A1* expression in *ETV6/RUNX1*-positive pre-B ALL blasts plays a role in the ETV6/RUNX1-mediated blockade of B-cell differentiation and in the preleukemic events induced by ETV6/RUNX1. First, REH cells were transduced by a lentiviral vector carrying *MIR181A1* (181A1-LV) to express miR-181a stably and constitutively (Fig 4A). We found that ectopic overexpression of miR-181a resulted in growth retardation of the cells, and 181A1-LV-transduced REH cells showed a nearly 40% decrease in both MTT activity and cell density after 72 hours of seeding (Figs 4B and 4C). Moreover, 181A1-LV transduction increased the annexin V–positive (apoptotic) cell population (Fig 4D). Further assessment of the proliferation activity by biparametric BrdU/DNA flow cytometry showed that miR-181a expression did not affect the percentage of BrdU-positive cells but rather increased the proportion of cells in G0/G1 phase (Fig 4E).

The stages of B cell maturation are characterized by specific expression patterns of immunoglobulins and other membrane proteins. To gain insight into the effect of miR-181a overexpression on REH cell maturation, we stained cells for differentiation markers and found an increase in CD10-negative, CD20-positive, surface

IgM-positive, κ-chain-positive, and λ-chain-positive cell populations in 181A1-LV-transduced cells compared with infection control cells (Fig 5A and S1 Fig). Decreased CD10 expression and increased CD20, IgM, κ-chain, and λ-chain expression may represent a gradual progression of B lymphoid cells from pre-BI cells to immature B cells [30]. Because the decrease in CD10 expression was the most notable change of 181A1-LV-transduced cells, we further stained cells for CD10 and annexin V and found that most apoptotic cells were CD10-negative (Fig 5B).

miR-181a induces partial differentiation by diminishing CD10 expression in *ETV6/RUNX1*-positive pre-B ALL blasts

Loss of the marker CD10 and a gain of CD20 have been associated with differentiation of normal B-cell precursors from hematopoietic stem cells to naive mature B cell in the bone marrow [31]. The infection of primary blasts isolated from the bone marrow of pre-B ALL patients with a lentiviral vector expressing miR-181a increased the level of miR-181a by an average of 2.5-fold (range from 1.5- to 3-fold) in three *ETV6/RUNX1*-positive samples compared with the controls (Fig 5C). This induction partially altered the lymphocytic differentiation as shown by the CD10 hyperexpression decrease in cells from two of three *ETV6/RUNX1*-positive samples (Fig 5D and S2 Fig), suggesting that the level of miR-181a expression is important for the perturbation of the lymphocytic differentiation program in ETV6/RUNX1 ALL.

Discussion

The critical roles of miRNAs in hematopoiesis and their ubiquitous dysregulation in leukemia allow us an opportunity to understand the driving force of leukemogenesis and the consequences of aberrant miRNA expression. By applying miRNA profiling to samples from 50 pre-B ALL patients, we determined the gene expression signatures of specific ALL subtypes. The miRNA expression profile showed that most miRNAs are downregulated in *ETV6/RUNX1*-positive samples, indicating that ETV6/RUNX1 affects the functions of miRNAs primarily by downregulating their expression. We identified miR-181a-1 as the most differentially underexpressed miRNA in patients carrying t(12;21). This is consistent with the expression profile of another patient cohort; Schotte et al. measured 397 miRNAs in 81 pediatric ALL cases and also demonstrated that miR-181a-1 expression is 5-fold lower in patients with t(12;21) than in patients with other ALL subtypes [32]. To address how ETV6/RUNX1 regulates miR-181a-1 level, we performed siRNA-mediated knockdown of *ETV6/RUNX1* followed by ChIP in an ETV6/RUNX1-expressing leukemic cell line. Our data reveal the upregulation of miR-181a-1 in ETV6/RUNX1-knockdown cells and direct ETV6/RUNX1 binding and recruitment of

HDAC3 to the regulatory region of *MIR181A1*, suggesting that ETV6/RUNX1 negatively regulates *MIR181A1* expression.

The miR-181 family is highly conserved and comprises six miRNAs transcribed from three separate gene loci and organized into three clusters including miR-181a/b-1, miR-181a/b-2, and miR-181c/d. The finding that both miR-181a-1 and miR-181c/d are significantly downregulated in ETV6/RUNX1 ALL (Table 1) and that all members of the miR-181 family share the same seed sequence within their 5′ arms and in targets led us to investigate which downstream genes are regulated by miR-181a. We found not only was miR-181a-1 suppressed by ETV6/RUNX1, but feedback inhibition of miR-181a on ETV6/RUNX1 was observed in the cell line experiments, suggesting that *MIR181A1* and *ETV6/RUNX1* can regulate each other.

In fact, such a regulatory network between transcription factors and miRNAs has been described before; for example, regulatory circuitry comprising miR-223 and transcription factors NFI-A and C/EBPα has been shown to sustain the level of miR-223, which may be important in granulopoiesis [33]. Moreover, recently a ‘mutual negative feedback loop’ involving MYC and miR-548m was described in non-Hodgkin B-cell lymphomas, in that this regulatory loop is important for sustaining a high level of MYC and low level of miR-548m during lymphomagenesis and drug resistance [34]. According to previous findings and our current data, we propose a new mechanism of ETV6/RUNX1 action: a double negative loop in which ETV6/RUNX1 can bind to the regulatory region of *MIR181A1* keeps hsa-mir-181a-1 expression low, which consequently reduces the miR-181a-mediated translational repression of ETV6/RUNX1. By doing so, ETV6/RUNX1 can enhance its own oncogenic potential (S3 Fig).

In conclusion, our study enhances the understanding of the molecular mechanism underlying ETV6/RUNX1-mediated attenuation of B-cell differentiation and offers the opportunity to identify new targets for development of therapeutic approaches to leukemia.

Acknowledgments

The authors thank Dr. Sheng-Kai Chang for the lentivirus package and Prof. Wen-Chien Chou for providing the MP-100 microporator device to transfect siRNA into REH cells.

Correspondence: Shu-Wha Lin, National Taiwan University, No. 7, Chung-San S. Rd., Taipei 100, Taiwan; e-mail: mtshuwha@ntu.edu.tw.; Shu-Rung Lin, Chung-Yuan Christian University, No. 200, Chung Pei Rd., 320 Taoyuan, Taiwan; e-mail: shurung@cycu.edu.tw

References

1. Pui CH, Carroll WL, Meshinchi S, Arceci RJ. Biology, risk stratification, and therapy of pediatric acute leukemias: an update. Journal of clinical oncology : official journal of the American Society of Clinical Oncology. 2011;29(5):551-65. Epub 2011/01/12. doi: 10.1200/JCO.2010.30.7405. PubMed PMID: 21220611; PubMed Central PMCID: PMC3071256.

2. Hong D, Gupta R, Ancliff P, Atzberger A, Brown J, Soneji S, et al. Initiating and cancer-propagating cells in TEL-AML1-associated childhood leukemia. Science. 2008;319(5861):336-9. Epub 2008/01/19. doi: 10.1126/science.1150648. PubMed PMID: 18202291.

3. Morrow M, Samanta A, Kioussis D, Brady HJ, Williams O. TEL-AML1 preleukemic activity requires the DNA binding domain of AML1 and the dimerization and corepressor binding domains of TEL. Oncogene. 2007;26(30):4404-14. Epub 2007/01/24. doi: 10.1038/sj.onc.1210227. PubMed PMID: 17237815.

4. Gunji H, Waga K, Nakamura F, Maki K, Sasaki K, Nakamura Y, et al. TEL/AML1 shows dominant-negative effects over TEL as well as AML1. Biochemical and biophysical research communications. 2004;322(2):623-30. Epub 2004/08/25. doi: 10.1016/j.bbrc.2004.07.169. PubMed PMID: 15325275.

5. Guidez F, Petrie K, Ford AM, Lu H, Bennett CA, MacGregor A, et al. Recruitment of the nuclear receptor corepressor N-CoR by the TEL moiety of the childhood leukemia-associated TEL-AML1 oncoprotein. Blood. 2000;96(7):2557-61. Epub 2000/09/26. PubMed PMID: 11001911.

6. Wang L, Hiebert SW. TEL contacts multiple co-repressors and specifically associates with histone deacetylase-3. Oncogene. 2001;20(28):3716-25. Epub 2001/07/06. doi: 10.1038/sj.onc.1204479. PubMed PMID: 11439334.

7. Karagianni P, Wong J. HDAC3: taking the SMRT-N-CoRrect road to repression. Oncogene. 2007;26(37):5439-49. Epub 2007/08/19. doi: 10.1038/sj.onc.1210612. PubMed PMID: 17694085.

8. Starkova J, Madzo J, Cario G, Kalina T, Ford A, Zaliova M, et al. The identification of (ETV6)/RUNX1-regulated genes in lymphopoiesis using histone deacetylase inhibitors in ETV6/RUNX1-positive lymphoid leukemic cells. Clinical cancer research : an official journal of the American Association for Cancer Research. 2007;13(6):1726-35. Epub 2007/02/28. doi: 10.1158/1078-0432.CCR-06-2569. PubMed PMID: 17325341.

9. Torrano V, Procter J, Cardus P, Greaves M, Ford AM. ETV6-RUNX1 promotes survival of early B lineage progenitor cells via a dysregulated erythropoietin receptor.

Blood. 2011;118(18):4910-8. Epub 2011/09/09. doi: 10.1182/blood-2011-05-354266. PubMed PMID: 21900195.

10. Kaindl U, Morak M, Portsmouth C, Mecklenbrauker A, Kauer M, Zeginigg M, et al. Blocking ETV6/RUNX1-induced MDM2 overexpression by Nutlin-3 reactivates p53 signaling in childhood leukemia. Leukemia : official journal of the Leukemia Society of America, Leukemia Research Fund, UK. 2014;28(3):600-8. Epub 2013/11/19. doi: 10.1038/leu.2013.345. PubMed PMID: 24240203; PubMed Central PMCID: PMC3948158.

11. Diakos C, Zhong S, Xiao Y, Zhou M, Vasconcelos GM, Krapf G, et al. TEL-AML1 regulation of survivin and apoptosis via miRNA-494 and miRNA-320a. Blood. 2010;116(23):4885-93. Epub 2010/09/03. doi: 10.1182/blood-2009-02-206706. PubMed PMID: 20807887; PubMed Central PMCID: PMC3265147.

12. Musilova K, Mraz M. MicroRNAs in B-cell lymphomas: how a complex biology gets more complex. Leukemia : official journal of the Leukemia Society of America, Leukemia Research Fund, UK. 2015;29(5):1004-17. Epub 2014/12/30. doi: 10.1038/leu.2014.351. PubMed PMID: 25541152.

13. Vasilatou D, Papageorgiou S, Pappa V, Papageorgiou E, Dervenoulas J. The role of microRNAs in normal and malignant hematopoiesis. European journal of haematology. 2010;84(1):1-16. Epub 2009/09/12. doi: 10.1111/j.1600-0609.2009.01348.x. PubMed PMID: 19744129.

14. Roehle A, Hoefig KP, Repsilber D, Thorns C, Ziepert M, Wesche KO, et al. MicroRNA signatures characterize diffuse large B-cell lymphomas and follicular lymphomas. British journal of haematology. 2008;142(5):732-44. Epub 2008/06/10. doi: 10.1111/j.1365-2141.2008.07237.x. PubMed PMID: 18537969.

15. Vargova K, Curik N, Burda P, Basova P, Kulvait V, Pospisil V, et al. MYB transcriptionally regulates the miR-155 host gene in chronic lymphocytic leukemia. Blood. 2011;117(14):3816-25. Epub 2011/02/08. doi: 10.1182/blood-2010-05-285064. PubMed PMID: 21296997.

16. Vigorito E, Perks KL, Abreu-Goodger C, Bunting S, Xiang Z, Kohlhaas S, et al. microRNA-155 regulates the generation of immunoglobulin class-switched plasma cells. Immunity. 2007;27(6):847-59. Epub 2007/12/07. doi: 10.1016/j.immuni.2007.10.009. PubMed PMID: 18055230; PubMed Central PMCID: PMC4135426.

17. Fazi F, Racanicchi S, Zardo G, Starnes LM, Mancini M, Travaglini L, et al. Epigenetic silencing of the myelopoiesis regulator microRNA-223 by the AML1/ETO oncoprotein. Cancer cell. 2007;12(5):457-66. Epub 2007/11/13. doi: 10.1016/j.ccr.2007.09.020. PubMed PMID: 17996649.

18. Gefen N, Binder V, Zaliova M, Linka Y, Morrow M, Novosel A, et al.

Hsa-mir-125b-2 is highly expressed in childhood ETV6/RUNX1 (TEL/AML1) leukemias and confers survival advantage to growth inhibitory signals independent of p53. Leukemia : official journal of the Leukemia Society of America, Leukemia Research Fund, UK. 2010;24(1):89-96. Epub 2009/11/06. doi: 10.1038/leu.2009.208. PubMed PMID: 19890372; PubMed Central PMCID: PMC2811577.

19. Yang YL, Lin SR, Chen JS, Lin SW, Yu SL, Chen HY, et al. Expression and prognostic significance of the apoptotic genes BCL2L13, Livin, and CASP8AP2 in childhood acute lymphoblastic leukemia. Leuk Res. 2010;34(1):18-23. Epub 2010/01/30. doi: 10.1016/j.leukres.2009.07.023. PubMed PMID: 20109966.

20. Gabert J, Beillard E, van der Velden VHJ, Bi W, Grimwade D, Pallisgaard N, et al. Standardization and quality control studies of 'real-time' quantitative reverse transcriptase polymerase chain reaction of fusion gene transcripts for residual disease detection in leukemia - A Europe Against Cancer Program. Leukemia : official journal of the Leukemia Society of America, Leukemia Research Fund, UK. 2003;17(12):2318-57. doi: DOI 10.1038/sj.leu.2403135. PubMed PMID: ISI:000187183200002.

21. Yu SL, Chen HY, Chang GC, Chen CY, Chen HW, Singh S, et al. MicroRNA signature predicts survival and relapse in lung cancer. Cancer cell. 2008;13(1):48-57. Epub 2008/01/03. doi: 10.1016/j.ccr.2007.12.008. PubMed PMID: 18167339.

22. Wang X, Xuan Z, Zhao X, Li Y, Zhang MQ. High-resolution human core-promoter prediction with CoreBoost_HM. Genome research. 2009;19(2):266-75. Epub 2008/11/11. doi: 10.1101/gr.081638.108. PubMed PMID: 18997002; PubMed Central PMCID: PMC2652208.

23. Zaliova M, Madzo J, Cario G, Trka J. Revealing the role of TEL/AML1 for leukemic cell survival by RNAi-mediated silencing. Leukemia : official journal of the Leukemia Society of America, Leukemia Research Fund, UK. 2011;25(2):313-20. Epub 2010/11/27. doi: 10.1038/leu.2010.277. PubMed PMID: 21109770.

24. Diakos C, Krapf G, Gerner C, Inthal A, Lemberger C, Ban J, et al. RNAi-mediated silencing of TEL/AML1 reveals a heat-shock protein- and survivin-dependent mechanism for survival. Blood. 2007;109(6):2607-10. Epub 2006/11/11. doi: 10.1182/blood-2006-04-019612. PubMed PMID: 17095626.

25. Benjamini YaH, Yosef. Controlling the false discovery rate: a practical and powerful approach to multiple testing. Journal of the Royal Statistical Society, Series B. 1995;57(1):289-300.

26. Pallasch CP, Patz M, Park YJ, Hagist S, Eggle D, Claus R, et al. miRNA deregulation by epigenetic silencing disrupts suppression of the oncogene PLAG1 in chronic lymphocytic leukemia. Blood. 2009;114(15):3255-64. Epub 2009/08/21. doi: 10.1182/blood-2009-06-229898. PubMed PMID: 19692702; PubMed Central PMCID:

PMC2925729.
27. Li X, Zhang J, Gao L, McClellan S, Finan MA, Butler TW, et al. MiR-181 mediates cell differentiation by interrupting the Lin28 and let-7 feedback circuit. Cell death and differentiation. 2012;19(3):378-86. Epub 2011/10/08. doi: 10.1038/cdd.2011.127. PubMed PMID: 21979467; PubMed Central PMCID: PMC3278736.
28. Ouyang YB, Lu Y, Yue S, Giffard RG. miR-181 targets multiple Bcl-2 family members and influences apoptosis and mitochondrial function in astrocytes. Mitochondrion. 2012;12(2):213-9. Epub 2011/10/01. doi: 10.1016/j.mito.2011.09.001. PubMed PMID: 21958558; PubMed Central PMCID: PMC3250561.
29. Fischer M, Schwieger M, Horn S, Niebuhr B, Ford A, Roscher S, et al. Defining the oncogenic function of the TEL/AML1 (ETV6/RUNX1) fusion protein in a mouse model. Oncogene. 2005;24(51):7579-91. Epub 2005/07/27. doi: 10.1038/sj.onc.1208931. PubMed PMID: 16044150.
30. Mesquita Junior D, Araujo JA, Catelan TT, Souza AW, Cruvinel Wde M, Andrade LE, et al. Immune system - part II: basis of the immunological response mediated by T and B lymphocytes. Revista brasileira de reumatologia. 2010;50(5):552-80. Epub 2010/12/03. PubMed PMID: 21125191.
31. Perez-Andres M, Paiva B, Nieto WG, Caraux A, Schmitz A, Almeida J, et al. Human peripheral blood B-cell compartments: a crossroad in B-cell traffic. Cytometry Part B, Clinical cytometry. 2010;78 Suppl 1:S47-60. Epub 2010/09/21. doi: 10.1002/cyto.b.20547. PubMed PMID: 20839338.
32. Schotte D, De Menezes RX, Akbari Moqadam F, Khankahdani LM, Lange-Turenhout E, Chen C, et al. MicroRNA characterize genetic diversity and drug resistance in pediatric acute lymphoblastic leukemia. Haematologica. 2011;96(5):703-11. Epub 2011/01/19. doi: 10.3324/haematol.2010.026138. PubMed PMID: 21242186; PubMed Central PMCID: PMC3084917.
33. Fazi F, Rosa A, Fatica A, Gelmetti V, De Marchis ML, Nervi C, et al. A minicircuitry comprised of microRNA-223 and transcription factors NFI-A and C/EBPalpha regulates human granulopoiesis. Cell. 2005;123(5):819-31. Epub 2005/12/06. doi: 10.1016/j.cell.2005.09.023. PubMed PMID: 16325577.
34. Lwin T, Zhao X, Cheng F, Zhang X, Huang A, Shah B, et al. A microenvironment-mediated c-Myc/miR-548m/HDAC6 amplification loop in non-Hodgkin B cell lymphomas. The Journal of clinical investigation. 2013;123(11):4612-26. Epub 2013/11/13. doi: 10.1172/JCI64210. PubMed PMID: 24216476; PubMed Central PMCID: PMC3809771.

Supporting information

S1 file. Primer sequences **(Table A)**. Clinical features of the ALL patients included in expression profiling study **(Table B)**. The signature of 13 miRNAs/miRNA cluster and the location of RUNX1 binding sites **(Table C)**.

S1 Fig. Surface antigen of lymphoid lineage expressed on lentivirus-infected REH cells. Expression of (A) CD20, (B) IgM, (C) κ-chain, and (D) λ-chain were detected by flow cytometric analysis (left). The results were quantified and represented as the average of three independent evaluations ± SD (right). *P ≤ 0.05, **P ≤ 0.01, ***P ≤ 0.001 (ANOVA)

S2 Fig. Surface CD10 expression of lentivirus infected $CD45^+$ $CD19^+$ ETV6/RUNX1-positive pre-B ALL blasts. Flow cytometric analysis of CD10 expression on $CD45^{w+}$or+ $CD19^+$ *ETV6/RUNX1*-positive pre-B ALL blasts derived from patient #3. The MFI of CD10 in each groups were: NC 49.62, 181A1 51.68.

S3 Fig. Schematic representation of the reciprocal downregulation of *ETV6/RUNX1* and *MIR181A1*. In leukemia cells with frequent chromosome rearrangement t(12;21)(p13;q22), ETV6/RUNX1 oncoprotein occupies the putative RUNX1-binding site upstream of *MIR181A1* and restricts transcription by recruiting co-repressors such as HDAC3. This repression of *MIR181A1* expression consequently upregulates the target of miR-181a, ETV6/RUNX1, the oncoprotein itself.

Figure Legends

Fig 1. siRNA-mediated silencing of ETV6/RUNX1 increases the level of mature miR-181a-1.

(A) Stem-loop sequence of human precursor mir-181a-1. Mature miR-181a (red) and miR181a-1 (blue) are indicated. (B) Validation of miR-181a-1 expression in primary pre-B ALL samples (*ETV6/RUNX1*-positive, n = 7; *ETV6/RUNX1*-negative, n = 8) using TaqMan qRT-PCR. ETV6/RUNX1-expressing REH cells (control) were transfected with siRNAs. After 48 hours of transfection with functional siETV6/RUNX1 (siE/R) or nonfunctional siRNA (siRNA-S), (C) *ETV6/RUNX1* mRNA was detected by qRT-PCR, and (D) protein was analyzed by Western blotting with anti-RUNX1; anti-β-actin was used as a loading control. Relative expression as determined by densitometry is indicated below the blots. (E) Mature miR-181a-1 was measured by qRT-PCR. Bars represent the mean ± SE of at least three independent experiments. *GAPDH* and *RNU6B* were used as calibration controls for mRNA and miRNA expression, respectively. $*P \leq 0.05$, $**P \leq 0.01$ (ANOVA).

Fig 2. ETV6/RUNX1 inhibits *MIR181A1* transcription via binding to the endogenous RUNX1 site.

(A) Schematic representation of the genomic structure of human *MIR181A1*. The location of the *MIR181A1* gene and the RUNX1-binding site are numbered relative to the TSS (+1). Arrows indicate the locations of the primers used in the ChIP assay. (B) ChIP was carried out using anti-RUNX1 or in the absence of specific antibody (Control) (left). DNA sequences surrounding the putative RUNX1-binding site were amplified by PCR using P1 primers. To evaluate the specificity of RUNX1 binding, a positive control and a negative control were performed using PC and P2, respectively, for the ChIP assay. Amplification of the upstream region near the RUNX1-binding site on *MIR223*, which is a known direct target of RUNX1, was performed using PC primers. P2 primers were designed to amplify a distal region lacking the RUNX1-binding site. Input shows the amplification from sonicated chromatin, and genomic DNA (gDNA) was used as a positive PCR control. The PCR products were quantified by densitometry (right). (C) The ChIP assay was performed using anti-HDAC3 (left). Treatment with valproic acid and amplification of the promoter region of *GAPDH* were used as controls. The PCR products were quantified by densitometry (right). Bars show the mean ± SD from three independent experiments. $*P \leq 0.05$, $**P \leq 0.01$ (ANOVA).

Fig 3. miR-181a regulates the level of ETV6/RUNX1.

Overexpression of miR-181a in REH cells was performed by transfection with precursor miRNA. A final 50 nM concentration of nontargeting-miR (NC) or pre-mir-181a (181a) were transfected twice and cells were harvested after 48 hours of the second transfection for further examination. (A) miR-181a level was detected by TaqMan qRT-PCR. (B) Regulation of ETV6/RUNX1 by miR-181a was confirmed by Western blotting with RUNX1-specific (E/R) antibody. Relative expression as determined by densitometry is indicated below the blots. (C) The putative miR-181a binding site in the *RUNX1* 3' UTR. nt, nucleotides. (D) The last 678 bp of the human *RUNX1* 3' UTR containing normal (WT) or mutated (mut) miR-181a targeting sequences were cloned downstream of a pGL3-luciferase vector and transfected into 293FT cells with expression vectors for miR-181a (181a) or negative control shRNA (NC). All experiment was conducted in triplicate. Bars represent the mean ± SD of three independent experiments. $*P \leq 0.05$, $**P \leq 0.01$, $***P \leq 0.001$ (ANOVA).

Fig 4. Ectopic expression of miR-181a suppresses growth and induces apoptosis of REH cells.

REH cells were infected with lentiviral vector expressing the negative control shRNA

(NC) or miR-181a (181A1). (A) Relative miR-181a levels were determined by qRT-PCR. (B) Growth curve was determined as following: Cells were cultured for 48, 96, and 144 hours and then assessed with the MTT assay. (C) Cells were seeded at a density of 1×10^5 cells/mL and cultured. After 72 hours, cells were stained with trypan blue, and viable cells were counted. (D) Apoptosis was assessed by flow cytometric analysis of annexin V/propidium iodide (PI) staining of lentivirus-transduced cells (left). Representative histograms demonstrate the proportion of annexin V-positive cells (right). (E) Biparametric BrdU/DNA analysis: During the last 30 minutes of culture, 1 mM BrdU was added to the cells, and then the cells were stained with anti-BrdU and 7-aminoactinomycin D (7-AAD) and detected by flow cytometry (left). The percentage of cells in each of the cell-cycle phases G0/G1, S, and G2+M was quantified (right). Bars show the mean ± SD from three independent experiments. 181A1 vs. NC $*P \leq 0.05$, $**P \leq 0.01$, $***P \leq 0.001$ (ANOVA); NC vs. REH $^{\#\#}P \leq 0.01$.

Fig 5. Ectopic expression of miR-181a enhances lymphoid differentiation in the ETV6/RUNX1-positive cell line and primary ALL blasts.

(A) Percentage of lentivirus-infected REH cells stained for cell-surface marker CD10 as analyzed by flow cytometry (left). The results were quantified and are presented as the average ± SD of three independent evaluations (right). (B) 181A1-LV-infected REH cells were co-stained for annexin V and CD10 and measured by flow cytometry (left). The percentage of each of CD10-positive and -negative annexin V-positive cells was quantified, and the average ± SD of three independent evaluations is shown (right). (C) Primary ALL blasts were infected with NC- or 181A1-LV. Mature miR-181a expression level in lentivirus-infected primary pre-B ALL blasts from three ETV6/RUNX1-positive patients was determined by qRT-PCR. The results are shown as average ± SD. (D) CD10 expression in $CD45^{w+or+}$ $CD19^{+}$ ETV6/RUNX1-positive pre-B ALL blasts was analyzed by flow cytometry. In the comparison with the infection control (NC), 181A1-LV-transduced cells derived from patient #1 and #2 both showed a decrease in $CD10^{High}$ cells (Patient #1: NC 10.1% / MFI 40.92, 181A1 6.95% / MFI 39.51; Patient #2: NC 40.1% / MFI 424.28, 181A1 29.5% / MFI 444.24) and a relative increase in $CD10^{Low}$ cells (Patient #1: NC 87.98% / MFI 165.49, 181A1 91.05% / MFI 156.68; Patient #2: NC 58.1% / MFI 1929.88, 181A1 69 % / 1854.4). $*P \leq 0.05$, $**P \leq 0.01$ (ANOVA).

Fig 1.

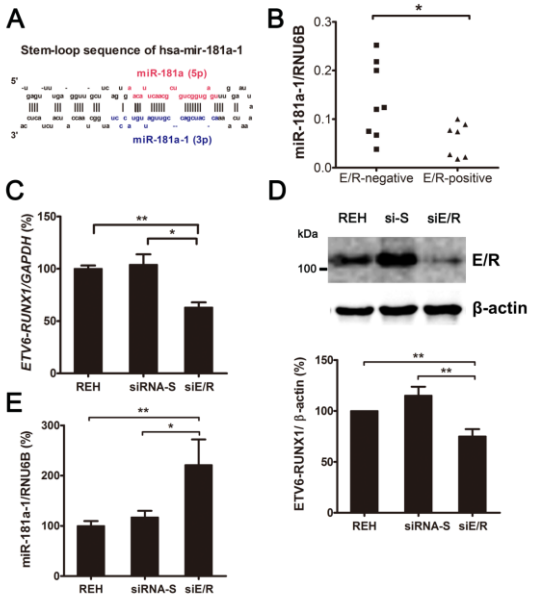

Fig 2.

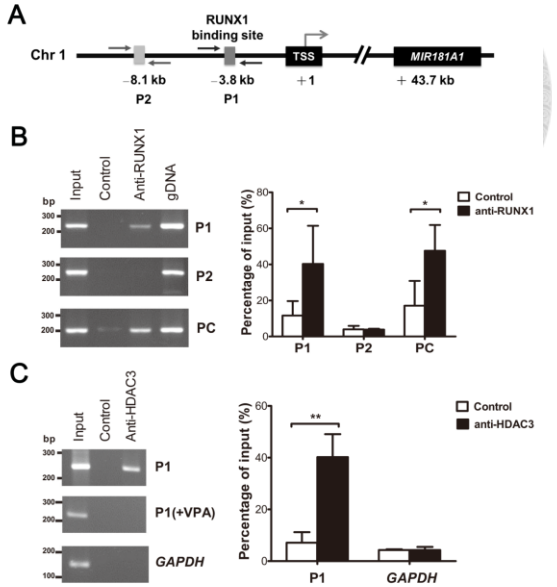

Fig 3.

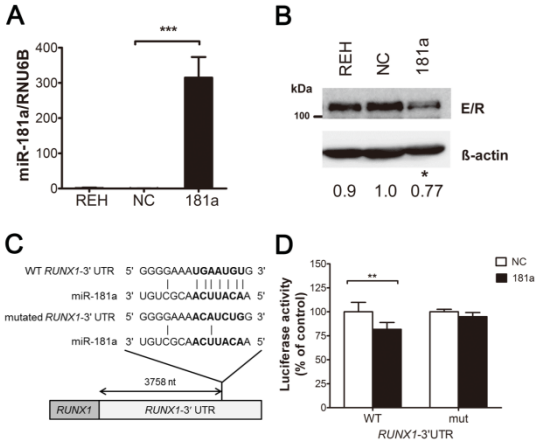

Fig 4.

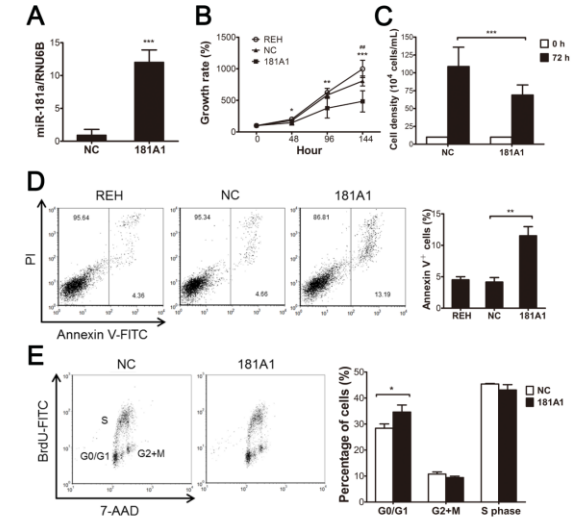

Fig 5.

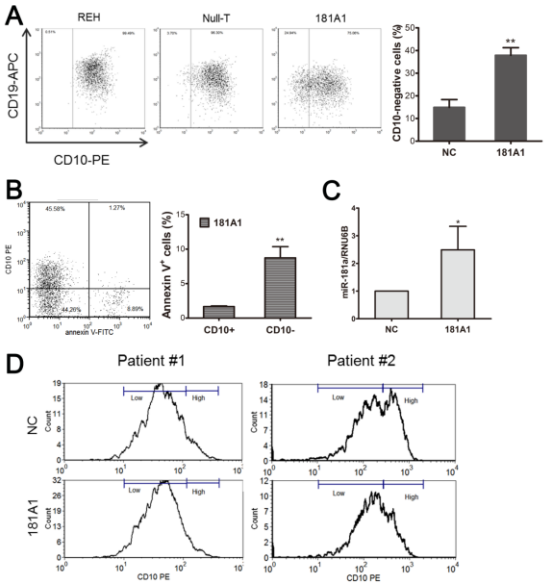

S1 file.

1. Supplemental table：3 tables

Table A. Primer sequences

Primers for ChIP assays	
P1-forward	5'-CACCATACACAAACCACTTG -3'
P1-reverse	5'-GAGCTCTGTGTATGATTGTC-3'
P2-forward	5'-AG CTCAGTAGAGAGATGTTG-3'
P2-reverse	5'-GGCACACAAGCTAAA ACTTG-3'
GAPDH coding region forward	5'-GAAGGTGAAGGTCGGAGT-3'
GAPDH coding region reverse	5'-ACCTTGAG CTCTCCTTGC-3'

Table B. Clinical features of the ALL patients included in expression profiling study

	ETV6/RUNX1^{-}		ETV6/RUNX1^{+}		
	n	%	n	%	*P*
Gender					
Female	20	50	4	40	.728*
Male	20	50	6	60	
Onset age					
Mean ± SD	6.15 ± 3.23		5.77 ± 2.97		.738†
Less than 10	36	90	9	90	1.000*
More than 10	4	10	1	10	
WBC count × k/μL					
Less than 100	32	80	9	90	.665*
More than 100	8	20	1	10	
t(9;22)					
Non	37	92.5	10	100	1.000*
With	3	7.5	0	0	
Risk groups					
SR	20	50	6	60	.899*
HR	9	22.5	2	20	
VHR	11	27.5	2	20	

SR: standard risk; HR: high risk; VHR: very high risk

*Calculated by Fisher's Exact test

†Calculated by Student's *t*-test

Table C. The signature of 13 miRNAs/miRNA clusters and the locations of RUNX1 binding sites

miRNA/miRNA cluster	Location	Input (NCBI36)	TSS* (+1)	RUNX1 binding site†
hsa-miR-181a-1	1q32.1	chr1 197094905 197144905 −	197138675	-3845
hsa-miR-30e-3p	1p34.2	chr1 40942614 40992614 +	40947610	-3749, -3185, -2321
hsa-miR-425	3p21.31	chr3 49033146 49083146 −	49041875	-3879, -3488, -2863, -1349
hsa-miR-19a/92a-1	13q31.3	chr13 90750860 90800860 +	90798075‡	-242
hsa-miR-342	14q32.2	chr14 99595745 99645745 +	99601480	-1909, -1322, -548, +31
hsa-miR-195	17p13.1	chr17 6862065 6912065 −	6919137‡	-2916, -889
hsa-miR-423	17q11.2	chr17 25418223 25468223 +	25468010	-3293, -2389
hsa-miR-181c/d	19p13.13	chr19 13796513 13846513 +	13837455	158
hsa-miR-155	21q21.3	chr21 25818163 25868163 +	26934221‡	no binding site is found
hsa-miR-130b	22q11.21	chr22 20287270 20337270 +	20326560	-1999, -545
hsa-let-7a-3/7b	22q13.31	chr22 44837293 44887293 +	44846680	-3453, -1882
hsa-miR-221/222	Xp11.3	chrX 45490638 45540638 −	45518410	-3561, -675
hsa-miR-660	Xp11.23	chrX 49604494 49654494 +	49613885	-3396, -3320, +708

TSS, transcriptional start site. *TSS is predicted by CoreBoost_HM.

†RUNX1 binding site in the upstream 4kb and downstream 1kb of TSS.

‡TSS of host gene

S1 Fig

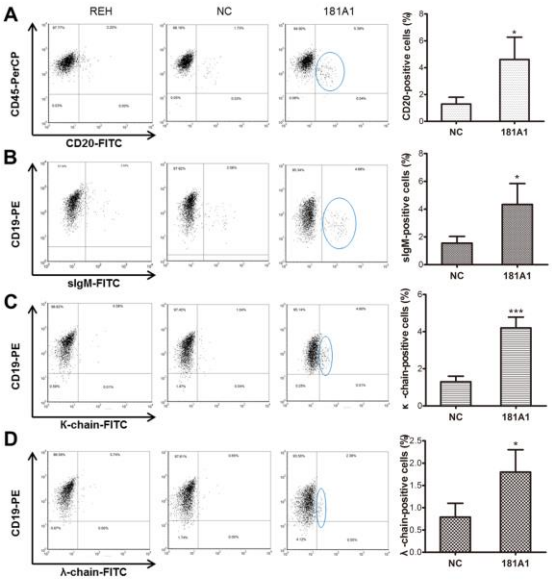

S2 Fig.

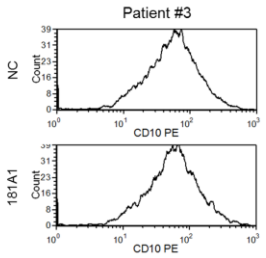

S3 Fig.

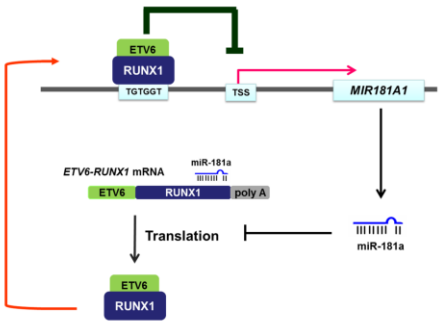

Clinica Chimica Acta 413 (2012) 246–250

Contents lists available at SciVerse ScienceDirect

Clinica Chimica Acta

journal homepage: www.elsevier.com/locate/clinchim

Functional importance of apolipoprotein A5 185G in the activation of lipoprotein lipase

Yi-Jan Huang [a], Yen-Lin Lin [a], Chi-I Chiang [a], Ching-Tzu Yen [a], Shu-Wha Lin [a,b], Jau-Tsuen Kao [a,b,*]

[a] Department of Clinical Laboratory Sciences and Medical Biotechnology, College of Medicine, National Taiwan University, Taiwan
[b] Department of Laboratory Medicine, National Taiwan University Hospital, Taipei 100, Taiwan

ARTICLE INFO

Article history:
Received 24 June 2011
Received in revised form 12 August 2011
Accepted 29 September 2011
Available online 8 October 2011

Keywords:
Apolipoprotein A5
Triglyceride
Mutagenesis
Lipoprotein lipase
Mutant

ABSTRACT

Background: Apolipoprotein A5 (APOA5) over-expression enhances lipolysis of triglyceride (TG) through stimulation of lipoprotein lipase (LPL) activity; however, an APOA5 G185C variant was found associated with hypertriglyceridemia. The aim of this study was, therefore, to explore the importance of APOA5 185GG in the activation of LPL.
Methods: A fragment containing mature human *APOA5* cDNA was obtained by RT-PCR and subcloned into pET-15b vector. Site-directed mutagenesis was performed to generate 19 variants. Recombinant human APOA5 wild type and variants were produced in *Escherichia coli*, and then activation of LPL was measured.
Results: Activity of APOA5 variants on LPL-mediated 1,2-dimyristoyl-sn-glycero-3-phosphocholine hydrolysis was reduced by 17 to 74% in comparison to wild type APOA5 ($P<0.0001$). All variants also showed reduced activation ($P<0.0001$) of LPL-mediated hydrolysis of very low-density lipoprotein (VLDL); activation abilities of APOA5 variants ranged from 31 to 81% of wild-type APOA5.
Conclusions: APOA5 residue 185G is very important in LPL-mediated VLDL hydrolysis, and any mutation at this residue will decrease LPL activation and concomitant TG modulation.

1. Introduction

The role of increased triglyceride (TG) in the pathogenesis of coronary heart disease remains controversial, however, increasing evidence indicates an association between increased plasma TG and the disease [1–3]. Hypertriglyceridemia is a metabolic disorder common in the general population. Although it can be caused by many factors, a relatively large number of individuals have a genetic tendency to manifest this disorder. Transgenic mice over-expressing human apolipoprotein A5 (APOA5) decreased plasma triglyceride concentrations to one-third of those in control mice; conversely, knockout mice lacking *apoa5* had four times as much plasma TG as controls [4], suggesting that *APOA5* plays a role in hypertriglyceridemia.

Human APOA5 protein has been detected at very low concentrations (24 to 406 μg/l) in serum as a component of high-density lipoprotein (HDL), very low-density lipoprotein (VLDL), and chylomicron particles [5]. Moreover, plasma APOA5 levels have been negatively associated with plasma TG and positively associated with HDL-C concentration [5,6] indicating the importance of APOA5 in lipid metabolism and homeostasis. APOA5 over-expression enhances lipolysis of triglyceride-rich lipoproteins through stimulation of lipoprotein lipase (LPL) activity [7,8]. Fruchart-Najib et al. reported increased VLDL hydrolysis by free LPL in vitro in the presence of very high concentrations of recombinant APOA5 [9].

Our previous report described an *APOA5* variant, c.553G>T (a substitution of a cysteine for a glycine at residue 185) that is associated with hypertriglyceridemia [10]. Individuals carrying the 553T allele were found to have odds of 11.73 of developing hypertriglyceridemia in comparison with individuals without the allele. Moreover, the minor T allele at this residue was significantly associated with increased risk of coronary artery disease after adjustment for common cardiovascular risk factors [11]. By using case control design, Yamada et al. demonstrated that c.553G>T (Gly185Cys) was significantly associated with the prevalence of metabolic syndrome in a large-scale study [12]. Furthermore the minor T allele remained a risk factor for metabolic syndrome using multivariable logistic regression analysis.

The aim of the present study was to explore the importance of APOA5 185G in the activation of LPL.

2. Materials and methods

2.1. Construction of vector

A fragment containing the mature human *APOA5* cDNA (nt 77–1109, accession number AF202889) was obtained by RT-PCR from HepG2 cell

* Corresponding author at: Department of Clinical Laboratory Sciences and Medical Biotechnology, College of Medicine, National Taiwan University, Taiwan. Tel.: +886 2 23123456x66904; fax: +886 2 23711574.
E-mail address: jtkao@ntu.edu.tw (J.-T. Kao).

0009-8981/$ – see front matter © 2011 Elsevier B.V. All rights reserved.
doi:10.1016/j.cca.2011.09.045

total RNA by using the forward primer 5′-CGGAGTTCATATGCG-GAAAGGCTTCTGGGACT-3′ and the reverse primer 5′-CGGAATTCATA TGCTCAGGGGTCCCCCAGATG-3′. The PCR product was subcloned into pET-15b vector (Novagen, Madison, WI, USA) by use of *Nde*I. A 6-amino acid HHHHHH tag was added to the N terminus to facilitate purification by nickel affinity chromatography. Site-directed mutagenesis was performed with the QuikChange site-directed mutagenesis kit (Stratagene, La Jolla, CA, USA) employing the mismatch primers (Table 1) to create 19 variants at residue 185 of human APOA5. The correctness of the mutagenesis was verified by DNA sequencing (Supplementary file).

2.2. Expression and purification of recombinant APOA5

Recombinant human APOA5 wild type and variants were produced in *Escherichia coli* BL21 (DE3) pLysS (Yeastern Biotech Co., Ltd., Taipei, Taiwan) by transformation with plasmids, and isolated as described by Beckstead et al. [13]. The expressed protein contained 343 amino acids plus a vector encoded N-terminal His tag extension. Recombinant APOA5 was purified with nickel magnetic beads (Millipore, Billerica, MA) [14]. Protein concentrations were determined by the BCA™ protein assay kit (Pierce Biotechnology Inc., Rockford, IL).

2.3. Enzyme-linked immunosorbent assay for APOA5

APOA5 concentrations were measured using a sandwich enzyme-linked immunosorbent assay (ELISA) as described previously with some modification [6]. Briefly, microtiter plates were coated overnight with 100 μl of 100 ng/μl anti-human APOA5 polyclonal antibody (Genesis Biotech Inc., Taipei, Taiwan) diluted in TPBSA (PBS containing 0.5% BSA and 0.05% Triton 20) in each well at 25 °C. After washing with TPBS, wells were blocked for 1 h at 37 °C with 3% BSA-TPBS. After washing, wells were incubated for 2 h at 37 °C with 100 μl samples (1:100 dilution in PBS). Next, wells were washed and incubated with 100 μl of 100 ng/μl mouse anti-APOA5 monoclonal antibody 2-11H-3E (Oncoprobe Biotech Inc., Taipei, Taiwan) for 2 h at 37 °C. After washing, wells were incubated with alkaline phosphatase conjugated anti-mouse IgG (MP Biomedicals, Irvine, CA, USA) diluted 1:3000 dilution in TPBSA for 1 h. After extensive washing, the plates were incubated with *p*-nitrophenylphosphate disodium (Sigma, Amherst, NJ). The color reaction was stopped after exactly 30 min with 50 μl of 1 mol/l NaOH, and the absorbance was read at 410 nm with M5 microplate reader (Kelowna Scientific, Inc, Taiwan).

Table 1
Primers used for site-directed mutagenesis.

Primer	Sequences
ApoA5-185ADV-F	5′-GGTGCACCACACC***GnC***CGCTTCAAAGA-3′
ApoA5-185ADV-R	5′-TCTTTGAAGCG***GnC***GGTGTGGTGCACC-3′
ApoA5-185RHLP-F	5′-GGTGCACCACACC***CnC***CGCTTCAAAGA-3′
ApoA5-185RHLP-R	5′-TCTTTGAAGCG***GnG***GGTGTGGTGCACC-3′
ApoA5-185EQK-F	5′-GGTGCACCACACC***VAG***CGCTTCAAAGA-3′
ApoA5-185EQK-R	5′-TCTTTGAAGCG***CTB***GGTGTGGTGCACC-3′
ApoA5-185CFY-F	5′-GGTGCACCACACC***TDC***CGCTTCAAAGA-3′
ApoA5-185CFY-R	5′-TCTTTGAAGCG***GHA***GGTGTGGTGCACC-3′
ApoA5-185SNIT-F	5′-GGTGCACCACACC***AnC***CGCTTCAAAGA-3′
ApoA5-185SNIT-R	5′-TCTTTGAAGCG***GnT***GGTGTGGTGCACC-3′
ApoA5-185W-F	5′-GGTGCACCACACC***TGG***CGCTTCAAAGA-3′
ApoA5-185W-R	5′-TCTTTGAAGCG***CCA***GGTGTGGTGCACC-3′
ApoA5-185M-F	5′-GGTGCACCACACC***ATG***CGCTTCAAAGA-3′
ApoA5-185M-R	5′-TCTTTGAAGCG***CAT***GGTGTGGTGCACC-3′

Mixed bases: R(A,G);Y(C,T);M(A,C);K(G,T);S(C,G);W(A,T);H(A,C,T);B(C,G,T);V(A,C,G);D(A,G,T);N,X(A,C,G,T).

2.4. Immunoblotting

For immunoblotting, recombinant purified proteins were separated through a 10% SDS-PAGE gel. The proteins were electrophoretically transferred to a 0.2-μm polyvinylidene difluoride membrane at a constant current of 100 mA for 1 h. Nonspecific binding sites on the membrane were blocked with PBS (containing 5% skim milk) overnight at 4 °C with rotation. Mouse anti-APOA5 monoclonal antibody (1:10,000 dilution in 1% BSA-TPBS) was incubated with the membrane for 1 h with rotation. The membrane was washed 3 times in TPBS, and then goat anti-mouse IRDye 680 (Li-Cor Biosciences, Lincoln NE) secondary antibody was incubated with the membrane for 1 h. After washing, the membrane was read by Li-Cor Odyssey.

2.5. Apolipoprotein AV-1,2-dimyristoyl-sn-glycero-3-phosphocholine (DMPC) disks

APOA5-DMPC disks were prepared by dissolving 10 mg of DMPC (Sigma, Amherst, NJ) in chloroform:methanol (3:1 v/v). Solvent was evaporated under a stream of N_2, and the DMPC was subsequently dispersed in 1 ml of 50 mmol/l sodium citrate (pH 3.0), and DMPC vesicles were generated by extrusion through a 0.22 μm filter. The concentration of lipid was determined by the Phospholipids B kit (Wako, Pure Chemical Industries, Ltd., Japan). 1.5 μg of APOA5 wild-type or variants was added to 20 μl of the DMPC vesicle preparation, and the sample was gently vortexed for 3 h at 24 °C until homogeneous mixture was obtained.

2.6. Incubation of APOA5-DMPC with LPL

Twenty-five microliters of APOA5-DMPC vesicles was added to 3 μl of LPL working solution. It was then incubated for 10 min at 37 °C. After addition of 12.5 μl of stop reagent, the amount of free fatty acids liberated was determined with a Clinimate NEFA kit (Daiichi Pure Chemicals Co., Ltd, Tokyo, Japan).

2.7. Isolation of VLDL

Blood from apoa5-deficient mice (Mutant Mouse Regional Resource Centers, The Jackson Laboratory, Bar Harbor, ME) was collected. After centrifugation at 2000×*g* for 10 min at 4 °C, the serum was removed, pooled, and stored at 4 °C. VLDL was isolated from pooled serum by sequential ultracentrifugation as described by Lindgren et al. [15].

2.8. Incubation of APOA5 with VLDL

Ten micrograms of APOA5 was added to 12.5 μg of VLDL, and the sample was gently vortexed until it was homogeneous. It was then incubated for 1 h at 37 °C. LPL working solution (1.5 μl) was added then incubated for 1 h at 37 °C. After addition of 15 μl of stop reagent, the amount of free fatty acids liberated was determined with a Clinimate NEFA kit (Daiichi).

2.9. Assay of lipoprotein lipase activity

LPL activity was determined by measuring the amount of free fatty acids released from a predetermined amount of DMPC vesicles or VLDL isolated from *apoa5* knockout mice. The amount of free fatty acids was determined with a free fatty acid Clinimate NEFA kit (Daiichi Pure Chemicals Co., Ltd, Tokyo, Japan). Briefly, 45 μl of reagent I was added into either APOA5-DMPC with LPL or APOA5-VLDL with LPL solution then incubated for 5 min at 37 °C. After addition of 90 μl of reagent II and incubation for another 5 min at 37 °C, the absorbance was measured at 546 nm and 660 nm. The amount of free fatty acids was obtained from the standard calibration curves.

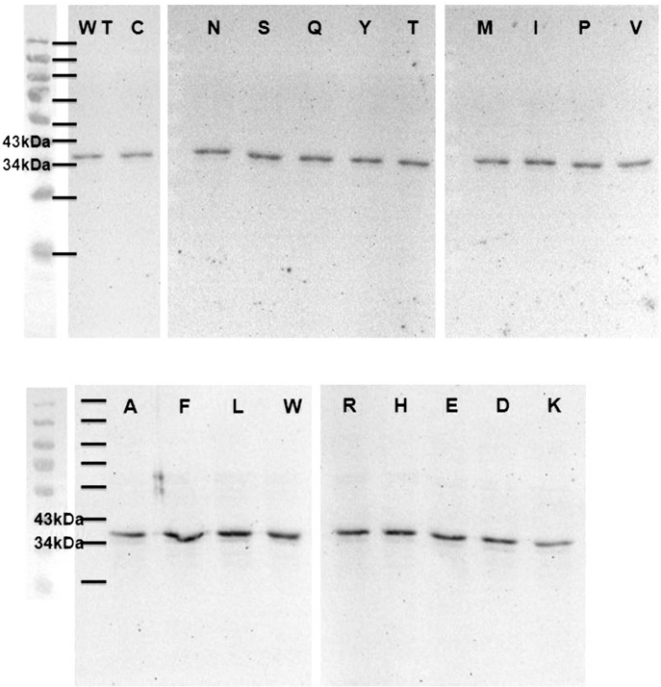

Fig. 1. Immunoblotting of APOA5 proteins. The left lane represents protein low molecular mass marker; other lanes represent wild-type APOA5 and other variants. WT: wild type; glycine, C: cysteine, N: asparagine, S: serine, Q: glutamine, Y: tyrosine, T: threonine, M: methionine, I: isoleucine, P: proline, V: valine, A: alanine, F: phenylalanine, L: leucine, W: tryptophan, R: arginine, H: histidine, E: glutamic acid. D: aspartic acid, K: lysine.

2.10. Statistical analysis

Data are expressed as mean ± SD. Statistical analyses were performed using SPSS (ver. 12.0, Chicago, IL). Comparisons between groups were performed using two-tailed Student's *t* test. A $P<0.05$ was considered statistically significant.

3. Results

3.1. Expression of recombinant APOA5 proteins

In order to investigate the importance of APOA5 185G, site-directed mutagenesis was performed to replace the glycine with the 19 possible substitute amino acids. Mismatch primers were used to create the 19 variants at residue 185 of human APOA5. Introduction of the desired variants was verified by DNA sequencing (Supplementary file). Recombinant human APOA5 wild type and 19 variants were then produced in *E. coli* BL21 (DE3) pLysS. After purification, the concentrations of recombinant APOA5 were measured with ELISA. Wild type and variants of APOA5 purified from the *E. coli* system were equally recognized by anti-APOA5 monoclonal antibody 2-11H-3E. The calculated molecular weights were as expected (Fig. 1).

3.2. Decreased hydrolysis of APOA5 variant-DMPC vesicles by LPL

DMPC hydrolysis by LPL was used to assess whether APOA5 variants were able to activate LPL hydrolysis. Analysis of variants revealed that the ability of APOA5 variants to generate free fatty acids was reduced to between 26% and 83% of that of wild type APOA5 ($P<0.0001$) (Fig. 2).

3.3. APOA5 variants show reduced activation of LPL

To confirm whether APOA5 variants also reduced LPL-mediated hydrolysis of VLDL, apoa5-deficient VLDL was incubated with wild-type APOA5 and variant proteins. After mixing with LPL solution, the free fatty acids released were measured to evaluate the extent of LPL hydrolysis. All variants showed reduced LPL activation (Fig. 3). LPL activations by APOA5 variants were between 31% (lysine) and 81% (glutamine) of that of wild type APOA5. Most variants retained some activation activity, however, arginine, threonine, and

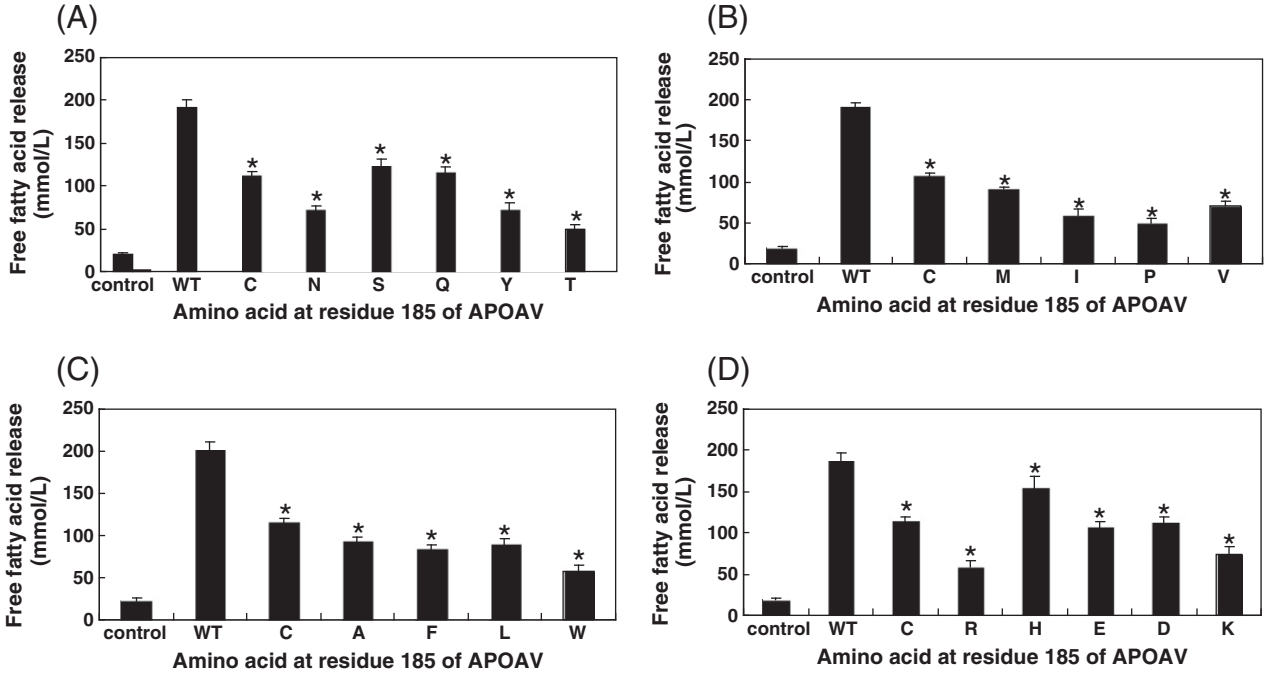

Fig. 2. Activation of lipoprotein lipase by recombinant wild-type APOA5 and variants. Purified DMPC vesicles containing wild-type APOA5 or variants were incubated with LPL (2.2 pmol) in a total volume of 28 μl assay mixture. The control contained no APOA5 protein. (A) Hydrophilic amino acids at residue 185; (B) hydrophobic amino acids at residue 185; (C) hydrophobic amino acids at residue 185; (D) acidic or basic amino acids at residue 185. Each bar is the mean of three independent determinations. Data are mean ± SD. *, $P<0.0001$ vs. wild-type APOA5 by Student's *t* test.

proline variants showed only approximately one third of the activation of the wild type.

4. Discussion

Apolipoprotein A5 185C has been reported to be associated with plasma triglyceride concentrations [16,17]. In the current study we explored the importance of glycine at residue 185 of APOA5 by using site-directed mutagenesis to produce a panel of variant proteins. We found that all variants tested had reduced LPL activation thus verifying that residue 185G of human APOA5 is indispensable for LPL activation.

Loss of activation was not caused by the hydrophilic nature of the variants, as both glycine and cysteine hydrophilic uncharged polar amino acid, but substitution of glycine with cysteine at residue 185 of APOA5 resulted in hypertriglyceridemia. In addition, neither acidic nor basic characteristics can explain this loss of activation as glutamine retained 81% of its LPL activation; even though, its molecular weight is larger than that of cysteine and almost 2-fold that of glycine. Size difference could also not explain the loss of LPL activation either. Due to the multimers of APOA5 185C protein in vitro [18], a change in tertiary structure might affect LPL activation ability. This hypothesis is supported by the fact that glycine at residue 185 was absolutely required for LPL activation. However, the exact mechanism will need further study.

A highly hydrophobic and amphipathic domain at APOA5 residues 171 to 188 has a potentially significant lipid binding ability [19]. By engineering a panel of deletion mutants, Sun et al. showed that the domain between residues 192 and 238 is critical for APOA5 both to bind lipids and to activate LPL [20]. In contrast, deletion of residues 132–188 resulted in about 2-fold higher lipid turbidity clearance ability. However, APOA5 mutant without residues 132–188 reduced activation of LPL by 46%, finding that agrees with the results of the current study. Dorfmeister et al. expressed APOA5 185C in BL21 (DES) cells with a C-terminal His-tag sequence; reporting that compared to wild-type APOA5 activation of LPL; APOA5 185C reduced LPL activation by 23% [18].

Lookene et al. suggested that residues 186–242 of APOA5 are responsible for the heparin binding ability of APOA5 [21]. As residue 185 lies next to this domain, this heparin binding might affect its LPL activation ability. Merkel et al. [8] demonstrated that LPL bound to heparan sulfate proteoglycan hydrolyzed VLDL TG much more efficiently in the presence of APOA5. APOA5 also served as a ligand for members of the low-density lipoprotein receptor family. The association resulted in binding of human chylomicrons to receptor-covered sensor chips [22]. However, APOA5 185C showed normal binding to receptors LR8 and LRP1 [18], indicating that residue 185 is more likely to be important in LPL activation than receptor binding.

While APOA5 bound to glycosylphosphatidylinositol high-density lipoprotein binding protein 1 which is important in lipolytic processing of triglycerides within chylomicrons [23], whether APOA5 185C has decreased binding affinity needs further study.

In addition to the association between APOA5 185C and plasma triglyceride concentration, this variant has been reported to be significantly associated with other diseases. Comparisons of genotype distributions revealed that APOA5 185C was significantly associated with prevalence of metabolic syndrome in a Japanese population [12].

Genetic variation at the APOA5 locus has also been implicated in the modulation of the effects of drugs that raise or lower blood lipids. Fenofibrate therapy had a greater triglyceride-lowering effect in carriers of the APOA5 56G than in those who were homozygous for the 56C allele [24]. Fortunately similar gene–drug interactions were not observed for the APOA5 185C polymorphism [25].

In summary, the data presented in the current study suggest that APOA5 residue 185G is very important in LPL-mediated VLDL hydrolysis. Any mutation at this residue will decrease its LPL activation and result in loss of TG modulation.

Supplementary materials related to this article can be found online at doi:10.1016/j.cca.2011.09.045.

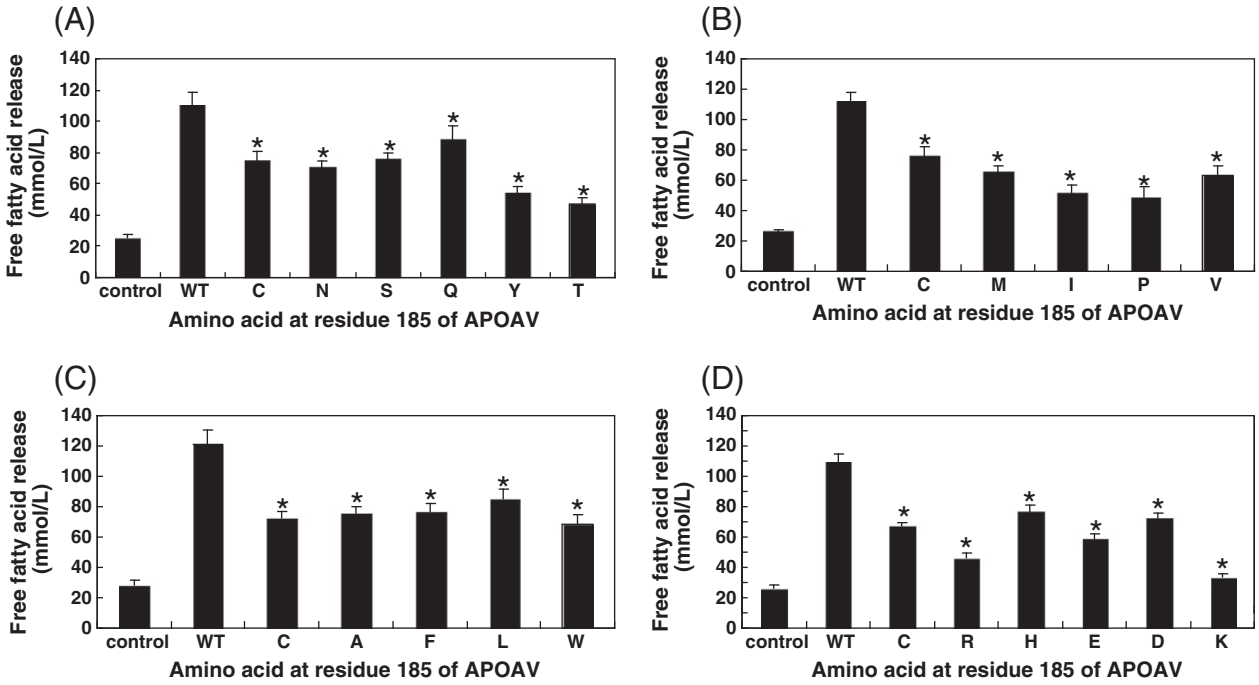

Fig. 3. Hydrolysis of VLDL from *apoa5*-deficient mice incubated with recombinant wild-type APOA5 and variants by lipoprotein lipase. Ten micrograms of APOA5 wild-type or variants was incubated with 12.5 μg of apoa5-deficient VLDL, then LPL (2.2 pmol) was added in a total volume of 31.5 μl assay mixture. The control contained no APOA5 protein. (A) Hydrophilic amino acids at residue 185; (B) hydrophobic amino acids at residue 185; (C) hydrophobic amino acids at residue 185; (D) acidic or basic amino acids at residue 185. Each bar is the mean of three independent determinations. Data are mean ± SD. *, $P<0.0001$ vs. wild-type APOA5 by Student's *t* test.

Acknowledgments

This work was supported in part by grants from the National Science Council of Taiwan (NSC 96-2320-B-002-038-MY3 and NSC 98-2320-B-002-019-MY3).

References

[1] Assmann G, Schulte H, von Eckardstein A. Hypertriglyceridemia and increased levels of lipoprotein (a) are risk factors for major coronary events in middle-aged men. Am J Cardiol 1996;77:1179–84.
[2] Hokanson JE, Austin MA. Plasma triglyceride level is a risk factor for cardiovascular disease independent of high-density lipoprotein cholesterol level: a meta-analysis of population-based prospective studies. J Cardiovasc Risk 1996;3:213–9.
[3] Jeppesen J, Hein HO, Suadicani P, Gyntelberg F. Triglyceride concentration and ischemic heart disease—an eight-year follow-up in the Copenhagen male study. Circulation 1998;97:1029–36.
[4] Pennacchio LA, Olivier M, Hubacek JA, et al. An apolipoprotein influencing triglycerides in humans and mice revealed by comparative sequencing. Science 2001;294:169–73.
[5] O'Brien PJ, Alborn WE, Sloan JH, et al. The novel apolipoprotein A5 is present in human serum, is associated with VLDL, HDL, and chylomicrons, and circulates at very low. Clin Chem 2005;51:351–9.
[6] Ishihara M, Kujiraoka T, Iwasaki T, et al. A sandwich enzyme-linked immunosorbent assay for human plasma apolipoprotein A-V concentration. J Lipid Res 2005;46: 2015–22.
[7] Schaap FG, Rensen PC, Voshol PJ, et al. ApoAV reduces plasma triglycerides by inhibiting very low density lipoprotein-triglyceride (VLDL-TG) production and stimulating lipoprotein lipase-mediated VLDL-TG hydrolysis. J Biol Chem 2004;279: 27941–7.
[8] Merkel M, Loeffler B, Kluger M, et al. Apolipoprotein AV accelerates plasma hydrolysis of triglyceride-rich lipoproteins by interaction with proteoglycan-bound lipoprotein lipase. J Biol Chem 2005;280:21553–60.
[9] Fruchart-Najib J, Bauge E, Niculescu LS, et al. Mechanism of triglyceride lowering in mice expressing human apolipoprotein A5. Biochem Biophys Res Commun 2004;319:397–404.
[10] Kao JT, Wen HC, Chien KL, Hsu HC, Lin SW. A novel genetic variant in the apolipoprotein A5 gene is associated with hypertriglyceridemia. Hum Mol Genet 2003;12:2533–9.
[11] Hsu LA, Ko YL, Chang CJ, et al. Genetic variations of apolipoprotein A5 gene is associated with the risk of coronary artery disease among Chinese in Taiwan. Atherosclerosis 2006;185:143–9.
[12] Yamada Y, Ichihara S, Kato K, et al. Genetic risk for metabolic syndrome: examination of candidate gene polymorphisms related to lipid metabolism in Japanese people. J Med Genet 2008;45:22–8.
[13] Beckstead JA, Oda MN, Martin DDO, et al. Structure–function studies of human apolipoprotein A-V: a regulator of plasma lipid homeostasis. Biochemistry 2003;42: 9416–23.
[14] Dyke MWV, Sirito M, Sawadogo M. Single-step purification of bacterially expressed polypeptides containing an oligo-histidine domain. Gene 1992;111: 99–104.
[15] Lindgren FT, Jensen LC, Hatch FT. In: Nelson GJ, editor. Blood lipids and lipoproteins: quantitation, composition, and metabolism. New York: Wiley-Interscience; 1972.
[16] Matsunaga A, Arishima H, Niimura H, et al. Strong linkage disequilibrium and association of −1131T>C and c.553G>T polymorphisms of the apolipoprotein A5 gene with hypertriglyceridemia in a Japanese population. Circ J 2007;71:746–52.
[17] Chien KL, Fang WH, Wen HC, et al. APOA1/C3/A5 haplotype and risk of hypertriglyceridemia in Taiwanese. Clin Chim Acta 2008;390:56–62.
[18] Dorfmeister B, Zeng WW, Dichlberger A, et al. Effects of six APOA5 variants, identified in patients with severe hypertriglyceridemia, on in vitro lipoprotein lipase activity and receptor binding. Arterioscler Thromb Vasc Biol 2008;28:1866–71.
[19] Weinberg RB, Cook VR, Beckstead JA, et al. Structure and interfacial properties of human apolipoprotein A-V. J Biol Chem 2003;278:34438–44.
[20] Sun GT, Bi N, Li GP, et al. Identification of lipid binding and lipoprotein lipase activation domains of human apoAV. Chem Phys Lipids 2006;143:22–8.
[21] Lookene A, Beckstead JA, Nilsson S, Olivecrona G, Ryan RO. Apolipoprotein A-V–heparin interactions: implications for plasma lipoprotein metabolism. J Biol Chem 2005;280:25383–7.
[22] Nilsson SK, Lookene A, Beckstead JA, Gliemann J, Ryan RO, Olivecrona G. Apolipoprotein A-V interaction with members of the low density lipoprotein receptor gene family. Biochemistry 2007;46:3896–904.
[23] Beigneux AP, Davies BS, Gin P, et al. Glycosylphosphatidylinositol-anchored high density lipoprotein-binding protein 1 plays a critical role in the lipolytic processing of chylomicrons. Cell Metab 2007;5:279–91.
[24] Lai CQ, Arnett DK, Corella D, et al. Fenofibrate effect on triglyceride and postprandial response of apolipoprotein A5 variants: the GOLDN study. Arterioscler Thromb Vasc Biol 2007;27:1417–25.
[25] Chien KL, Lin YL, Wen HC, et al. Common sequence variant in the lipoprotein lipase gene conferring triglyceride response to fibrate treatment. Pharmacogenomics 2009;10:267–76.

Leukemia Research 34 (2010) 18–23

Contents lists available at ScienceDirect

Leukemia Research

journal homepage: www.elsevier.com/locate/leukres

Expression and prognostic significance of the apoptotic genes *BCL2L13*, *Livin*, and *CASP8AP2* in childhood acute lymphoblastic leukemia

Yung-Li Yang[a,b], Shu-Rung Lin[c], Jiann-Shiuh Chen[d,j], Shu-Wha Lin[e,f], Sung-Liang Yu[a,e,f,g], Hsuan-Yu Chen[h], Ching-Tzu Yen[f], Chien-Yu Lin[h], Jing-Fang Lin[f], Kai-Hsin Lin[b], Shiann-Tarng Jou[b], Chung-Yi Hu[f], Sheng-Kai Chang[f], Meng-Yao Lu[b], Hsiu-Hao Chang[b], Wan-Hui Chang[i], Kuo-Sin Lin[i], Dong-Tsamn Lin[a,b,*]

[a] *Department of Laboratory Medicine, College of Medicine, National Taiwan University, Taipei, Taiwan*
[b] *Department of Pediatrics, College of Medicine, National Taiwan University, Taipei, Taiwan*
[c] *Department of Bioscience Technology, College of Science, Chung-Yuan Christian University, Taoyuan, Taiwan*
[d] *Department of Internal Medicine, College of Medicine, National Taiwan University, Taipei, Taiwan*
[e] *Department of Medical Research, College of Medicine, National Taiwan University, Taipei, Taiwan*
[f] *National Taiwan University Hospital, Department of Clinical Laboratory Sciences and Medical Biotechnology, College of Medicine, National Taiwan University, Taipei, Taiwan*
[g] *NTU Center for Genomic Medicine, College of Medicine, National Taiwan University, Taipei, Taiwan*
[h] *Institute of Statistical Science Academia Sinica, Taiwan*
[i] *Taiwan Childhood Cancer Foundation, Taipei, Taiwan*
[j] *Department of Pediatrics, National Cheng Kung University Hospital, Tainan, Taiwan*

ARTICLE INFO

Article history:
Received 15 January 2009
Received in revised form 12 July 2009
Accepted 14 July 2009

Keywords:
Childhood acute lymphoblastic leukemia (ALL)
BCL2L13
Livin
CASP8AP2

ABSTRACT

Improved treatment of childhood acute lymphoblastic leukemia (ALL) depends on the identification of new molecular markers that are able to predict treatment response and clinical outcome. The development of impaired apoptosis in leukemic cells is one factor that may influence their response to treatment. We investigated the expression of three apoptosis related genes, *BCL2L13*, *CASP8AP2*, and *Livin*, as well as their prognostic significance, in a retrospective study of 90 pediatric ALL patients diagnosed between 1996 and 2007 in Taiwan. Univariant analysis revealed that high expression of *BCL2L13* was associated with inferior event-free survival and overall survival ($p < 0.001$ and 0.005, respectively). Multivariate analysis for EFS and OS demonstrated that high expression of *BCL2L13* was an independent prognostic factor for childhood ALL in this ethnic group.

1. Introduction

Recent progress in the use of DNA microarrays has identified genes that regulate cell cycle control, DNA repair, and apoptosis which may also participate in disordered cell proliferation and cancer progression in leukemia [1,2]. Alterations in the basal level of expression of these genes may also affect the drug response and clinical outcome of leukemic patients. The cure rate of childhood acute lymphoblastic leukemia (ALL) has increased from 10 to 80% in the developed countries, a fact which may largely be a consequence of the stringent application of prognostic factors for risk-factor-directed therapy [3,4]. The identification of new such gene markers is therefore important not only to gain a basic understanding of the signaling pathways that operate in leukemogenesis, but also to implement enhancements to disease classification systems and to productively target disease with novel therapies.

It has been shown that decreased apoptosis may be an important step in the acquisition of cellular drug resistance in pediatric acute leukemia. Holleman et al. used microarrays to investigate the expression of 70 apoptosis genes, and revealed that *BCL2L13* expression was an independent prognostic factor [5]. Flotho et al. analyzed gene expression in diagnostic lymphoblasts, and compared the findings to minimal residual disease (MRD) levels on days 19 and 46 of remission induction therapy. They identified 17 genes that were significantly associated with MRD level. Among these, the gene coding for caspase 8-associated protein 2 (*CASP8AP2*) was studied further and showed a strong correlation with prog-

* Corresponding author at: Department of Laboratory Medicine and Pediatrics, National Taiwan University Hospital, College of Medicine, National Taiwan University, No. 7 Chung-San S. Rd., Sec. 1, Taipei 100, Taiwan. Tel.: +886 2 23123456x65399; fax: +886 2 23224263.
E-mail address: dtlin@ntuh.gov.tw (D.-T. Lin).

0145-2126/$ – see front matter © 2009 Elsevier Ltd. All rights reserved.
doi:10.1016/j.leukres.2009.07.023

nosis [6]. Chio et al. studied the expression of *Livin*, a member of the IAP family of childhood ALL [7]. Unexpectedly, *Livin* expression was an independent prognostic factor in their cohort. These studies demonstrated an association between dysregulated apoptosis pathways and treatment prognosis, and suggested that the identified genes might serve as functionally defined risk factors for treatment stratification, in addition to those factors currently used.

If specific patterns of gene expression can be correlated with clinical features in childhood ALL, a refinement of current prognosis-based stratification systems might be possible. Thus, we analyzed *BCL2L13*, *CASP8AP2*, and *Livin* gene expression in the childhood ALL of a specific ethnic group, and investigated their correlation with treatment outcomes.

2. Design and methods

2.1. Patients

Viable diagnostic bone marrow (BM) or peripheral blood (PB) was obtained from 90 children who were diagnosed with ALL between July 1996 and August 2007 at National Taiwan University Hospital (NTUH) and National Cheng Kung University Hospital (NCKUH). Of these, 78 patients had been newly diagnosed with B-precursor ALL, and 12 patients with T-cell ALL. Forty-seven patients were treated with TPOG-93-ALL protocols and 43 patients were treated with TPOG-2002-ALL protocols, which are described in detail elsewhere [8,9]. The diagnosis of ALL was made based on the morphologic findings of BM aspirates, as well as on immunophenotype analyses of leukemic cells by flow cytometry. Conventional cytogenetics analyses were performed as part of the routine workup.

Patients were prospectively assigned to one of three risk groups (standard, high, and very high) based on their presenting clinical features and the biological features of their leukemic cells. Patients were considered to have standard-risk (SR) ALL if they were between 1 and 9 years old with a presenting leukocyte count less than 10×10^9 (cells/L) or were between 2 and 7 years old with a presenting leukocyte count between 10×10^9 and 50×10^9. Patients were considered to have high-risk (HR) ALL if they were between 1 and 9 years old with a presenting leukocyte count between $50 \times 10^9$and 100×10^9, or between 1 and 2 or 7 and 10 years old with a presenting leukocyte count between 10×10^9 and 50×10^9. Patients with at least one of the following were assigned to the very-high-risk (VHR) group: age younger than 1 year, initial leukocyte count greater than 100×10^9, T-cell ALL, or presence of *BCR-ABL*, *MLL-AF4* or other *MLL* rearrangements in pre-B ALL.

The risk-directed Taiwan Pediatric Oncology Group (TPOG) protocols consisted of multiple chemotherapeutic agents of different intensities. The treatment protocol was upgraded if complete remission was not achieved after initial induction therapy. Events were defined as any relapse, death, or secondary malignancy. This study was approved by the Medical Ethics Committee of National Taiwan University Hospital. Informed consent was obtained from the patients or their parents before sample collection.

2.2. Methods

2.2.1. RNA isolation

Mononuclear cells from bone marrow (BM) or peripheral blood (PB) were Ficoll-purified and immediately stored in liquid nitrogen. Cryopreserved samples were thawed and washed in FBS-supplemented RPMI 1640 medium prior to RNA extraction. Total RNA was extracted using Trizol reagent according to the manufacturer's instructions (Invitrogen, Paisley, United Kingdom).

2.2.2. Determination of BCL2L13, Livin and CASP8AP2 expression by comparative real-time quantitative-reverse transcriptase polymerase chain reaction (Q-RT-PCR)

The mRNA expression levels of *BCL2L13*, *Livin*, *CASP8AP2* and *glyceraldehydes-3-phosphate dehydrogenase* (*GAPDH*) were measured by Q-RT-PCR using an ABI 7300 real-time PCR system (Applied Biosystems, Foster City, CA). Mature mRNAs were reverse-transcribed into cDNA using oligo-dT and random hexamers as primers by standard methods as described previously [10]. Quantitative PCR amplification of individual cDNAs was performed using the pre-developed Taqman gene expression assay for *BCL2L13* (Hs00209789_m1), *Livin* (Hs00223384_m1) and *CASP8AP2* (Hs01594281_m1)(Applied Biosystems, Foster City, CA). TaqMan endogenous control assay for the *GAPDH* was combined with the assay for target gene in the same reaction (Applied Biosystems). All reactions were performed in duplicate at a minimum. The 20 μl PCR reaction mixture contained 12.5 ng cDNA, 900 nM primers, 250 nM probe, and 1× Taqman universal master mix, combining AmpliTaq Gold® DNA Polymerase, AmpErase® UNG, dNTPs with dUTP, and optimized buffer components. After an initial incubation at 50 °C for 2 min, and a denaturing step at 95 °C for 10 min, a 2-step PCR (95 °C for 15 s followed by 60 °C for 1 min) was performed for 45 cycles to amplify and detect the target sequence.

The expression levels of the target genes in unknown samples were normalized standardized for expression of *GAPDH* and analyzed by the ΔΔCt method [$\Delta\Delta Ct = (Ct_{target\ gene} - Ct_{GAPDH})$ sample − $(Ct_{target\ gene} - Ct_{GAPDH})$ calibrator]. The average of ΔCt ($Ct_{target\ gene} - Ct_{GAPDH}$) from all samples combined was defined as 0, as the calibrator. The amplification efficiencies for target genes and *GAPDH* were calculated and showed the same slopes. A negative control without the templates was also included in each experiment.

2.2.3. Statistical methods

Comparison of baseline clinical variables across groups was made using the Fisher's exact test for categorical data. The nonparametric Mann–Whitney *U*-test was applied for continuous variables. A p-value < 0.05 (two-sided) was considered significant.

Patients analyzed for *BCL2L13* expression were initially divided into two groups according to their median level of *BCL2L13* (median = 5.91 as cut-off point). We divided the patients into three groups of 30 patients each according to the *CASPS8AP2* expression levels (5.5 and 10.5 as cut-off point). The patients were categorized into two groups according to the presence or absence of the *Livin* expression.

OS was calculated using the Kaplan–Meier method, and the log-rank test was used to compare differences between survival curves. OS was measured from the protocol commencement date until the date of death regardless of cause, excluding patients who were alive at last follow-up. EFS was defined only for patients who achieved complete remission, and was measured from the date of attaining CR until the date of relapse. Patients with no report of relapse by the end of the follow-up observation were censored on the date of last follow-up.

Cox proportional hazard models were constructed for EFS and OS. The following covariates were included in the full model of OS and EFS: *BCL2L13* expression (low vs. high), *CASP8AP2* expression (low, median and high), *Livin* expression (presence or absence), sex, WBC (<100,000/μL vs. 100,000/μL), age (<10 years vs. >10 years), immunophenotypes (B or T), hospital, and genetic subtypes. Stepwise backward selection was performed. All calculations were performed using the SAS software package, version 9 (SAS Inc.).

3. Results

3.1. Patient characteristics (Table 1)

The clinical characteristics of patients at the time of diagnosis are presented in Table 1. The median age among 90 patients (46 boys and 44 girls) was 4.3 years (range: 0–17 years), and their median leukocyte count was 20.0 (range: 0.2–1826). The number of SR, HR, and VHR patients was 24, 31, and 35 respectively.

3.2. The association of BCL2L13, CASP8AP2 and Livin expression level with clinical outcomes

Patients were defined as low and high *BCL2L13* as described in Section 2. The *BCL2L13* expression level did not differ among the different risk groups (Table 1). Patients with lower *BCL2L13* expression had better EFS ($p < 0.001$), and better OS ($p = 0.005$) (Fig. 1).

Patients were defined as low, median and high *CASP8AP2* as described above. The *CASP8AP2* expression level did not differ among the different risk groups (Table 1). The prognosis did not differ between different *CASP8AP2* expression groups (Fig. 2).

As expected, approximately 21.1% of patients expressed *Livin*, as was reported by Choi et al. In our series, 20 patients expressed *Livin* and 70 patients did not. We compared EFS and OS between patients who did and did not express *Livin*. There was no statistically significant difference between these two groups of patients (Fig. 3).

3.3. Multiple variable (Cox regression) analysis reveals that BCL2L13 was an independent prognostic factor

We performed multivariable Cox regression analyses examining the correlation between EFS or OS and *BCL2L13, CAP8AP2and Livin* status, other known prognostic factors, and age and white count listed in Table 1. When other significant predictors of EFS were controlled for in the final model, *MLL* gene rearrangement, initial white counts more than 100,000/μL, risk groups and the expression level of *BCL2L13* were correlated with EFS (hazard ratio for *BCL2L13* = 4.11, $p = 0.0025$) (Table 2). When other significant predictors of OS were controlled for in the final model, *MLL* gene rearrangement, initial white counts more than 100,000/μL, and the expression level of

Table 1
The clinical features of patients at diagnosis and their association with three genes studied.

	BCL2L13			*CASP8AP2*				*Livin*		
	Low number	High number	*p*-value*	Low number	Median number	High number	*p*-value*	Positive number	Negative number	*p*-value*
WBC										
<100,000/μL	36	12	0.462	24	21	23	0.749	16	52	0.771
>100,000/μL	9	13		6	9	7		4	18	
Immunophenotype										
B	36	42	0.118	23	24	27	0.578	18	16	1.000
T										
Age										
<10 years	33	32	1.000	21	22	22	1.000	16	49	0.572
>10 years	12	13		9	8	8		4	21	
Risk groups										
Standard risk	14	10	0.335	9	7	8	0.929	7	17	0.592
High risk	17	14		11	11	9		7	24	
Very high risk	14	21		10	12	13		6	29	
Hyperdiplopid										
Negative	36	41	0.230	23	28	26	0.217	58	19	0.283
Positive	9	4		7	2	4		12	1	
t(9;22)										
Negative	45	43	0.494	30	28	30	0.326	20	69	1.000
Positive	0	2		2	0	2		0	4	
MLL gene										
Negative	45	41	0.117	28	30	28	0.54	20	66	0.572
Positive	0	4		2	0	2		0	4	
Hospital										
NTUH	29	38	0.052	24	20	23	0.565	52	15	1.000
MCKUH	16	7		6	10	7		18	5	

* Fisher exact test.

BCL2L13 were correlated with OS (hazard ratio for *BCL2L13* = 3.41, $p = 0.0244$) (Table 3).

3.4. Three gene signature as a predictor as outcome

We attempted to develop a risk signature using the combination of three markers studied. The signature was *CASP8AP2* × 0.03869 + *BCL2L13* × 0.02747 + *Livin* code (0 or 1) − 0.59135. The patients with high-risk signature had inferior EFS than patients with low-risk signature ($p = 0.0084$, median = 0.463 as cut-off point) (Fig. 4). We performed multivariable Cox regression analyses examining the correlation between EFS and other known prognostic factors, genetic types, age and white count listed in Table 1. The results were shown in Table 4. When other significant predictors of EFS were controlled for in the final model, *MLL* gene rearrangement,

Table 3
Multivariate Cox regression analysis for OS.

Variables	Hazard ratio (HR)	95% HR CI	*p*-value
Livin	0.49	0.11–2.29	0.365
CASP8AP2	1.12	0.58–2.17	0.738
BCL2L13	2.45	0.67–9.04	0.178
WBC > 100,000/μL	3.30	0.81–13.43	0.095
B vs. T	0.43	0.07–2.89	0.388
Age > 10	1.39	0.36–5.35	0.630
Risk groups	1.85	0.61–5.57	0.277
Hyperdiplopid	0	0	0.992
t(9;22)	1.38	0.25–7.67	0.716
MLL gene rearrangements	6.28	1.38–28.56	0.017
Step selection			
BCL2L13	3.41	1.17–9.93	0.0244
WBC > 100,000/μL	5.25	2.05–13.44	0.0005
MLL gene rearrangements	8.05	1.99–32.54	0.0034

Table 2
Multivariate Cox regression analysis for EFS.

Variables	Hazard ratio (HR)	95% HR CI	*p*-value
Livin	0.73	0.24–2.25	0.587
CASP8AP2	1.12	0.53–2.00	0.695
BCL2L13	3.25	1.09–9.72	0.035
WBC > 100,000/μL	2.77	0.89–8.60	0.079
B vs. T	0.74	0.18–3.03	0.679
Age > 10	1.39	0.49–3.95	0.537
Risk groups	2.02	0.82–4.98	0.127
Hyperdiplopid	0.44	0.06–3.52	0.44
t(9;22)	2.65	0.48–14.52	0.261
MLL gene rearrangements	5.75	1.42–23.23	0.014
Step selection			
BCL2L13	4.11	1.64–10.30	0.0025
WBC > 100,000/μL	2.72	1.02–7.26	0.0452
Risk groups	2.28	1.04–4.97	0.0386
MLL gene rearrangements	5.75	1.45–17.55	0.0110

Table 4
Multivariate Cox regression analysis for EFS using three gene signature as a parameter.

Variables	Hazard ratio (HR)	95% HR CI	*p*-value
Three gene signature	2.68	1.07–6.70	0.035
WBC > 100,000/μL		0.78–6.83	0.129
B vs. T	0.54	0.15–1.99	0.356
Age > 10	1.47	0.53–4.07	0.461
Risk groups	2.42	1.00–5.88	0.051
Hyperdiplopid	0.47	0.06–3.77	0.478
t(9;22)	2.89	0.53–15.72	0.220
MLL gene rearrangements	6.98	1.78–27.30	0.005
Step selection			
Three gene signature	2.85	1.21–6.70	0.0163
WBC > 100,000/μL	6.36	1.83–22.08	0.0036
MLL gene rearrangements	3.51	1.82–6.76	0.0002

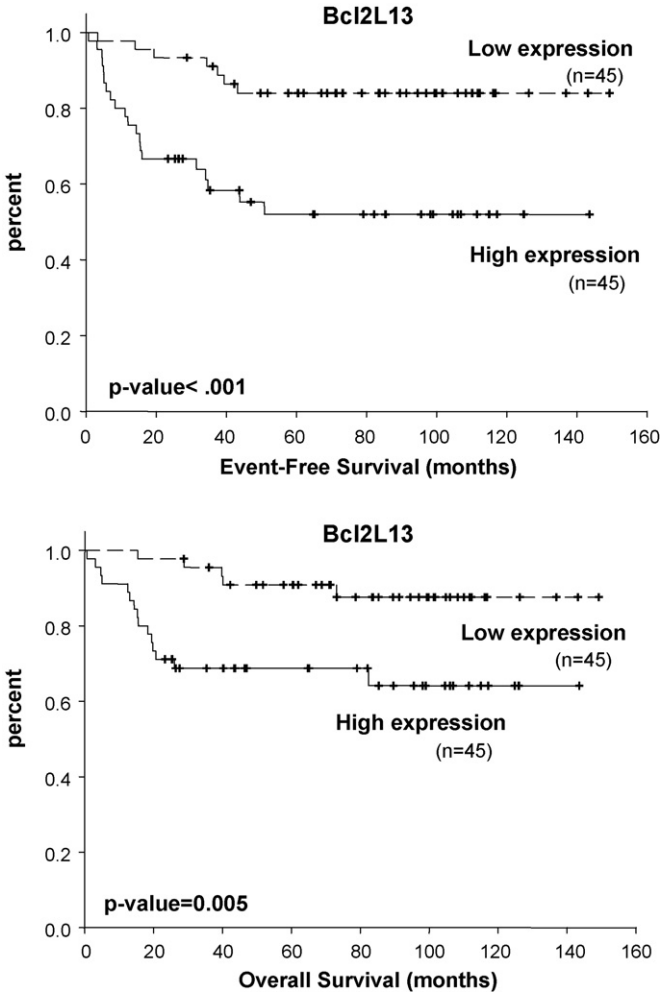

Fig. 1. Patients with lower *BCL2L13* expression had better EFS ($p < 0.001$), and better OS ($p = 0.005$).

risk groups and the three gene signature were correlated with EFS (hazard ratio for three gene signature = 2.85, $p = 0.0163$).

4. Discussion

The principal goal of this study was to measure the expression, in pediatric ALL patients, of three genes involved in apoptotic pathways, and to determine whether these showed any correlation with clinical outcomes. In our study, higher expression of *BCL2L13* was associated with inferior EFS and OS. The expressions of *CASP8AP2* and *Livin* were not associated with clinical outcomes in our cohort. We also attempted to develop a three gene signature to predict the clinical outcome in this study cohort.

BCL2L13 is a member of the *BCL-2* family, and has pro-apoptotic activity [11]. Our results were consistent with those of Holleman et al., who reported that high expression of *BCL2L13* was associated with inferior outcome, a finding that was validated by another cohort [5]. In theory, impaired apoptosis of leukemia cells might allow them to resist chemotherapy, and thus low expression of *BCL2L13* would be expected to indicate a better prognosis following cancer treatment. These apparently conflicting results suggest that *BCL2L13* may have a different apoptotic role in childhood ALL in comparison to its behavior in the cell lines that were used to characterize its apoptotic functions. One possible mechanism to explain this difference is alternative splicing, which is known to generate both anti- and pro-apoptic variants of apoptosis genes such as *Apaf-1* and *Livin* [12–14]. The explanation for the finding that high expression of *BCL2L13* was associated with inferior treatment response will thus require further study.

We attempted to develop a risk signature by the combination of three genes studied. We can use this signature to predict the clinical outcome in this cohort. After multivariate regression including this signature and other known risk factor, this signature can predict the EFS but not OS. However, the *p*-value and hazard ratio were less powerful than the expression of *BCL2L13* alone (HR: 2.81 and $p = 0.0163$ vs. HR: 4.11 and $p = 0.0025$ for EFS). This may be due to the clinical significance of the expression *BCL2L13* but not *Livin* and *CASP8AP2* in this ethical group. A larger prospective study cohort may be needed to validate this finding.

Genome-wide, gene-expression profiling offers a powerful new approach to the study of leukemia cell biology and potentially provides a new molecular classification of leukemia [15–19]. Although our sample size was small, the results differed in some respects from those previously reported. First, we found *BCL2L13* expression to predict survival in the same way as previously reported. We did not find any clinical significance of *CASP8AP2* and *Livin individually*. Several recent studies attempted to identify prognostically relevant genes in ALL by correlating in vitro drug sensitivities or treatment outcomes to chemotherapy drugs with gene expression profiles on microarrays [2,20,21]. Although several genes were identified, and were subsequently confirmed independently in patient populations, there was little overlap between gene expression signatures and established subgroups of patients, such as *t*(12;21), hyperdiploid BP-ALL, or T-cell ALL, or with established drug resistance genes. Catchpoole and colleagues [22] examined the set of 14 genes that Floth et al. [23] recently identified. The results were not

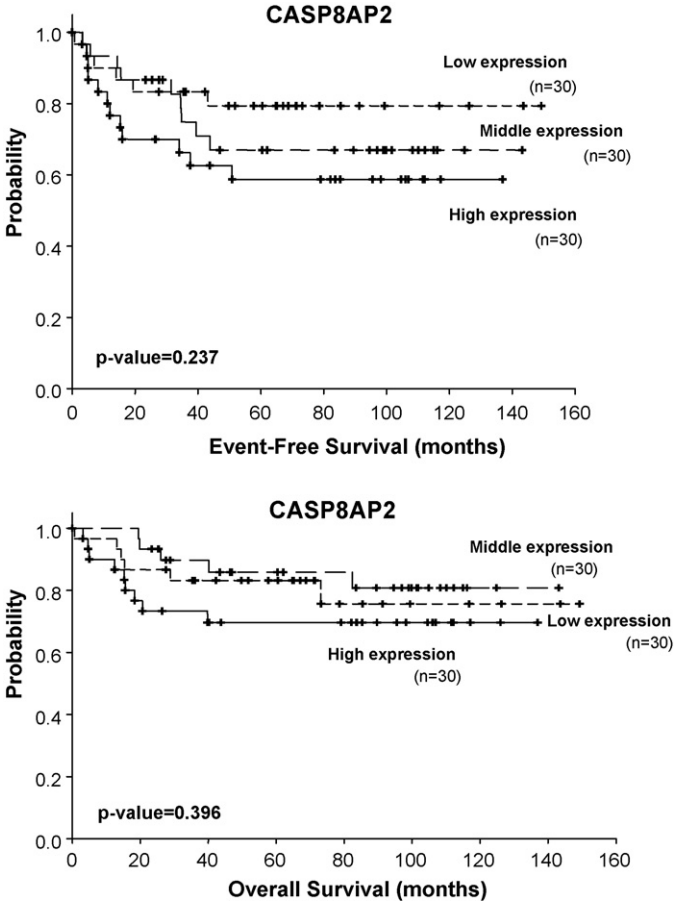

Fig. 2. The EFS and OS did not differ between different *CASP8AP2* expression groups.

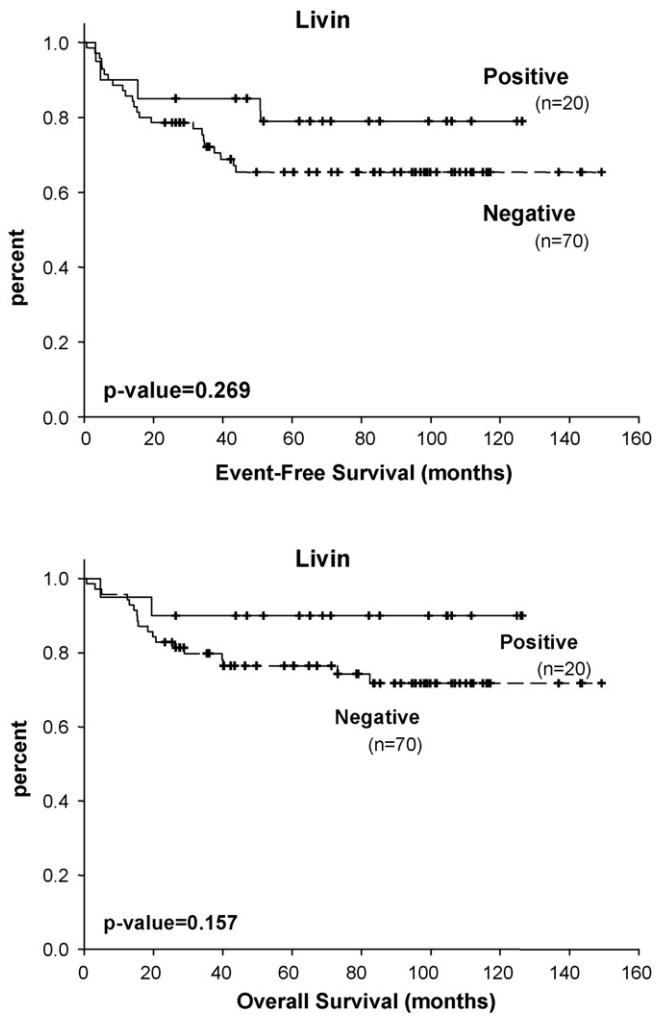

Fig. 3. There was no statistically significant difference for EFS and OS between these two groups of patients with *Livin* expression or not.

in agreement with the original report, suggesting that treatment outcome may be influenced by the other factors, such as pharmacogenetics, the intensity of chemotherapy, and the gene expression of primary leukemia cells. The value of gene expression profiles as

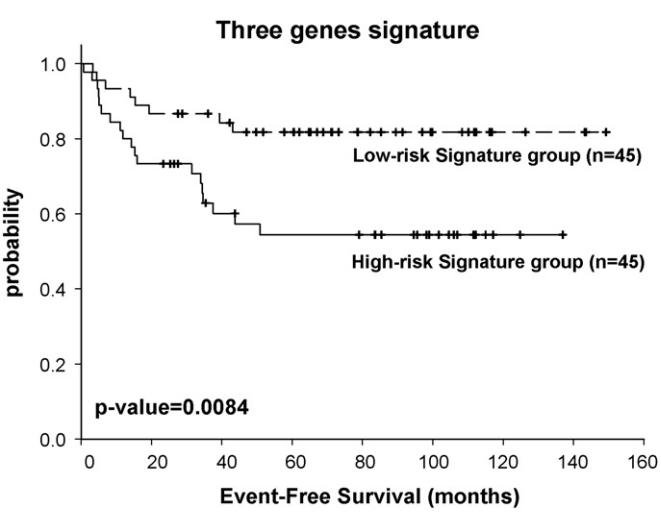

Fig. 4. The patients with high-risk signature had inferior EFS than patients with low-risk signature.

prognostic indicators depends on the treatment regimen. In fact, this caveat applies to any prognostic factor.

Over the past 10–20 years, chromosomal translocation has also emerged as an extremely important prognostic factor and means to assign patients to protocols. However, the importance of even the *t*(12;21) event remains under debate. For example, two large prospective studies focused on the prognostic impact of *t*(12;21) but reached different conclusions [24,25]. If more molecular prognostic factors can be found, it might be possible to provide accurately tailored individualized chemotherapy regimens. Despite this, the number of genes identified as being able to predict clinical outcome in ALL remains small. For examples, Cario et al. reported that expression of *MADL2* was associated with MRD on week 12 in the BFM2000 study [26]. *MADL2* was one of 14 genes identified by Flotho et al. [2]. Low expression of *TTK* (a gene encoding a kinase involved in cell-cycle regulation) was identified by two groups [26,27]. Searching for genes related to treatment response across different regimens might provide clues about general mechanisms that regulate drug sensitivity in leukemic cells.

In summary, in our retrospective studies, *BCL2L13* expression was an independent prognostic factor in childhood ALL. Upon confirmation of their prognostic significance in a larger ALL population, *BCL2L13* may be incorporated into a new classification system. Furthermore, these genes, or other genes related to treatment failure, might themselves represent molecular targets allowing ALL cells to be sensitized to chemotherapy drugs.

Conflict of interest

The authors declare no competing financial interests.

Acknowledgements

We would like to thank all the patients and their parents who participated in this study. We also acknowledge TPOG for data collection and management. This work was supported by NTUH-96-022 and Mr. Chang Han-Sen's research fund for pediatric blood disease.

Contributions. Yung-Li Yang and Shu-Rung Lin contributed equally to this article.

References

[1] Holleman A, den Boer ML, Kazemier KM, Janka-Schaub GE, Pieters R. Resistance to different classes of drugs is associated with impaired apoptosis in childhood acute lymphoblastic leukemia. Blood 2003;102:4541–6.
[2] Flotho C, Coustan-Smith E, Pei D, et al. A set of genes that regulate cell proliferation predicts treatment outcome in childhood acute lymphoblastic leukemia. Blood 2007;110:1271–7.
[3] Pui CH, Evans WE. Treatment of acute lymphoblastic leukemia. N Engl J Med 2006;354:166–78.
[4] Pui CH, Robison LL, Look AT. Acute lymphoblastic leukaemia. Lancet 2008;371:1030–43.
[5] Holleman A, den Boer ML, de Menezes RX, et al. The expression of 70 apoptosis genes in relation to lineage, genetic subtype, cellular drug resistance, and outcome in childhood acute lymphoblastic leukemia. Blood 2006;107:769–76.
[6] Flotho C, Coustan-Smith E, Pei D, et al. Genes contributing to minimal residual disease in childhood acute lymphoblastic leukemia: prognostic significance of CASP8AP2. Blood 2006;108:1050–7.
[7] Choi J, Hwang YK, Sung KW, et al. Expression of Livin, an antiapoptotic protein, is an independent favorable prognostic factor in childhood acute lymphoblastic leukemia. Blood 2007;109:471–7.
[8] Liang DC, Hung IJ, Yang CP, et al. Unexpected mortality from the use of *E. coli* L-asparaginase during remission induction therapy for childhood acute lymphoblastic leukemia: a report from the Taiwan Pediatric Oncology Group. Leukemia 1999;13:155–60.
[9] Lin WY, Liu HC, Yeh TC, Wang LY, Liang DC. Triple intrathecal therapy without cranial irradiation for central nervous system preventive therapy in childhood acute lymphoblastic leukemia. Pediatr Blood Cancer 2008;50:523–7.
[10] Yu IS, Lin SR, Huang CC, et al. TXAS-deleted mice exhibit normal thrombopoiesis, defective hemostasis, and resistance to arachidonate-induced death. Blood 2004;104:135–42.

[11] Kataoka T, Holler N, Micheau O, et al. Bcl-rambo, a novel Bcl-2 homologue that induces apoptosis via its unique C-terminal extension. J Biol Chem 2001;276:19548–54.
[12] Benedict MA, Hu Y, Inohara N, Nunez G. Expression and functional analysis of Apaf-1 Isoforms. Extra WD-40 repeat is required for cytochrome c binding and regulated activation of procaspase-9. J Biol Chem 2000;275:8461–8.
[13] Seol D-W, Billiar TR. A caspase-9 variant missing the catalytic site is an endogenous inhibitor of apoptosis. J Biol Chem 1999;274:2072–6.
[14] Nachmias B, Ashhab Y, Bucholtz V, et al. Caspase-mediated cleavage converts Livin from an antiapoptotic to a proapoptotic factor: implications for drug-resistant melanoma. Cancer Res 2003;63:6340–9.
[15] Moos PJ, Raetz EA, Carlson MA, et al. Identification of gene expression profiles that segregate patients with childhood leukemia. Clin Cancer Res 2002;8:3118–30.
[16] Fine BM, Stanulla M, Schrappe M, et al. Gene expression patterns associated with recurrent chromosomal translocations in acute lymphoblastic leukemia. Blood 2004;103:1043–9.
[17] Ross ME, Zhou X, Song G, et al. Classification of pediatric acute lymphoblastic leukemia by gene expression profiling. Blood 2003;102:2951–9.
[18] Yeoh EJ, Ross ME, Shurtleff SA, et al. Classification, subtype discovery, and prediction of outcome in pediatric acute lymphoblastic leukemia by gene expression profiling. Cancer Cell 2002;1:133–43.
[19] Ferrando AA, Neuberg DS, Staunton J, et al. Gene expression signatures define novel oncogenic pathways in T cell acute lymphoblastic leukemia. Cancer Cell 2002;1:75–87.
[20] Holleman A, Cheok MH, den Boer ML, et al. Gene-expression patterns in drug-resistant acute lymphoblastic leukemia cells and response to treatment. N Engl J Med 2004;351:533–42.
[21] Lugthart S, Cheok MH, den Boer ML, et al. Identification of genes associated with chemotherapy crossresistance and treatment response in childhood acute lymphoblastic leukemia. Cancer Cell 2005;7:375–86.
[22] Catchpoole D, Guo D, Jiang H, Biesheuvel C. Predicting outcome in childhood acute lymphoblastic leukemia using gene expression profiling: Prognostication or protocol selection? Blood 2008;111:2486-a–7-a.
[23] Flotho C, Coustan-Smith E, Pei D, et al. A set of genes that regulate cell proliferation predict treatment outcome in childhood acute lymphoblastic leukemia. Blood 2007.
[24] Loh ML, Goldwasser MA, Silverman LB, et al. Prospective analysis of TEL/AML1-positive patients treated on Dana-Farber Cancer Institute Consortium Protocol 95-01. Blood 2006;107:4508–13.
[25] Rubnitz JE, Wichlan D, Devidas M, et al. Prospective analysis of TEL gene rearrangements in childhood acute lymphoblastic leukemia: a Children's Oncology Group study. J Clin Oncol 2008;26:2186–91.
[26] Cario G, Stanulla M, Fine BM, et al. Distinct gene expression profiles determine molecular treatment response in childhood acute lymphoblastic leukemia. Blood 2005;105:821–6.
[27] Chiaretti S, Li X, Gentleman R, et al. Gene expression profile of adult T-cell acute lymphocytic leukemia identifies distinct subsets of patients with different response to therapy and survival. Blood 2004;103:2771–8.

Leukemia Research 34 (2010) 18–23

Contents lists available at ScienceDirect

Leukemia Research

journal homepage: www.elsevier.com/locate/leukres

Expression and prognostic significance of the apoptotic genes *BCL2L13*, *Livin*, and *CASP8AP2* in childhood acute lymphoblastic leukemia

Yung-Li Yang[a,b], Shu-Rung Lin[c], Jiann-Shiuh Chen[d,j], Shu-Wha Lin[e,f], Sung-Liang Yu[a,e,f,g], Hsuan-Yu Chen[h], Ching-Tzu Yen[f], Chien-Yu Lin[h], Jing-Fang Lin[f], Kai-Hsin Lin[b], Shiann-Tarng Jou[b], Chung-Yi Hu[f], Sheng-Kai Chang[f], Meng-Yao Lu[b], Hsiu-Hao Chang[b], Wan-Hui Chang[i], Kuo-Sin Lin[i], Dong-Tsamn Lin[a,b,*]

[a] *Department of Laboratory Medicine, College of Medicine, National Taiwan University, Taipei, Taiwan*
[b] *Department of Pediatrics, College of Medicine, National Taiwan University, Taipei, Taiwan*
[c] *Department of Bioscience Technology, College of Science, Chung-Yuan Christian University, Taoyuan, Taiwan*
[d] *Department of Internal Medicine, College of Medicine, National Taiwan University, Taipei, Taiwan*
[e] *Department of Medical Research, College of Medicine, National Taiwan University, Taipei, Taiwan*
[f] *National Taiwan University Hospital, Department of Clinical Laboratory Sciences and Medical Biotechnology, College of Medicine, National Taiwan University, Taipei, Taiwan*
[g] *NTU Center for Genomic Medicine, College of Medicine, National Taiwan University, Taipei, Taiwan*
[h] *Institute of Statistical Science Academia Sinica, Taiwan*
[i] *Taiwan Childhood Cancer Foundation, Taipei, Taiwan*
[j] *Department of Pediatrics, National Cheng Kung University Hospital, Tainan, Taiwan*

ARTICLE INFO

Article history:
Received 15 January 2009
Received in revised form 12 July 2009
Accepted 14 July 2009

Keywords:
Childhood acute lymphoblastic leukemia (ALL)
BCL2L13
Livin
CASP8AP2

ABSTRACT

Improved treatment of childhood acute lymphoblastic leukemia (ALL) depends on the identification of new molecular markers that are able to predict treatment response and clinical outcome. The development of impaired apoptosis in leukemic cells is one factor that may influence their response to treatment. We investigated the expression of three apoptosis related genes, *BCL2L13*, *CASP8AP2*, and *Livin*, as well as their prognostic significance, in a retrospective study of 90 pediatric ALL patients diagnosed between 1996 and 2007 in Taiwan. Univariant analysis revealed that high expression of *BCL2L13* was associated with inferior event-free survival and overall survival ($p < 0.001$ and 0.005, respectively). Multivariate analysis for EFS and OS demonstrated that high expression of *BCL2L13* was an independent prognostic factor for childhood ALL in this ethnic group.

1. Introduction

Recent progress in the use of DNA microarrays has identified genes that regulate cell cycle control, DNA repair, and apoptosis which may also participate in disordered cell proliferation and cancer progression in leukemia [1,2]. Alterations in the basal level of expression of these genes may also affect the drug response and clinical outcome of leukemic patients. The cure rate of childhood acute lymphoblastic leukemia (ALL) has increased from 10 to 80% in the developed countries, a fact which may largely be a consequence of the stringent application of prognostic factors for risk-factor-directed therapy [3,4]. The identification of new such gene markers is therefore important not only to gain a basic understanding of the signaling pathways that operate in leukemogenesis, but also to implement enhancements to disease classification systems and to productively target disease with novel therapies.

It has been shown that decreased apoptosis may be an important step in the acquisition of cellular drug resistance in pediatric acute leukemia. Holleman et al. used microarrays to investigate the expression of 70 apoptosis genes, and revealed that *BCL2L13* expression was an independent prognostic factor [5]. Flotho et al. analyzed gene expression in diagnostic lymphoblasts, and compared the findings to minimal residual disease (MRD) levels on days 19 and 46 of remission induction therapy. They identified 17 genes that were significantly associated with MRD level. Among these, the gene coding for caspase 8-associated protein 2 (*CASP8AP2*) was studied further and showed a strong correlation with prog-

* Corresponding author at: Department of Laboratory Medicine and Pediatrics, National Taiwan University Hospital, College of Medicine, National Taiwan University, No. 7 Chung-San S. Rd., Sec. 1, Taipei 100, Taiwan. Tel.: +886 2 23123456x65399; fax: +886 2 23224263.
E-mail address: dtlin@ntuh.gov.tw (D.-T. Lin).

0145-2126/$ – see front matter © 2009 Elsevier Ltd. All rights reserved.
doi:10.1016/j.leukres.2009.07.023

nosis [6]. Chio et al. studied the expression of *Livin*, a member of the IAP family of childhood ALL [7]. Unexpectedly, *Livin* expression was an independent prognostic factor in their cohort. These studies demonstrated an association between dysregulated apoptosis pathways and treatment prognosis, and suggested that the identified genes might serve as functionally defined risk factors for treatment stratification, in addition to those factors currently used.

If specific patterns of gene expression can be correlated with clinical features in childhood ALL, a refinement of current prognosis-based stratification systems might be possible. Thus, we analyzed *BCL2L13*, *CASP8AP2*, and *Livin* gene expression in the childhood ALL of a specific ethnic group, and investigated their correlation with treatment outcomes.

2. Design and methods

2.1. Patients

Viable diagnostic bone marrow (BM) or peripheral blood (PB) was obtained from 90 children who were diagnosed with ALL between July 1996 and August 2007 at National Taiwan University Hospital (NTUH) and National Cheng Kung University Hospital (NCKUH). Of these, 78 patients had been newly diagnosed with B-precursor ALL, and 12 patients with T-cell ALL. Forty-seven patients were treated with TPOG-93-ALL protocols and 43 patients were treated with TPOG-2002-ALL protocols, which are described in detail elsewhere [8,9]. The diagnosis of ALL was made based on the morphologic findings of BM aspirates, as well as on immunophenotype analyses of leukemic cells by flow cytometry. Conventional cytogenetics analyses were performed as part of the routine workup.

Patients were prospectively assigned to one of three risk groups (standard, high, and very high) based on their presenting clinical features and the biological features of their leukemic cells. Patients were considered to have standard-risk (SR) ALL if they were between 1 and 9 years old with a presenting leukocyte count less than 10×10^9 (cells/L) or were between 2 and 7 years old with a presenting leukocyte count between 10×10^9 and 50×10^9. Patients were considered to have high-risk (HR) ALL if they were between 1 and 9 years old with a presenting leukocyte count between $50 \times 10^9$and 100×10^9, or between 1 and 2 or 7 and 10 years old with a presenting leukocyte count between 10×10^9 and 50×10^9. Patients with at least one of the following were assigned to the very-high-risk (VHR) group: age younger than 1 year, initial leukocyte count greater than 100×10^9, T-cell ALL, or presence of *BCR-ABL*, *MLL-AF4* or other *MLL* rearrangements in pre-B ALL.

The risk-directed Taiwan Pediatric Oncology Group (TPOG) protocols consisted of multiple chemotherapeutic agents of different intensities. The treatment protocol was upgraded if complete remission was not achieved after initial induction therapy. Events were defined as any relapse, death, or secondary malignancy. This study was approved by the Medical Ethics Committee of National Taiwan University Hospital. Informed consent was obtained from the patients or their parents before sample collection.

2.2. Methods

2.2.1. RNA isolation

Mononuclear cells from bone marrow (BM) or peripheral blood (PB) were Ficoll-purified and immediately stored in liquid nitrogen. Cryopreserved samples were thawed and washed in FBS-supplemented RPMI 1640 medium prior to RNA extraction. Total RNA was extracted using Trizol reagent according to the manufacturer's instructions (Invitrogen, Paisley, United Kingdom).

2.2.2. Determination of BCL2L13, Livin and CASP8AP2 expression by comparative real-time quantitative-reverse transcriptase polymerase chain reaction (Q-RT-PCR)

The mRNA expression levels of *BCL2L13*, *Livin*, *CASP8AP2* and *glyceraldehydes-3-phosphate dehydrogenase* (*GAPDH*) were measured by Q-RT-PCR using an ABI 7300 real-time PCR system (Applied Biosystems, Foster City, CA). Mature mRNAs were reverse-transcribed into cDNA using oligo-dT and random hexamers as primers by standard methods as described previously [10]. Quantitative PCR amplification of individual cDNAs was performed using the pre-developed Taqman gene expression assay for *BCL2L13* (Hs00209789_m1), *Livin* (Hs00223384_m1) and *CASP8AP2* (Hs01594281_m1)(Applied Biosystems, Foster City, CA). TaqMan endogenous control assay for the *GAPDH* was combined with the assay for target gene in the same reaction (Applied Biosystems). All reactions were performed in duplicate at a minimum. The 20 μl PCR reaction mixture contained 12.5 ng cDNA, 900 nM primers, 250 nM probe, and 1× Taqman universal master mix, combining AmpliTaq Gold® DNA Polymerase, AmpErase® UNG, dNTPs with dUTP, and optimized buffer components. After an initial incubation at 50 °C for 2 min, and a denaturing step at 95 °C for 10 min, a 2-step PCR (95 °C for 15 s followed by 60 °C for 1 min) was performed for 45 cycles to amplify and detect the target sequence.

The expression levels of the target genes in unknown samples were normalized standardized for expression of *GAPDH* and analyzed by the ΔΔCt method [$\Delta\Delta Ct = (Ct_{target\ gene} - Ct_{GAPDH})$ sample − $(Ct_{target\ gene} - Ct_{GAPDH})$ calibrator]. The average of ΔCt ($Ct_{target\ gene} - Ct_{GAPDH}$) from all samples combined was defined as 0, as the calibrator. The amplification efficiencies for target genes and *GAPDH* were calculated and showed the same slopes. A negative control without the templates was also included in each experiment.

2.2.3. Statistical methods

Comparison of baseline clinical variables across groups was made using the Fisher's exact test for categorical data. The nonparametric Mann–Whitney *U*-test was applied for continuous variables. A p-value < 0.05 (two-sided) was considered significant.

Patients analyzed for *BCL2L13* expression were initially divided into two groups according to their median level of *BCL2L13* (median = 5.91 as cut-off point). We divided the patients into three groups of 30 patients each according to the *CASPS8AP2* expression levels (5.5 and 10.5 as cut-off point). The patients were categorized into two groups according to the presence or absence of the *Livin* expression.

OS was calculated using the Kaplan–Meier method, and the log-rank test was used to compare differences between survival curves. OS was measured from the protocol commencement date until the date of death regardless of cause, excluding patients who were alive at last follow-up. EFS was defined only for patients who achieved complete remission, and was measured from the date of attaining CR until the date of relapse. Patients with no report of relapse by the end of the follow-up observation were censored on the date of last follow-up.

Cox proportional hazard models were constructed for EFS and OS. The following covariates were included in the full model of OS and EFS: *BCL2L13* expression (low vs. high), *CASP8AP2* expression (low, median and high), *Livin* expression (presence or absence), sex, WBC (<100,000/μL vs. 100,000/μL), age (<10 years vs. >10 years), immunophenotypes (B or T), hospital, and genetic subtypes. Stepwise backward selection was performed. All calculations were performed using the SAS software package, version 9 (SAS Inc.).

3. Results

3.1. Patient characteristics (Table 1)

The clinical characteristics of patients at the time of diagnosis are presented in Table 1. The median age among 90 patients (46 boys and 44 girls) was 4.3 years (range: 0–17 years), and their median leukocyte count was 20.0 (range: 0.2–1826). The number of SR, HR, and VHR patients was 24, 31, and 35 respectively.

3.2. The association of BCL2L13, CASP8AP2 and Livin expression level with clinical outcomes

Patients were defined as low and high *BCL2L13* as described in Section 2. The *BCL2L13* expression level did not differ among the different risk groups (Table 1). Patients with lower *BCL2L13* expression had better EFS ($p < 0.001$), and better OS ($p = 0.005$) (Fig. 1).

Patients were defined as low, median and high *CASP8AP2* as described above. The *CASP8AP2* expression level did not differ among the different risk groups (Table 1). The prognosis did not differ between different *CASP8AP2* expression groups (Fig. 2).

As expected, approximately 21.1% of patients expressed *Livin*, as was reported by Choi et al. In our series, 20 patients expressed *Livin* and 70 patients did not. We compared EFS and OS between patients who did and did not express *Livin*. There was no statistically significant difference between these two groups of patients (Fig. 3).

3.3. Multiple variable (Cox regression) analysis reveals that BCL2L13 was an independent prognostic factor

We performed multivariable Cox regression analyses examining the correlation between EFS or OS and *BCL2L13, CAP8AP2and Livin* status, other known prognostic factors, and age and white count listed in Table 1. When other significant predictors of EFS were controlled for in the final model, *MLL* gene rearrangement, initial white counts more than 100,000/μL, risk groups and the expression level of *BCL2L13* were correlated with EFS (hazard ratio for *BCL2L13* = 4.11, $p = 0.0025$) (Table 2). When other significant predictors of OS were controlled for in the final model, *MLL* gene rearrangement, initial white counts more than 100,000/μL, and the expression level of

Table 1
The clinical features of patients at diagnosis and their association with three genes studied.

	BCL2L13			*CASP8AP2*				*Livin*		
	Low number	High number	*p*-value*	Low number	Median number	High number	*p*-value*	Positive number	Negative number	*p*-value*
WBC										
<100,000/μL	36	12	0.462	24	21	23	0.749	16	52	0.771
>100,000/μL	9	13		6	9	7		4	18	
Immunophenotype										
B	36	42	0.118	23	24	27	0.578	18	16	1.000
T										
Age										
<10 years	33	32	1.000	21	22	22	1.000	16	49	0.572
>10 years	12	13		9	8	8		4	21	
Risk groups										
Standard risk	14	10	0.335	9	7	8	0.929	7	17	0.592
High risk	17	14		11	11	9		7	24	
Very high risk	14	21		10	12	13		6	29	
Hyperdiplopid										
Negative	36	41	0.230	23	28	26	0.217	58	19	0.283
Positive	9	4		7	2	4		12	1	
t(9;22)										
Negative	45	43	0.494	30	28	30	0.326	20	69	1.000
Positive	0	2		2	0	2		0	4	
MLL gene										
Negative	45	41	0.117	28	30	28	0.54	20	66	0.572
Positive	0	4		2	0	2		0	4	
Hospital										
NTUH	29	38	0.052	24	20	23	0.565	52	15	1.000
MCKUH	16	7		6	10	7		18	5	

* Fisher exact test.

BCL2L13 were correlated with OS (hazard ratio for *BCL2L13* = 3.41, $p = 0.0244$) (Table 3).

3.4. Three gene signature as a predictor as outcome

We attempted to develop a risk signature using the combination of three markers studied. The signature was *CASP8AP2* × 0.03869 + *BCL2L13* × 0.02747 + *Livin* code (0 or 1) − 0.59135. The patients with high-risk signature had inferior EFS than patients with low-risk signature ($p = 0.0084$, median = 0.463 as cut-off point) (Fig. 4). We performed multivariable Cox regression analyses examining the correlation between EFS and other known prognostic factors, genetic types, age and white count listed in Table 1. The results were shown in Table 4. When other significant predictors of EFS were controlled for in the final model, *MLL* gene rearrangement,

Table 3
Multivariate Cox regression analysis for OS.

Variables	Hazard ratio (HR)	95% HR CI	*p*-value
Livin	0.49	0.11–2.29	0.365
CASP8AP2	1.12	0.58–2.17	0.738
BCL2L13	2.45	0.67–9.04	0.178
WBC > 100,000/μL	3.30	0.81–13.43	0.095
B vs. T	0.43	0.07–2.89	0.388
Age > 10	1.39	0.36–5.35	0.630
Risk groups	1.85	0.61–5.57	0.277
Hyperdiplopid	0	0	0.992
t(9;22)	1.38	0.25–7.67	0.716
MLL gene rearrangements	6.28	1.38–28.56	0.017
Step selection			
BCL2L13	3.41	1.17–9.93	0.0244
WBC > 100,000/μL	5.25	2.05–13.44	0.0005
MLL gene rearrangements	8.05	1.99–32.54	0.0034

Table 2
Multivariate Cox regression analysis for EFS.

Variables	Hazard ratio (HR)	95% HR CI	*p*-value
Livin	0.73	0.24–2.25	0.587
CASP8AP2	1.12	0.53–2.00	0.695
BCL2L13	3.25	1.09–9.72	0.035
WBC > 100,000/μL	2.77	0.89–8.60	0.079
B vs. T	0.74	0.18–3.03	0.679
Age > 10	1.39	0.49–3.95	0.537
Risk groups	2.02	0.82–4.98	0.127
Hyperdiplopid	0.44	0.06–3.52	0.44
t(9;22)	2.65	0.48–14.52	0.261
MLL gene rearrangements	5.75	1.42–23.23	0.014
Step selection			
BCL2L13	4.11	1.64–10.30	0.0025
WBC > 100,000/μL	2.72	1.02–7.26	0.0452
Risk groups	2.28	1.04–4.97	0.0386
MLL gene rearrangements	5.75	1.45–17.55	0.0110

Table 4
Multivariate Cox regression analysis for EFS using three gene signature as a parameter.

Variables	Hazard ratio (HR)	95% HR CI	*p*-value
Three gene signature	2.68	1.07–6.70	0.035
WBC > 100,000/μL		0.78–6.83	0.129
B vs. T	0.54	0.15–1.99	0.356
Age > 10	1.47	0.53–4.07	0.461
Risk groups	2.42	1.00–5.88	0.051
Hyperdiplopid	0.47	0.06–3.77	0.478
t(9;22)	2.89	0.53–15.72	0.220
MLL gene rearrangements	6.98	1.78–27.30	0.005
Step selection			
Three gene signature	2.85	1.21–6.70	0.0163
WBC > 100,000/μL	6.36	1.83–22.08	0.0036
MLL gene rearrangements	3.51	1.82–6.76	0.0002

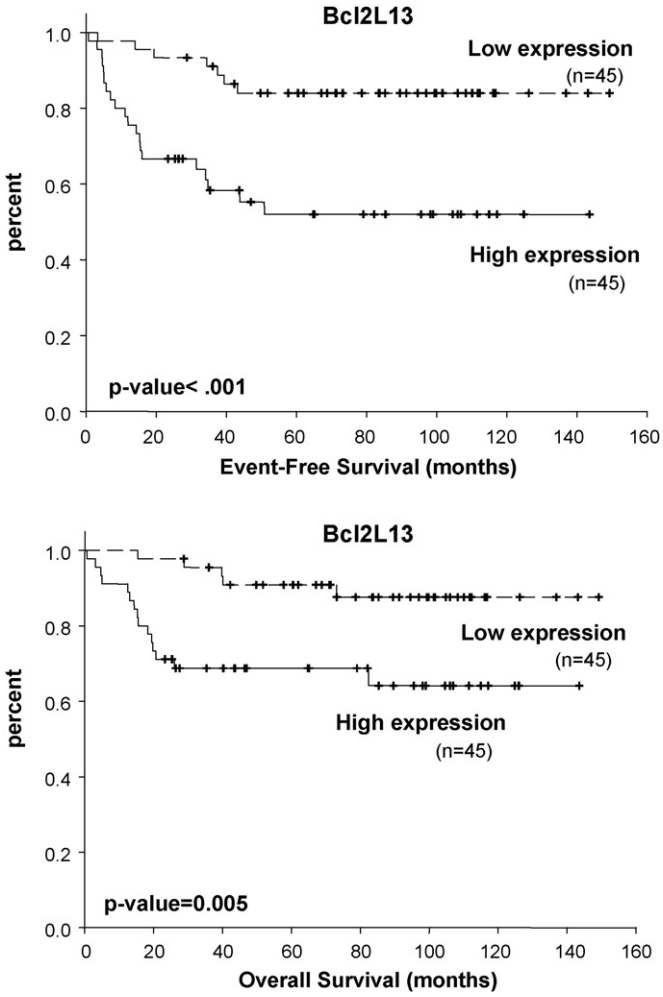

Fig. 1. Patients with lower *BCL2L13* expression had better EFS ($p < 0.001$), and better OS ($p = 0.005$).

risk groups and the three gene signature were correlated with EFS (hazard ratio for three gene signature = 2.85, $p = 0.0163$).

4. Discussion

The principal goal of this study was to measure the expression, in pediatric ALL patients, of three genes involved in apoptotic pathways, and to determine whether these showed any correlation with clinical outcomes. In our study, higher expression of *BCL2L13* was associated with inferior EFS and OS. The expressions of *CASP8AP2* and *Livin* were not associated with clinical outcomes in our cohort. We also attempted to develop a three gene signature to predict the clinical outcome in this study cohort.

BCL2L13 is a member of the *BCL-2* family, and has pro-apoptotic activity [11]. Our results were consistent with those of Holleman et al., who reported that high expression of *BCL2L13* was associated with inferior outcome, a finding that was validated by another cohort [5]. In theory, impaired apoptosis of leukemia cells might allow them to resist chemotherapy, and thus low expression of *BCL2L13* would be expected to indicate a better prognosis following cancer treatment. These apparently conflicting results suggest that *BCL2L13* may have a different apoptotic role in childhood ALL in comparison to its behavior in the cell lines that were used to characterize its apoptotic functions. One possible mechanism to explain this difference is alternative splicing, which is known to generate both anti- and pro-apoptic variants of apoptosis genes such as *Apaf-1* and *Livin* [12–14]. The explanation for the finding that high expression of *BCL2L13* was associated with inferior treatment response will thus require further study.

We attempted to develop a risk signature by the combination of three genes studied. We can use this signature to predict the clinical outcome in this cohort. After multivariate regression including this signature and other known risk factor, this signature can predict the EFS but not OS. However, the *p*-value and hazard ratio were less powerful than the expression of *BCL2L13* alone (HR: 2.81 and $p = 0.0163$ vs. HR: 4.11 and $p = 0.0025$ for EFS). This may be due to the clinical significance of the expression *BCL2L13* but not *Livin* and *CASP8AP2* in this ethical group. A larger prospective study cohort may be needed to validate this finding.

Genome-wide, gene-expression profiling offers a powerful new approach to the study of leukemia cell biology and potentially provides a new molecular classification of leukemia [15–19]. Although our sample size was small, the results differed in some respects from those previously reported. First, we found *BCL2L13* expression to predict survival in the same way as previously reported. We did not find any clinical significance of *CASP8AP2* and *Livin individually*. Several recent studies attempted to identify prognostically relevant genes in ALL by correlating in vitro drug sensitivities or treatment outcomes to chemotherapy drugs with gene expression profiles on microarrays [2,20,21]. Although several genes were identified, and were subsequently confirmed independently in patient populations, there was little overlap between gene expression signatures and established subgroups of patients, such as *t*(12;21), hyperdiploid BP-ALL, or T-cell ALL, or with established drug resistance genes. Catchpoole and colleagues [22] examined the set of 14 genes that Floth et al. [23] recently identified. The results were not

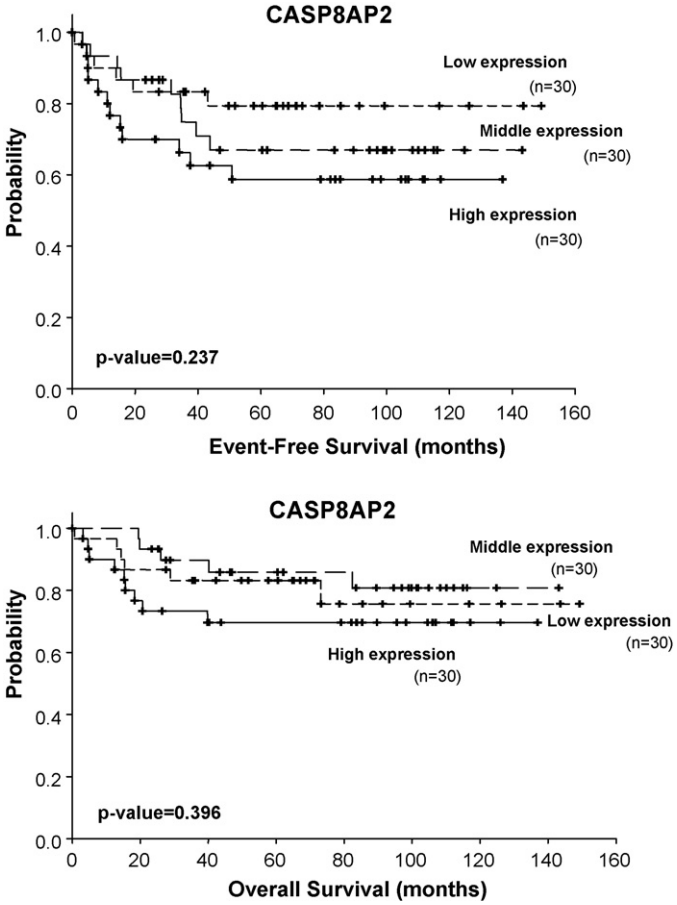

Fig. 2. The EFS and OS did not differ between different *CASP8AP2* expression groups.

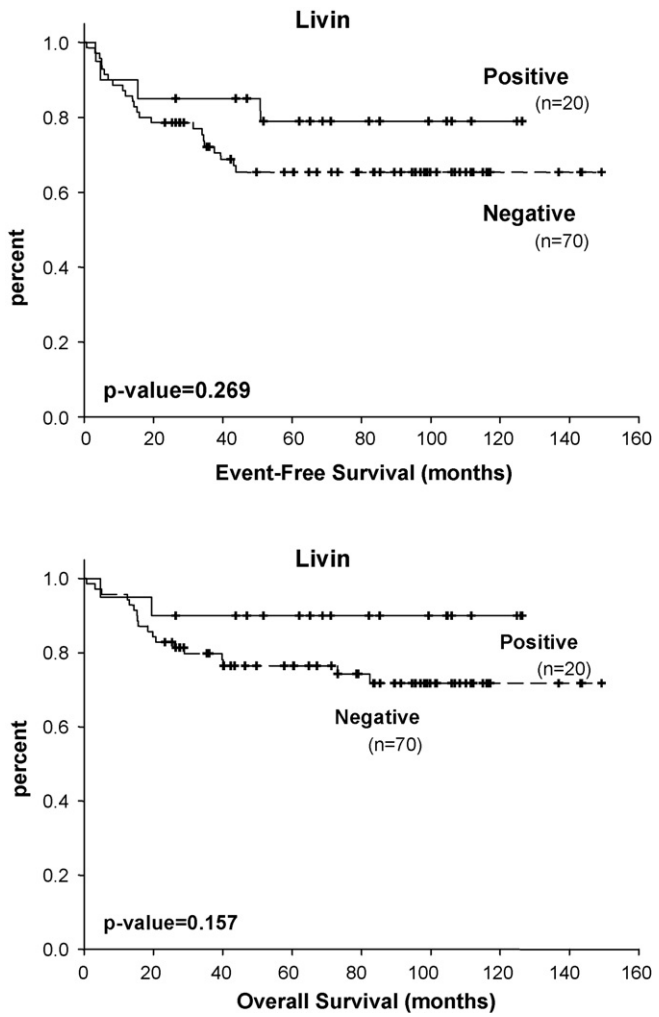

Fig. 3. There was no statistically significant difference for EFS and OS between these two groups of patients with *Livin* expression or not.

in agreement with the original report, suggesting that treatment outcome may be influenced by the other factors, such as pharmacogenetics, the intensity of chemotherapy, and the gene expression of primary leukemia cells. The value of gene expression profiles as

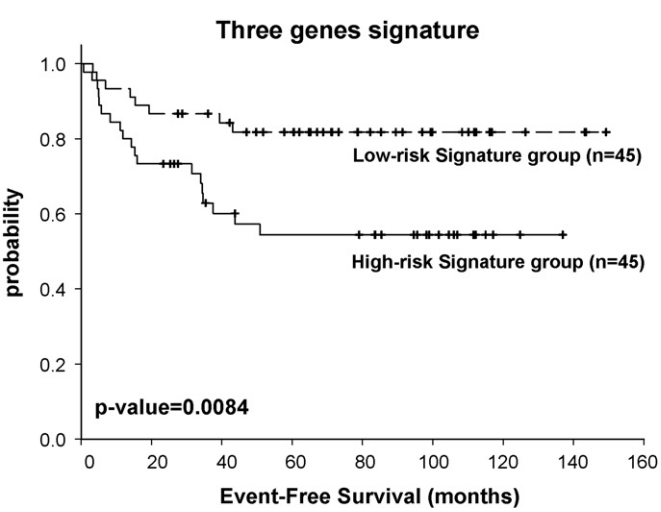

Fig. 4. The patients with high-risk signature had inferior EFS than patients with low-risk signature.

prognostic indicators depends on the treatment regimen. In fact, this caveat applies to any prognostic factor.

Over the past 10–20 years, chromosomal translocation has also emerged as an extremely important prognostic factor and means to assign patients to protocols. However, the importance of even the *t*(12;21) event remains under debate. For example, two large prospective studies focused on the prognostic impact of *t*(12;21) but reached different conclusions [24,25]. If more molecular prognostic factors can be found, it might be possible to provide accurately tailored individualized chemotherapy regimens. Despite this, the number of genes identified as being able to predict clinical outcome in ALL remains small. For examples, Cario et al. reported that expression of *MADL2* was associated with MRD on week 12 in the BFM2000 study [26]. *MADL2* was one of 14 genes identified by Flotho et al. [2]. Low expression of *TTK* (a gene encoding a kinase involved in cell-cycle regulation) was identified by two groups [26,27]. Searching for genes related to treatment response across different regimens might provide clues about general mechanisms that regulate drug sensitivity in leukemic cells.

In summary, in our retrospective studies, *BCL2L13* expression was an independent prognostic factor in childhood ALL. Upon confirmation of their prognostic significance in a larger ALL population, *BCL2L13* may be incorporated into a new classification system. Furthermore, these genes, or other genes related to treatment failure, might themselves represent molecular targets allowing ALL cells to be sensitized to chemotherapy drugs.

Conflict of interest

The authors declare no competing financial interests.

Acknowledgements

We would like to thank all the patients and their parents who participated in this study. We also acknowledge TPOG for data collection and management. This work was supported by NTUH-96-022 and Mr. Chang Han-Sen's research fund for pediatric blood disease.

Contributions. Yung-Li Yang and Shu-Rung Lin contributed equally to this article.

References

[1] Holleman A, den Boer ML, Kazemier KM, Janka-Schaub GE, Pieters R. Resistance to different classes of drugs is associated with impaired apoptosis in childhood acute lymphoblastic leukemia. Blood 2003;102:4541–6.
[2] Flotho C, Coustan-Smith E, Pei D, et al. A set of genes that regulate cell proliferation predicts treatment outcome in childhood acute lymphoblastic leukemia. Blood 2007;110:1271–7.
[3] Pui CH, Evans WE. Treatment of acute lymphoblastic leukemia. N Engl J Med 2006;354:166–78.
[4] Pui CH, Robison LL, Look AT. Acute lymphoblastic leukaemia. Lancet 2008;371:1030–43.
[5] Holleman A, den Boer ML, de Menezes RX, et al. The expression of 70 apoptosis genes in relation to lineage, genetic subtype, cellular drug resistance, and outcome in childhood acute lymphoblastic leukemia. Blood 2006;107:769–76.
[6] Flotho C, Coustan-Smith E, Pei D, et al. Genes contributing to minimal residual disease in childhood acute lymphoblastic leukemia: prognostic significance of CASP8AP2. Blood 2006;108:1050–7.
[7] Choi J, Hwang YK, Sung KW, et al. Expression of Livin, an antiapoptotic protein, is an independent favorable prognostic factor in childhood acute lymphoblastic leukemia. Blood 2007;109:471–7.
[8] Liang DC, Hung IJ, Yang CP, et al. Unexpected mortality from the use of *E. coli* L-asparaginase during remission induction therapy for childhood acute lymphoblastic leukemia: a report from the Taiwan Pediatric Oncology Group. Leukemia 1999;13:155–60.
[9] Lin WY, Liu HC, Yeh TC, Wang LY, Liang DC. Triple intrathecal therapy without cranial irradiation for central nervous system preventive therapy in childhood acute lymphoblastic leukemia. Pediatr Blood Cancer 2008;50:523–7.
[10] Yu IS, Lin SR, Huang CC, et al. TXAS-deleted mice exhibit normal thrombopoiesis, defective hemostasis, and resistance to arachidonate-induced death. Blood 2004;104:135–42.

[11] Kataoka T, Holler N, Micheau O, et al. Bcl-rambo, a novel Bcl-2 homologue that induces apoptosis via its unique C-terminal extension. J Biol Chem 2001;276:19548–54.
[12] Benedict MA, Hu Y, Inohara N, Nunez G. Expression and functional analysis of Apaf-1 Isoforms. Extra WD-40 repeat is required for cytochrome c binding and regulated activation of procaspase-9. J Biol Chem 2000;275:8461–8.
[13] Seol D-W, Billiar TR. A caspase-9 variant missing the catalytic site is an endogenous inhibitor of apoptosis. J Biol Chem 1999;274:2072–6.
[14] Nachmias B, Ashhab Y, Bucholtz V, et al. Caspase-mediated cleavage converts Livin from an antiapoptotic to a proapoptotic factor: implications for drug-resistant melanoma. Cancer Res 2003;63:6340–9.
[15] Moos PJ, Raetz EA, Carlson MA, et al. Identification of gene expression profiles that segregate patients with childhood leukemia. Clin Cancer Res 2002;8:3118–30.
[16] Fine BM, Stanulla M, Schrappe M, et al. Gene expression patterns associated with recurrent chromosomal translocations in acute lymphoblastic leukemia. Blood 2004;103:1043–9.
[17] Ross ME, Zhou X, Song G, et al. Classification of pediatric acute lymphoblastic leukemia by gene expression profiling. Blood 2003;102:2951–9.
[18] Yeoh EJ, Ross ME, Shurtleff SA, et al. Classification, subtype discovery, and prediction of outcome in pediatric acute lymphoblastic leukemia by gene expression profiling. Cancer Cell 2002;1:133–43.
[19] Ferrando AA, Neuberg DS, Staunton J, et al. Gene expression signatures define novel oncogenic pathways in T cell acute lymphoblastic leukemia. Cancer Cell 2002;1:75–87.
[20] Holleman A, Cheok MH, den Boer ML, et al. Gene-expression patterns in drug-resistant acute lymphoblastic leukemia cells and response to treatment. N Engl J Med 2004;351:533–42.
[21] Lugthart S, Cheok MH, den Boer ML, et al. Identification of genes associated with chemotherapy crossresistance and treatment response in childhood acute lymphoblastic leukemia. Cancer Cell 2005;7:375–86.
[22] Catchpoole D, Guo D, Jiang H, Biesheuvel C. Predicting outcome in childhood acute lymphoblastic leukemia using gene expression profiling: Prognostication or protocol selection? Blood 2008;111:2486-a–7-a.
[23] Flotho C, Coustan-Smith E, Pei D, et al. A set of genes that regulate cell proliferation predict treatment outcome in childhood acute lymphoblastic leukemia. Blood 2007.
[24] Loh ML, Goldwasser MA, Silverman LB, et al. Prospective analysis of TEL/AML1-positive patients treated on Dana-Farber Cancer Institute Consortium Protocol 95-01. Blood 2006;107:4508–13.
[25] Rubnitz JE, Wichlan D, Devidas M, et al. Prospective analysis of TEL gene rearrangements in childhood acute lymphoblastic leukemia: a Children's Oncology Group study. J Clin Oncol 2008;26:2186–91.
[26] Cario G, Stanulla M, Fine BM, et al. Distinct gene expression profiles determine molecular treatment response in childhood acute lymphoblastic leukemia. Blood 2005;105:821–6.
[27] Chiaretti S, Li X, Gentleman R, et al. Gene expression profile of adult T-cell acute lymphocytic leukemia identifies distinct subsets of patients with different response to therapy and survival. Blood 2004;103:2771–8.